Methodologies for Screening Metal-Chelating Peptides in Protein Hydrolysates for their Antioxidant Properties

Sarah El Hajj

Ecole Doctorale Sciences et Ingénierie des Molécules Procédés Produits et Énergie

Thèse de doctorat

Methodologies for Screening Metal-Chelating Peptides in Protein Hydrolysates for their Antioxidant Properties

Présentée et soutenue publiquement pour l'obtention du titre de

DOCTEURE DE L'UNIVERSITE DE LORRAINE

Spécialité : Procédés Biotechnologiques

par

Sarah EL HAJJ

Le 22 Mars 2022

Devant le jury composé de

Rapporteurs :	M. Peter FALLER	Professeur, Université de Strasbourg
	Mme Charlotte JACOBSEN	Professeure, Denmark Technical University
Examinateurs :	M. Jean-Michel GIRARDET	Ingénieur de recherche, HDR, Université de Lorraine
Président du jury :	M. Chibuike UDENIGWE	Professeur, University of Ottawa
Directrice de thèse :	Mme Laetitia CANABADY-ROCHELLE	Chargée de recherche, HDR, Université de Lorraine
Co-Directrice de thèse :	Mme Caroline GAUCHER	Maître de conferences, HDR, Université de Lorraine
Membres invités :	Mme Sandrine BOSCHI-MULLER	Professeure, Université de Lorraine
	M. Saïd BOUHALLAB	Directeur de recherche, INRAE

Abstract

Currently, the discovery of new biomolecules is essential for various industrial applications. Peptides produced by hydrolysis of plant or animal proteins are of interest because of their potential bioactivities. Some peptides, by their ability to complex iron(II), can inhibit and slow down oxidation phenomena. To date, the discovery of new bioactive molecules is generally based on long and fastidious empirical approaches, involving large quantities of solvents, harmful to the environment. Therefore, it is important to develop new and highly sensitive screening methods before implementing a selective separation process of these peptides of interest present in mixture. The objective of this thesis is therefore to (1) develop highly sensitive screening methods to identify the presence of these metal chelating peptides (MCPs) in hydrolysates, produced in the laboratory, before undertaking a time-consuming separation phase and (2) to study their antioxidant activities, using cellular assays.

In the first approach, time-resolved molecular dynamics (switchSENSE®) was first implemented on model peptides capable of complexing metals and then applied to non-filtrated soy and tilapia protein hydrolysates. It has proven to be very sensitive for detecting the presence of MCPs in peptide hydrolysates. This technology is based on the electrical movement of DNA strands, present on the surface of gold microelectrodes, on which are immobilized metal ions. When a peptide has an affinity for an immobilized metal ion and thus forms a peptide-metal complex, a variation of the measured fluorescence signal is observed. On the other hand, MCPs were screened in ultrafiltrated soy and pea protein hydrolysates using Surface Plasmon Resonance (SPR). This advanced technique allows to determine an affinity constant between a peptide and a metal ion immobilized on a microchip at the molecular scale. It is used here in an original way to study different hydrolysates and thus, to screen the best hydrolysis condition to produce MCPs.

The biological interest in exploring metal-chelating activity in these hydrolysates is to evaluate their antioxidant power *in cellulo*. These peptides could be promising for ferroptosis inhibition by chelating excess iron ions and thus contribute to the prevention of cell death in several diseases including atherosclerosis (AS). We aimed to develop a ferroptosis model (induction and rescuing) on human aortic smooth muscle cells to mimic ferroptosis happening during AS development. The ferroptosis model was developed in three steps taking into consideration three essential parameters such as the concentration of ferroptosis inducers (erastin and ferric ions), the time and the medium of incubation. At each step, 2 biomarkers *i.e.,* intracellular concentration of glutathione and peroxidized lipids were followed by NDA and TBARS methods, respectively. The rescue of the ferroptosis model was validated using metal chelators such as deferoxamine and deferiprone, which are also control molecules regarding MCP activity.

Keywords: Metal-chelating peptides, Hydrolysis, Antioxidants, Screening, Ferroptosis.

Acknowledgements

I deeply believe that we are the fruit of the experiences we live and the people we meet. Many, no doubt, are those without whom this thesis could not have been carried out as it has been.

I can never thank enough my PhD director **Laetitia CANABADY-ROCHELLE** and co-director **Caroline GAUCHER** for having given me the opportunity to do this PhD. From the beginning, their trust and support have been unfailing. They have always put everything in place so that my research is conducted in the best possible conditions. I thank **Mrs. CANABADY-ROCHELLE** and **Mrs. GAUCHER** for all their teachings, advices, and their permanent availability.

I also wish to thank all the staff of LRGP and CITHEFOR laboratories, in particular **Philippe ARNOUX** (LRGP) and **Isabelle FRIES** (CITHEFOR) who helped me in certain experiments. Thanks as well for my doctoral students and post-docs friends for their support and for the quality time we spent together.

I gratefully acknowledge the funding received towards my PhD from the "Impact Biomolecules" project of the "Lorraine Université d'Excellence" (ANR-15-IDEX-04-LUE-LUE-Lorraine Université d'Excellence, 2016). I also appreciate the support received through the collaborative work undertaken in the different laboratories (LCPM, LIBIO, L2CM, IMoPA & URAFPA) and platforms (ASIA & B2S) of Université de Lorraine. Special thanks for **Jean-Michel GIRARDET** and **Sandrine BOSCHI-MULLER** for their supervision during the SwitchSENSE® and SPR experiments.

My thanks also go to Professor **Peter FALLER** and Professor **Charlotte JACOBSEN** for accepting to review my thesis. As well, thanks for the other members of the jury: **Jean-Michel GIRARDET** and **Chibuike UDENIGWE**.

I would like to say a heartfelt "thank you" to my **Mum** and **Dad** for being there day after day to make sure I have this wonderful education. To my **siblings**, to my whole **family**, and to my **friends**: You have all contributed in one way or another to this thesis, so thank you!

And finally, to **Mohamad**, who has always been there with his endless support and continuous encouragement.

Table of Contents

Abstract 1
Acknowledgements 3
List of Figures 9
List of Tables 13
List of abbreviations 15

Chapter 1 Introduction (English & Français) 17
1.1 Oxidative stress and antioxidant: terms and concepts 17
1.2 Ferroptosis: Iron-catalyzed oxidative cell damage 18
1.3 Metal-chelating peptides: antioxidant properties and discovery limitations 20
1.4 General context and objective of this PhD 21
1.5 Thesis structure 23
1.6 References 33

Chapter 2 State of the art 35
2.1 Mineral-Binding Peptides: applications in nutrition 36
2.1.1 Introduction 36
2.1.2 Importance of minerals for nutrition 37
2.1.3 Bioavailability and metabolism of minerals 41
2.1.4 Mineral-binding peptides: potential applications, sources, production and commercialization 43
2.1.5 Selective extraction of mineral-binding peptides from complex hydrolysates 50
2.1.6 Evidence of health effects of mineral-binding peptides 66
2.1.7 Summary 68
2.1.8 References 69
2.2 Ferroptosis: A cell death mechanism driven by Iron overload 84
2.2.1 Introduction 84
2.2.2 Lipid peroxidation 84
2.2.3 Iron catalysed lipid peroxidation in cells 85
2.2.4 Discovery of ferroptosis and speed of research in this field 86
2.2.5 Morphological and biochemical features of ferroptosis 88
2.2.6 Pharmacological modulation of ferroptosis 92
2.2.7 Ferroptosis and human diseases 98
2.2.8 Conclusion 102
2.2.9 References 103

Chapter 3 Electrically switchable nanolever technology for the screening of metal-chelating peptides in hydrolysates 115
3.1 Introduction 117
3.2 Material and Methods 119
3.2.1 Production of protein hydrolysates 119
3.2.2 Peptide characterization 122
3.2.3 Real-time switchSENSE® analysis 123
3.2.4 Metal-chelation test 125
3.3 Results and Discussion 125
3.3.1 SwitchSENSE® measurements with model peptides 125
3.3.2 Metal-chelation capacity of Tilapia viscera and soy proteins hydrolysates 130
3.3.3 SwitchSENSE® measurements for screening MCPs in hydrolysates 134
3.4 References 138

Chapter 4 Metal-chelating activity of soy and pea protein hydrolysates obtained after different enzymatic treatments 143
4.1 Introduction 144
4.2 Material and Methods 146
4.2.1 Production of protein hydrolysates 146
4.2.2 Ultrafiltration 146
4.2.3 Efficiency of the different hydrolysis protocols 147
4.2.4 Physico-chemical characterization of the produced hydrolysates 148
4.2.5 Determination of the metal-chelation properties 149
4.3 Results and Discussion 150
4.3.1 Efficiency of the different hydrolysis protocols 150
4.3.2 Characterization of the produced hydrolysates 152
4.3.3 Determination of the metal-chelation properties 155
4.4 Conclusion 161
4.5 References 162

Chapter 5 Development of a ferroptosis model on Aortic smooth muscle cells 167
5.1 Introduction 167
5.2 Material and Methods 168
5.2.1 Reagents 168
5.2.2 Cell culture 169
5.2.3 Cytocompatibility test 169
5.2.4 Induction of ferroptosis 169
5.2.5 Quantification of intracellular glutathione concentration 170
5.2.6 Quantification of peroxidized lipids 170
5.2.7 Quantification of intracellular proteins 171

5.2.8 Statistical analysis 171
5.3 Results and Discussion 171
5.3.1 Cytocompatibility of Erastin 171
5.3.2 Ferroptosis evaluation upon Erastin incubation in different media by GSH quantification 172
5.3.3 Ferroptosis evaluation upon erastin incubation in different media by MDA quantification 175
5.3.4 Ferroptosis evaluation upon iron introduction in different media by MDA quantification 177
5.3.5 Ferroptosis rescue model evaluation by GSH and MDA quantifications 179
5.4 Conclusion and Perspectives 180
5.5 References 182

Chapter 6 General Conclusion and Perspectives 183
6.1 Conclusion 185
6.2 Perspectives 188

List of Figures

Figure 1.1 Oxidation state balance 18

Figure 1.2 Effect of free and bound iron ions on the formation of ROS 19

Figure 1.3 Diseases where ferroptosis is reported (left). Plaques buildups in arteries in atherosclerosis (AS) disease (Right) 20

Figure 1.4 The empirical approach to discover MCPs 21

Figure 1.5 The fields covered in this interdisciplinary PhD project 22

Figure 1.6 The thesis structure 23

Figure 1.1 (français) Équilibre de l'état d'oxydation 26

Figure 1.2 (français) Effet des ions fer libres et liés sur la formation de ERO 27

Figure 1.3 (français) Maladies où la ferroptose est signalée (à gauche). Accumulation de plaques dans les artères dans l'athérosclérose (AS) (à droite) 28

Figure 1.4 (français) L'approche empirique pour découvrir les PCMs 29

Figure 1.5 (français) Les matières couvertes par ce projet de doctorat interdisciplinaire 31

Figure 1.6 (français) Structure de la thèse 32

Figure 2.1 Synoptic scheme of this bibliographic part 37

Figure 2.2 Proteolysis parameters to act on to produce various MBP sequences and most common mode of action of the commonly used enzymes. Figure adapted from Chabanon, 2005 47

Figure 2.3 Principle of solid phase synthesis commonly used for peptide synthesis 49

Figure 2.4 Various complementary spectroscopic techniques used for the investigation of peptide-metal interaction 52

Figure 2.5 Principle of Isothermal Titration Calorimetry. Example of the VP-ITC microcalorimeter from microCal (North-Hampton, MA, U.S.A) 56

Figure 2.6 Principle of the Surface Plasmon Resonance 58

Figure 2.7 Principle of switchSENSE adapted for peptide-metal interaction study**.** (A) Single strands of DNA having 48 base pairs are bound on the chip gold surface and hybridized with a complementary DNA activated by trisNTA. The hybridization is followed by fluorescence measurement of a Cy5 probe fixed at the extremity of the nanolever (kcps: kilocounts per second). A multivalent ion like Ni^{2+} is then immobilized onto the trisNTA group. (B) Binding of metal-chelating peptides (MCP) increases friction forces and leads to decrease the

dynamic response DR (dru: dynamic response unit) of the nanolevers. (C) The kinetic (k_{on}, k_{off}) and affinity constants ($K_D = k_{off}/k_{on}$) of the interaction between Ni^{2+} and MCP can be determined by real-time measurements of the quenching of the normalized fluorescence $F_{norm.}$. 61

Figure 2.8 Mass spectrum of a solution containing 2.5 mM Cd (II) and 10 mM glutathione-**G.** The inset shows the comparison of the enlarged experimental isotopic pattern (solid line) and the theoritical pattern (histogram) for selected cadmium complexes. Reprinted from Keith-Roach (2010) with kind permission from Elsevier. 63

Figure 2.9 Principle of MBP-screening in complex mixture of peptides such as hydrolysates using mass spectra differential analysis 64

Figure 2.10 Principle of Immobilized Metal ion Affinity Chromatography (IMAC) 65

Figure 2.11 Process of lipid peroxidation 85

Figure 2.12 Timeline for the major discoveries concerning ferroptosis 87

Figure 2.13 Network of ferroptosis signalling pathways 91

Figure 2.14 Chemical structures for ferroptosis inducers 94

Figure 2.15 Network of ferroptosis inducers and inhibitors 97

Figure 2.16 Chemical structures of iron chelators: (A) Deferoxamine chelating iron and (B) 3 deferiprones chelating iron, and lipophilic antioxidants: (C) Ferrostatin-1 and (D) Lipoxstatin-1 98

Figure 2.17 Ferroptosis evidence in Atherosclerosis 100

Figure 3.1 The switchSENSE® method was first set up on synthetic peptides known for their metal-chelating properties and on soy and tilapia viscera protein hydrolysates 116

Figure 3.2 Production of the soy protein hydrolysate 120

Figure 3.3 Production of the Tilapia protein hydrolysate 121

Figure 3.4 Chemical structures of the investigated peptides 124

Figure 3.5 (A) Schematic principles of switchSENSE® and **(B)** Structures of the NTA-Ni^{2+} chelate bound at the extremity of the DNA nanolever and on the surface of the biosensor chip 124

Figure 3.6 Association kinetics analysis of synthetic peptides onto immobilized nickel ions by using the switchSENSE® technology. Raw data are superimposed by global exponential fits for various concentrations of each peptide. A blank control performed with T40 buffer instead of analyte was subtracted to normalize the signal. The k_{obs} were determined for each kinetics measurement. F_{norm}, normalized fluorescence. 126

Figure 3.7 Real-time switchSENSE® analysis of molecular interaction between the investigated analyte (synthetic peptides or hydrolysates (TPH, SPHs)) and nickel ions immobilized on DNA nanolevers attached to the gold surface of the chip. The chip is composed of six switchable

electrodes, all in contact with the running buffer or analytes loaded into the microfluidic. In molecular dynamics mode, nanolevers are deliberately moved by way of alternating the voltage across the surface. The motion of the levers is tracked in real time. Upon analyte binding, the hydrodynamic friction of the nanolevers and their movement are affected. **(A)** Reference electrodes E1 and E2 in the presence of T40 buffer, **(B)** Sample electrodes E3 to E6 in the presence of T40 buffer, **(C)** Reference electrodes in the presence of analyte (i.e. synthetic peptides or hydrolysates), **(D)** Sample electrodes in the presence of analyte. 128

Figure 3.8 Molecular dynamics experiments performed by switchSENSE® technology with synthetic peptides. Experiments were performed in T40 buffer, then in the presence of sample (at 10 µM). Nanolevers' motions were expressed as dynamic response (DR). The relative difference **Δ**DR (in %) was calculated from the various motions determined in the presence and in the absence of sample. Unspecific binding onto the DNA double strands was determined from the **Δ**DR of the reference electrodes E1 and E2 free of nickel, whereas specific interaction with nickel was determined from the **Δ**DR of the sample electrodes E3 to E6 129

Figure 3.9 Copper chelation capacity (%) of the different hydrolysates **(A),** EDTA and carnosine **(B)** as a function of molar ratio (mM eq NH_2 of hydrolysate or mM EDTA, carnosine/ mM $CuSO_4$). SPHs were prepared by Alcalase®, Protamex®, or Flavourzyme® one- or three-hour treatment. The TPH was prepared by Alcalase® three-hours treatment 132

Figure 3.10 SDS-PAGE analysis of the soy protein hydrolysates generated after 1 or 3 h treatment by Alcalase® (Alc), Protamex® (Prt) and Flavourzyme® (Flv). Std, molecular mass standards 134

Figure 3.11 Association kinetics analysis (**A**) and Molecular dynamics experiments (**B**) of SPHs and TPH onto immobilized nickel ions by using the switchSENSE® technology. The SPHs were prepared by Alcalase®, Protamex®, or Flavourzyme® one-hour treatment. The TPH was prepared by Alcalase® three-hours treatment. The kinetics raw data are superimposed by global exponential fits for various concentrations of each analyte. The k_{obs} were determined for each kinetics measurement. F_{norm}, normalized fluorescence. For the motion determination, experiments were performed in T40 buffer, then in the presence of sample (SPH at 1000 µM eq. NH_2 & TPH at 100 µM eq. NH_2) and the nanolevers' motions were expressed as dynamic response (DR). The relative difference **Δ**DR (in %) was calculated from the various motions determined in the presence and in the absence of sample. Unspecific binding onto the DNA double strands was determined from the **Δ**DR of the reference electrodes E1 and E2 free of nickel, whereas specific interaction with nickel was determined from the **Δ**DR of the sample electrodes E3 to E6. 136

Figure 5.1 AoSMC cell viability after 24 h incubation of different erastin concentration. Results are presented as mean ± sem of n=3 and compared using one-way ANOVA. Results are calculated in respect to 100% viability, which is for [Erastin]=0 µM. 172

Figure 5.2 GSH and proteins concentrations in AoSMCs after an overnight incubation with and without erastin in non-diluted complete medium (A & B), complete medium diluted 2 times (C &

D) and complete medium diluted 10 times (E & F). Results are presented as mean ± sem of n=3 and compared using one sample t test; *p < 0.05. 174

Figure 5.3 MDA quantification and protein dosage of AoSMC after an overnight incubation with and without erastin in non-diluted complete medium (A & B) and, complete medium diluted 2 times (C & D). Results are presented as mean ± sem of n=3 and compared using one sample t test; *p < 0.05. 176

Figure 5.4 MDA quantification and protein dosage of AoSMC after an overnight incubation with and without erastin ± 50 µM ferric citrate (FC) in non-diluted complete medium (A & B) and in complete medium diluted 2 times (C & D). Results are presented as mean ± sem of n=3 and compared using one way ANOVA; *p < 0.05 (Tukey's multiple comparisons test). 178

Figure 5.5 Ratio of GSH quantity over protein mass (A) and the ratio of MDA quantity over protein mass (B) Smooth muscle cells were incubated in complete medium diluted 2 times for 1 night with and without erastin ± 50 µM ferric citrate ± 50 µM deferoxamine (or 150 µM deferiprone). Results are presented as mean ± sem of n=3 and compared using one-way ANOVA; *p < 0.05 (Tukey's multiple comparisons test). 180

Figure 6.1 Schematic representation for this PhD's goal, achievements and proposed future work. 184

Figure 6.2 The outcomes of this PhD 187

List of Tables

Table 1.1 The HSAB theory 21

Table 2.1 Safety considerations and standard regulations 39

Table 2.2 Comparison between apoptosis, necrosis and ferroptosis cell deaths 89

Table 3.1 Peptide concentrations in tilapia protein hydrolysate (TPH) and soy protein hydrolysate (SPH) determined by OPA quantification 122

Table 3.2 Observed rate constants (kobs) of synthetic peptides, SPHs and TPH association to immobilized nickel ions determined with the switchSENSE® method. Results are presented as mean ± standard deviation. 127

Table 3.3 EECC and CECC values determined for TPH and SPHs 133

Table 4.1 EDTA equivalent chelating capacity (EECC) and carnosine equivalent chelating capacity (CECC) values determined for 1kDa-ultrafiltrated SPHs and PPHs. Results are presented as mean ± standard deviation from 5 replicates 157

Table 4.2 Peptide concentration (mM equivalent glycine) determined by OPA dosage, Dissociation (KD, mM), Affinity constants (KA, mM-1), and Rmax (R.U) determined by SPR ± standard deviation for the 1kDa-ultrafiltrated SPHs and PPHs 160

List of abbreviations

Aa	Amino acids
ACSL4	Acyl-Co1 Synthase Long-Chain Family 4
Alc (1h)	Alcalase® treatment for 1 hour
Alc (1h) + Flv (2h)	Alcalase® treatment for 1 hour followed by Flavourzyme® treatment for 2 hours
Alc (3h)	Alcalase® treatment for 3 hours
AS	Atherosclerosis
BHT	Butylated Hydroxytoluene
CD	Circular Dichroism
CPPs	Caseinphosphopeptides
DFO	Deferoxamine
DFr	Deferiprone
DH	Degree of Hydrolysis
DMT1	Divalent Metal Transporter 1
EPR	Electron Paramagnetic Resonance
ESI	Electrospray Ionization
ESI-MS	Electrospray Ionization-Mass Spectrometry
ESR	Electron Spin Resonance
EXAFS	Extended X-ray Absorption Fine Structure
Fer-1	Ferrostatin-1
FIN I	Class 1 Ferroptosis Inducing Compounds
FIN II	Class 2 Ferroptosis Inducing Compounds
Flv (1h)	Flavourzyme® treatment for 1 hour
Flv (3h)	Flavourzyme® treatment for 3 hours
FS	Fluorescence Spectroscopy
FTH1	Ferritin Heavy Chain 1
FTIR	Fourier-Transform InfraRed
GPx4	Glutathione peroxidase 4
GSH	Glutathione
HCP1	Heme Transporter
HILIC	Hydrophilic Interaction Liquid Chromatography
HNE	4- Hydroxynonenal
HSAB	Hard and Soft Acid and Bases
IDA	Iminodiacetic Acid
IKE	Imidazole Ketone Erastin
IMAC	Immobilized Metal-ion Affinity Chromatography
IRE-BP	Iron-Responsive Element Binding Protein
IREBP2	Iron Responsive Element Binding Protein 2
ITC	Isothermal Titration Calorimetry

L-AT	L-Aminoacid Transporter
LDL	Low-Density Lipoproteins
LIP	Labile Iron Pool
Lip-1	Liproxstatin-1
LOX	Lipoxygenase
LPCAT3	Lysophosphatidyl Choline Acyl Transferase 3
MBPs	Metal-Binding Peptides
MCPs	Metal-Chelating Peptides
MDA	Malondialdehyde
MnBPs	Mineral-Binding Peptides
MS	Mass Spectrometry
MT	Metallothioneins
NMR	Nuclear Magnetic Resonance
NTA	Tetradentate Nitriloacetic Acid
PE	Piperazine-Erastin
PG	Propyl Gallate
PPHs	Pea Protein Hydrolysates
Prt (1h)	Protamex® treatment for 1 hour
Prt (1h) + Flv (2h)	Protamex® treatment for 1 hour followed by Flavourzyme® treatment for 2 hours
Prt (3h)	Protamex® treatment for 3 hours
PUFA	PolyUnsaturated Fatty Acids
ROS	Reactive Oxygen Species
RSL3	Ras Selective Lethal 3
SEC	Size-Exclusion Chromatography
SOD	Superoxide Dismutase
SPHs	Soy Protein Hydrolysates
SPPs	Solid-Phase Peptide Synthesis
SPR	Surface Plasmon Resonance
TBHQ	Tert-Butyl Hydroquinone
TFR1	Transferrin Receptor 1
TFR2	Transferrin Receptor 2
TPHs	Tilapia Protein Hydrolysates
TRPV6	Transient Receptor Potential V6
XANES	X-ray Absorption Near Edge Structure
XAS	X-ray Absorption Spectroscopy

Chapter 1 Introduction

The human body is constantly at risk of developing serious diseases due to lifestyle stresses and environmental toxins. Therefore, the discovery or/and the development of health-promoting agents is a worldwide scientific interest. Food-derived bioactive peptides are widely studied nowadays as alternatives to pharmacological treatments. These peptides have shown a variety of bioactivities such as anticancer, anti-inflammation, antihypertensive and antioxidant activities. While this thesis focuses specifically on metal-chelation related to antioxidant activity, it is worth to have a brief look in this chapter on the health and biotechnological aspects that lead to our interest in metal-chelation.

1.1 Oxidative stress and antioxidant: terms and concepts

"Oxidative stress" is a term used to describe the situation in which pro-oxidants concentration is transiently or chronically higher than that of antioxidants, causing metabolic disorders and cellular damages (Lushchak, 2014). Reactive oxygen species (**ROS**), byproducts of the physiological metabolism of oxygen, are present at low levels in normal cells. However, their accumulation caused by the exposure to ultraviolet radiation and other environmental stresses leads to oxidative damage (Gross and Bhattacharya, 2010). The three main biological components attacked and modified by ROS are proteins, lipids and nucleic acids. The attack on lipids causes lipid peroxidation, which ultimately leads to cellular membrane breakdown; the attack on DNA causes mutagenic lesions, and the attack on proteins leads to modifications in their activities or to their elimination (Halliwell, 1994). Oxidative stress-induced damages are involved in the process of aging as well as several chronic diseases (Liguori *et al.*, 2018) (*i.e.,* cancer, cardiovascular, and neurodegenerative diseases). The study of oxidative stress is an important field of research with thousands of publications related to its causes, consequences and prevention (Breitenbach and Eckl, 2015).

Antioxidants are compounds that reacts - directly or indirectly - against or / and inhibits oxidative phenomena. Living organisms have set up a complex, multilevel antioxidant defense mechanisms. There are plenty of mitochondrial and cytosolic antioxidant enzymes such as, the superoxide dismutase (**SOD**) that converts superoxide ions ($2O_2^{\bullet -} + 2\ H^+ \rightarrow O_2 + H_2O_2$) to

hydrogen peroxide, the catalase that removes hydrogen peroxide, and the glutathione peroxidase that reduces peroxides like lipid peroxides or H_2O_2 to the corresponding alcohol or H_2O, respectively, while oxidizing glutathione (**GSH**) (Lushchak, 2014). In reality, the power of oxidative stress is higher than that of the organisms' antioxidant defense (Poljsak, 2011). Therefore, exogenous antioxidants are required **(Figure 1.1.)**.

Exogenous antioxidant substances can be either synthetic or natural. The most known synthetic antioxidants are butylated hydroxytoluene (**BHT**), propyl gallate (**PG**) and tert-butyl hydroquinone (**TBHQ**) and are commonly used in cosmetic products to stabilize the products' raw materials. These display higher stability and performance than natural antioxidants but also higher health risks. Natural antioxidants are obtained from plant resources such as vegetables, fruits, herbs and seeds. Vitamins C and E, carotenoids and polyphenols are examples of natural antioxidants that can re-equilibrate the oxidation state (Lourenço, Moldão-Martins, and Alves, 2019). Due to consumers' demand for natural antioxidant ingredients, research studies to obtain, process, increase and preserve their nutritional value has been a scientific spotlight since so many years.

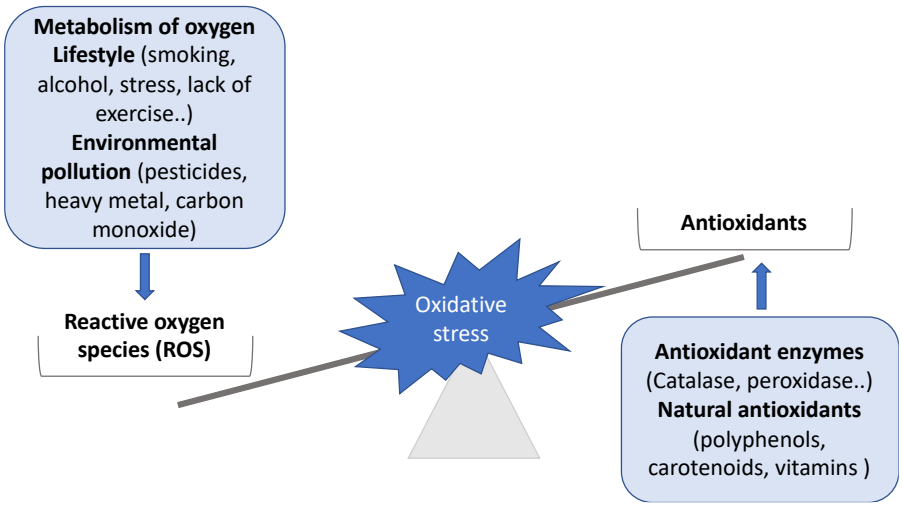

Figure 1.1. Oxidation state balance

1.2 Ferroptosis: Iron-catalyzed oxidative cell damage

Free iron ions catalyzes the formation of hydroxyl radicals *via* the Haber-Weiss reaction (Haber and Weiss, 1934), or can be a direct reactant for their production such as Fe(II) in the Fenton reaction (Fenton, 1894). Recommended dietary allowance for iron is 1.5 mg per day for adult

males and 1.5 mg to 2 mg (to compensate the losses during menstrual bleeding) per day for adult females. Maintaining iron homeostasis is critically essential for human health to prevent diseases such as iron deficiency anemia and hemochromatosis caused by iron overload **(Figure 1.2.)**. Concentration of intracellular iron is regulated at several cellular levels that comprise: iron uptake *via* transferrin receptors (**TFR1 and TFR2**), iron storage in ferritin and transferrin, and iron export *via* ferroportin. Dysregulation of iron homeostasis causes iron-mediated cell death, recently described as ferroptosis (Mou *et al*. 2019; Tang *et al.* 2019).

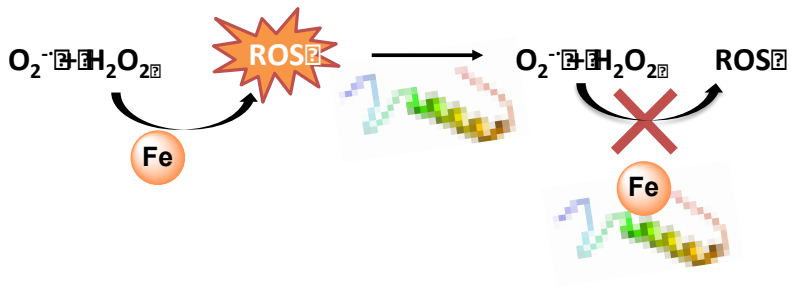

Figure 1.2. Effect of free and bound iron ions on the formation of ROS

The main feature of ferroptosis is lipid peroxidation catalysed by iron-overload. It is first discovered as a pathway to kill cancer cells, and then it was reported in several diseases such as atherosclerosis **(AS)**, Alzheimer disease, type I diabetes, acute kidney injury, *etc.* (Wu *et al.,* 2020; Yang and Stockwell, 2016) **(Figure 1.3)**. However, very few studies in literature report treatments for ferroptosis related to these diseases. AS refers to the restriction or even the blockage of blood flow due to the narrowing of blood vessels as a result of the build-up of plaques made up of oxidized lipids (Kobayashi *et al*., 2018; Ross, 1990). To date, there is no model of ferroptosis based on cardiovascular cells in order to test molecules able to inhibit ferroptosis with potential application in cardiovascular diseases treatment.

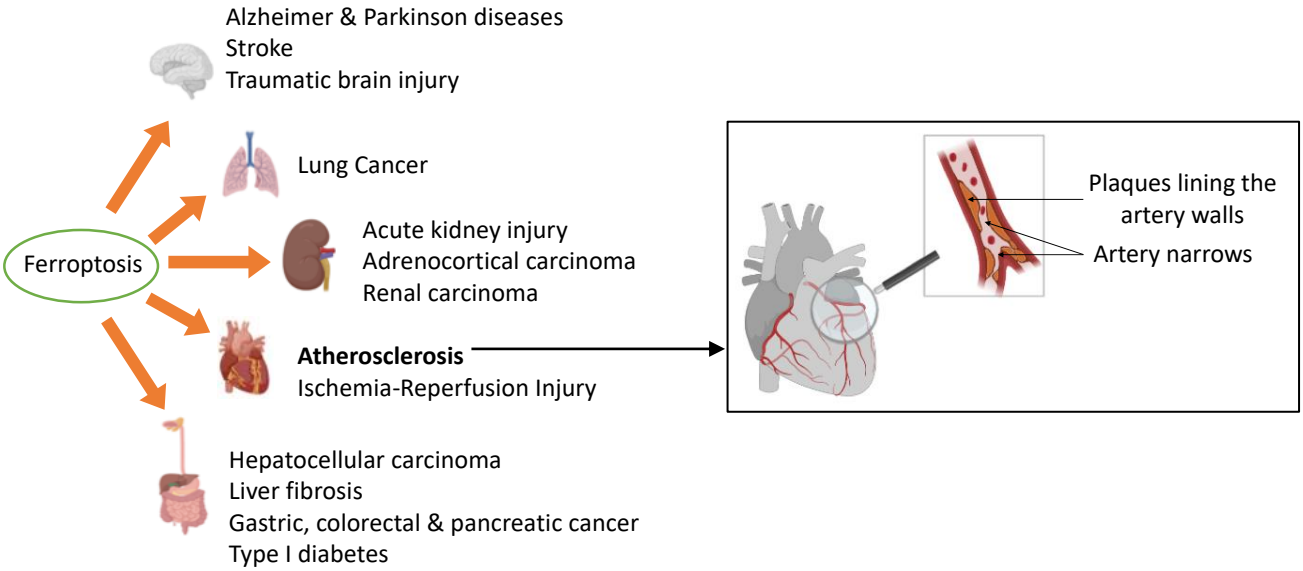

Figure 1.3. Diseases where ferroptosis is reported (left). Plaques buildups in arteries in atherosclerosis (AS) disease (Right)

1.3 Metal-chelating peptides: antioxidant properties and discovery limitations

Plant (or animal)-based proteins can inhibit multiple oxidative pathways by reducing ROS, scavenging free radicals, and chelating transient metals. Sometimes, the antioxidant power of these proteins is trapped within their 3-dimentional structures. Therefore, enzymatic hydrolysis can reveal this antioxidant activity. Indeed, during proteolysis, bioactive peptides are released with exposure of characteristic amino acids, which are inaccessible prior the disruption of proteins' tertiary structure (Puntarulo, 2005; Luza and Speisky, 1996). In our work, we focus our attention on the metal-chelation capacity of peptides. Indeed, amino acids residues present in the peptide sequence can participate to coordination bonds with metals through their α-amino group, carboxyl group, and R side-chain for some of them. The carboxylate function, COO^-, and the nitrogen element, N, interact with metals to establish metal carboxylate salt, amine complex, and 5 or 6 membered chelating rings (Wang *et al.*, 2018; Chen *et al.*, 1998). The reaction between amino acids and metals is a general acid-base reaction and is applied according to the Hard and Soft Acid and Bases theory (**HSAB**) (**Table 1.1**). In general, reactions take place between soft acid and soft base or, between hard acid and hard base (Hancock, 1992). Metal-chelating peptides (**MCPs**) can be promising bioactive

peptides to treat ferroptosis in cardiovascular diseases. MCPs are known to reduce cell oxidative stress caused by the Haber-Weiss and Fenton reactions, which are catalyzed by Fe^{2+}.

Table 1.1. The HSAB theory

	Hard	Moderate	Soft
Acids	Li^{+}, Na^{+}, Mg^{2+}, Ca^{2+}, Ba^{2+}, Al^{3+}, Ga^{3+}, V^{3+}, Cr^{3+}, Co^{3+}, Fe^{3+}	Mn^{2+}, Fe^{2+}, Co^{2+}, Ni^{2+}, Cu^{2+}, Zn^{2+}, Pd^{2+}	Cu^{+}, Ag^{+}, Cd^{2+}, Au^{+}, Hg^{+}
Bases	Carboxylates (Glu & Asp), hydroxyl group (Ser, Thr, Tyr), guanidinium (Arg)	Imidazole (His), amides (Asn, Gln), indole (Trp)	Thiols (Cys), thioethers (Met), phenyl (Phe)

To date, many experimental limitations are encountered by researchers who are trying to screen or identify MCPs in protein hydrolysates from natural resources. The empirical approach to discover MCPs consists in separating hydrolysates in various fractions and in evaluating their antioxidant activity. These sequential steps are reiterated until reaching pure MCPs identified by mass spectrometry **(Figure 1.4)**. Nevertheless, this empirical approach is fastidious, presents a high cost and is uncertain regarding the presence of desired peptides in hydrolysates, which would make it time consuming.

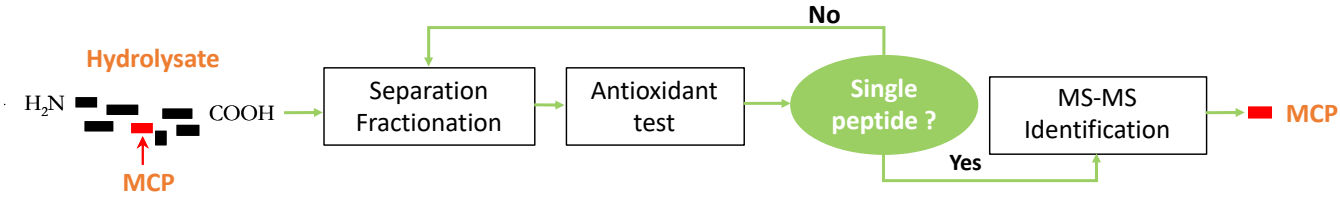

Figure 1.4. The empirical approach to discover MCPs

1.4 General context and objective of this PhD

Nowadays, there is an increasing need for new biomolecules for various industrial applications related to pharmacy, foods or cosmetics. As some synthetic antioxidants are considered hazardous for human health, the interest in bioactive peptides generated from protein

hydrolysis has been widely studied to fulfill consumers' needs. MCPs from food proteins present great health benefits due to their ability to suppress the formation of free radicals catalyzed by transient metal ions. The scientific field of MCPs is interdisciplinary and can cover studies related to: their production (by proteolysis or chemical synthesis), biotechnological tools used for their screening and/or separation in a complex mixture of biomolecules, their interaction with metal ions and/or the surrounding environment, and their applications in human health, cosmetics, environment, biotechnology…

As biotechnological objective, this PhD project aimed at discovering and testing MCPs produced by enzymatic proteolysis of natural resources, taking advantage of the efficiency of Surface Plasmon Resonance (SPR) technique to screen MCPs in hydrolysates. However, since SPR showed some limitations related to the length of peptides when present in non-ultrafiltrated hydrolysates, we set up a methodology to screen MCPs in non-filtrated hydrolysates based on an electrically switchable nanolever technology, switchSENSE®. For the biological objective, the interest is to evaluate the effect of MCPs in inhibiting ferroptosis in cardiovascular cells by chelating iron ions. To do so, we aimed first to develop the ferroptosis model based on human aortic smooth muscle cells **(Figure 1.5)**.

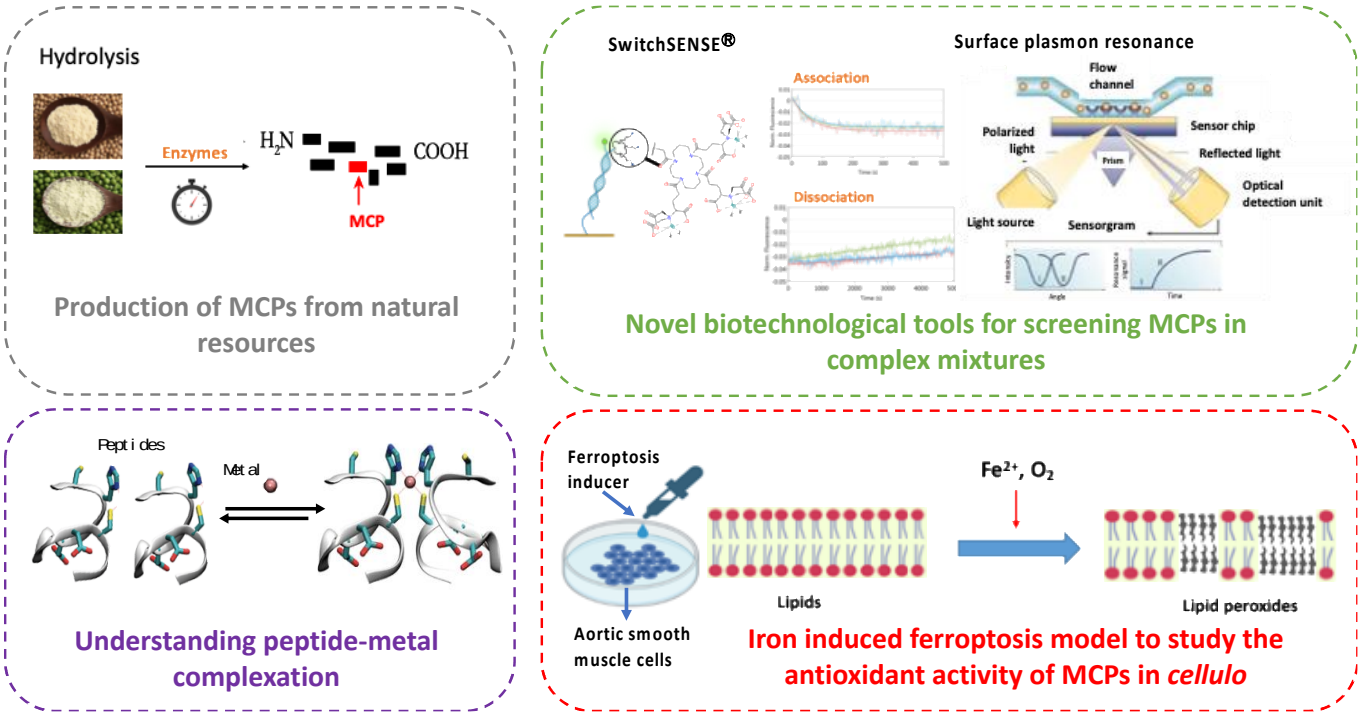

Figure 1.5. The fields covered in this interdisciplinary PhD project

1.5 Thesis structure

After this introducing chapter (Chapter 1), a literature review will be conducted to gain an in depth understanding of concepts (Chapter 2). Then three main contributions will be made to fulfill PhD objectives (Chapters 3, 4 and 5 mainly).

- Chapter 3: Developing a novel methodology based on electrically switchable DNA nanolevers to cross peptides' size limitations for screening MCPs in hydrolysates.
- Chapter 4: Screening of metal-chelating activity of soy and pea protein hydrolysates obtained after different enzymatic treatments using surface plasmon resonance.
- Chapter 5: Developing a cardiovascular cell-based ferroptosis model in order to test MCPs antioxidant activity.

Finally, conclusions will be then drawn and perspectives to go deeper in this research area will be stressed out (Chapter 6) **(Figure 1.6).**

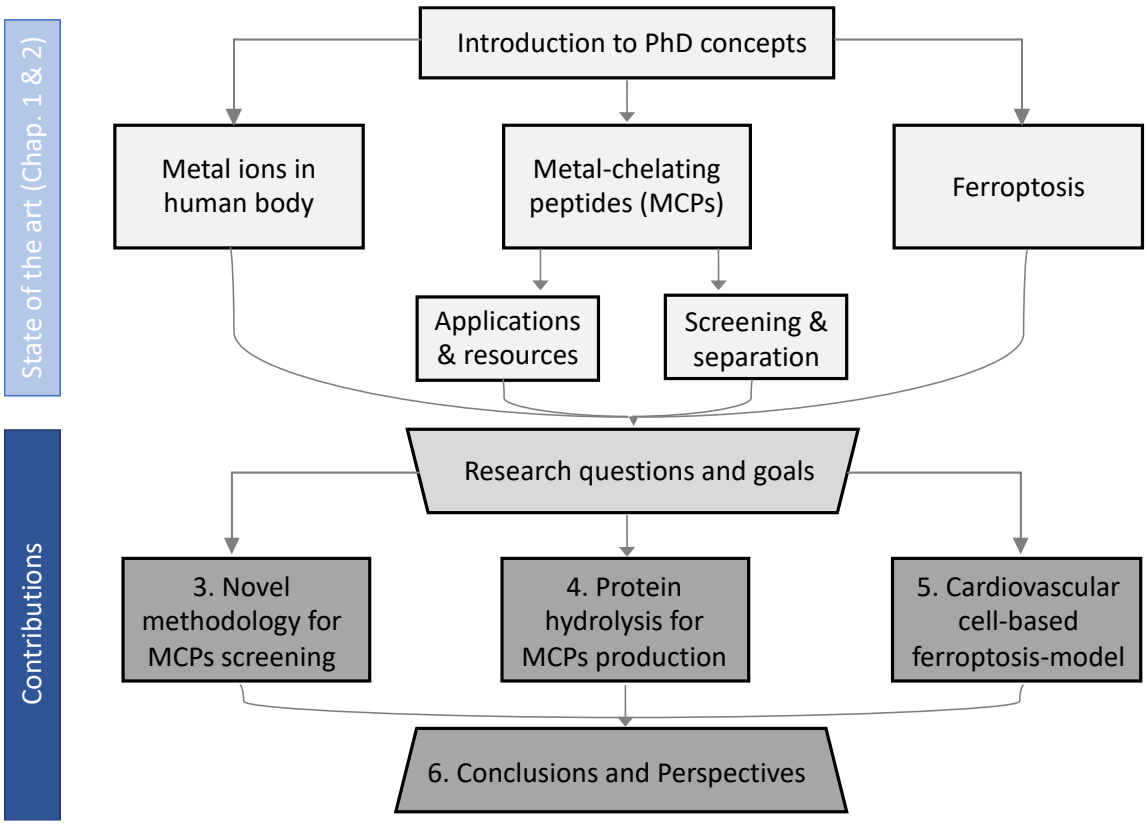

Figure 1.6. The thesis structure

Chapitre 1 Introduction

Le corps humain est constamment exposé au stress de son mode de vie et aux toxines environnementales augmentant le risque de développement des maladies graves. C'est pourquoi, la découverte et/ou le développement d'agents bénéfiques pour la santé suscite un intérêt scientifique. Les peptides bioactifs d'origine alimentaire sont aujourd'hui largement étudiés comme alternative aux traitements pharmacologiques. Ces peptides ont montré une variété de bioactivités telles que des activités anticancéreuses, anti-inflammatoires, antihypertensives et antioxydantes. Bien que cette thèse se concentre spécifiquement sur la chélation des métaux en lien avec leur activité antioxydante, il est nécessaire de contextualiser brièvement dans ce chapitre, les aspects sanitaires et biotechnologiques qui ont conduit à notre intérêt pour les peptides chélateurs de métaux.

1.1 Stress oxydant et antioxydant : termes et concepts.

" Le stress oxydant " est un terme utilisé pour décrire la situation dans laquelle la concentration en pro-oxydants est transitoirement ou chroniquement supérieure à celle des antioxydants, provoquant des troubles métaboliques et des dommages cellulaires (Lushchak, 2014). Les espèces réactives de l'oxygène (**ERO)**, sous-produits du métabolisme de l'oxygène, sont maintenues à de faibles concentration dans les cellules saines. Cependant, leur accumulation causée par l'exposition aux rayons ultraviolets et à d'autres stress environnementaux entraîne des dommages oxydatifs (Gross et Bhattacharya, 2010). Les trois principaux composants biologiques attaqués et modifiés par les ERO sont les protéines, les lipides et les acides nucléiques. L'attaque des lipides provoque la peroxydation lipidique, qui conduit finalement à la dégradation de la membrane cellulaire ; l'attaque de l'ADN provoque des lésions mutagènes, et celle des protéines conduit à des modifications de leurs activités ou à leur élimination (Halliwell, 1994). Les dommages induits par le stress oxydant sont impliqués dans le processus de vieillissement ainsi que dans plusieurs maladies chroniques (Liguori *et al.,* 2018) (ex. le cancer, les maladies cardiovasculaires et neurodégénératives). L'étude du

stress oxydant est un domaine de recherche important avec des milliers de publications concernant ses causes, ses conséquences et les moyens de le prévenir (Breitenbach et Eckl, 2015).

Les antioxydants sont des composés qui inhibent - directement ou indirectement - les phénomènes oxydants. Les organismes vivants ont mis en place des mécanismes de défense complexes agissant à plusieurs niveaux appelés « antioxydants ». Il existe de nombreuses enzymes antioxydantes mitochondriales et cytosoliques telles que, les superoxyde dismutases (**SOD**) qui convertissent les ions superoxydes ($2O_2^{\circ-} + 2\ H^+ \rightarrow O_2 + H_2O_2$) en peroxyde d'hydrogène (H_20_2), les catalases qui éliminent ce dernier, et les glutathion peroxydases qui réduisent les peroxydes lipidique ou H_2O_2 en l'alcol correspondant ou H_2O, respectivement tout en oxydant le glutathion (**GSH**) (Lushchak, 2014). La puissance du stress oxydant est plus grande que celle de la défense antioxydante des organismes (Poljsak, 2011). Par conséquent, des antioxydants exogènes sont nécessaires pour lutter contre le stress oxydant **(Figure 1.1)**. Les substances antioxydantes peuvent être synthétiques ou naturelles. Les antioxydants synthétiques les plus connus sont l'hydroxytoluène butylé (**BHT**), le gallate de propyle (**PG**) et la tert-butyl hydroquinone (**TBHQ**) et sont couramment utilisés dans les produits cosmétiques pour stabiliser les matières premières des produits. Ils présentent une stabilité et des performances supérieures à celles des antioxydants naturels, mais aussi des risques plus élevés pour la santé. Les antioxydants naturels sont obtenus à partir de ressources végétales telles que les légumes, les fruits, les herbes et les graines. Les vitamines C et E, les caroténoïdes et les polyphénols sont des exemples d'antioxydants naturels qui peuvent rééquilibrer la balance redox (Lourenço, Moldão-Martins et Alves, 2019). En raison de la demande des consommateurs pour des ingrédients antioxydants naturels, les études de recherche pour obtenir, traiter, augmenter et préserver leur valeur nutritionnelle constitue un challenge scientifique depuis de nombreuses années.

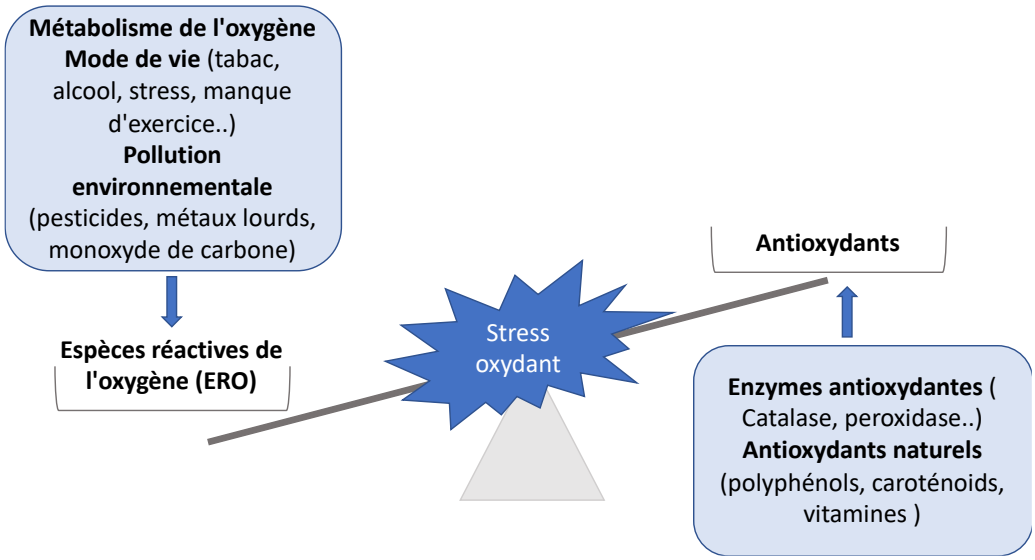

Figure 1.7. Équilibre de l'état d'oxydation

1.2 Ferroptose : dommages cellulaires oxydants catalysés par le fer

Les ions fer libres catalysent la formation de radicaux hydroxyles *via* la réaction de Haber-Weiss (Haber et Weiss, 1934), ou peuvent être un réactif direct pour leur production comme le Fe(II) dans la réaction de Fenton (Fenton, 1894). Les apports nutritionnels recommandés en fer sont de 1,5 mg par jour pour les hommes adultes et de 1,5 mg à 2 mg (pour compenser les pertes menstruelles) par jour pour les femmes adultes. Le maintien de l'homéostasie du fer est essentiel pour la santé humaine afin de prévenir des maladies telles que l'anémie ferriprive et l'hémochromatose causée par une surcharge en fer **(Figure 1.2).** La concentration de fer intracellulaire est régulée à plusieurs niveaux cellulaires qui comprennent : l'absorption du fer *via* les récepteurs de la transferrine **(TFR1 et TFR2)**, le stockage du fer dans la ferritine et la transferrine, et l'exportation du fer *via* la ferroportine. La dérégulation de l'homéostasie du fer entraîne la mort cellulaire médiée par le fer, récemment décrite comme la ferroptose (Mou *et al.,* 2019 ; Tang *et al.,* 2019).

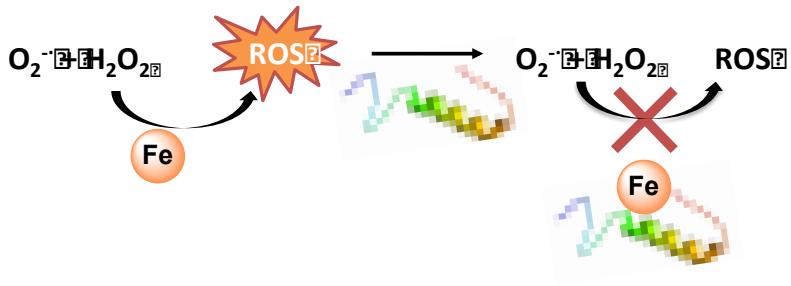

Figure 1.8. Effet des ions fer libres et liés sur la formation de ERO

La principale caractéristique de la ferroptose est la peroxydation lipidique catalysée par la surcharge en fer. Elle est d'abord découverte comme une voie pour tuer les cellules cancéreuses, puis elle a été rapportée dans plusieurs maladies dont l'athérosclérose (**AS**), la maladie d'Alzheimer, le diabète de type I, les lésions rénales aiguës (Wu *et al.,* 2020 ; Yang et Stockwell, 2016) **(Figure 1.3).** Cependant, très peu d'études dans la littérature rapportent des traitements de la ferroptose liés à ces maladies. L'AS désigne la restriction, voire le blocage, de la circulation sanguine en raison du rétrécissement des vaisseaux sanguins suite à l'accumulation de plaques constituées de lipides oxydés (Kobayashi *et al.,* 2018 ; Ross, 1990). A ce jour, il n'existe pas de modèle de ferroptose développé sur des cellules cardiovasculaires qui permettrait de tester des molécules potentiellement capables d'inhiber la ferroptose, avec une application ultérieure dans le traitement des maladies cardiovasculaires.

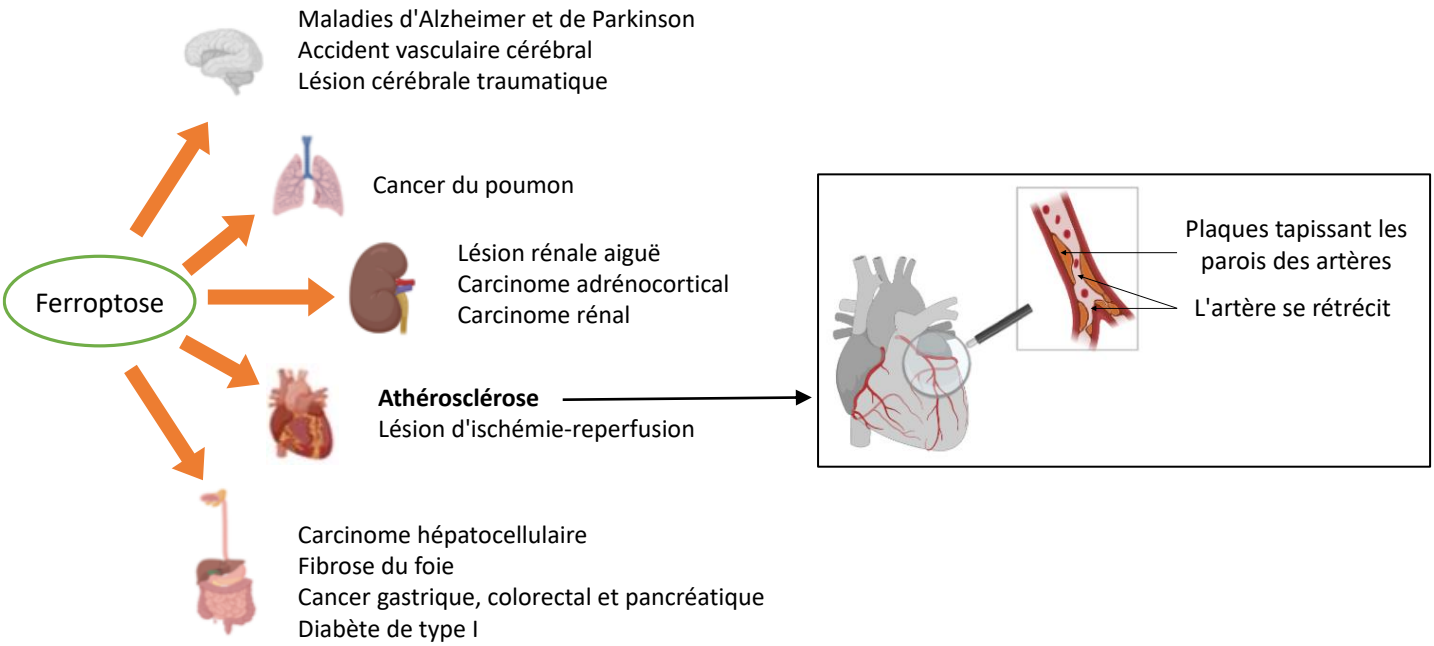

Figure 1.9. Maladies où la ferroptose est signalée (à gauche). Accumulation de plaques dans les artères dans l'athérosclérose (AS) (à droite)

1.3 Peptides chélateurs de métaux : propriétés antioxydantes et verrous liés à leur découverte

Les protéines d'origine végétale (ou animale) peuvent inhiber de multiples voies d'oxydation en réduisant les ERO en piégeant les radicaux libres et en chélatant les métaux de transition. Parfois, le pouvoir antioxydant de ces protéines est « piégé » dans leurs structures tridimensionnelles. Par conséquent, l'hydrolyse enzymatique peut révéler cette activité antioxydante. En effet, au cours de la protéolyse, les peptides bioactifs sont libérés avec l'exposition des acides aminés caractéristiques, inaccessibles avant la rupture des structures tertiaires des protéines (Puntarulo, 2005 ; Luza et Speisky, 1996). Dans notre travail, nous nous sommes intéressés à la capacité qu'ont certains peptides de chélater des métaux. En effet, les résidus d'acides aminés présents dans la séquence peptidique peuvent établir des liaisons de coordination avec les métaux par l'intermédiaire de leur groupe α-aminé, carboxyle, et de leur chaîne latérale R pour certains d'entre eux. La fonction carboxylate (COO^-) et l'atome d'azote (N) interagissent avec les métaux pour établir un carboxylate métallique, un complexe aminé et des cycles chélateurs à 5 ou 6 chaînons (Wang *et al.*, 2018 ; Chen *et al.*, 1998). La réaction

entre les acides aminés et les métaux est une réaction acide-base générale et s'applique selon la théorie des acides et des bases durs et mous (**HSAB**) (**Tableau 1.1**). En général, les réactions ont lieu entre un acide mou et une base molle, ou entre un acide dur et une base dure (Hancock, 1992). Les peptides chélateurs de métaux (**PCMs**) peuvent être des peptides bioactifs prometteurs pour inhiber la ferroptose dans les maladies cardiovasculaires. En effet, les PCMs sont connus pour réduire le stress oxydant cellulaire causé par les réactions d'Haber-Weiss et de Fenton, qui sont catalysées par le Fe^{2+}.

Tableau 1.1. La théorie HSAB

	Durs	**Modéré**	**Doux**
Acides	Li^{+}, Na^{+}, Mg^{2+}, Ca^{2+}, Ba^{2+}, Al^{3+}, Ga^{3+}, V^{3+}, Cr^{3+}, Co^{3+}, Fe^{3+}	Mn^{2+}, Fe^{2+}, Co^{2+}, Ni^{2+}, Cu^{2+}, Zn^{2+}, Pd^{2+}	Cu^{+}, Ag^{+}, Cd^{2+}, Au^{+}, Hg^{+}
Bases	Carboxylates (Glu & Asp), groupe hydroxyle (Ser, Thr, Tyr), guanidinium (Arg)	Imidazole (His), amides (Asn, Gln), indole (Trp)	Thiols (Cys), thioéthers (Met), phényl (Phe)

Jusqu'à présent, de nombreuses limitations expérimentales ont été rencontrées par les chercheurs qui tentent de cribler ou d'identifier les PCMs dans les hydrolysats de protéines provenant de ressources naturelles. L'approche empirique pour découvrir les PCMs consiste à séparer les hydrolysats en différentes fractions et à évaluer leur activité antioxydante. Ces étapes séquentielles sont répétées jusqu'à obtenir une fraction pure en PCMs, dont la séquence est identifiée par spectrométrie de masse **(Figure 1.4).** Néanmoins, cette approche empirique est longue et fastidieuse : elle présente un coût élevé et une présence incertaine en peptides cibles dans les hydrolysats.

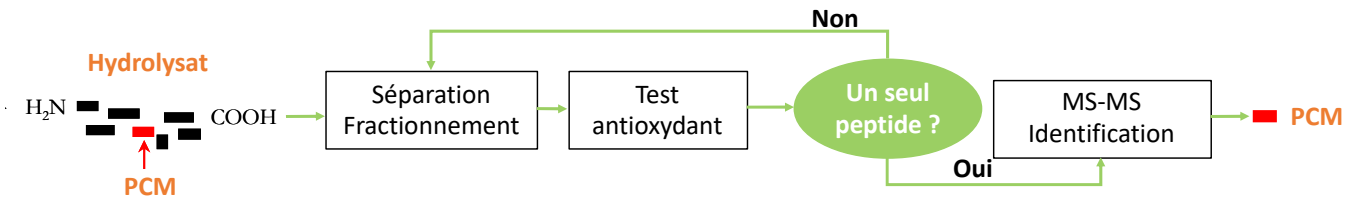

Figure 1.10. L'approche empirique pour découvrir les PCMs

1.4 Contexte général et objectifs de cette thèse

De nos jours, il existe un besoin croissant de nouvelles biomolécules pour diverses applications industrielles liées à la pharmacie, à l'alimentation ou aux cosmétiques. Certains antioxydants synthétiques étant considérés comme dangereux pour la santé humaine, l'intérêt pour les peptides bioactifs générés par l'hydrolyse des protéines a été largement étudié pour répondre aux besoins des consommateurs. Les PCMs issus des protéines alimentaires présentent de grands avantages pour la santé en raison de leur capacité à ralentir/inhiber la formation de radicaux libres catalysés par des ions métalliques de transition. Les recherches autour des PCMs sont interdisciplinaires et concernent leur production (par protéolyse ou synthèse chimique), les outils biotechnologiques utilisés pour leur criblage et/ou leur séparation dans un mélange complexe de biomolécules, leur interaction avec les ions métalliques et/ou le milieu environnant, et leurs applications en santé humaine, cosmétique, en environnement, biotechnologie…

Ce projet de thèse visait à découvrir et à tester les PCMs produits par hydrolyse enzymatique de protéines issues de ressources naturelles, en utilisant notamment la résonance plasmonique de surface (SPR) pour cribler les PCMs dans les hydrolysats peptidiques. Cependant, la SPR a montré certaines limites liées à la taille des peptides lorsqu'ils sont présents dans des hydrolysats non ultrafiltrés. Aussi, une autre méthodologie de criblage des PCMs dans les hydrolysats a été mise au point à l'aide du switchSENSE®. Par ailleurs, nous avions comme second objectif d'évaluer l'effet des PCMs dans l'inhibition de la ferroptose dans les cellules cardiovasculaires. Pour ce faire, nous avons d'abord cherché à développer un modèle de ferroptose basé sur les cellules musculaires lisses aortiques humaines **(Figure 1.5).**

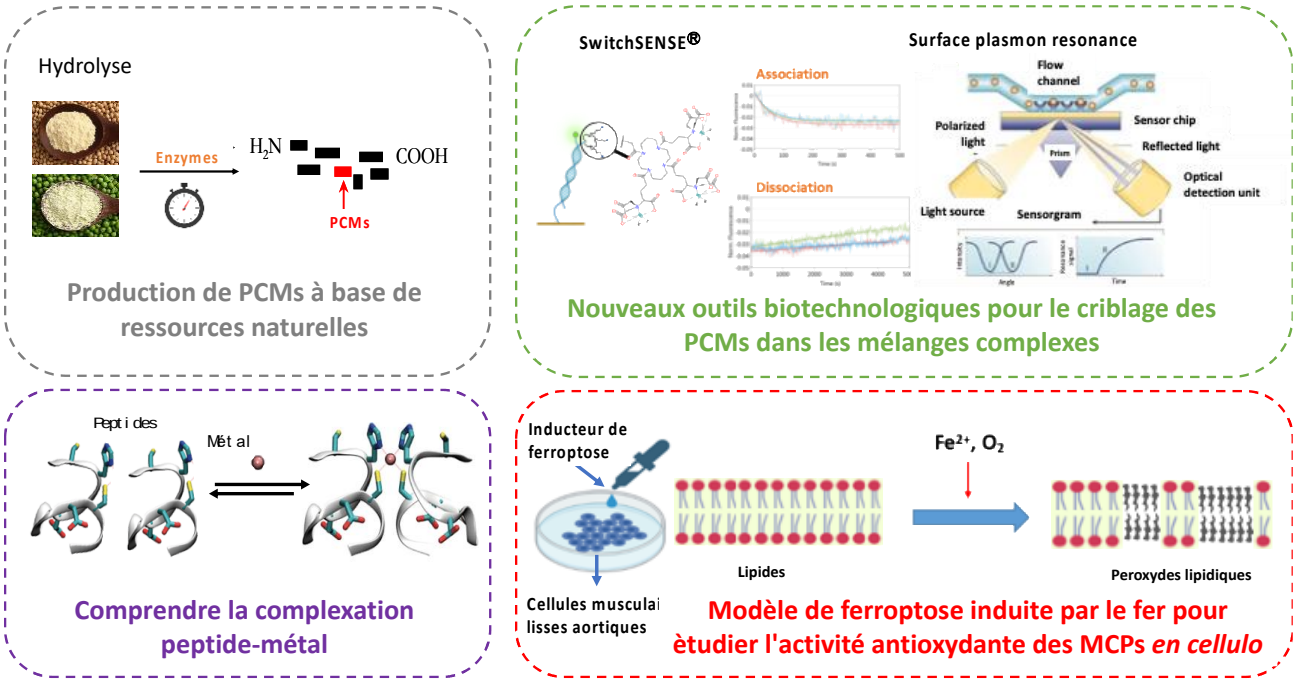

Figure 1.11. Les matières couvertes par ce projet de doctorat interdisciplinaire

1.5 Structure de la thèse

Après cette introduction (Chapitre 1), une étude bibliographique sera effectuée afin de comprendre en profondeur les différents concepts (Chapitre 2). Ensuite, trois contributions principales seront apportées pour répondre aux objectifs de la thèse (Chapitres 3, 4 et 5 principalement).

- Chapitre 3 : Développement d'une nouvelle méthodologie basée sur des nanolevers d'ADN électriquement commutables pour dépasser les limites de taille des peptides afin de cribler les PCMs dans les hydrolysats.
- Chapitre 4 : Activité chélatrice de métaux des hydrolysats de protéines de soja et de pois obtenus après différents traitements enzymatiques.
- Chapitre 5 : Développement d'un modèle de ferroptose à base de cellules cardiovasculaires afin de tester l'activité antioxydante des PCMs.

Enfin, des conclusions seront tirées et les perspectives d'approfondissement de ce domaine de recherche seront soulignées en chapitre 6 **(Figure 1.6).**

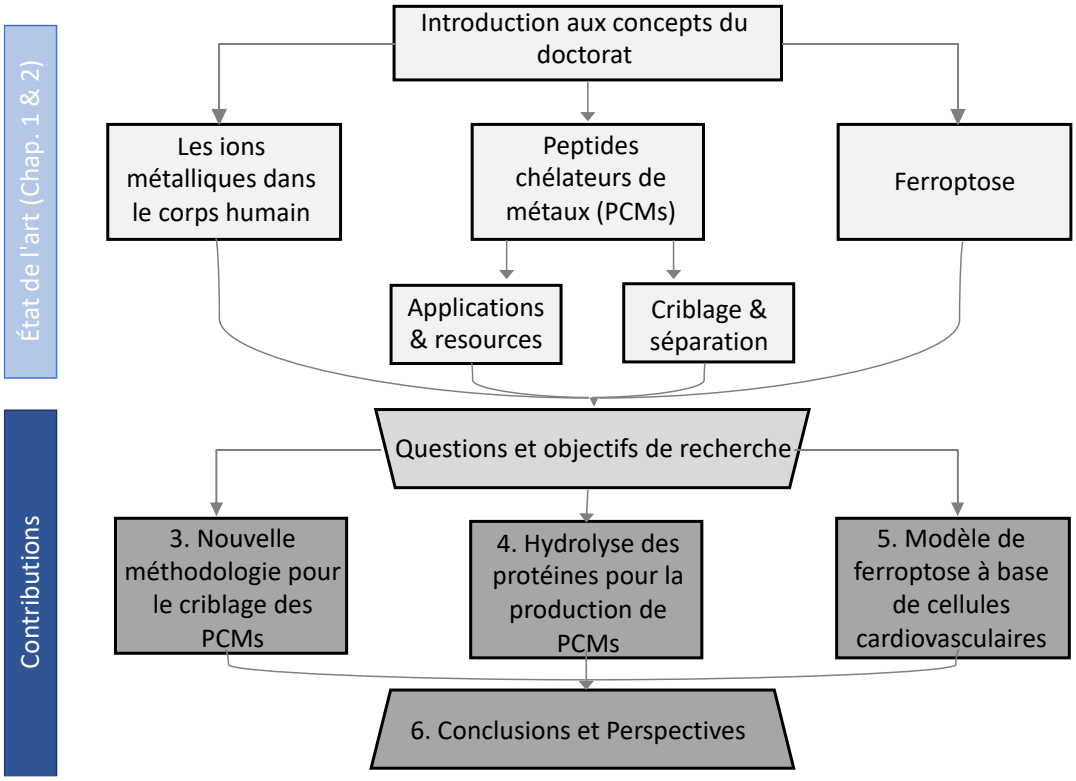

Figure 1.12. Structure de la thèse

1.6 References

Breitenbach, and Eckl. 2015. "Introduction to Oxidative Stress in Biomedical and Biological Research." *Biomolecules* 5 (2): 1169–77. https://doi.org/10.3390/biom5021169.

Chen, Muramoto, Yamauchi, Fujimoto, and Nokihara. 1998. "Antioxidative Properties of Histidine-Containing Peptides Designed from Peptide Fragments Found in the Digests of a Soybean Protein." *Journal of Agricultural and Food Chemistry* 46 (1): 49–53. https://doi.org/10.1021/jf970649w.

Fenton. 1894. "LXXIII.—Oxidation of Tartaric Acid in Presence of Iron." *Journal of the Chemical Society, Transactions* 65 (0): 899–910. https://doi.org/10.1039/CT8946500899.

Gross, and Bhattacharya. 2010. "Uniting Sex and Eukaryote Origins in an Emerging Oxygenic World." *Biology Direct* 5 (1): 53. https://doi.org/10.1186/1745-6150-5-53.

Haber, and Weiss. 1934. "The Catalytic Decomposition of Hydrogen Peroxide by Iron Salts." *Proceedings of the Royal Society of London. Series A - Mathematical and Physical Sciences* 147 (861): 332–51. https://doi.org/10.1098/rspa.1934.0221.

Halliwell. 1994. "Free Radicals, Antioxidants, and Human Disease: Curiosity, Cause, or Consequence?" *The Lancet* 344 (8924): 721–24. https://doi.org/10.1016/S0140-6736(94)92211-X.

Hancock. 1992. "Chelate Ring Size and Metal Ion Selection. The Basis of Selectivity for Metal Ions in Open-Chain Ligands and Macrocycles." *Journal of Chemical Education* 69 (8): 615. https://doi.org/10.1021/ed069p615.

Kobayashi, Suhara, Baba, Kawasaki, Higa, and Matsui. 2018. "Pathological Roles of Iron in Cardiovascular Disease." *Current Drug Targets* 19 (9): 1068–76. https://doi.org/10.2174/1389450119666180605112235.

Liguori, Russo, Curcio, Bulli, Aran, Della-Morte, Gargiulo, et al. 2018. "Oxidative Stress, Aging, and Diseases." *Clinical Interventions in Aging* 13 (April): 757–72. https://doi.org/10.2147/CIA.S158513.

Lourenço, Moldão-Martins, and Alves. 2019. "Antioxidants of Natural Plant Origins: From Sources to Food Industry Applications." *Molecules* 24 (22): 4132. https://doi.org/10.3390/molecules24224132.

Lushchak. 2014. "Free Radicals, Reactive Oxygen Species, Oxidative Stress and Its Classification." *Chemico-Biological Interactions* 224 (December): 164–75. https://doi.org/10.1016/j.cbi.2014.10.016.

Luza and Speisky. 1996. "Liver Copper Storage and Transport during Development: Implications for Cytotoxicity." *The American Journal of Clinical Nutrition* 63 (5): 812S-**20S.** https://doi.org/10.1093/ajcn/63.5.812.

Mou, Wang, Wu, He, Zhang, Duan, and Li. 2019. "Ferroptosis, a New Form of Cell Death: Opportunities and Challenges in Cancer." *Journal of Hematology & Oncology* 12 (1): 1–16. https://doi.org/10.1186/s13045-019-0720-y.

Poljsak. 2011. "Strategies for Reducing or Preventing the Generation of Oxidative Stress." *Oxidative Medicine and Cellular Longevity* 2011: 194586. https://doi.org/10.1155/2011/194586.

Puntarulo. 2005. “Iron, Oxidative Stress and Human Health.” *Molecular Aspects of Medicine*, Trace Elements and Human Health, 26 (4): 299–312. https://doi.org/10.1016/j.mam.2005.07.001.

Ross. 1990. “Mechanisms of Atherosclerosis--a Review.” *Advances in Nephrology from the* ***Necker Hospital*** **19 (January): 79–86.**

Tang, Kang, Berghe, Vandenabeele, and Kroemer. 2019. “The Molecular Machinery of Regulated Cell Death.” *Cell Research* 29 (5): 347–64. https://doi.org/10.1038/s41422-019-0164-5.

Wang, Luo, Liang, Zhang, Yin, Zhang, Yang, and Liu. 2018. “Spectrum-Effect Relationships between High-Performance Liquid Chromatography (HPLC) Fingerprints and the Antioxidant and Anti-Inflammatory Activities of Collagen Peptides.” *Molecules* 23 (12): 3257. https://doi.org/10.3390/molecules23123257.

Wu, Yu, Luo, Cen, Qiu, Zhang, and Hu. 2020. “Ferroptosis in Cancer Treatment: Another Way to Rome.” *Frontiers in Oncology* 10. https://doi.org/10.3389/fonc.2020.571127.

Yang, and Stockwell. 2016. “Ferroptosis: Death by Lipid Peroxidation.” *Trends in Cell Biology* 26 (3): 165–76. https://doi.org/10.1016/j.tcb.2015.10.014.

Chapter 2 State of the art

This chapter provides a comprehensive overview about the current knowledge concerning the scientific field of metal-chelating peptides, related to our main objectives. The chapter is divided into 2 part:

2.1 Applications of mineral (metal)-binding peptides in nutrition: Here, the chemical and biotechnological aspects of the thesis are mainly covered. This part gives a wide range of information and studies concerning several mineral (metal) elements, their interactions with peptides and a variety of methodologies related to their production, screening and separation. However, it is worth to note that this PhD focused mainly on the following metal ions, Fe^{3+}/Fe^{2+}, Cu^{2+} and Ni^{2+}, the production of metal-binding peptides **(MBPs)** by proteolysis and their screening using surface plasmon resonance and switchSENSE® as novel approach. This part led to the writing of a book chapter already published in Elsevier**. El Hajj, Sarah, Tatiana Sepulveda-Rincon, Cédric Paris, Tristan Giraud, Gizella Csire, Loic Stefan, Katalin Selmeczi, Jean-Michel Girardet, Stéphane Desobry, Said Bouhallab, Laurence Muhr, Caroline Gaucher, Laetitia Canabady-Rochelle. 2021. "Chapter 19 - Application in Nutrition: Mineral Binding." In *Biologically Active Peptides*, edited by Fidel Toldrá and Jianping Wu, 455–94. Academic Press. https://doi.org/10.1016/B978-0-12-821389-6.00016-9.**

2.2 Ferroptosis: A cell death mechanism driven by iron overload: The biological aspect of the PhD is introduced here. The literature on ferroptosis is described in this part. We present its timeline discoveries, mechanisms, and its relation with several human diseases. In fact, ferroptosis is a health illness, which can be targeted by the antioxidant activity of metal-binding peptides.

2.1 Mineral-Binding Peptides: applications in nutrition

2.1.1 Introduction

Minerals are essentials for human health since they are involved in the inherent structure of the organism (bone and teeth constitution), in its metabolism (enzyme, hormone composition) or its functions (cardiac rhythm, muscle contraction, neuronal conductivity, and acid-basic equilibrium). Constituting about 4% of the body weight, their presence varies in the organism according to the type of mineral. They are either classified as main minerals (needs higher than 100 mg/day; including calcium, magnesium, potassium, phosphorus, sulfur, sodium and chlorine) or as trace elements (less than 15 g in total in a human body, including iron, zinc, copper, fluorine, iodine, chrome and selenium). An equilibrated and diversified nutrition brings the required daily intake in minerals and compensates their natural loss in urine, sweat or cell peeling. Nevertheless, due to our industrial way of life, the level of minerals in food decreases related either to the intensive agriculture that depletes the soil in mineral or to the industrial processes (pre-washing treatment, ionization, pasteurization). Besides, some external factors increase our needs, notably the stress of daily life, smoking, pollution, sport, age or drugs consumption.

In this part, we focus our attention principally on calcium and magnesium as examples of main minerals, and iron and copper as trace elements. First, we report on the importance of minerals for nutrition. Secondly, the potential applications of mineral-binding peptides (MnBPs), their natural source of obtention and their way of production are discussed. In the third part, the peptide-metal ion interactions, the various ways for MBP screening and separation processes commonly used - based on these specific peptide-metal interactions - are reviewed. The last part of this chapter is dedicated to the evident effects of mineral-binding peptides on nutrition.

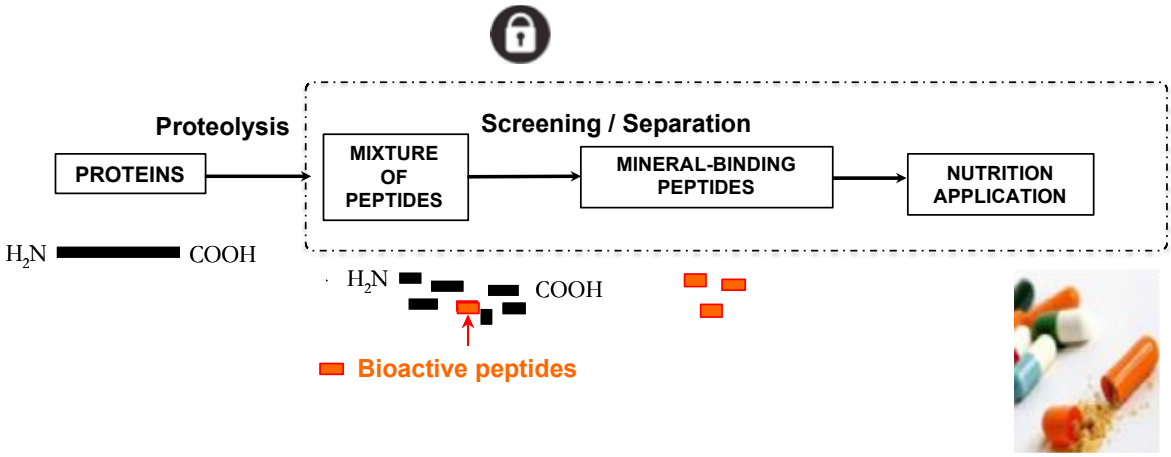

Figure 2.1. Synoptic scheme of this bibliographic part

2.1.2 Importance of minerals for nutrition

2.1.2.1 Main mineral involved in nutrition and their needs in human

As essential micro-nutrients, minerals needs are satisfied with diet. Their repartition and their role in the human body depends on the nature of the mineral, and on physiological parameters of each individual (*i.e.* age, sex, specific period of life such as pregnancy, lactation, or illness). For instance, calcium accounts for about 1-2% of the body weight (1200 g for an adult). Mainly related to the skeleton edification (99% in bone and teeth), calcium is also involved in other functions such as intracellular metabolism, muscles contraction, cardiac functions, cellular exchange, membrane permeability, hormone release and transmission of the nerve impulses (Peng *et al.*, 2017). Magnesium is one of the most important minerals in human, with half of its total mass located in bones as well. An adult body contains approximately 25 g of magnesium (DiNicolantonio *et al.*, 2018). It regulates the metabolism of carbohydrates (*via* the glucose degradation) and lipids present in the muscular, cardiac and nerves tissues. This latter mineral participates also to the protein synthesis, to hormones activity (*i.e.* insulin) and is involved in the functioning of more than 300 enzymes.

In humans, iron is present in the body at about 3-4 g (~ 50 mg/kg body weight) and is mainly included in the hemoglobin of red blood cells, the remaining being incorporated in the myoglobin present in skeletal muscle cells or stored (ferritin) in liver, spleen or bone marrow. Iron is mainly involved in the oxygen transport and in antioxidant enzymes activity (*e.g.*, peroxidase, catalase).

Finally, copper plays a vital role as a cofactor for various enzymes, although as a trace element (1.4-2.1 mg/kg body weight). It is involved in anti-inflammation, neural communication, and acts as anti-bacterial. More, copper is involved in the metabolism of iron, taking part in the heme synthesis through its insertion in the cytochrome oxidase and also being able to inhibit iron absorption by binding to transferrin receptors (Chan *et al*., 1980).

2.1.2.2 Safety considerations and standards/regulation

The recommended daily allowance for the various minerals investigated is stated hereafter according to the FAO specifications (**Table 2.1**).

Table 2.1. Safety considerations and standard

Mineral	Repartition within the human body	Role	Recommended Daily Allowances	Specific needs	Illness in case of deficiency or excess	Mineral-containg food	*Reference*
Calcium	2% of the body-weight, 99% in skeleton	Skeleton, metabolism (muscles activity, nerves impulse, enzymes, hormone activity)	400-550 mg/day (children), 700 mg/day (adult), 1200 mg/day (lactation)	Growth, pregnancy , lactation, ageing	Deficiency (osteoporosis), toxicity in case of high calcium when calcium given as carbohydrate form.	Dairy products, some vegetables and legumes	FAO, Guegen and Pointillard, 2000
Magnesium	In muscles and soft tissues (30-40%), 1% in extracellular fluid, the reminder in skeleton (50-60%)	Involved in metabolism (protein, RNA, DNA), cofactor of many enzymes	280-370 mg/day for an adult (France)	Supplementary needs: lactation(50-55 mg/day)	Rare dietary deficiency, Hypermagnesia (nausea, hypotension, diarrhoea, relatively innocuous)	Green vegetables, legume seeds, cocoa, nuts, seaffood, cereals, dried fruits	In: Hong *et al.*, 2015
Iron	3-4 g (haemoglobine in red globules, myoglobines, ferritine)	O_2 transport, enzymes activity (peroxydases, catalases, cytochromes)	0.7-0.9 mg/day for infant (< 1 year)), 1.46 mg/day in adult women, 1.06 mg/day in adult men.	Women of childbearing age, pregnancy, lactation, children	Ferriprive anemia or hemochromatosis	Meat (liver), fish, poultry, eggs, legume, green vegetables	FAO
Zinc	All body tissues and fluid. 60% in the skeletal muscle. 2-3 g (Adult)	In the skeleton, enzymes involved in metabolism (carbohydrate, lipid, proteins and nucleic acid), maintenance of cell and organ integrity, immune system	2.1 mg/day (adult women), 3.2 mg/day (Adult men)	Children, adolescence, pregnant women	Zinc deficiency: growth retardation, delay sexual & bone maturation, skin lesion, diarrhoea, alopecia, defects of immune system. Zinc toxicity (nausea, vomiting, diarrhoea, fever) in case of excess.	Meat (liver), fish, eggs	FAO
Copper	1.4-2.1 mg /kg	Constituting several enzymes, iron metabolism, anti-inflammatory and antibacterian process, neural communication	1.5-2 mg/day (adult)		Anemia, Menkes syndrome (copper malabsorption) or neurodegenerative pathologies (excess)	Liver, shellfish, chocolate, legume	www.musculaction.com

Calcium needs are comprised between 400-500 mg/day and up to 1 g/day for adults, with recommendations varying between countries (Guegen and Pointillart, 2000). Calcium needs are higher during growth (400-700 mg/day for a child) or specific periods such as pregnancy or lactation. Milk and dairy products are the main natural sources of highly bioavailable calcium. Calcium deficiency involves rickets in children and osteoporosis in the elderly, a disease that affects more than 75 million people in the world (Guéguen and Pointillard, 2000). Calcium nutrition, bioavailability, and fortification were nicely reviewed by Vavrusova and Skibsted (2014).

Concerning magnesium, the recommended daily intake of 6 mg/kg/day is raised to 25 mg during growth, 40 mg during pregnancy and 30 mg during lactation. Magnesium is found in cocoa, various nuts, seafood, cereals or dried fruits. Normal magnesium concentration protects against various diseases and its deficiency induces anxiety, headache, a general fatigue in addition to a low morale (Vormann, 2003).

Iron needs are about 10 mg/day for an adult, with higher recommended daily intake for children (increase of the blood volume during growth), childbearing-aged women due to menses, during pregnancy and lactation. Anemia is related to iron-deficiency while hemochromatosis is due to an excess of iron in the body. In this latter genetic illness, responsible of an excessive iron intestinal absorption, iron excess settles down in the liver, the heart and the skin with chronic fatigue as main symptom. Meat (animal liver, especially), fish, seafood, eggs, beans, legumes, and green vegetables (spinach, broccoli…) are the main sources of iron-containing food.

Adult daily recommended intake for copper is ~2-5 mg/day, while 0.8-1.9 mg/day is recommended for children (Lonnërdal, 1996). These recommendations are easily satisfied by copper-containing food (*i.e.* animal liver and kidney, shellfish, chocolate, legumes, cereals, and nuts), which are reviewed in Lönnerdal (1996). Although copper intake in infants and adults is often lower than the recommendations, the status of this element is still adequate for the majority of the people. Hence, copper deficiency is rare but responsible for anemia or Menkes syndrome rather related to copper malabsorption. Inversely, an excess of copper (also known as Wilson's disease) is toxic; it would act as a pro-oxidant and is involved in neurodegenerative diseases (*i.e.* Parkinson and Alzheimer disease) as reported in the literature (Kaden *et al.*,

2011; Rivera-Mancia *et al*., 2010). Similarly, to other sources of trace elements, iron and copper in the diet depends on their concentration in the soil (Lönnerdal, 1996).

2.1.3 Bioavailability and metabolism of minerals

The metabolism of minerals from food depends first on their bioavailability. In nutrition, this is defined as the part of nutrients present in food, effectively assimilated by the organism, and is dependent on various parameters, either physiological (age, sex, *etc.*) or related to supplementation. Indeed, the nature of salt, the quantity used for supplementation, and the presence or absence of other components in the formulation can increase or decrease the mineral bioavailability. For instance, mineral-binding peptides and non-digestible carbohydrates are reported to improve mineral absorption (Greger, 1999). On the contrary, some components (*i.e.* phytate, cellulose and fat) present in food can negatively affect the mineral absorption, in particular calcium (Reinhold *et al*., 1973; Slavin & Marlett, 1980 in: Chen *et al.,* 2014), magnesium (Pallauf, 1998), and iron**,** which can be inhibited by the presence of some phytates, oxalate, and tannins**.** In a general way, free minerals cannot cross the intestinal barrier; they need either to be solubilized or complexed with other components in order to cross the intestinal barrier to become bioavailable.

Calcium is hardly absorbed from foods due to the precipitation of its insoluble salts formed in a basic environment (Jin *et al*., 2011 in Peng *et al*., 2017). Calcium needs to be dissolved as Ca^{2+} in an acidic environment or complexed to organic molecules such as peptides in order to be absorbed by the small intestine (Wasserman, 2004; in Vavrusova and Skibsted, 2014). Besides, vitamin D also aids to increase the calcium intestinal absorption since it is a fat-soluble secosteroid (Holick, 2004). Calcium absorption decreases from 55-60 years old in women or 60-65 years old in men, (Bullamore *et al*., 1970). In the elderly, calcium malabsorption is related to the reduced production of gastric acid, inducing the entrance of calcium in the intestines under the precipitated form (Straub, 2007; Vavrusova and Skibsted, 2014).

Magnesium is absorbed all over the intestine, especially on the distal part of the small intestine (jejunum and ileum), *via* a passive intercellular process mainly (concomitant with an electrochemical gradient and solvent drag) and an active transport for a small part solely

(Coudray *et al*., 2005). Considering this passive process of absorption, the quantity of Mg absorbed depends on the quantity of the Mg concentration in the intestine. The bioavailability of Mg salt used for supplementation also depends on the type of salt (Coudray *et al*., 2005).

Dietary iron is provided either under heme or non-heme form. The first one, present in food of animal origin, is mainly absorbed at 15-35% mainly in the duodenum (Pereira and Vicente, 2013; in Sun *et al*., 2017). In comparison, less than 10% of the non-heme form of iron is absorbed (in Guo *et al*., 2013). The poorer absorption of this latter form of iron is related to its low solubility at pH near neutrality and its complexation to phytic acid, polyphenols, or fibers. Indeed, as inhibitors of iron-absorption, these food components decrease its bioavailability (Hurrell and Egli, 2010, mentioned in Sun *et al.,* 2017). Inversely, some other dietary compounds such as peptides or amino acids can form soluble complexes with iron, which improve its absorption. Compared to the widely used inorganic iron salts (*i.e.* ferrous sulfate, ferrous gluconate, ferrous fumarate), iron entrapped into biomolecules/organic molecules has a better bioavailability and lower side effects, as reviewed by Li and co-workers, (2017b) on protein hydrolysates, which promote iron absorption. Indeed, the mineral-binding peptides present in hydrolysate complex iron, increase its stability and facilitate its direct absorption in the small intestine (Wang *et al*., 2013; mentioned in Kim *et al*., 2014), which finally improve the bioavailability of iron. As stated latter in this chapter, mineral-binding peptides obtained from various proteins constitute potential resources to overcome the mineral deficiency.

Copper is absorbed mainly from the stomach but also from the duodenum to some extent. The absorption of this trace element is greatly affected by age. As reviewed by Lönnerdal (1996), the bioavailability of copper is also affected by the source of proteins (animal *versus* vegetal) and the presence of specific amino acids (*e.g.,* histidine has a high affinity for copper). Other compounds negatively affect the copper bioavailability, such as phytate and fibers, ascorbic acid, or other minerals with similar properties than copper (*e.g.*, zinc, iron). Finally, copper bioavailability can be disturbed upon illness, particularly in the case of Alzheimer's disease (Kaden *et al*., 2011).

2.1.4 Mineral-binding peptides: potential applications, sources, production and commercialization

2.1.4.1 Application of mineral-binding peptides in nutrition

i) In case of mineral deficiency

Some mineral-binding-peptides obtained from protein hydrolysis were reported for their positive effect on mineral absorption. Indeed, such peptides could be used as potential functional ingredients to prevent mineral deficiency. Calcium-chelating peptides were obtained from various hydrolyzed resources such as shrimp (Huang *et al*., 2011; Le Vo *et al*., 2018), whey proteins (Huang *et al*., 2015; Zhao *et al*., 2014), soy proteins (Lv *et al*., 2009), tilapia protein hydrolysate (Charoenphun *et al*., 2013), and pacific cod bone (Peng *et al*., 2017). Calcium-chelating peptide (GPAGPHGPPG) derived from skin Alaska pollock improved calcium absorption up to 113% in Caco-2 intestinal cells (Chen *et al.*, 2017). There are few reports on the effects of magnesium-chelating peptides on regulating magnesium absorption. The main dietary protein source studied is milk caseins which yield bioactive multiphosphorylated peptides (Cuomo *et al*., 2011; Zidane *et al*., 2012; Cao *et al*., 2017). The latter remain stable chelates during *in vitro* simulated gastrointestinal digestion (Hong *et al*., 2015). Whey proteins are also source of bioactive peptides that carry various minerals like magnesium and enhance their bioavailability (Vegarud *et al*., 2000).

Several natural protein resources are potentially rich in iron-chelating peptides, once hydrolyzed, notably those from sugar cane (De la Hoz, 2014), barley (Eckert *et al*., 2016), whey (Caestano-Silva *et al*., 2015 and 2017), Alaska pollock skin (Guo *et al.*, 2013 and 2015), hairtail (Huang *et al*., 2015), α_s-casein (Jaishwal *et al.*, 2015), spirulina (Kim *et al*., 2014), porcine blood plasma (Lee *et al*., 2009) or anchovy muscle (Wu *et al.*, 2012). Li *et al* (2017) nicely reviewed the potential of protein hydrolysates for improving non-heme iron absorption. Indeed, protein hydrolysates can promote iron absorption either by keeping the iron soluble, by reducing the Fe(III) to Fe(II), or by promoting the iron transport through the intestinal cell membrane. Lin *et al.* (2016) investigated the effect of ferrous-chelating hairtail peptides on iron deficiency and demonstrated that such functional peptides could improve the iron-deficiency status in anemic patients. In an extensive study, our group showed that iron deficiency in rats was repleted with iron complexed with CPP from casein (Aît-Oukhatar *et al*., 1999). Similarly, the binding of copper ion to small peptides or amino acids (*i.e.* histidine, methionine, cysteine)

favors the absorption of copper through an amino acid transporter. Copper-chelating peptides were produced by the hydrolysis of sunflower proteins, with various enzymes used either pure (Megias *et al*., 2008) or in mixture (Megias *et al.,* 2007). Phaseolin hydrolysate was also reported to be rich in Cu^{2+}-chelating peptides (Carasco-Castilla *et al*., 2012).

ii) In case of oxidation phenomena

Transition metals, such as iron and copper, are powerful promoters for the production of ROS since they are able to donate and accept electrons *via* intracellular reactions and help in creating free radicals. Metals can act as catalysts accelerating the formation of hydroxyl radicals *via* the Haber-Weiss reaction (Haber and Weiss 1934), or can be a direct reactant for their production such as Fe(II) in Fenton reaction (Fenton, 1894). Copper is also able to catalyze such reactions (Gutteridge and Wilkins, 1982). Aging and neurodegenerative diseases (*i.e*. Alzheimer) are mainly caused by the dysregulation of metal ion homeostasis, which induces oxidative stress in the brain (Adlard and Bush, 2006). Since the free forms of metals are powerful pro-oxidants, a network of transport and storage systems is expected in order to control their absorption, distribution and excretion. Besides, once stored or bound to biomolecules, bioactive metals are much less toxic and cannot induce as much oxidative stress than when present in their free form (Halliwel, 1994). In addition, the exogenous metal-chelators reduce the oxidative stress resulting from environmental toxins and modern life stresses. Nevertheless, related to the Alzheimer's disease, a recent study evidenced that copper can still catalyze the formation of ROS in the brain when complexed to the amyloid-β peptide (Cheignon *et al*., 2017).

The antioxidant metal-chelating properties of peptides are related to characteristic amino acids and their proper positioning within the peptide sequence. Indeed, amino acids can form coordination bounds with metals through their α-amino group, carboxyl group, and the side chain of certain amino acids. The carboxylate function (COO^-) as well as nitrogen atoms (NH_2) can coordinate metals to form metal carboxylate salt, amine complex, and 5 or 6 membered chelating rings (Hancock, 1992; Wong, Albright, and Wang 1991). Among all 20 amino acids, histidine, cysteine and tryptophan are well-known for their metal chelating affinity *via* their respective functional groups (*i.e.* imidazole, thiol, and indole) (Nieba *et al.*, 1997). Thus, the

metal-chelating capacity of bioactive peptides strongly depends on various parameters (see part 2.1.5.1. Peptide-metal ion interactions).

2.1.4.2 Sources of mineral-binding peptides

i) MnBP in natural ressources

MnBPs in living organisms, such as microorganisms and plants play various biological functions, namely defensive and absorption functions. Rauser reviewed in his work the metal-binding peptides present in plants (Rauser, 1995). Generally known as metallothioneins (MT), these conserved sequences of peptides are rich in cysteine and comprise three classes: MT-I, MT-II, and MT-III, the later one constituting the so-called phytochelatins. As oligomers of glutathione, phytochelatins are found in plant cell's cytosol and serve as chelators useful for metal tolerance and detoxification (Rascio and Navari-Izzo, 2011). More, minerals uptake by the plants' roots is an important phenomenon for their growth; therefore, MnBPs with mineral ion homeostasis roles can be extracted from the roots of plants (Nakayama *et al.,* 2017).

Besides, microbial communities can be found wherever minerals are present and their various mechanisms of interaction with such elements have always served themselves as energy providers (Dunbar, 2017). In fact, minerals were key players in the evolution of microbes over the years (Hazen and Ferry, 2010). In a recent study, the term "mineral microbiome" was identified for the first time as the reservoir of microbial communities, in and near mineral sources. This rich source of genetic information could be used either to create synthetic and/or modified microbiomes or to modify and/or extract MnBPs (Gilbert *et al*., 2014). Microorganisms were even engineered to take advantage of the MnBPs they produce. By constructing clones in *Escherichia coli,* Kjærgaard and colleagues discovered a unique peptide sequence (HARAERHHQ) able to bind Zn^{2+} independently from the protein scaffold (Kjærgaard, Schembri, and Klemm, 2001). As another example, it was shown that the parasitic glutathione S-transferase, *Schistosoma japonicum* (SjGST) can bind Ni^{2+} with high affinity when its Glu26 residue is muted to His residue, and thus can be used in recombinant *E.coli* to purify recombinant proteins (Han *et al*., 2010).

Due to their numerous advantages related to their metal-chelation properties, the metal-binding peptides naturally produced in plants and microorganisms were a source of bio-inspiration for their biological and chemical production. Therefore, many studies have developed certain methodologies to produce pure MBPs such as proteolysis of proteins and chemical synthesis of peptides.

ii) Production of MBPs by proteolysis and chemical synthesis

Over the past few decades, protein hydrolysates have been widely considered in human nutrition applications. Indeed, the short-chain peptides obtained upon proteolysis contain characteristic amino acid residues, some of them being highly advantageous for targeting specific physiological or nutritional requirements (Clemente, 2000). The hydrolysis of proteins changes their functionality, resulting in the loss of their native structures, and the production of low molecular weight peptides, with enhanced interactions with their surrounding environment. Mineral-binding peptides obtained by proteolysis can improve minerals absorption (by avoiding precipitation) and bioavailability *via* peptide transporter *in vivo*. For the *in vitro* hydrolysis carried out in a reactor, the protein source and the used proteolytic enzymes specificity are important parameters to consider in addition to other physicochemical parameters in order to control the MBPs production (**Figure 2.2)**. Digestive enzymes panel, with many and various proteinases activity and their combinations – including pure (trypsin, pepsin, chymotrypsin) and crude (Alcalase®, Protamex®, Flavourzyme®) enzymes – have been listed in the literature with their hydrolyzing optimum conditions (Korhonen and Pihlanto, 2006).

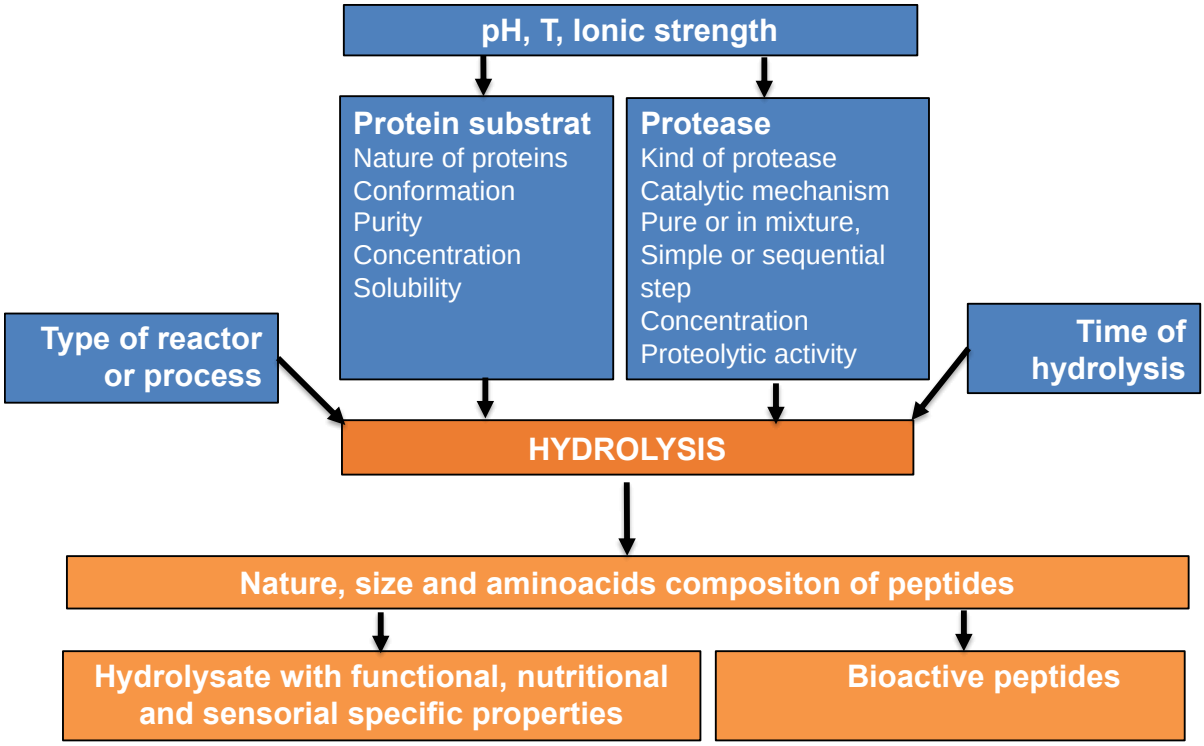

Figure 2.2. Proteolysis parameters to act on to produce various MBP sequences and most common mode of action of the commonly used enzymes. Figure adapted from Chabanon, 2005

As an example, many MBPs were produced from the proteolysis of milk proteins, especially casein and whey proteins, and have been widely reported in the literature. Calcium and iron-binding motifs were discovered in these proteins after enzymatic hydrolysis (Vegarud, Langsrud, and Svenning, 2000). For instance, the tryptic digestion of α_{S1}- α_{S2}- and β caseins produce specific sequences of caseinphosphopeptides (**CPPs**) featured with variable calcium-binding properties depending on their content in phosphoryl groups (Bouhallab and Bouglé, 2004; Hartmann and Meisel, 2007). More generally, metal-binding peptides were discovered in animals' protein hydrolysates. Calcium-binding peptides were notably derived from the hydrolysis of tilapia protein and shrimp processing by-products (Charoenphun *et al.*, 2013; Chen *et al.*, 2014; Cheung *et al.*, 2012). From the digestion of other fish related proteins, scientists evidenced iron and zinc-chelating peptides and identified the contributing amino acid sequences (Wu *et al.*, 2017; Sun *et al.*, 2017; Chen *et al.*, 2017).

Similarly, MBPs were obtained from food proteins derived from plant sources. Due to their wide nutritional values, soybean protein hydrolysates were extensively examined for their bioactivity, and many studies reported the extraction and screening of calcium, copper and iron-chelating peptides after various enzymatic soy proteolysis (Bao *et al.*, 2007; Bao *et al.*,

2008; Canabady-Rochelle *et al.*, 2018; Lv *et al*., 2009). Other protein hydrolysates from plants such as chickpea, rapeseed, sunflower, and bean proteins also contain bioactive MBPs (Torres-Fuentes, Alaiz, and Vioque, 2011; Xie *et al*., 2015; Megías *et al.*, 2007; Carrasco-Castilla *et al.*, 2012).

For MBPs production, chemical peptide synthesis is an alternative to proteolysis. Peptides are chains of amino acids (**Aa**) linearly linked together *via* amide bonds. The synthetic formation of an amide function requires the condensation of a carboxylic acid and an amine group. However, this coupling does not occur spontaneously at ambient temperature (Valeur and Bradley, 2009) and needs to be activated. Despite the existence of thermal activation techniques (Pedersen *et al.*, 2012), in most cases, chemical activation is performed by turning the acid group into a more reactive specie like an acyl halide, an azide, an active ester or an anhydride (Pattabiraman *et al*., 2011). The main challenge is then to choose an efficient activator (*e.g.*, DCC, CDI, onium salts) compatible with the experimental conditions and which prevents from side-reactions (*e.g.*, epimerization, guanidinization, formation of *N*-carboxyanhydride) (El-Faham *et al*., 2011). The original whole protocol for synthetizing peptides was developed by Fisher in the 1900's (Fischer, 1903, 1907) in solution phase. This method, still used for short peptides synthesis, is very laborious for long sequences mainly due to many isolation and purification steps between each coupling (Verlander, 2007). In the 1960's, Merrifield proposed the so-called solid phase peptide synthesis (SPPS) (Merrifield *et al*. 1963); this new procedure enables to perform all coupling reactions successively in a single reactor. SPPS is based on the covalent attachment of the first amino acid on a solid phase followed by the stepwise addition of each amino acid of the sequence (**Figure 2.3**), the peptide sequence being usually synthesized from C-term to the N-term, whereas other strategies are possible (*e.g.*, reversed SPPS (Jaradat *et al.*, 2017)). For SPPS, peptides are fixed on insoluble solid particles, generally polymer-based resin beads, which offer good contact of the grafted compound with the dissolved reagents (Moss, 2005); hence, the reaction media can easily be washed, getting rid of reagent excess and byproducts, renewing completely the medium before the next coupling step.

To avoid side reactions, lateral chains of the amino acids must be protected until the end of the synthesis, whereas N-terminal amino protecting groups are removed at the beginning of each coupling cycle. Several systems of orthogonal protective groups have been elaborated,

like the popular Boc/Cbz and Fmoc/^{t}Bu couples (Isidro-Llobet *et al.*, 2009). Once the whole sequence synthetized, the peptide is cleaved from the solid support and the side chain protecting groups are discarded – sometimes both steps at once (Moss, 2005), and purification are performed through precipitation, crystallization and/or chromatography techniques. SPPS is therefore a simple and fast method offering high efficiency and yields (Palomo *et al.*, 2014), widely used in both academia and industry. Thus, plenty of antioxidant peptides with an original design or with a sequence previously determined from antioxidant hydrolysates have been reported in the literature (Zheng *et al.*, 2016; Wu *et al.*, 2019; Liu *et al.*, 2020), including from our group (Csire *et al.*, 2020). However, peptide synthesis still suffers from deficiencies regarding "difficult peptide sequences" prone to side reactions or aggregation, requiring other chemical synthesis strategies (Paradis-Bas *et al.*, 2016, Coin *et al.*, 2007, Bondalapati *et al.*, 2016). Recently, new methodologies to form peptide bonds have been established, in a greener and healthier way using green solvents and reagents (Varnava and Sarojini, 2019) or no solvent at all (Friscic *et al.*, 2020), or seeking for atom economy through original amide formation pathways (Pattabiraman *et al.*, 2011).

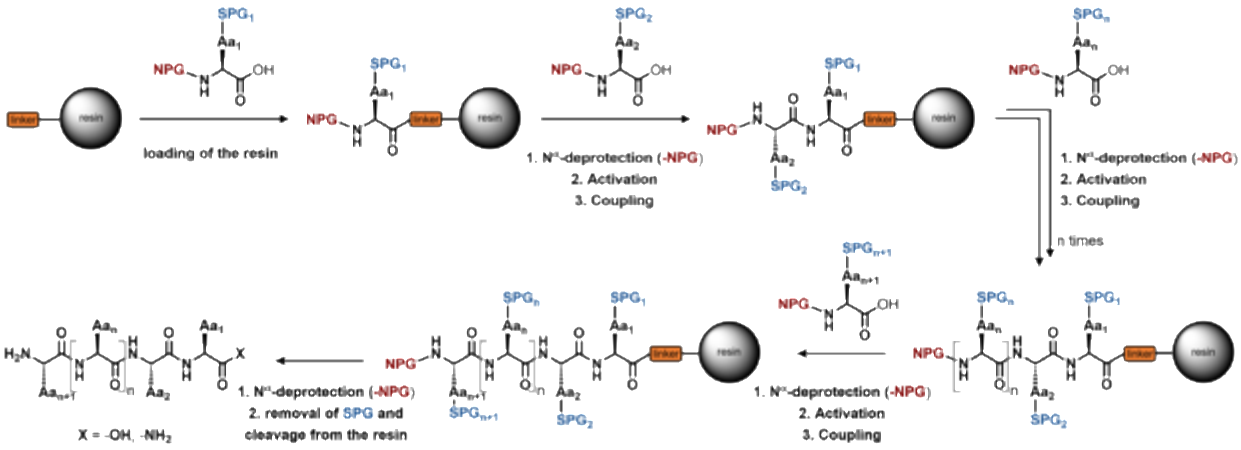

Figure 2.3. Principle of solid phase synthesis commonly used for peptide synthesis

2.1.5 Selective extraction of mineral-binding peptides from complex hydrolysates

2.1.5.1 Peptides- metal ion interactions

Peptides are very efficient and versatile ligands for almost all groups of metal ions (Rodzik *et al*. 2020). Both the thermodynamic stability and the coordination geometry of metal-peptide complexes are greatly influenced by the amino acid composition and their sequence. Naturally-occurring amino acids (Aa) are usually classified by their structure, side-chain nature, electronic, hydrophilic, or steric properties according to the specific research needs (Wu, 2010). In coordination chemistry, two classes are distinguished: Aa with non-coordinating side chains and those with side chains carrying functional groups, endowed with metal coordinating properties (strong donor atom, Lewis base character). The latter includes the imidazole group of histidine (His), the extra carboxylate function of aspartate (Asp) and glutamate (Glu), the phenolic-OH of tyrosine (Tyr), alcoholic-OH of serine (Ser) and threonine (Thr), the extra amino nitrogen of lysine (Lys) and arginine (Arg) and the sulphur atom from cysteine (Cys) and methionine (Met) side chains. His is able to strongly coordinate metal cations by the imidazole nitrogen (Sóvágó *et al*. 2016). Besides, the thioether S-donors in Met or in S-methyl-cysteine (MeCys) have a rather low basicity compared to the thiolate-type S-donor atom in Cys, which is one of the most frequent metal binding sites (like His) of proteinous molecules (Farkas and Sovago, 2017). Despite being a strong donor, the γ-carboxylic group of Glu forms only a low stability 7-membered chelate ring, as the ε-amino function of Lys is too far to form stable chelate with other N/O-donor atoms of the chain (Sóvágó *et al*. 2012). In addition of the Aa residue composition of a peptide, their arrangement within the primary sequence also affect the peptide-metal ion interaction. Indeed, due to the large number and many different arrangements of donor atoms both in the backbone and in the side chains, small modifications in the amino acid sequences can cause significant changes in the formation processes of peptide-metal complex.

On the other side, peptides with non-coordinating side chains can use terminal-amino and amide nitrogens and/or carbonyl and terminal-carboxyl oxygens as donor atoms. At acidic pH, the metal ion is anchored to the N-terminal α-amino nitrogen, and with increasing pH, the Cu^{2+} and Ni^{2+} metal ion can deprotonate the skeletal amide nitrogen atoms with formation of metal–anionic nitrogen bonds. This metal ion-promoted amide deprotonation and

coordination process has a p*K* values around 4 - 8 (Sóvágó *et al*. 2006), much lower than the p*K* value of the amide N-donor atom deprotonation (p*K* ~15) (Sigel and Matin, 1982).

Other factors affect the binding of a metal to peptide including the properties of metal ion, such as the oxidation state, the ionic radius, and the Lewis acidity. The hard/soft acid distinction introduced by Pearson (Pearson, 1963) is often used to explain the metal ion behaviour in the presence of peptide. According to this so-called Pearson theory, Fe(III), Ca(II) and Mg(II) have hard acidic character, Cu(II), Ni(II), Fe(II) are classed as borderline, while Cu(I) is presented as soft Lewis acidic metal ion. The more stable complexes are formed between Lewis acid and Lewis base having the same character, namely hard acid with hard base, and soft acid with soft base. For example, Cu(I) has a particular affinity to bind sulphur-containing ligands. The deprotonated phenol of Tyr, β- and γ-carboxylic group of Asp and Glu, as oxygen donor atom, are good ligands for Fe(III), alkali and alkaline earth metal ions (Shimazaki *et al*. 2009). Transition metals like nickel(II), copper(II) and iron(II) interact preferentially with N-donor atoms from His or N-terminal amino groups (Kozłowski *et al*. 2005, Sóvágó *et al*. 2016).

Finally, the effect of pH on such interactions should also be mentioned because the protonation state of amino acids in peptides depends on this former parameter. As stated above, metal ion promoted deprotonation and coordination process can also occur for all O/N/S-donor atom containing groups with p*K*s lower than their natural p*K* values in the absence of metal ion. However, at acidic pH, the dissociation of the complexes takes place by protonation of the same donor atoms, this process being a reversible equilibrium depending on pH. In addition, the ionic strength, the type of buffers used, as well as the effect of temperature on the binding constants are important factors.

2.1.5.2 MBP screening techniques

i) Spectroscopic techniques

Spectroscopic techniques (**Figure 2.4**), commonly applied for examining the interaction, structure and conformational changes of peptides in metal-peptide complexes, go from simple instrumental analytical techniques to combined application of thermodynamic (potentiometric), spectroscopic, and theoretical (density functional theory) tools.

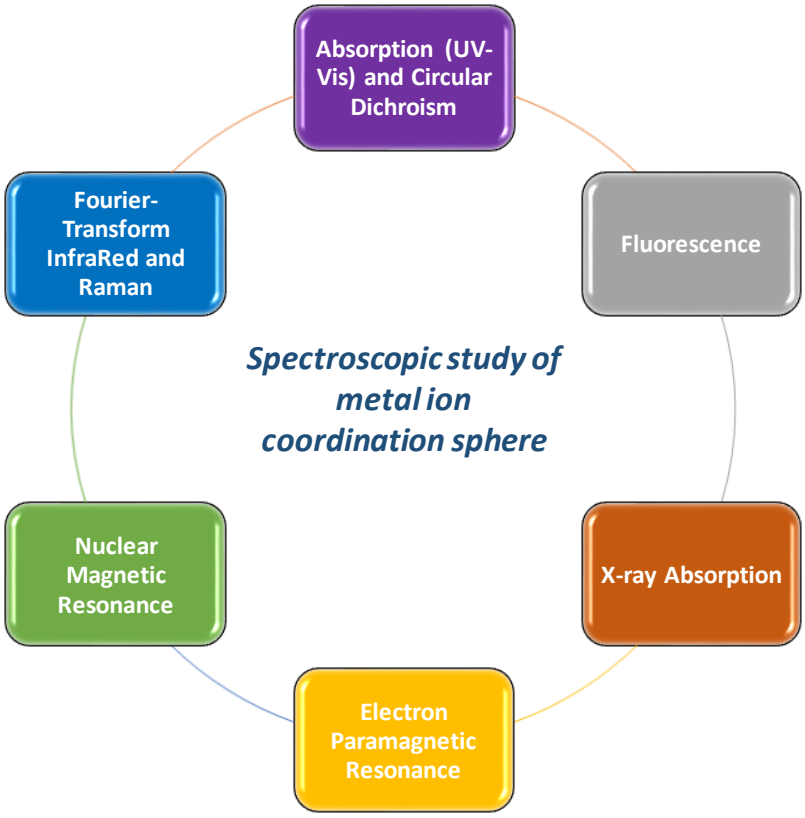

Figure 2.4. Various complementary spectroscopic techniques used for the investigation of peptide-metal interaction

Electronic absorption (**UV-Vis-NIR**) and Circular Dichroism (**CD**) spectra consist of a series of bands, corresponding to the transition from an electronic ground state to an excited state after absorption of isotropic or circularly polarized light, respectively (Jiskoot and Crommelin, 2005; Polavarapu, 2017). Each band is characterized by its position (λ_{max} or ν_{max}), intensity (ε_{max} for absorption and $\Delta\varepsilon_{max}$ for CD), and shape (negative or positive Cotton effect in CD). Peptide molecules can be divided into identifiable functional groups, so-called chromophores, including the amide group and the phenyl, phenolic, imidazolyl and indolyl groups of the side chains in Phe, Tyr, His and Trp, respectively. Upon metal ion binding, the electronic distribution at various atoms of these chromophores is altered in the UV region, the intensity depending on the binding strength. More, the presence of transition metal ions involves two less intense transitions in the visible and near infrared regions: the charge-transfer transition (metal-to-ligand (MLCT) or ligand-to-metal (LMCT)), and the d-d transition of the metal ion. The addition of metal ions can induce hypo-/hyperchromic (decrease/increase in band intensity) and hypso-/bathochromic shifts (blue/red shift) of the characteristic spectral bands.

The isosbestic points, seen in the spectra upon cations addition, indicates the presence of two species in equilibrium and enable the binding constant determination. For peptides conformational analysis, changes caused by metal ion binding, if any, are monitored by CD spectra variation.

Vibrational spectroscopies, *i.e.* Fourier-Transform InfraRed (**FTIR**; Barth, 2007) and Raman (Buckley and Ryder, 2017), are sensitive tools to analyse the effect of metal ions interactions on the peptide conformations. Raman, based on an inelastic scattering process of light, results in polarizability change during the molecular motion, while IR absorption spectroscopy is associated with changes in the dipole moment during molecular vibrations. Thus, both spectroscopies are complementary: transitions allowed in Raman may be forbidden in IR or *vice versa*. For example, O-H stretching modes of water and alcohols absorb strongly in the IR region but give relatively weak bands in Raman, which is ideal for solution measurements. The effect of the metal ion coordination to the specific peptide groups is revealed by comparing the band frequencies of the complex with those of the peptide alone (shift in wavenumber, $\Delta\nu$).

Nuclear Magnetic Resonance (**NMR**) is a powerful spectroscopy for determining the structural and dynamic properties of metal–peptide interactions in solution (de Ricco *et al.* 2014). Any change in the electronic environment surrounding the nuclei due to interactions with metal ions leads to selective variations in the NMR parameters (chemical shifts and nuclear relaxation rates (^{1}H, ^{13}C, ^{15}N) of the residues directly involved in the metal coordination or close to the metal binding site). For example, metal ion can induce an electric field *via* its charge only (*i.e.* Ca(II), Mg(II), Cu(I), tetra-coordinated Ni(II), low spin Fe(II); classical diamagnetic NMR) or by the presence of unpaired electrons (*i.e.* Cu(II), hexa-coordinated Ni(II), high spin Fe(II) and Fe(III) ions; paramagnetic NMR). The latter group can also cause line broadening, the effect of which can be selective and used to locate the metal binding sites.

Electron Paramagnetic Resonance (**EPR**) or Electron Spin Resonance (**ESR**) is a versatile tool for probing structural information on systems with unpaired electrons such as organic radicals or biological systems with paramagnetic metal centres (Sahu *et al*. 2013). The EPR active metal ions have an odd spin, *e.g.* Cu(II) (S = 1/2), high spin Fe(III) (S = 5/2) and the not common Ni(I) and Ni(III) (S = 1/2) ions. The EPR 'silent' metals are the diamagnetic metals with spin equal to zero (Ca(II), Mg(II), Cu(I)) or those with even spin (Ni(II) (S = 1) and Fe(II) (S = 2) high spin) for

which in most cases the signals cannot be detected. The values of g-factor and hyperfine coupling constant (A) determined by simulation of the experimental spectra, and the line shape are necessary to characterise the type of metal ion, its spin state, the type and number of donor atoms and the geometry around the metal ion (Abragam and Bleaney, 1970).

X-ray Absorption Spectroscopy (**XAS**) is an element-specific spectroscopy, sensitive to the local chemical and structural order of the absorber element. X-ray Absorption Near Edge Structure (**XANES**) and Extended X-ray Absorption Fine Structure (**EXAFS**) are two complementary methods. While XANES provides information on the metal oxidation state and the geometry of coordination sphere, EXAFS gives structural information on the metal binding site (*i.e.* coordinating atoms (O/N/S), coordination number and bond lengths; Ortega *et al*. 2012).

Another important technique, Fluorescence Spectroscopy (**FS**) allows the binding affinity determination by measuring in static manner the fluorescence quenching of the peptide upon metal ion addition (Tabak *et al*. 1989). For FS, peptide must contain aromatic amino acids (Trp, Tyr, Phe), inherently fluorescent when excited with UV light. Due to tryptophan's greater absorptivity, higher quantum yield, and resonance energy transfer, the fluorescence spectrum of a peptide containing the three amino acids usually resembles that of tryptophan (Ghisaidoobe *et al.* 2014). The metal sensitive property of Tyr near the chelation site highly depends on metal binding strength. While no change is observed in fluorescence emission intensity for weak complexes, strong metal-peptide complexes cause dramatic changes in the electronic environment of Tyr, strongly quenching the fluorescence. FS, suitable for moderate/strong affinities, includes some details to consider during measurements (van de Weert *et al*. 2011).

The previously detailed analytical techniques, particularly suitable to characterise metal-peptide complexes (Rolinger *et al*. 2020, Faller *et al*. 2012), are more advantageous when combined given their complementarity. They are chosen according to the metal ion and its spin state, which determines the type of bonding and the donor atoms involved. The stoichiometry and geometry of the complex depending mainly on the metal-ligand ratio and the applied pH, the effect of these latter parameters must be investigated upon spectroscopic measurements. The chemistry of metal–peptide complexes has long been studied spectroscopically and thermodynamically by coupling spectroscopic techniques to potentiometry in bioinorganic chemistry field (Farkas and Sovago, 2012 and 2017).

The potentiometric measurement allows to describe the solution equilibria (stability constants, log*K* or logβ) with a species distribution model containing complexes with different metal (M) and ligand (L: peptide, Aa) stoichiometry at various protonation degrees ($M_pL_qH_r$) according to $pM + qL + rH = M_pL_qH_r$ equilibrium (Irving and Williams, 1953). Thus, information on the $M_pL_qH_r$ species present in solution supplemented by spectral parameters observed as a function of the pH allows to deduce the inner coordination sphere of the metal-peptide complexes. Complemented by theoretical calculations and the solid phase structure, more and more information can be obtained on the interaction of peptides with metal ions (Lamshöft and Ivana, 2011).

ii) Isothermal Titration Calorimetry

Biomolecular interactions, and especially mineral-peptide interactions, can be investigated by Isothermal Titration Calorimetry (**ITC**) (Ladbury and Chowdhry, 1996). This technology presents the advantage of allowing characterization of weak interactions between two partner biomolecules (defined as ligands). Theory of the ITC approach of metal chelation by proteins was developed by Nielsen *et al.* (2003). ITC is a thermodynamic approach where the binding equilibrium is directly determined by measuring the heat involved in the association of a ligand with its binding partner. When two molecules interact, heat is either absorbed or released. The measurement of this heat allows the accurate determination of the Gibbs free energy $\Delta G = \Delta H - T\Delta S$ of the reaction, where ΔH is the enthalpy change and ΔS the entropy change of the thermodynamic system. According to the enthalpy change, the reaction is characterized either of endothermic ($\Delta H > 0$) or exothermic ($\Delta H < 0$). This determination provides general information on the nature of the linkages, *i.e.* either electrostatic bonds enthalpically driven such as van der Waals interactions or hydrogen bonds, or hydrophobic bonds entropically driven, or both. In addition, the molar ratio of mineral bound with peptides (stoichiometry, N) and the binding constants (K_A) can be measured (in: Vanhooren *et al.*, 2002). More, the temperature dependence of the ΔH parameter, measured by performing the titration at various temperatures, describes the heat capacity (ΔCp). Finally, the stronger the binding, the less positive the ΔCp is. In a typical ITC experiment, a syringe containing a "ligand" solution is titrated into a cell containing a solution of the "macromolecule" kept at constant temperature as described hereafter (**Figure 2.5**). When ligand is injected into the cell, the two materials interact. The heat (and also ΔH), released or absorbed, is related to the

amount of binding occurring over the time (**Figure 2.5**, top panel, right). As the macromolecule in the cell becomes saturated with ligand, the heat signal diminishes until the background heat of dilution is observed only. A binding curve and its specific binding parameters (N, K_A, **Δ**H, **Δ**S) are then obtained after integration from a plot of the heats of binding obtained from each injection against the ratio of ligand (**Figure 2.5**, **down panel, right).** The binding titration curve and the appropriate fit of experimental data determine whether there are one or more classes of mineral binding sites, independent or not, involving or not cooperativity phenomenon. A modern ITC instrument operates on the heat compensation principle. Upon titration, the amount of uncomplexed peptide available progressively decreases after each injection and the magnitude of the peak becomes progressively smaller. Once the saturation reached, subsequent injections produce similar peaks corresponding to dilution or mechanical effects.

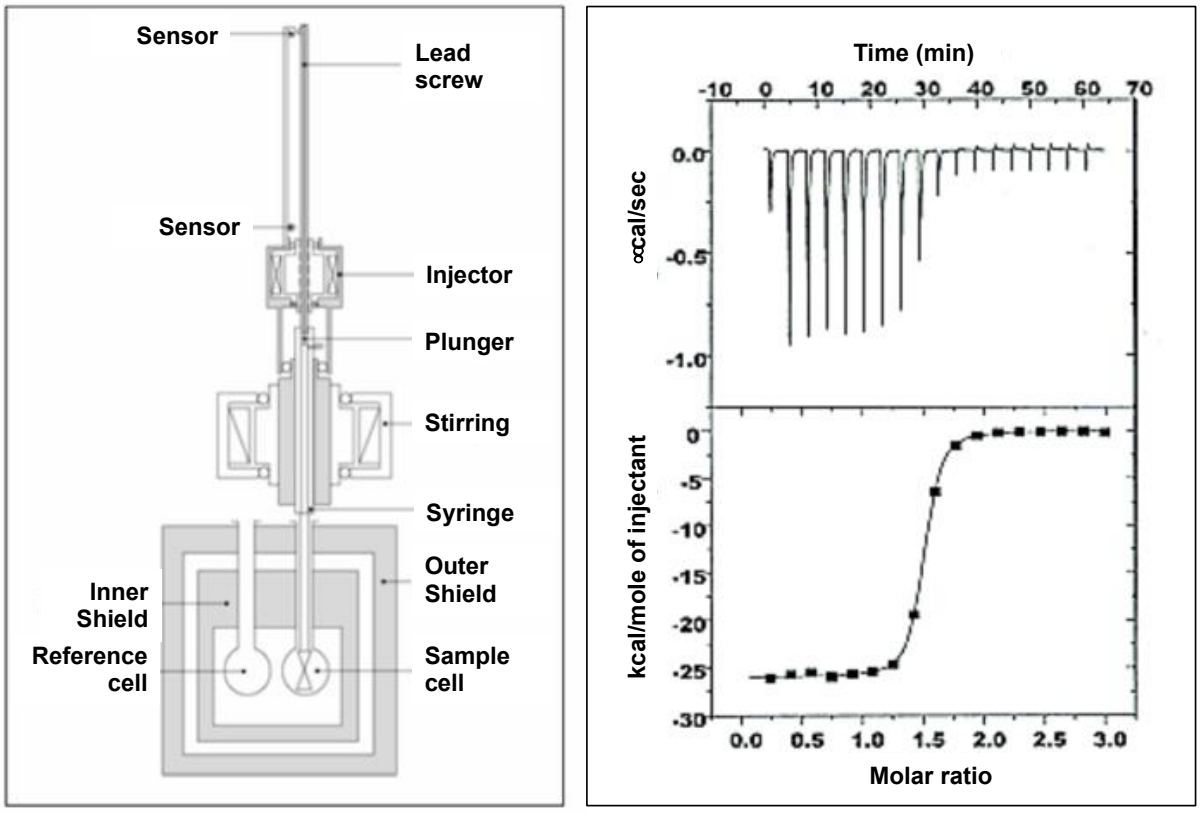

Figure 2.5. Principle of Isothermal Titration Calorimetry. Example of the VP-ITC microcalorimeter from microCal (North-Hampton, MA, U.S.A)

Several studies reported the use of isothermal titration calorimetry for the thermodynamic characterization of the interaction between metal and peptides, mainly pure synthetic peptides as short fragment of proteins. For instance, Grossoehme *et al*. (2005) investigated

metal-binding thermodynamics of the histidine-rich sequence from the metal-transport protein IRT1 of *Arabidopsis thaliana, an* iron transporter overexpressed in iron-deficient conditions. The sequence investigated showed high and low binding to Fe^{3+} and Fe^{2+}, respectively. Comba *et al*. (2013) studied the copper binding with synthetic derivatives of naturally-occurring pseudo-octapeptides by ITC combined with square wave voltammetry (SWV) and they observed that the complex stabilities of these derivatives to Cu^{2+} are in agreement with stabilities corresponding to natural ligands. In all of these studies, pure synthetic peptides were considered as model for a better understanding of their biological function *in vivo* (Guillereau *et al*., 2006; Rich *et al*., 2012; Sacco *et al*., 2012; Sheftic *et al*., 2012). Regarding natural peptides released by digestion, Zidane and co-workers (2012) reported the chelation of calcium, magnesium, zinc, and copper by the caseinophosphopeptide β-CN(1-25)4P investigated by ITC under experimental conditions mimicking the physiological conditions of ileum. At pH 8.0, the peptide binds 2 ions of calcium, magnesium or zinc, but no copper ion. In another application, ITC is used for screening the presence of metal-binding peptides in hydrolysates. In their work, Canabady-Rochelle *et al.* (2009, 2010) investigated the calcium-peptide interactions in the soy protein hydrolysate and in other proteinous systems (soy or milk proteins). Whatever the system, former authors evidenced a calcium-peptide interaction endothermic in nature and fitted by a one set of site model. As compared to non-hydrolyzed protein, soy protein hydrolysate bound less calcium (2 mg/g of proteins), probably due to the conformational change and destructuration of the protein. The coupling with electrophoretic measurement or pH-cycle enabled a better understanding of calcium-peptide interactions. More recently, ITC experiments were completed by tandem mass spectrometry (MS/MS) to study the interaction between iron(II) and an heptapeptide (SNVVPLY) from barley protein hydrolysate under physiological conditions (Eckert *et al*., 2016). The peptide complexed iron(II) spontaneously, with a binding constant reaching 10^7 M^{-1} suggesting its potential application as dietary supplement to improve iron absorption.

Similarly, Liao *et al*. (2019) evidenced a novel calcium-binding peptides (VLPVPQK) from casein hydrolysate, that could potentially be developed as nutraceutical additive.

iii) Surface Plasmon Resonance

Developed recently, Surface Plasmon Resonance (**SPR**) is at the forefront of evolving technologies in terms of medical, nutritional and environmental applications (Rich and Myszka 2011; Shankaran, Gobi, and Miura 2007; Mir and Shinohara 2013). Wood (1902) was the first to observe surface plasmons, however, surface plasmon resonance for biosensing goals was illustrated by Liedberg in 1983 (Liedberg, Nylander, and Lunström 1983). The Biacore® technology was the first to evolve in the commercial markets based on the SPR principle, and has been developed for its application since 1990. Since then, researchers have screened various interactions by SPR technology among them drug-protein, antigen-antibody, inhibitor-enzyme, and small molecule-nucleic acid (Sandblad *et al.*, 2009; Tam *et al.*, 2017; Navratilova *et al.*, 2007; Liu and Wilson, 2010). In SPR, the so-called "ligand" is immobilized onto the surface of the sensor chip and when there is an affinity, captures the target molecule or "analyte", this latter being directly injected in solution and flows over the sensor chip. In case of ligand-analyte binding, the refractive index (RI) is modified at the chip surface, proportionally to the change in mass concentration (**Figure 2.6**). The analyte capture produces measurable signals represented by the sensorgram and expressed in resonance unit. Among various advantages, the SPR technology is simple, in real-time and rapid, and does not require analyte pre-labeling. Applied with low amounts of the interacting partners – pure or in a mixture –, the obtained sensorgram can determine the rate of complex formation and dissociation (k_{on}, and k_{off}, respectively). Finally, the sensor chip can be reused several times due to the regeneration treatment (Treiber *et al.*, 2007; Achilleos *et al.*, 2009; Maalouli *et al.*, 2011).

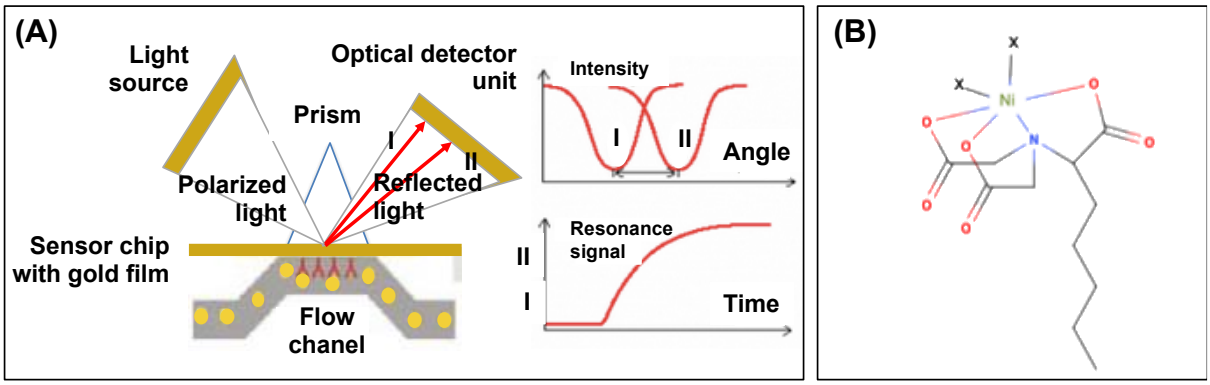

Figure 2.6. Principle of the Surface Plasmon Resonance

No longer after its introduction to the biochemical society, SPR technology has gained the scientists curiosity to detect interactions between metal ions and proteins/peptides. It offers the clearest advantages in speed and sample quantity over other alternative techniques such as Immobilized Metal-ion Affinity Chromatography (**IMAC**) (Bernaudat and Bülow, 2005). In fact, SPR signal is detected when the peptide/protein is surrounding the ion in its favorable geometry. Some available tetradentate nitriloacetic acid (**NTA**) sensor chips were commercialized by Biacore® and allowed the development of a sensitive and selective screening of mineral-peptide complexes. In literature, nickel and copper ions immobilized on NTA chip were the most common methodology to screen MBPs (Knecht *et al*., 2009; Canabady-Rochelle *et al.*, 2018; Maalouli *et al.,* 2011). Inversely, in other studies, peptides were immobilized on the sensor chips surface and minerals were injected as the analytes. With convenient and well-functional platforms, the kinetics of interactions between peptides/proteins and minerals such as copper, magnesium, calcium, and zinc, can be determined (Chen *et al*., 2015; Balliu and Baltzer, 2017).

iv) Electrically switchable nanolever technology

The innovative switchSENSE® technology utilizes a novel electro-switchable biosurface to characterize interactions between molecules in real-time. This technology is unlike existing methodologies in that it combines high sensitivity kinetics with structural information on size, shape and conformation providing a new depth and understanding of the interaction. Studies are performed on a re-usable biochip, generated using familiar coupling and hybridization methods. Within this biochip, DNA levers are embedded onto a series of gold electrodes. These nanolevers serve either as target for molecular interactions themselves, or hold other interaction partners. To characterize interactions, the DRX instrument is used to bring about deliberate movement of these nanolevers by altering the voltage across the gold surface. When interactions occur, these movements (expressed as dynamic response DR) are affected and in turn, used in the calculation of kinetic and biophysical information, such as the kinetics constants of association (k_{on}) and dissociation (k_{off}), the affinity constant (K_D) and the hydrodynamic diameter (D_H) in the case where the ligand is a protein immobilized on the DNA nanolevers (Knezevic et al. 2012).

For proteins or peptides adsorption onto an immobilized-metal chromatographic column for instance, nickel ions are widely used due to their affinity with the exposed side chains of histidine and cysteine residues (Hainfeld et al. 1999). With six coordination sites, Ni^{2+} can strongly bind to a complexing agent *e.g.* the tetradentate nitrilotriacetic acid (NTA) while some sites remains available to interact with the target peptide (Hainfeld et al. 1999). With the switchSENSE® technology, the ssDNA bound on the chip gold surface is hybridized with a cDNA-trisNTA, and a multivalent ion like Ni^{2+} is loaded onto trisNTA; an excess of Ni^{2+} is used in order to load each NTA moiety with one Ni^{2+} ion (**Figure 2.7-A**). Binding of nickel-chelating peptides increases friction forces and leads to decrease the dynamic response DR of the nanolevers (**Figure 2.7-B**). The kinetic (k_{on}, k_{off}) and affinity constants *(*$K_D = k_{off}/k_{on}$*)* of the interaction between Ni^{2+} and MCP can be determined by real-time measurements of the quenching of the fluorescence (**Figure 2.7-C**). Hence, direct evidence of MCPs using switchSENSE® would enable the faster detection of metal-chelating peptides before launching time-consuming separation, which should be engaged solely in the case of positive screening. For the first time, our team just developed a new screening method to highlight MCPs in dietary hydrolysates with the switchSENSE® technology using immobilized nickel (El Hajj *et al.,* 2021).

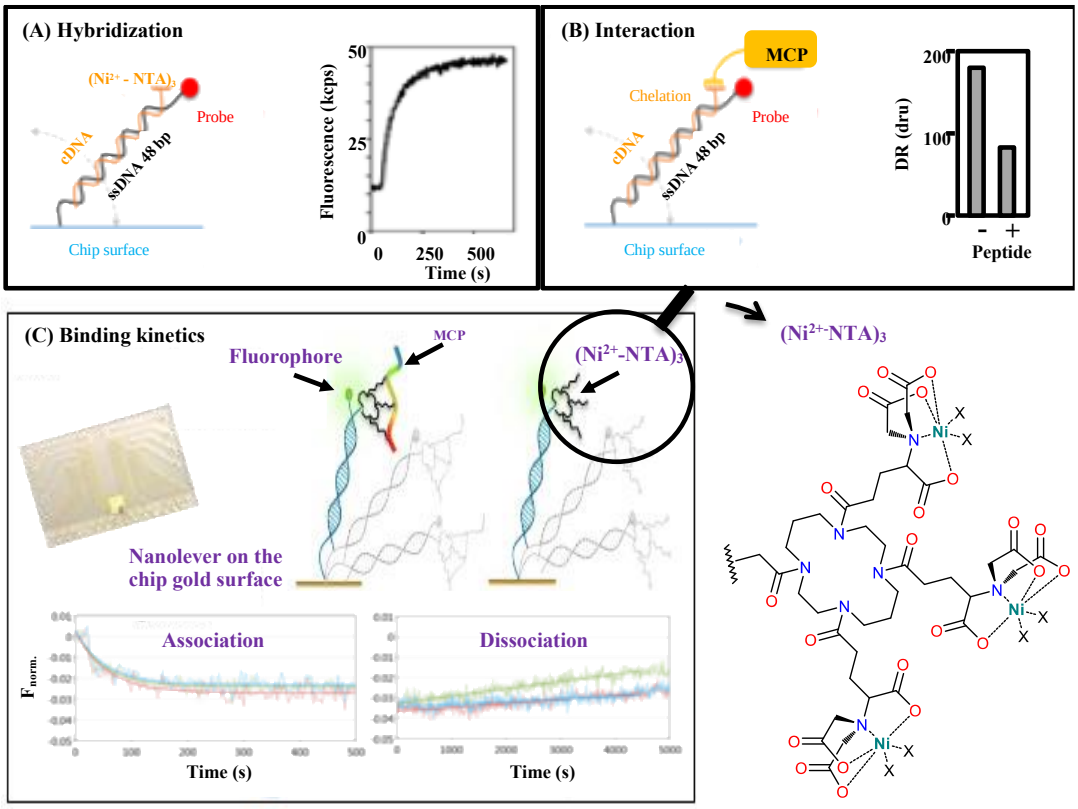

Figure 2.7. Principle of switchSENSE adapted for peptide-metal interaction study**.** (A) Single strands of DNA having 48 base pairs are bound on the chip gold surface and hybridized with a complementary DNA activated by trisNTA. The hybridization is followed by fluorescence measurement of a Cy5 probe fixed at the extremity of the nanolever (kcps: kilocounts per second). A multivalent ion like Ni^{2+} is then immobilized onto the trisNTA group. (B) Binding of metal-chelating peptides (MCP) increases friction forces and leads to decrease the dynamic response DR (dru: dynamic response unit) of the nanolevers. (C) The kinetic (k_{on}, k_{off}) and affinity constants ($K_D = k_{off}/k_{on}$) of the interaction between Ni^{2+} and MCP can be determined by real-time measurements of the quenching of the normalized fluorescence $F_{norm.}$.

v) Electro-Spray Ionisation Mass spectrometry

Electrospray ionization-mass spectrometry (**ESI-MS**) is a well-known technique for the structural analysis of small and large biomolecules of variable polarity (Ho *et al*., 2003). For several years, ESI-MS has shown a great potential for the qualitative analysis of metal-organic ligand complexes (Keith-Roach, 2010).

Electrospray ionization (ESI) is a soft atmospheric pressure ionization allowing the ions transfer from the liquid phase to the gas phase, before their filtering according to their mass-to-charge ratio (*m/z*) in a mass spectrometer (MS). The near-total absence of fragmentation in the electrospray source allows preferential observation of the pseudo-molecular ion,

corresponding to a simple case where the analyte is in its mono-protonated (ESI^+) or mono-deprotonated (ESI^-) form. In addition, non-covalent bonds can be preserved, which is of major interest for coordination complexes study.

In practice, a liquid sample circulates at a low flow rate in a capillary tube (made of stainless steel or quartz) maintained at a high electrical potential (positive or negative) relative to the entry into the MS (2.5 - 6 kV) (Ho *et al*., 2003). Under the influence of this electric field and an inert nebulizing gas (N_2) applied coaxially to the capillary, fine charged droplets are formed with the same polarity as the applied potential. The solvent is then evaporated by application of a drying gas (N_2) and / or gentle heating of the capillary tube (100 to 300 °C) leading to the gradual decrease in droplets size. When the droplets are small enough, the electric field on the surface reaches a critical intensity allowing the direct expulsion of ions in the gas phase (Schalley and Armentrout, 2003).

With ESI-MS, the MS signature is directly provided from samples in solution, and therefore the species of interest are analyzed *in situ* (Di Marco and Bombi, 2006). Thanks to its high sensitivity, this method can be applied to biological samples containing very low concentrations of complexes (10^{-6} M). ESI-MS is an effective tool for determining the number of coordination species formed in solution as well as their stoichiometry, since these parameters are directly obtained from the mass spectrum (Di Marco and Bombi, 2006). In fact, the values of *m/z* ratios at low or high resolution as well as the isotopic patterns enable to identify the complex structure with reliability (**Figure 2.8)**. In addition, the complexes stoichiometry can be studied with robustness as a function of the metal:organic ligand ratio and of the pH (Keith-Roach, 2010).

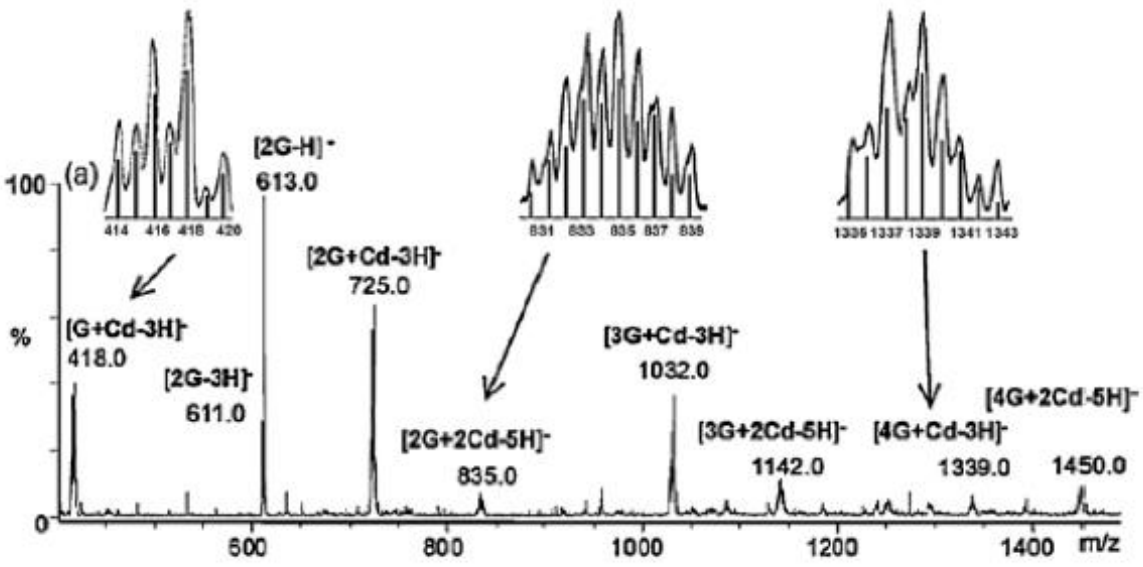

Figure 2.8. Mass spectrum of a solution containing 2.5 mM Cd (II) and 10 mM glutathione-**G.** The inset shows the comparison of the enlarged experimental isotopic pattern (solid line) and the theoritical pattern (histogram) for selected cadmium complexes. Reprinted from Keith-Roach (2010) with kind permission from Elsevier.

ESI-MS has notably been used to characterize a few metal-peptide complexes. The study of the interaction between the small synthetic peptide (αMeAla-Ha AGHa, GGGHa) and nickel(II) or copper(II) was carried out and validated the formation of different complexes in solution (Selmeczi *et al.* 2010, Gizzi, *et al*., 2005, Jancsó *et al.* 2011). Another work - based on histidine-containing synthetic oligopeptides - successfully used the ESI-MS technique to study the impact of conformational changes on the binding affinity with copper(II) and nickel(II) (Murariu *et al.*, 2010). A recent study also described the identification of several iron(II)-peptide complexes from purified peptides, thanks to a ESI-MS differential analysis conducted in the absence and in the presence of iron(II) (Wu *et al*., 2017).

In the case of complex samples, coupled LC-ESI-MS technique allows the matrix effects suppression and is therefore able to provide relevant information on stable non-covalent species (Keith-Roach, 2010). As an example, hydrophilic interaction liquid chromatography (**HILIC**) and ESI-MS, the so-called HILIC-ESI-MS, was proven effective for the targeted analysis of iron(II)- and iron(III)-phytosiderophore complexes (Xuan *et al*., 2006).

Recently, a promising preliminary study carried out on a pool of small synthetic peptides showed that a LC-ESI-MS based methodology (**Figure 2.9**) could be used for an efficient non-targeted screening of peptides with high iron(II)-chelating abilities (Paris *et al.*, 2020).

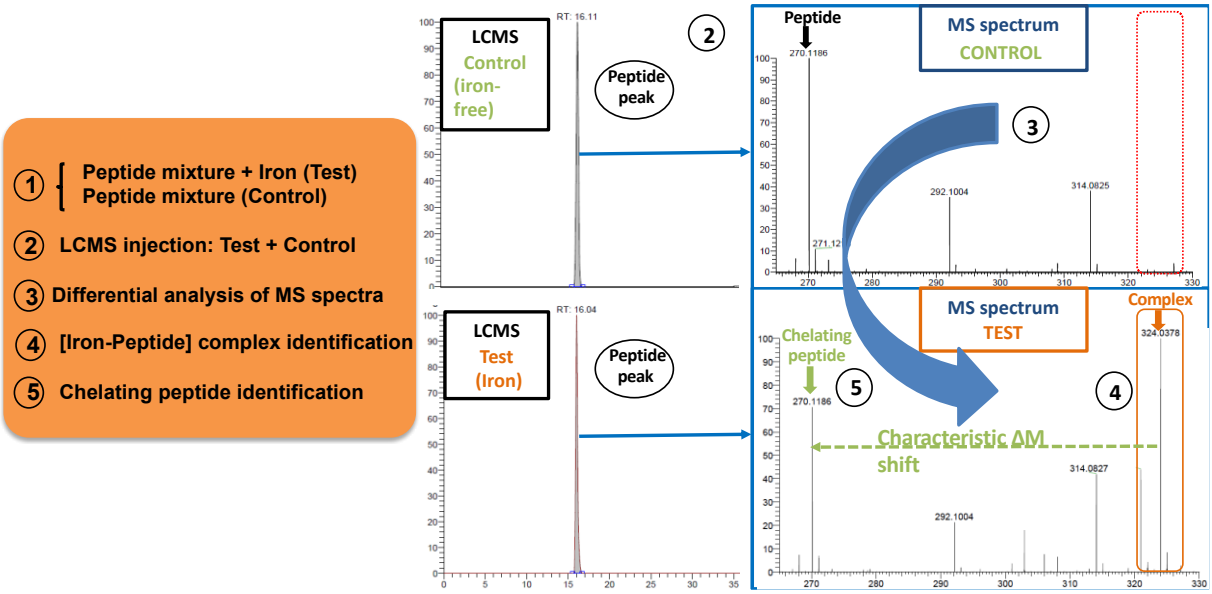

Figure 2.9. Principle of MBP-screening in complex mixture of peptides such as hydrolysates using mass spectra differential analysis

vi) IMAC separation

IMAC principle is briefly constituted of 4 main steps (**Figure 2.10**): (1) metal ion immobilization onto the matrix, (2) Sample injection and target protein/peptide retention, (3) washing step to eliminate the unbound components and (4) finally, elution of the target biomolecule. IMAC is constituted of several parts (Amiri, 2017). First, the matrix (*i.e.* agarose, sepharose, cellulose, silica, dextran) must be highly hydrophilic and characterized by low non-specific adsorption, in addition to a high porosity for a high amount of ligand immobilization, or fairly large pore size and narrow pore size distribution (Gutierrez *et al.*, 2007). *Via* a spacer arm (usually short alkyl chain), a chelating agent is covalently bound onto the matrix for further M^{n+} immobilization, this latter is generally tridentate such as iminodiacetic acid (**IDA**) or tretradentate such as NTA. The higher its denticity, the stronger the immobilization of metal-ions, and hence, a lower metal-ion leakage. Yet, the fewer coordination bonds remain available for protein or peptides adsorption (Garberc-Porekar and Menart, 2001). Once the M^{n+} loaded onto the column, the complexing agent and the metal ions form complexes, letting

some free coordination sites on the immobilized metal ions to further coordinate peptides or proteins (Gutierrez *et al*., 2007). Besides the specific coordination interactions of some amino-acid residues exposed on the biomolecule surface with the immobilized metal-ions, some other aspecific interactions may occur notably, like electrostatic and hydrophobic interactions (Gutierrez *et al*., 2007). The nature of the surrounding chemical environment (*i.e*., buffer salts used and their concentration, pH, and ionic strength) can reduce these aspecific interactions. In this aim, relatively high-ionic strength buffers (often NaCl, 0.1–1.0 M) could be used during adsorption or washing while the buffer itself should not coordinate to the immobilized metal-ions (Garberc-Porekar and Menart, 2001). Various ways of elution are considered in IMAC like acting on pH (González-Ortega & Guzman, 2015), on higher salt concentration, using a competition elution (*e.g*., imidazole, ligand exchange method) (Bresolin *et al.*, 2015), or a complexing agent elution (*e.g.*, EDTA) (Sun *et al.*, 2013). Sometimes, IMAC protocols couple two way of elution to obtain a better chromatographic resolution (Gutierrez *et al*., 2007).

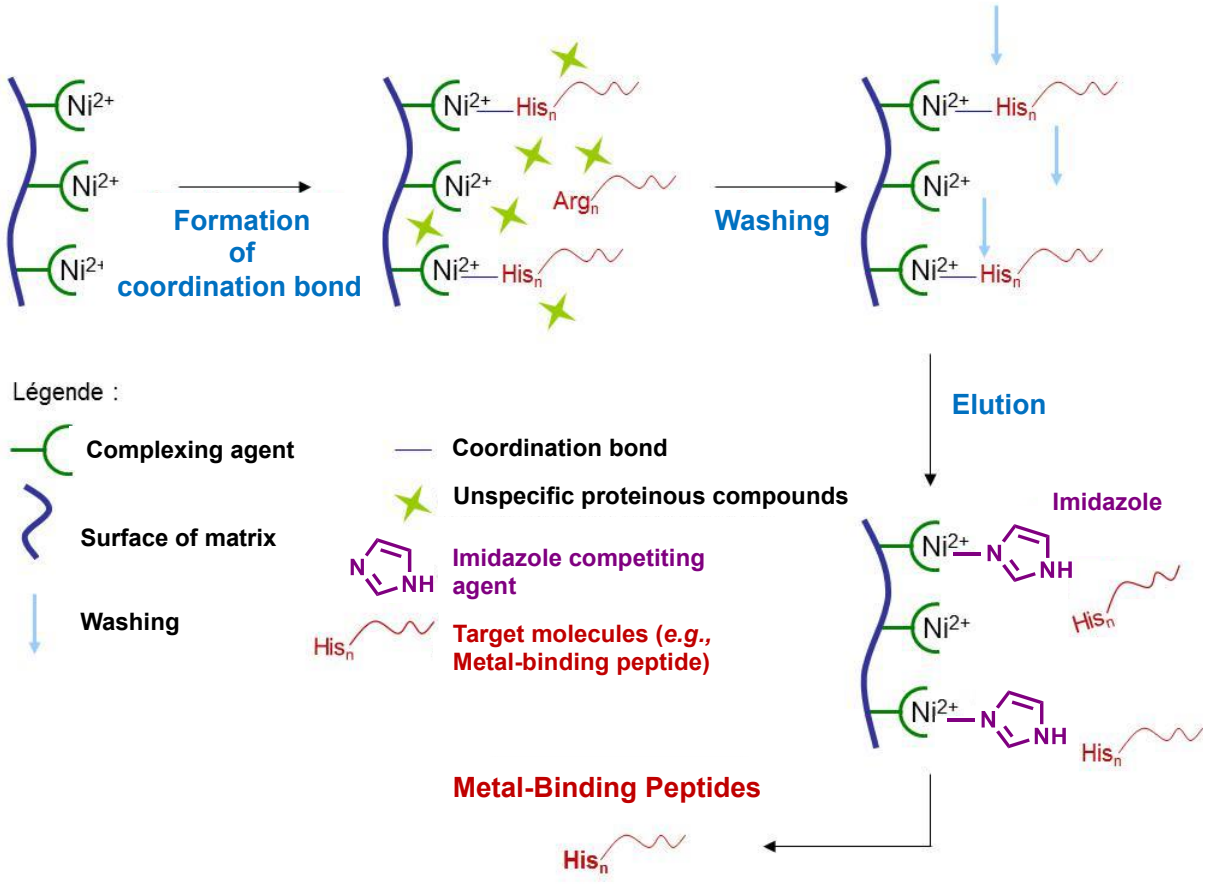

Figure 2.10. Principle of Immobilized Metal ion Affinity Chromatography (IMAC)

More, IMAC chromatography columns can be modelled using mathematical equations. Simulations are useful to predict liquid and solid phase concentration profiles as a function of time, for given operating parameters. The influence of various operating parameters is thus studied numerically, reducing the number of experiments to perform for unit operation optimization. Modelling requires an understanding of the mechanisms governing the chromatographical process, *i.e.* equilibria, hydrodynamics and kinetics. The simulation of IMAC chromatographic separation of metal-chelating peptides was carried out in our team, from binding parameters determined in SPR (Muhr *et al.*, 2020). Despite the high interest of this approach and considering the readership of this book, modelling of IMAC separation was not developed in this chapter.

Introduced by Porath and colleagues (1975), IMAC was first applied on proteins fractionation, based on their differential affinity towards immobilized metal ions due to their specific coordinating amino acid residues exposed in surface (Gutiérrez *et al.*, 2007). In the late 1980s, recombined proteins with engineered histidine tag were efficiently purified, especially using Ni^{2+}-NTA matrix, selective for adjacent histidine groups binding (Hochuli *et al.*, 1987).

However, other matrices can be used: For instance, Fe^{3+}-IDA matrix was used to investigate the role of the phosphoseryl cluster (Ser*P*-Ser*P*-Ser*P*-Glu-Glu or □□□EE) and diphosphoseryl pattern in the complexation of ferric iron and calcium by the purified caseins and the proteose peptone 3 component of milk and to determine the adsorption efficiency of free amino acids (Tyr, Trp, Cys, His, etc.) with the immobilized Fe^{3+}-IDA matrix (Bernos *et al.*, 1997). IMAC has a high selectivity, a high recovery yield of the target proteins/peptide, a high protein loading, and a complete regeneration of the solid supports (Ha *et al.*, 2008). Today, this is one of the main methodologies used for peptide or protein purification, from laboratory to pilot/industrial scale.

2.1.6 Evidence of health effects of mineral-binding peptides

The presence of several minerals is required in food diets for life. Mineral absorption occurs across the gastrointestinal mucosa *via* passive and active transport mechanisms. Sometimes minerals can interact with other substances in the diet during their gastrointestinal tract crossing, which may consequently enhance or impair mineral permeability in the small intestine (Kiela and Ghishan 2016). Mineral-chelating peptides derived from food proteins

display stability properties, enabling mineral transport across the gastrointestinal tract and improving the mineral bioavailability (Chen *et al.*, 2017). The effect of mineral-chelating peptides on mineral bioavailability - especially calcium and iron - have been widely evaluated *in vitro* on cell models and *in vivo* in animal and human studies (Guo *et al.*, 2014).

Calcium is one of the major required minerals in human physiology. Its absorption is mediated by passive paracellular diffusive pathway *via* the epithelial tight junctions claudins Cldn-2, Cldn-12 and Cldn-15 (Kiela and Ghishan 2016). Calcium-rich foods (milk, cheese and other dairy products) contain key proteins such as caseins, hydrolyzed upon tryptic digestion in CPPs (Cross, Huq, and Reynolds 2007). Extensively reported in mineral absorption studies, CPPs promoted calcium permeability through Caco-2 cells intestinal barrier model (Cosentino *et al.*, 2010). Ferraretto *et al.* 2001, suggested that CPPs enhance calcium absorption by acting either on calcium channels at plasma membranes or as calcium-carrier proteins by endocytosis (Ferraretto *et al*. 2001).To favour calcium absorption, CPPs directly interact with Transient Receptor Potential V6 (**TRPV6**), a selective calcium channel (Perego *et al*., 2013). Sato, Noguchi, and Naito (1985) evidenced that the increase of calcium absorption at the rat small intestine level (ligated loops) was related to the inhibition of calcium precipitation due to CPPs calcium chelation properties. Indeed, increased calcium absorption by rats small intestine level was also observed when calcium solution and phytate deficient deaminated soybean globulins (another calcium chelator) were administrated together (Kumagai *et al*., 2004). Chabance *et al.* (1998) recovered casein-derived peptides from the duodenum of six healthy individuals after milk ingestion, in addition to other peptides related to casein found in the subjects' plasma. In addition, researchers detected in human volunteers with ileostomy, the presence of CPPs in ileostomy fluid after 10 hours of milk ingestion, evidencing that these peptides can survive to the intestinal tract environment up to the ileum (Meisel *et al.*, 2003). Moreover, fish bone peptides from fish meals prevent also calcium deficiency by increasing calcium absorption and bone mineral density in ovariectomised rats (Jung, Lee, and Kim, 2006).

Iron absorption occurs at the level of duodenal brush border, where cytochrome b reductase 1 reduces the ferric form of iron (Fe^{3+}) to its ferrous form (Fe^{2+}), the latter crossing through the brush membrane *via* the Divalent Metal Transporter 1 (**DMT1**). Only heme iron is not absorbed *via* DMT1 but *via* a Heme Transporter (**HCP1**) (Kiela and Ghishan, 2016). Certain

studies demonstrated the positive effect of iron bound to peptides for iron deficiency treatment. Kapsokefalou and Miller (1995) explained that the solubility of iron in the small intestine was related to its binding to peptides and not to the free amino acids or fatty acids. Indeed, iron bound to CPPs was shown to be soluble and stable in the digestive tract of iron deficient rats with increased bioavailability compared to the free iron forms (Aît-Oukhatar *et al.*, 2002; Kibangou *et al.* 2008; Pérès *et al.* 1999). Kibangou *et al.* (2008) followed the protective effect of CPPs against enterocyte peroxidation, induced by the increase of iron absorption. Layrisse *et al.* (1984) conducted a study on 113 subjects to determine the effect of cysteine, histidine, reduced glutathione and beef consumption on iron bioavailability. They showed that free cysteine had the same effect as beef consumption concerning the enhancement of food iron bioavailability and that this amino acid residue maintained its activity when present in the reduced form of glutathione peptide.

Although mineral absorption is physiologically a well-regulated phenomenon, pre-clinical and clinical trials on mineral-chelating peptides are needed in order to prove their health benefits in malabsorption syndromes.

2.1.7 Summary

Minerals are essential to different biological processes in living beings. Likewise, free transition metals such as copper and iron promote the formation of reactive oxygen species (ROSs). However, metal-binding-peptides obtained by enzymatic hydrolysis of proteins or synthesized by solid-phase peptide synthesis (**SPPS**) avoid ROS formation catalysed by free transition metals. Interactions between metals and mineral-binding-peptides are usually studied using spectroscopic techniques, ITC, and more recently by SPR and switchSENSE®. Through electrospray ionization-mass spectrometry, the changes on the binding affinities can be studied. Mineral-binding-peptides can be purified using immobilized IMAC, and its process simulation. Various cellular models are used to investigate the health effects of mineral-binding peptides.

2.1.8 References

Abragam, and Bleaney. (1970). "Electron Paramagnetic Resonance of Transition Ions", Oxford University Press, London, pp 911.

Achilleos, Tailhardat, Courtellemont, Varlet, Le, and Dupont. (2009). Investigation of surface plasmon resonance biosensor for skin sensitizers studies. *Toxicology in Vitro*, **23**(2), 308–318. https://doi.org/10.1016/j.tiv.2008.11.007

Adlard, and Bush. (2006). Metals and Alzheimer's disease. *Journal of Alzheimer's Disease*, **10**(2–3), 145–163. https://doi.org/10.3233/JAD-2006-102-303

Aît-Oukhatar, Bouhallab, Arhan, Maubois, Drosdowsky, and Bouglé. (1999). Iron tissue storage and hemoglobin levels of defiscient rats repleted with iron bound to the caseinophosphopeptide 1-25 of b-casein. *Journal of Agricultural and Food Chemistry*, 47(7): 2786-2790. https://doi.org/10.1021/jf981018k

Aît-Oukhatar, Peres, Bouhallab, Neuville, Bureau, Bouvard, Arhan, and Bougle. (2002). Bioavailability of caseinophosphopeptide-bound iron. *Journal of Laboratory and Clinical Medicine,* **140** (4): 290–94. https://doi.org/10.1067/mlc.2002.128146

Amiri, Mehrnia, Sobhanifard, Pourasgharian Roudsari, and Hoseini. (2017). Evaluation of agarose-entrapped magnetic nanoparticles influence on protein adsorption isotherm and kinetics using nickel-iminodiacetic acid ligand. *Separation and Purification Technology*, **188**, 423–430. https://doi.org/10.1016/j.seppur.2017.07.030

Balliu, and Baltzer (2017). Conjugation of a dipicolyl chelate to polypeptide conjugates increases binding affinities for human serum albumin and survival times in human serum. *ChemBioChem*, **18**(14), 1408–1414. https://doi.org/10.1002/cbic.201700049

Bao, Lv, Yang, Ren, and Guo. (2008). A study of the soluble complexes formed during calcium binding by soybean protein hydrolysates. *Journal of Food Science*, **73**(3), C117–C121. https://doi.org/10.1111/j.1750-3841.2008.00673.x

Bao, Song, Zhang, Chen, and Guo, (2007). Calcium-binding ability of soy protein hydrolysates. *Chinese Chemical Letters*, **18**(9), 1115–1118. https://doi.org/10.1016/j.cclet.2007.07.032

Barth. (2007). Infrared spectroscopy of proteins. *Biochimica et Biophysica Acta (BBA) - Bioenergetics*, **1767**(9), 1073–1101. https://doi.org/10.1016/j.bbabio.2007.06.004

Bernaudat, and Bullow. (2005). Rapid evaluation of nickel binding properties of His-tagged lactate dehydrogenases using surface plasmon resonance. *Journal of Chromatography A*, **1066**(1–2), 219–224. https://doi.org/10.1016/j.chroma.2005.01.079

Bernos, Girardet, Humbert, and Linden. (1997). Role of the O phosphoserine clusters in the interaction of the bovine milk □$_{s1}$-, □-, □-caseins and the PP3 component with immobilized iron(III) ions. *Biochimica et Biophysica Acta: Protein Structure and Molecular Enzymology*, **1337**(1), 149–159. https://doi.org/10.1016/S0167-4838(96)00159-8

Bondalapati, Jbara, and Brik. (2016). Expanding the chemical toolbox for the synthesis of large and uniquely modified proteins. *Nature Chemistry*, **8**(5), 407–418. https://doi.org/10.1038/nchem.2476

Bouhallab, and Bougl. (2004). Biopeptides of milk: caseinophosphopeptides and mineral bioavailability. *Reproduction Nutrition Development*, EDP Sciences, **44**(5), 493-498. https://doi.org/10.1051/rnd:2004053

Bouglé, and Bouhallab. Mineral-Binding Proteins and Peptides and Bioavailability of Trace Elements. In Nutraceutical proteins and peptides in health and disease, Y. Mine and F. Shahidi, eds., Taylor & Francis group 2006, pp 29-40.

Bresolin, Bresolin, and Pessoa. (2015). Purification of anti-interleukin-6 monoclonal antibody using precipitation and immobilized metal-ion affinity chromatography. *Adsorption Science and Technology*, **33**(2), 191–202. https://doi.org/10.1260/0263-6174.33.2.191

Buckley, and Ryder. (2017). Applications of Raman spectroscopy in biopharmaceutical manufacturing: a short review. *Applied Spectroscopy*, **71**(6), 1085–1116. https://doi.org/10.1177/0003702817703270

Bullamore, Wilkinson, Gallagher, Nordin, and Marshall. (1970). Effect of age on calcium absorption. *The Lancet*, **296**(7672), 535–537. https://doi.org/10.1016/S0140-6736(70)91344-9

Caetano-Silva, Alves, Lucena, Frem, Bertoldo-Pacheco, Lima-Pallone, and Netto. (2017). Synthesis of whey peptide-iron complexes: influence of using different iron precursor compounds. *Food Research International*, **101**(May), 73–81. https://doi.org/10.1016/j.foodres.2017.08.056

Caetano-Silva, Bertoldo-Pacheco, Paes-Leme, and Netto. (2015). Iron-binding peptides from whey protein hydrolysates: Evaluation, isolation and sequencing by LC-MS/MS. *Food Research International*, **71**, 132–139. https://doi.org/10.1016/j.foodres.2015.01.008

Canabady-Rochelle, Sanchez, Mellema, and Banon. (2009). Study of calcium–soy protein interactions by Isothermal Titration Calorimetry and pH cycle. *Journal of Agricultural and Food Chemistry*, 57: 5339-5347. https://doi.org/10.1021/jf900424b

Canabady-Rochelle, Sanchez, Mellema, and Banon. (2010). Calcium carbonate-hydrolysed soy proteins complexation in presence of citric acid. *Journal of Colloid and Interface Science*. **345**: 88-95. https://doi.org/10.1016/j.jcis.2010.01.037

Canabady-Rochelle, Selmeczi, Collin, Pasc, Muhr, and Boschi-Muller. (2018). SPR screening of metal chelating peptides in a hydrolysate for their antioxidant properties. *Food Chemistry*, **239**, 478–485. https://doi.org/10.1016/j.foodchem.2017.06.116

Cao, Miao, Liu, Luo, Xia, Liu, Yao, Cao, Sun, Lin, Lan, and Xiao. (2017). Bioactive peptides isolated from casein phosphopeptides enhance calcium and magnesium uptake in Caco-2 cell monolayers. *Journal of Agricultural and Food Chemistry*, ***65***(11), 2307–2314. https://doi.org/10.1021/acs.jafc.6b05711

Carrasco-Castilla, Hernández-Álvarez, Jiménez-Martínez, Jacinto-Hernández, Alaiz, Girón-Calle, Vioque, J., and Dávila-Ortiz, G. (2012). Antioxidant and metal chelating activities of peptide fractions from phaseolin and bean protein hydrolysates. *Food Chemistry*, **135**(3), 1789–1795. https://doi.org/10.1016/j.foodchem.2012.06.016

Chabance, Marteau, Rambaud, Migliore-Samour, Boynard, Perrotin, Guillet, Jollès, and Fiat. (1998). Casein peptide release and passage to the blood in humans during digestion of milk or yogurt. *Biochimie,* **80** (2): 155–65. https://doi.org/10.1016/S0300-9084(98)80022-9

Chabanon. (2005). Hydrolyses enzymatiques d'isolats protéiques issus de tourteaux de colza : cinétique, modélisation, caractérisation et fonctionnalités des peptides. Thèse de l'Institut National Polytechnique de Lorraine. 248 pages.

Chan, and Rennert. (1980). The Role of Copper in Iron Metabolism. *Annals of Clinical and Laboratory Science,* 10 (4): 338–44.

Charoenphun, Cheirsilp, Sirinupong, and Youravong. (2013). Calcium-binding peptides derived from tilapia (*Oreochromis niloticus*) protein hydrolysate. *European Food Research and Technology*, **236**(1), 57–63. https://doi.org/10.1007/s00217-012-1860-2

Cheignon, Jones, Atrián-Blasco, Kieffer, Faller, Collin, and Hureau. (2017). Identification of key structural features of the elusive Cu–Aβ complex that generates ROS in Alzheimer's disease. *Chemical Science*, **8**(7), 5107–5118. https://doi.org/10.1039/C7SC00809K

Chen, Mu, Huang, Nie, Liu, and Zeng. (2014). Isolation of a calcium-binding peptide from tilapia scale protein hydrolysate and its calcium bioavailability in rats. *Journal of Functional Foods*, **6**(1), 575–584. https://doi.org/10.1016/j.jff.2013.12.001

Chen, Jia, Zhang, Jang, Chen, Koh, and Wang. (2015). Sensitive detection of copper(II) ions based on the conformational change of peptides by surface plasmon resonance spectroscopy. *Analytical Methods*, **7**(20), 8942–8946. https://doi.org/10.1039/C5AY02047F

Chen, Guo, Du, Chen, Hou, and Li. (2017). The chelating peptide (GPAGPHGPPG) derived from Alaska pollock skin enhances calcium, zinc and iron transport in Caco-2 cells. *International Journal of Food Science and Technology*, **52**(5), 1283–1290. https://doi.org/10.1111/ijfs.13396

Cheung, Cheung, Tan, and Li-Chan. (2012). The role of molecular size in antioxidant activity of peptide fractions from Pacific hake (*Merluccius productus*) hydrolysates. *Food Chemistry*, **134**(3), 1297–1306. https://doi.org/10.1016/j.foodchem.2012.02.215

Clemente. (2000). Enzymatic protein hydrolysates in human nutrition. *Trends in Food Science and Technology*, **11**(7), 254–262. https://doi.org/10.1016/S0924-2244(01)00007-3

Coin, Beyermann, and Bienert. (2007). Solid-phase peptide synthesis: from standard procedures to the synthesis of difficult sequences. *Nature Protocols*, **2**(12), 3247–3256. https://doi.org/10.1038/nprot.2007.454

Comba, Dovalil, Haberhauer, Kowski, Mehrkens, and Westphal. Copper (2013). Copper solution chemistry of cyclic pseudo-octapeptides. *Zeitschrift für Anorganische und Allgemeine Chemie*, **639** (8-9), 1395-1400.

Cross, Huq, and Reynolds. (2007). Casein phosphopeptides in oral health--chemistry and clinical applications. *Current Pharmaceutical Design,* **13** (8): 793–800. https://doi.org/10.2174/138161207780363086

Cosentino, Gravaghi, Donetti, Donida, Lombardi, Bedoni, Fiorilli, Tettamanti, and Ferraretto, A. (2010). Caseinphosphopeptide-Induced calcium uptake in human intestinal cell lines HT-29 and Caco2 is correlated to cellular differentiation. *The Journal of Nutritional Biochemistry,* **21** (3): 247–54. https://doi.org/10.1016/j.jnutbio.2008.12.016

Coudray, Rambeau, Feillet-Coudray, Gueux, Tressol, Mazur, and Rayssiguier. (2005). Study of magnesium bioavailability from ten organic and inorganic Mg salts in Mg-depleted rats using a stable isotope approach. *Magnesium Research*, **18**(4), 215–223.

Cuomo, Ceglie, and Lopez. (2011). Temperature dependence of calcium and magnesium induced caseinate precipitation in H_2O and D_2O. *Food Chemistry*, **126**(1), 8–14. https://doi.org/10.1016/j.foodchem.2010.10.021

Csire, Canabady-Rochelle**,** Averlant-Petit, Selmeczi, Stefan. Both metal-chelating and free radical-scavenging synthetic pentapeptides as efficient inhibitors of reactive oxygen species generation. *Metallomics*, 2020, 1-10. https://doi.org/ 10.1039/d0mt00103a

De La Hoz, Ponezi, Milani, Da Silva, De Souza, and Bertoldo-Pacheco. (2014). Iron-binding properties of sugar cane yeast peptides. *Food Chemistry*, **142**, 114–120. https://doi.org/10.1016/j.foodchem.2013.06.133

Di Marco and Bombi. (2006). Electrospray mass spectrometry (ESI-MS) in the study of metal–ligand solution equilibria. *Mass Spectrometry Reviews*, **25**(3), 347-379. https://doi.org/10.1002/mas.20070

De Ricco, Potocki, Kozlowski, Valensin. (2014). NMR investigations of metal interactions with unstructured soluble protein domains. *Coordination Chemistry Review*, **269**, 1-12. https://doi.org/10.1016/j.ccr.2014.02.014

DiNicolantonio, Liu, O'Keefe. (2018). Magnesium for the prevention and treatment of cardiovascular disease. Open Heart, 5:e000775. http://doi.org/10.1136/ openhrt-2018-000775

Dunbar. (2017). Biotechnology and the mine of tomorrow. *Trends in Biotechnology*, **35**(1), 79–89. https://doi.org/10.1016/j.tibtech.2016.07.004

Eckert, Lu, Unsworth, Chen, Xie, and Xu. (2016). Biophysical and *in vitro* absorption studies of iron chelating peptide from barley proteins. *Journal of Functional Foods*, **25**, 291–301. https://doi.org/10.1016/j.jff.2016.06.011

El-Faham, and Albericio. (2011). Peptide coupling reagents, more than a letter soup. *Chemical Reviews*, **111**(11), 6557–6602. https://doi.org/10.1021/cr100048w

FAO specification Human vitamin and mineral requirements. Report of a Joint FAO/WHO Expert Consultation. FAO/WHO non-series publication. Rome: Food and Agriculture Organization, 2002. (En)

Faller, Hureau, Dorlet, Hellwig, Coppel, Collin, and Alies. (2012). Methods and techniques to study the bioinorganic chemistry of metal–peptide complexes linked to neurodegenerative diseases. *Coordination Chemistry Reviews*, **256**(19–20), 2381–2396. https://doi.org/10.1016/j.ccr.2012.03.015

Farkas, and Sóvágó. (2012). "Amino acids, peptides and proteins". In Amino Acids, Peptides and Proteins: Volume 37, The Royal Society of Chemistry. pp 66–118. https://doi.org/10.1039/9781849734677

Farkas, and Sóvágó. (2017). "Metal complexes of amino acids and peptides". In Amino Acids, Peptides and Proteins. The Royal Society of Chemistry, Vol. 41, pp 100–151. https://doi.org/10.1039/9781782626619-00100

Fenton. (1894). LXXIII.—Oxidation of tartaric acid in presence of iron. *Journal of the Chemical Society*, Transactions, 65, 899–910. https://doi.org/10.1039/CT8946500899

Ferraretto, Signorile, Gravaghi, Fiorilli, and Tettamanti. (2001). Casein phosphopeptides influence calcium uptake by cultured human intestinal HT-29 tumor cells. *The Journal of Nutrition,* **131** (6): 1655–61. https://doi.org/10.1093/jn/131.6.1655

Fisher. (1903). Synthese von derivaten der Polypeptide. *ChemPlusChem*, 36(2) 2094-2106. https://doi-org.bases-doc.univ-lorraine.fr/10.1002/cber.190303602127

Fisher. (1907). Synthese von Polypeptiden. *ChemPlusChem*, 40(2), 1754-1767. https://doi-org.bases-doc.univ-lorraine.fr/10.1002/cber.19070400273

Friščić, Mottillo, and Titi. (2020). Mechanochemistry for synthesis. *Angewandte Chemie International Edition*, **59**(3), 1018–1029. https://doi.org/10.1002/anie.201906755

Gaberc-Porekar, and Menart. (2001). Perspectives of immobilized-metal affinity chromatography. *Journal of Biochemical and Biophysical Methods*, **49**(1–3), 335–360. https://doi.org/10.1016/S0165-022X(01)00207-X

Ghisaidoobe, and Chung. (2014). Intrinsic tryptophan fluorescence in the detection and analysis of proteins: a focus on Förster Resonance Energy Transfer techniques. *International Journal of Molecular Sciences*, **15**(12), 22518–22538. https://doi.org/10.3390/ijms151222518

Gilbert, Jansson, and Knight. (2014). The earth microbiome project: successes and aspirations. *BMC Biology*, ***12***(1), 69. https://doi.org/10.1186/s12915-014-0069-1

Gizzi, Henry, Rubini, Giroux, and Wenger. (2005). A multi-approach study of the interaction of the Cu(II) and Ni(II) ions with alanylglycylhistamine, a mimicking pseudopeptide of the serum albumine N-terminal residue. *Journal of Inorganic Biochemistry*, **99**(5), 1182–1192. https://doi.org/10.1016/j.jinorgbio.2005.02.018

González-Ortega, and Guzmán. (2015). Purification of human serum immunoglogulins using immobilized metal affinity chromatography with ethylendiamine triacetic acid as chelating agent. *Journal of Liquid Chromatography and Related Technologies*, **38**(1):74-81. https://doi.org/10.1080/10826076.2014.883534

Greger. (1999). Nondigestible carbohydrates and mineral bioavailability. *The Journal of Nutrition*, **129**(7), 1434S-1435S. https://doi.org/10.1093/jn/129.7.1434S

Grossoehme, Akilesh, Guerinot, and Wilcox. (2006). Metal-binding thermodynamics of the histidine-rich sequence from the metal-transport protein IRT1 of Arabidopsis thaliana. *Inorganic Chemistry,* **45**(21), 8500-8508. https://doi.org/10.1021/ic0606431

Guéguen, and Pointillart. (2000). The bioavailability of dietary calcium. *Journal of the American College of Nutrition*, **19**(sup2), 119S-136S. https://doi.org/10.1080/07315724.2000.10718083

Guilloreau, Luminita, Coppel, Mazarguil, Winterhalter, Faller, P. (2006). Structural and thermodynamical properties of Cu amyloid-b16/28 complexes associated with Alzheimer's disease. *Journal of Biological Inorganic Chemistry*, **11**:1024-1038. https://doi.org/10.1007/s00775-006-0154-1

Guo, Hou, Li, Zhang, Wang, and Zhao. (2013). Preparation, isolation and identification of iron-chelating peptides derived from Alaska pollock skin. *Process Biochemistry*, **48**(5–6), 988–993. https://doi.org/10.1016/j.procbio.2013.04.013

Guo, Harnedy, Li, Hou, Zhang, Zhao, and FitzGerald. (2014). Food protein-derived chelating peptides: biofunctional ingredients for dietary mineral bioavailability enhancement. *Trends in Food Science & Technology,* **37** (2): 92–105. https://doi.org/10.1016/j.tifs.2014.02.007

Guo, Harnedy, O'Keeffe, Zhang, Li, Hou, and Fitzgerald. (2015). Fractionation and identification of Alaska pollock skin collagen-derived mineral chelating peptides. *Food Chemistry*, **173**, 536–542. https://doi.org/10.1016/j.foodchem.2014.10.055

Gutteridge, and Wilkins. (1982). Copper-dependent hydroxyl radical damage to ascorbic acid. *FEBS Letters*, **137**(2), 327–330. https://doi.org/10.1016/0014-5793(82)80377-3

Gutierrez, Martín del Valle, and Galan. (2007). Immobilized metal-ion affinity chromatography: status and trends. *Separation & Purification Reviews*, **36**: 71-111. https://doi.org/10.1080/15422110601166007

Ha, Kim, An, Kim, Lee, Lee, and Paik. (2008). Purification of His-tagged proteins using Ni^{2+}–poly(2-acetamidoacrylic acid) hydrogel. *Journal of Chromatography B*, **876**(1), 8–12. https://doi.org/10.1016/j.jchromb.2008.10.020

Haber, and Weiss. (1934). The catalytic decomposition of hydrogen peroxide by iron salts. *Proceedings of the Royal Society of London. Series A - Mathematical and Physical Sciences*, **147**(861), 332–351. https://doi.org/10.1098/rspa.1934.0221

Hainfeld, Liu, Halsey, Freimuth, and Powell. (1999). Ni-NTA-gold clusters target His-tagged proteins. *Journal of Structural Biology*, **127**(2), 185–198. https://doi.org/10.1006/jsbi.1999.4149

Halliwell. (1994). Free radicals, antioxidants, and human disease: curiosity, cause, or consequence? *The Lancet*, **344**(8924), 721–724. https://doi.org/10.1016/S0140-6736(94)92211-X

Han, Seo, Kim, Lee, Kang, Ryu, and Chung. (2010). A histidine substitution confers metal binding affinity to a *Schistosoma japonicum* Glutathione S-transferase. *Protein Expression and Purification*, **73**(1), 74–77. https://doi.org/10.1016/j.pep.2010.03.014

Hancock. (1992). Chelate ring size and metal ion selection. The basis of selectivity for metal ions in open-chain ligands and macrocycles. *Journal of Chemical Education*, **69**(8), 615. https://doi.org/10.1021/ed069p615

Hartmann, and Meisel. (2007). Food-derived peptides with biological activity: from research to food applications. *Current Opinion in Biotechnology*, **18**(2), 163–169. https://doi.org/10.1016/j.copbio.2007.01.013

Hazen, and Ferry. (2010). Mineral evolution: mineralogy in the fourth dimension. *Elements*, **6**(1), 9–12. https://doi.org/10.2113/gselements.6.1.9

Ho, Lam, Chan, Cheung, Law, Lit, … Tai. (2003). Electrospray ionisation mass spectrometry: principles and clinical applications. *The Clinical Biochemist. Reviews*, **24**(1), 3–12. Retrieved from https://pubmed.ncbi.nlm.nih.gov/18568044

Hochuli, Döbeli, and Schacher. (1987). New metal chelate adsorbent selective for proteins and peptides containing neighboring histidine residues. *Journal of Chromatography A*, **411**, 177–184. https://doi.org/10.1016/S0021-9673(00)93969-4

Holick. (2004). Sunlight and vitamin D for bone health and prevention of autoimmune diseases, cancers, and cardiovascular disease. *The American Journal of Clinical Nutrition,* **80** (6): 1678S-1688S. https://doi.org/10.1093/ajcn/80.6.1678S.

Hong, Kim, jin, Park, Ryu, Ryu, Kim, and Chung. (2015). Preparation and characterisation of an easily absorbable Mg-casein hydrolysate complex produced through enzymatic hydrolysis and ultrafiltration. *International Journal of Food Science and Technology*, **50**(2), 365–371. https://doi.org/10.1111/ijfs.12650

Huang, Ren, and Jiang. (2011). Purification of a histidine-containing peptide with calcium binding activity from shrimp processing byproducts hydrolysate. *European Food Research and Technology*, **232**(2), 281–287. https://doi.org/10.1007/s00217-010-1388-2

Huang, Zhao, Cai, Wang, Huang, Hong, and Rao. (2015). Purification and characterization of a glutamic acid-containing peptide with calcium-binding capacity from whey protein hydrolysate. *Journal of Dairy Research*, **82**(1), 29–35. https://doi.org/10.1017/S0022029914000715

Hurrell, and Egli. (2010). Iron bioavailability and dietary reference values. *The American Journal of Clinical Nutrition*, **91**(5), 1461S-1467S. https://doi.org/10.3945/ajcn.2010.28674F

Irving, and Williams. (1953). The stability of transition-metal complexes. *Journal of the Chemical Society*, 3192–3210. https://doi.org/10.1039/jr9530003192

Isidro-Llobet, Álvarez, and Albericio. (2009). Amino acid-protecting groups. *Chemical Reviews*, **109**(6), 2455–2504. https://doi.org/10.1021/cr800323s

Jaiswal, Bajaj, Mann, and Lata. (2015). Iron (II)-chelating activity of buffalo αS-casein hydrolysed by corolase PP, alcalase and flavourzyme. *Journal of Food Science and Technology*, **52**(6), 3911–3918. https://doi.org/10.1007/s13197-014-1626-x

Jancsó, Selmeczi, Gizzi, Nagy, Gajda, Henry. (2011). The role of terminal amino group and histidine at the fourth position in the metal ion binding of oligopeptides revisited: Copper(II) and nickel(II) complexes of glycyl-glycyl-glycyl-histamine and its N-Boc protected derivative, *Journal of Inorganic Biochemistry*, **105**, 92-101. https://doi.org/10.1016/j.jinorgbio.2010.09.004

Jaradat. (2017). Thirteen decades of peptide synthesis: key developments in solid phase peptide synthesis and amide bond formation utilized in peptide ligation. *Amino Acids*, **50**(1), 39–68. https://doi.org/10.1007/s00726-017-2516-0

Jin, Fu, & Ma. (2011). Preparation and structure characterization of soluble bone collagen peptide chelating calcium. *African Journal of Biotechnology*, **10**(50), 10204–10211. https://doi.org/10.5897/AJB10.1923

Jiskoot, and Crommelin. (2005). "Methods for Structural Analysis of Protein Pharmaceuticals". Springer Science and Business Media. vol. 3. pp 1–26.

Jung, Lee, and Kim. (2006). Fish-bone peptide increases calcium solubility and bioavailability in ovariectomised rats. *British Journal of Nutrition,* **95**(1): 124–28. https://doi.org/10.1079/BJN20051615

Kaden, Bush, Danzeisen, Bayer, and Multhaup. (2011). Disturbed copper bioavailability in Alzheimer's disease. *International Journal of Alzheimer's Disease*, 2011. https://doi.org/10.4061/2011/345614

Kapsokefalou, and Miller. (1995). Iron speciation in intestinal contents of rats Fed meals composed of meat and nonmeat sources of protein and fat. *Food Chemistry*, **52** (1): 47–56. https://doi.org/10.1016/0308-146(94)P4180-N

Kumagai, Koizumi, Suda, Sato, Sakurai, and Kumagai. (2004). Enhanced calcium absorption in the small intestine by a phytate-removed deamidated soybean globulin preparation. *Bioscience, Biotechnology, and Biochemistry,* **68**(7): 1598–1600. https://doi.org/10.1271/bbb.68.1598

Keith-Roach. (2010). A review of recent trends in electrospray ionisation–mass spectrometry for the analysis of metal–organic ligand complexes. *Analytica Chimica Acta*, **678**(2), 140–148. https://doi.org/10.1016/j.aca.2010.08.023

Kibangou, Bouhallab, Bureau, Allouche Thouvenin, and Bouglé. (2008). Caseinophosphopeptide-bound iron: protective effect against gut peroxidation. *Annals of Nutrition and Metabolism,* **52** (3): 177–80. https://doi.org/10.1159/000136384

Kiela, and Ghishan. (2016). Physiology of intestinal absorption and secretion. *Best Practice & Research. Clinical Gastroenterology,* **30** (2): 145–59. https://doi.org/10.1016/j.bpg.2016.02.007

Kim, Jung, Kim, Kim, Ahn, and Song. (2014). Purification of an iron-chelating peptide from spirulina protein hydrolysates. *Journal of the Korean Society for Applied Biological Chemistry*, **57**(1), 91–95. https://doi.org/10.1007/s13765-013-4211-5

Kjærgaard, Schembri, and Klemm. (2001). Novel Zn^{2+}-chelating peptides selected from a fimbria-displayed random peptide library. *Applied and Environmental Microbiology*, **67**(12), 5467–5473. https://doi.org/10.1128/AEM.67.12.5467-5473.2001

Knecht, Ricklin, Eberle, and Ernst. (2009). Oligohis-tags: mechanisms of binding to Ni^{2+}-NTA surfaces. *Journal of Molecular Recognition*, **22**(4), 270–279. https://doi.org/10.1002/jmr.941

Knezevic, Langer, Hampel, Kaiser, Strasser, and Rant. (2012). Quantitation of affinity, avidity, and binding kinetics of protein analytes with a dynamically switchable biosurface. *Journal of the American Chemical Society*, **134**(37), 15225–15228. https://doi.org/10.1021/ja3061276

Korhonen, and Pihlanto. (2006). Bioactive peptides: production and functionality. *International Dairy Journal*, **16**(9), 945–960. https://doi.org/10.1016/j.idairyj.2005.10.012

Kozłowski, Kowalik-Jankowska, and Jeżowska-Bojczuk. (2005). Chemical and biological aspects of Cu^{2+} interactions with peptides and aminoglycosides. *Coordination Chemistry Reviews*, **249**(21–22), 2323–2334. https://doi.org/10.1016/j.ccr.2005.04.027

Ladbury, and Chowdhry. (1996). Sensing the heat: the application of isothermal titration calorimetry to thermodynamic studies of biomolecular interactions. *Chemistry and Biology*, **3**(10), 791–801. https://doi.org/10.1016/S1074-5521(96)90063-0

Lamshöft, and Ivanova. (2011). Protonation and coordination ability of small peptides – theoretical and experimental approaches for elucidation. *Journal of Coordination Chemistry*, **64**(14), 2419–2442. https://doi.org/10.1080/00958972.2011.598926

Langer, Hampel, Kaiser, Knezevic, Welte, Villa, Maruyama, Svejda, Jähner, Fischer, Strasser& Rant. (2013). Protein analysis by time-resolved measurements with an electro-switchable DNA chip. *Nature Communications*, **4**, 2099. https://doi.org/10.1038/ncomms3099

Langer, Schräml, Strasser, Daub, Myers, Heindl, and Rant. (2015). Polymerase/DNA interactions and enzymatic activity: multi-parameter analysis with electro-switchable biosurfaces. *Scientific Reports*, **5**, 1–15. https://doi.org/10.1038/srep12066

Layrisse, Martínez-Torres, Leets, Taylor, and Ramírez. (1984). Effect of histidine, cysteine, glutathione or beef on iron absorption in humans. *The Journal of Nutrition,* **114** (1): 217–23. https://doi.org/10.1093/jn/114.1.217

Lee, and Song. (2009). Purification of an iron-binding nona-peptide from hydrolysates of porcine blood plasma protein. *Process Biochemistry*, **44**(3), 378–381. https://doi.org/10.1016/j.procbio.2008.12.001

Le Vo, Le, Pham, Le, and Nguyen. (2018). Identification of a new calcium-binding peptide from enzymatic proteolysate of *Acetes japonicus*. *Journal of Food Processing and Preservation*, **42**(12), 2–7. https://doi.org/10.1111/jfpp.13837

Li, Jiang, and Huang. (2017). Protein hydrolysates as promoters of non-haem iron absorption. *Nutrients*, **9**(6), 1–18. https://doi.org/10.3390/nu9060609

Liao, Yang, Liu, Duan, Xiao, Liu, and Miao. (2019). The purification, identification and bioactivity study of a novel calcium-binding peptide from casein hydrolysate. Food 1 Function, 2019, **10**, 7724-7732. https://doi.org/10.1039/c9fo01383k

Liedberg, Nylander, and Lunström. (1983). Surface plasmon resonance for gas detection and biosensing. *Sensors and Actuators*, **4**, 299–304. https://doi.org/10.1016/0250-6874(83)85036-7

Lin, Deng, Huang, Li, and Song. (2016). The effect of ferrous-chelating hairtail peptides on iron deficiency and intestinal flora in rats. *Journal of the Science of Food and Agriculture*, **96**(8), 2839–2844. https://doi.org/10.1002/jsfa.7452

Liu, and Wilson. (2010). Quantitative analysis of small molecule–nucleic acid interactions with a biosensor surface and surface plasmon resonance detection. In "*Drug-DNA Interaction Protocols"*, edited by Keith R. Fox, 613,1–23. Totowa, NJ: Humana Press. https://doi.org/10.1007/978-1-60327-418-0_1

Liu, Yang, Zhao, and Yang. (2020). Isolation of antioxidant peptides from yak casein hydrolysate. RSC Advance, 34. https://doi.org/10.1039/d0ra02644a

Lönnerdal. Bioavailability of copper. (1996). *The American Journal of Clinical Nutrition*, **63**(5), 821S-829S. 10.1093/ajcn/63.5.821

Lv, Liu, Bao, Tang, Yang, and Guo. (2009). Identification and characteristics of iron-chelating peptides from soybean protein hydrolysates using IMAC-Fe^{3+}. *Journal of Agricultural and Food Chemistry*, **57**(11), 4593–4597. https://doi.org/10.1021/jf9000204

Maalouli, Gouget-Laemmel, Pinchemel, Bouazaoui, Chazalviel, Ozanam, Yang, Burkhard, Boukherroub, and Szunerits. (2011). Development of a metal-chelated plasmonic interface for the linking of His-peptides with a droplet-based surface plasmon resonance read-off scheme. *Langmuir*, **27**(9), 5498–5505. https://doi.org/10.1021/la2005437

Megías, Pedroche, Yust, Girón-Calle, Alaiz, Millán, and Vioque. (2007). Affinity purification of copper-chelating peptides from sunflower protein hydrolysates. *Journal of Agricultural and Food Chemistry*, **55**(16), 6509–6514. https://doi.org/10.1021/jf0712705

Megías, Pedroche, Yust, Girón-Calle, Alaiz, Millán, and Vioque. (2008). Production of copper-chelating peptides after hydrolysis of sunflower proteins with pepsin and pancreatin. *LWT - Food Science and Technology*, **41**(10), 1973–1977. https://doi.org/10.1016/j.lwt.2007.11.010

Merrifield. (1963). Solid Phase Peptide Synthesis. I. The synthesis of a tetrapeptide. *Journal of the American Chemical Society*, **85**(14), 2149–2154. https://doi.org/10.1021/ja00897a025

Meisel, Meisel, Fairweather-Tait, FitzGerald, Hartmann, Lane, McDonagh, Teucher, and Wal. (2003). Detection of caseinophosphopeptides in the distal ileostomy fluid of human subjects. *British Journal of Nutrition,* **89** (3): 351–58. https://doi.org/10.1079/BJN2002803

Mir, and Shinohara. (2013). Two-dimensional surface plasmon resonance imager: an approach to study neuronal differentiation. *Analytical Biochemistry*, **443**(1), 46–51. https://doi.org/10.1016/j.ab.2013.08.008

Moss. (2005). Guide for resin and linker selection in solid-phase peptide synthesis. *Current Protocols in Protein Science*, **40**(1), 18.7.1-18.7.19 https://doi.org/10.1002/0471140864.ps1807s40

Muhr, Pontvianne, Selmeczi, Paris, Boschi-Muller, and Canabady-Rochelle. (2020). Chromatographic separation simulation of metal-chelating peptides from surface plasmon resonance binding parameters. *Journal of Separation Science*, **43**(11), 2031-2041. https://doi.org/10.1002/jssc.201900882

Murariu, Dragan, and Drochioiu. (2010). Model peptide-based system used for the investigation of metal ions binding to histidine-containing polypeptides. *Biopolymers*, **93**(6), 497-508. https://doi.org/10.1002/bip.21385

Nakayama, Shinohara, Tanaka, Baba, Ogawa-Ohnishi, and Matsubayashi. (2017). A peptide hormone required for Casparian strip diffusion barrier formation in *Arabidopsis* roots. *Science*, **355**(6322), 284–286. https://doi.org/10.1126/science.aai9057

Navratilova, Papalia, Rich, Bedinger, Brophy, Condon, Deng, Emerick, Guan, Hayden, Heutmekers, Hoorelbeke, McCroskey, Murphy, Nakagawa, Parmeggiani, Qin, Rebe, Tomasevic, Tsang, Waddell, Zhang, Leavitt, and Myszka. (2007). Thermodynamic benchmark study using Biacore technology. *Analytical Biochemistry*, **364**(1), 67–77. https://doi.org/10.1016/j.ab.2007.01.031

Nieba, Nieba-Axmann, Persson, Hämäläinen, Edebratt, Hansson, Lidholm, Magnusson, Karlsson, Plückthun. (1997). Biacore analysis of histidine-tagged proteins using a chelating NTA sensor chip. *Analytical Biochemistry*, **252**(2), 217–228. https://doi.org/10.1006/abio.1997.2326

Nielsen, Fuglsang, and Westh. (2003). Isothermal titration calorimetric procedure to determine protein–metal ion binding parameters in the presence of excess metal ion or chelator. *Analytical Biochemistry*, **314**(2), 227–234. https://doi.org/10.1016/S0003-2697(02)00655-3

Ortega, Carmona, Llorens, and Solari. (2012). X-ray absorption spectroscopy of biological samples. A tutorial. *Journal of Analytical Atomic Spectrometry*, **27**(12), 2054. https://doi.org/10.1039/c2ja30224a

Pallauf, Pietsch, and Rimbach. (1998). Dietary phytate reduces magnesium bioavailability in growing rats. *Nutrition Research*, **18**(6), 1029–1037. https://doi.org/10.1016/S0271-5317(98)00085-2

Palomo. (2014). Solid-phase peptide synthesis: an overview focused on the preparation of biologically relevant peptides. *RSC Advances*, **4**(62), 32658–32672. https://doi.org/10.1039/C4RA02458C

Paradís-Bas, Tulla-Puche, and Albericio. (2016). The road to the synthesis of "difficult peptides." *Chemical Society Reviews*, **45**(3), 631–654. https://doi.org/10.1039/C5CS00680E

Paris, Selmeczi, Chaimbault, Desobry, Canabady-Rochelle. Optimization of a LCMS Method for screening of iron-chelating peptides by differential mass spectrometry analysis. Pittcon Conference, Chicago, Mc Cormick place, 1-5 Marsh 2020. Oral communication.

Pattabiraman, and Bode. (2011). Rethinking amide bond synthesis. *Nature*, **480**(7378), 471–479. https://doi.org/10.1038/nature10702

Pearson. (1963). Hard and soft acids and bases. *Journal of the American Chemical Society*, **85**(22), 3533–3539. https://doi.org/10.1021/ja00905a001

Pedersen, Tofteng, Malik, and Jensen. (2012). Microwave heating in solid-phase peptide synthesis. *Chemical Society Reviews*, **41**(5), 1826–1844. https://doi.org/10.1039/C1CS15214A

Peng, Hou, Zhang, and Li. (2017). Effect of calcium-binding peptide from Pacific cod (*Gadus macrocephalus*) bone on calcium bioavailability in rats. *Food Chemistry*, **221**, 373–378. https://doi.org/10.1016/j.foodchem.2016.10.078

Perego, Zabeo, Marasco, Giussani, Fiorilli, Tettamanti, and Ferraretto. (2013). Casein phosphopeptides modulate calcium uptake and apoptosis in Caco2 cells through their interaction with the TRPV6 calcium channel. *Journal of Functional Foods,* **5** (2): 847–57. https://doi.org/10.1016/j.jff.2013.01.032

Pereira, and Vicente. (2013). Meat nutritional composition and nutritive role in the human diet. *Meat Science*, **93**(3), 586–592. https://doi.org/10.1016/j.meatsci.2012.09.018

Pérès, Bouhallab, Bureau, Neuville, Maubois, Devroede, Arhan, and Bouglé. (1999). Mechanisms of absorption of caseinophosphopeptide bound iron. *The Journal of Nutritional Biochemistry,* **10** (4): 215–22. https://doi.org/10.1016/S0955-2863(98)00101-6

Polavarapu. (2017). Chiroptical Spectroscopy. Boca Raton: CRC Press. 448 pages. https://doi.org/10.1201/9781315374888

Porath, Carlsson, Olsson, and Belfrage. (1975). Metal chelate affinity chromatography, a new approach to protein fractionation. *Nature*, **258**(5536), 598–599. https://doi.org/10.1038/258598a0

Rant. (2012). Sensing with electro-switchable biosurfaces. *Bioanalytical Reviews*, **4**(2–4), 97–114. https://doi.org/10.1007/s12566-012-0030-0

Rant, Arinaga, Scherer, Pringsheim, Fujita, Yokoyama, Tornow, and Abstreiter. (2007). Switchable DNA interfaces for the highly sensitive detection of label-free DNA targets. *Proceedings of the National Academy of Sciences of the United States of America*, **104**(44), 17364–17369. https://doi.org/10.1073/pnas.0703974104

Rascio, and Navari-Izzo. (2011). Heavy metal hyperaccumulating plants: How and why do they do it? And what makes them so interesting? *Plant Science*, **180**(2), 169–181. https://doi.org/10.1016/j.plantsci.2010.08.016

Rauser. (1995). Phytochelatins and related peptides (structure, biosynthesis, and function). *Plant Physiology*, **109**(4), 1141–1149. https://doi.org/10.1104/pp.109.4.1141

Reinhold, Lahimgarzadeh, Nasr, and Hedayati. (1973). Effects of purified phytate and phytate-rich bread upon metabolism of zinc, calcium, phosphorus, and nitrogen in man. *The Lancet*, **301**(7798), 283–288. https://doi.org/10.1016/S0140-6736(73)91538-9

Rich, and Myszka. (2011). Survey of the 2009 commercial optical biosensor literature. *Journal of Molecular Recognition*, **24**(6), 892–914. https://doi.org/10.1002/jmr.1138

Rich, Bombarda, Schenk, Lee, Cox, Spuches, Hudson, Kieffer, and Wilcox. (2012). Thermodynamics of Zn^{2+} binding to Cys_2His_2 and $Cys_2HisCys$ zinc fingers and a Cys_4 transcription factor site. *Journal of the American Society*, **134**, 10405-10418. https://doi.org/10.1021/ja211417g

Rivera-Mancía, Pérez-Neri, Ríos, Tristán-López, Rivera-Espinosa,and Montes. (2010). The transition metals copper and iron in neurodegenerative diseases. *Chemico-Biological Interactions*, **186**(2), 184–199. https://doi.org/10.1016/j.cbi.2010.04.010

Rodzik, Pomastowski, Sagandykova, and Buszewski. (2020). Interactions of whey proteins with metal ions. *International Journal of Molecular Sciences*, **21**(6), 2156. https://doi.org/10.3390/ijms21062156

Rolinger, Rüdt, and Hubbuch. (2020). A critical review of recent trends, and a future perspective of optical spectroscopy as PAT in biopharmaceutical downstream processing. *Analytical and Bioanalytical Chemistry*, **412**(9), 2047–2064. https://doi.org/10.1007/s00216-020-02407-z

Sacco, Skowronsky, Gade, Kenney, Spuches. (2012). Calorimetric investigation of copper(II) binding to Ab peptides: thermodynamics of coordination plasticity. Journal of Biollogical Inorganic Chemistry, **17**:531–541. https://doi.org/10.1007/s00775-012-0874-3

Sahu, McCarrick, and Lorigan. (2013). Use of Electron Paramagnetic Resonance to solve biochemical problems. *Biochemistry*, **52**(35), 5967–5984. https://doi.org/10.1021/bi400834a

Sandblad, Arnell, Samuelsson, and Fornstedt. (2009). Approach for reliable evaluation of drug proteins interactions using surface plasmon resonance technology. *Analytical Chemistry*, **81**(9), 3551–3559. https://doi.org/10.1021/ac900299p

Sato, Noguchi, and Naito. (1985). The formation and iron-binding property of phosphopeptides in the small intestinal contents of rats fed egg yolk diet. *Nutrition Reports International*, **31** (1): 245–52.

Sheftic, Snell, Jha, Alexandrescu. (2012). Inhibition of semen-derived enhancer of virus infection (SEVI) fibrillogenesis by zinc and copper. *European Biophysical Journal*, **41**:695-704. https://doi.org/10.1007/s00249-012-0846-0

Schalley, and Armentrout. (2003). Modern Mass Spectrometry. (Christoph A. Schalley, Ed.) (Vol. 225). Berlin: Springer.

Schiedel, Daub, Itzen, and Jung. (2020). Validation of the slow off-kinetics of sirtuin-rearranging ligands (SirReals) by means of label-free electrically switchable nanolever technology. *ChemBioChem*, **21**(8), 1161–1166. https://doi.org/10.1002/cbic.201900527

Selmeczi, Gizzi, Champmartin, Rubini, Aubert, Dahaoui, Henry. (2010). Nickel(II)-Dipeptidoamine-Based Tetrameric Complex: Structural Study in Solution and in Solid State. *Inorganic Chemistry*, **49**(18), 8222-8229. https://doi.org/10.1021/ic101167f

Shankaran, Gobi, and Miura. (2007). Recent advancements in surface plasmon resonance immunosensors for detection of small molecules of biomedical, food and environmental interest. *Sensors and Actuators B: Chemical*, **121**(1), 158–177. https://doi.org/10.1016/j.snb.2006.09.014

Shimazaki, Takani, and Yamauchi. (2009). Metal complexes of amino acids and amino acid side chain groups. Structures and properties. *Dalton Transactions*, (38), 7854. https://doi.org/10.1039/b905871k

Sigel, and Martin. (1982). Coordinating properties of the amide bond. Stability and structure of metal ion complexes of peptides and related ligands. *Chemical Reviews*, **82**(4), 385–426. https://doi.org/10.1021/cr00050a003

Slavin, and Marlett. (1980). Influence of refined cellulose on human bowel function and calcium and magnesium balance. *The American Journal of Clinical Nutrition*, **33**(9), 1932–1939. https://doi.org/10.1093/ajcn/33.9.1932

Sóvágó, Kállay, and Várnagy. (2012). Peptides as complexing agents: Factors influencing the structure and thermodynamic stability of peptide complexes. *Coordination Chemistry Reviews*, **256**(19–20), 2225–2233. https://doi.org/10.1016/j.ccr.2012.02.026

Sóvágó, and Ősz,. (2006). Metal ion selectivity of oligopeptides. *Dalton Transactions*, (32), 3841–3854. https://doi.org/10.1039/B607515K

Sóvágó, Várnagy, Lihi, and Grenács. (2016). Coordinating properties of peptides containing histidyl residues. *Coordination Chemistry Reviews*, **327–328**, 43–54. https://doi.org/10.1016/j.ccr.2016.04.015

Straub. (2007). Calcium supplementation in clinical practice: a review of forms, doses, and indications. *Nutrition in Clinical Practice*, **22**(3), 286–296. https://doi.org/10.1177/0115426507022003286

Sun, Cui, Jin, Wu, Wang, and Lin. (2017). Contributions of molecular size, charge distribution, and specific amino acids to the iron-binding capacity of sea cucumber (*Stichopus japonicus*) ovum hydrolysates. *Food Chemistry*, **230**, 627–636. https://doi.org/10.1016/j.foodchem.2017.03.077

Sun, Yu, Xu, Li, Xiao, Yin, Cao, Han, and He. (2013). Putative cobalt- and nickel-binding proteins and motifs in Streptococcus pneumoniae. *Metallomics*, **5**(7), 928. https://doi.org/10.1039/c3mt00126a

Tabak, Sartor, and Cavatorta. (1989). On the interactions of metal ions with tryptophan and glyciltryptophan: A fluorescence study. *Journal of Luminescence*, **43**(6), 355–361. https://doi.org/10.1016/0022-2313(89)90038-0

Tam, Zeenathul, Rezaei, Mustafa, Azmi, Bahaman, Lo, Hani, and Rasedee. (2017). Wide dynamic range of surface-plasmon-resonance-based assay for hepatitis B surface antigen antibody optimal detection in comparison with ELISA. *Biotechnology and Applied Biochemistry*, **64**(5), 735–744. https://doi.org/10.1002/bab.1528

Torres-Fuentes, C., Alaiz, M., and Vioque, J. (2011). Affinity purification and characterisation of chelating peptides from chickpea protein hydrolysates. *Food Chemistry*, **129**(2), 485–490. https://doi.org/10.1016/j.foodchem.2011.04.103

Treiber, Thompsett, Pipkorn, Brown, and Multhaup. (2007). Real-time kinetics of discontinuous and highly conformational metal-ion binding sites of prion protein. *JBIC Journal of Biological Inorganic Chemistry*, **12**(5), 711–720. https://doi.org/10.1007/s00775-007-0220-3

Valeur, and Bradley. (2009). Amide bond formation: beyond the myth of coupling reagents. *Chemical Society Reviews*, **38**(2), 606–631. https://doi.org/10.1039/B701677H

Van de Weert, and Stella. (2011). Fluorescence quenching and ligand binding: A critical discussion of a popular methodology. *Journal of Molecular Structure*, **998**(1–3), 144–150. https://doi.org/10.1016/j.molstruc.2011.05.023

Vanhooren, Vanhee, Noyelle, Majer, Joniau, and Hanssens. (2002). Structural basis for difference in heat capacity increments for Ca^{2+} binding to two α-lactalbumins. *Biophysical Journal*, **82**(1), 407–417. https://doi.org/10.1016/S0006-3495(02)75405-2

Varnava, and Sarojini. (2019). Making solid-phase peptide synthesis greener: a review of the literature. *Chemistry – An Asian Journal*, **14**(8), 1088–1097. https://doi.org/10.1002/asia.201801807

Vavrusova, and Skibsted. (2014). Calcium nutrition, bioavailability and fortification. *LWT - Food Science and Technology*, **59**(2), 1198–1204. https://doi.org/10.1016/j.lwt.2014.04.034

Vegarud, Langsrud, and Svenning. (2000). Mineral-binding milk proteins and peptides; occurrence, biochemical and technological characteristics. *British Journal of Nutrition*, **84**(S1), 91–98. https://doi.org/10.1017/S0007114500002300

Verlander. (2007). Industrial applications of solid-phase peptide synthesis – A status report. *International Journal of Peptide Research and Therapeutics*, **13**(1–2), 75–82. https://doi.org/10.1007/s10989-006-9075-7

Vormann. (2003). Magnesium: nutrition and metabolism. *Molecular Aspects of Medicine*, **24**(1–3), 27–37. https://doi.org/10.1016/S0098-2997(02)00089-4

Wang, Huang, and Jiang. (2013). Optimization of hydrolysis conditions for the production of iron-binding peptides from mackerel processing byproducts. *Advance Journal of Food Science and Technology*, **5**(7), 921–925. https://doi.org/10.19026/ajfst.5.3183

Wasserman. (2004). Vitamin D and the dual processes of intestinal calcium absorption. *The Journal of Nutrition*, **134**(11), 3137–3139. https://doi.org/10.1093/jn/134.11.3137

Wong, Albright, and Wang. (1991). Immobilized metal ion affinity chromatography (IMAC): chemistry and bioseparation applications. *Separation and Purification Methods*, **20**(1), 49–106. https://doi.org/10.1080/03602549108021408

Wood. (1902). On a remarkable case of uneven distribution of light in a diffraction grating spectrum. *Proceedings of the Physical Society of London*, **18**(1), 269–275. https://doi.org/10.1088/1478-7814/18/1/325

Wu. (2010). "Amino acids – Biochemistry and Nutrition", 1st Ed., CRC Press, Boca Raton. https://doi.org/10.1201/b14661

Wu, Liu, Zhao, and Zeng. (2012). Enzymatic preparation and characterization of iron-chelating peptides from anchovy (*Engraulis japonicus*) muscle protein. *Food Research International*, **48**(2), 435–441. https://doi.org/10.1016/j.foodres.2012.04.013

Wu, Li, Hou, Zhang, and Zhao. (2017). Identification of iron-chelating peptides from pacific cod skin gelatin and the possible binding mode. *Journal of Functional Foods*, **35**, 418–427. https://doi.org/10.1016/j.jff.2017.06.013

Wu, Sun, Ding, Zhu, and Lin. (2019). Evaluation and structure–activity relationship analysis of antioxidant shrimp peptides. Food & Function, **10**, 5605-5615. https://doi.org/10.1039/C9FO01280J

Xie, Huang, Li, Cheng, Wang, Yin, and Yan. (2015). Affinity purification and characterization of zinc chelating peptides from rapeseed protein hydrolysates: possible contribution of characteristic amino acid residues. *Food Chemistry*, **173**, 210–217. https://doi.org/10.1016/j.foodchem.2014.10.030

Xuan, Scheuermann, Meda, Hayen, von Wirén, and Weber. (2006). Separation and identification of phytosiderophores and their metal complexes in plants by zwitterionic hydrophilic interaction liquid chromatography coupled to electrospray ionization mass spectrometry. *Journal of Chromatography A*, **1136**(1), 73–81. https://doi.org/10.1016/j.chroma.2006.09.060

Zhao, Huang, Huang, Lin, Wang, Huang, Hong, and Rao. (2014). Novel peptide with a specific calcium-binding capacity from whey protein hydrolysate and the possible chelating mode. *Journal of Agricultural and Food Chemistry*, **62**(42), 10274–10282. https://doi.org/10.1021/jf502412f

Zheng, Li, Zhang, and Zhao. (2016). Purification, characterization and synthesis of antioxidant peptides from enzymatic hydrolysates of coconut (*Cocos nucifera* L.) cake protein isolates. RSC Advances, **6**(59), 54346-54356. https://doi.org/10.1039/C6RA07086H

Zidane, Matéos, Cakir-Kiefer, Miclo, Rahuel-Clermont, Girardet, and Corbier. (2012). Binding of divalent metal ions to 1-25 □-caseinophosphopeptide: an isothermal titration calorimetry study. *Food Chemistry*, **132**(1), 391–398. https://doi.org/10.1016/j.foodchem.2011.11.006

2.2 Ferroptosis: A cell death mechanism driven by Iron overload

2.2.1 Introduction

The definition of cell death was first coined in 1858 by the biologist Rudolf Virchow, but the apoptosis mechanism (programmed cell death) was only elucidated in the 20th century. Besides canonical mechanisms of cell death (apoptosis, necrosis), more exotic ones such as efferocytosis, necroptosis, pyroptosis, parthanatos, and ferroptosis have been described. Ferroptosis is a non-apoptotic cell death characterized by lipid peroxidation catalysed by iron-overload. In this bibliographic part, we answer questions concerning ferroptosis milestones, its importance in physiopathologic mechanisms and its downstream regulatory mechanisms.

2.2.2 Lipid peroxidation

Lipids are fundamental building blocks of cells as key components of the plasma membrane and membranes of cell compartments such as the nucleus, the endoplasmic reticulum, the Golgi apparatus, and trafficking vesicles (endosomes and lysosomes). Unsaturated lipids are sensitive to uncontrolled oxidative stress that causes lipid peroxidation. The process of lipid peroxidation involves 3 main steps: initiation, propagation, and termination **(Figure 2.11)**. For initiation, the lipid (L-H) is attacked by highly reactive species such as the hydroxyl radical $OH^{\bullet}$, which pulls a hydrogen atom from the lipid converting it to a radical ($L^{\bullet}$). $L^{\bullet}$ quickly reacts with dioxygen (O_2) and thus forms a lipid peroxyl radical ($LOO^{\bullet}$), which in turn extracts a hydrogen from another L-H to form lipid hydroperoxide (LOOH) and a new $L^{\bullet}$. This is the propagation step. Termination happens when a high concentration of lipid radical species is reached, so the probability of collision between two of them is high. When 2 radical lipid species interact ($2L^{\bullet}$, $2LOO^{\bullet}$, $L^{\bullet}$ + $LOO^{\bullet}$), a non-radical species is formed. (Ayala, Muñoz, and Argüelles 2014; Yin, Xu, and Porter 2011) Reactive aldehydes such as malondialdehyde (**MDA**) and 4-hydroxynonenal (**HNE**) are products formed due to the decomposition of lipid peroxides and that can be mutagenic and carcinogenic (Guéraud *et al.,* 2010; Negre-Salvayre *et al.,* 2010; Vaca, Wilhelm, and Harms-Ringdahl 1988). If lipid peroxidation is not rapidly terminated,

damage for cell membranes takes place. Moreover, lipid peroxidation is involved in the initiation and development of pathologies such as atherosclerosis. Atherosclerosis is a cardiovascular disease induced by an accumulation of oxidized lipids in the vascular wall forming atherosclerotic plaques. The early stage of plaque formation involves the oxidation of low-density lipoproteins (**LDL**), which attracts macrophages. Those macrophages phagocyte oxidized LDL forming foam cells, that compose the atherosclerotic plaque (Benzie 1996; Natto, Kawamura, and Yamamoto 1993; Nilsson *et al.,* 1992).

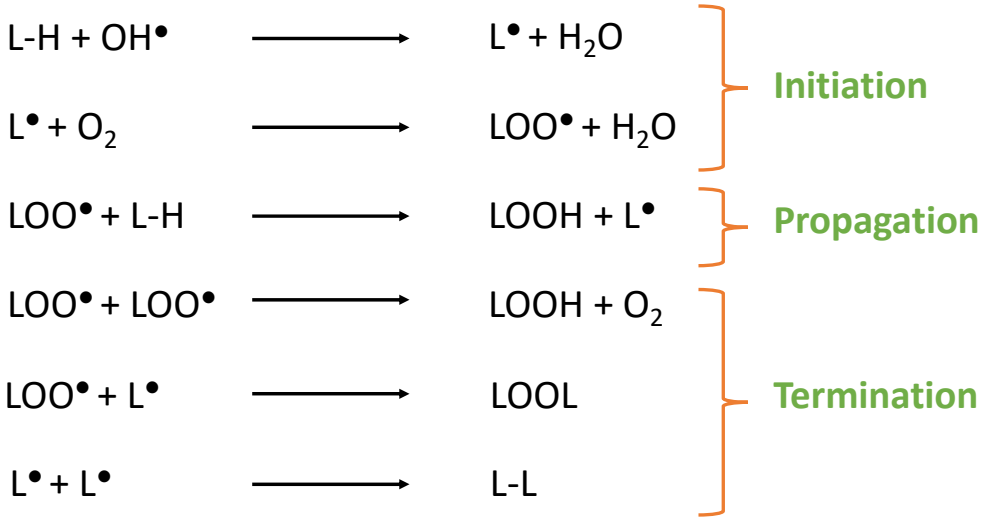

Figure 2.11. Process of lipid peroxidation

2.2.3 Iron catalysed lipid peroxidation in cells

Iron is an important trace element for cell functions (Abbaspour, Hurrell, and Kelishadi 2014). However, its distribution and content should be controlled constantly in order to prevent iron overload or iron deficiency related diseases (Yiannikourides and Latunde-Dada 2019). The safety of iron uptake is already presented in part 1. Iron is absorbed by the intestines at the duodenum and proximal jejunum level, where it exists in its ferrous (Fe^{2+}) form because of the low pH (~ 5-6) in the duodenum. When absorbed, Fe^{2+} is oxidized to Fe^{3+} by hephaestin and ceruloplasmin in the blood. The majority of iron is transported and stored as a complex with proteins. Indeed, in the bloodstream, Fe^{3+} binds to transferrin protein as a transport protein, which distributes Fe^{3+} to tissues by binding to transferrin receptors on the plasma membrane of target cells. The transferrin-Fe^{3+} complex is then endocytosed. The low pH of endocytosis

vesicles associated with a ferrireductase reduce Fe^{3+} to Fe^{2+}. Inside cells, Fe^{2+} is stored in ferritin and/or the labile iron pool (**LIP**) (Ems, St Lucia, and Huecker 2021; Knutson 2017; Andrews and Schmidt 2007). Free iron ions (Fe^{2+} and Fe^{3+}) provokes harmful reactions with proteins, nucleic acids and lipids in membrane. Notably, iron excess participates to lipid peroxidation *via* hydroxyl-dependent and hydroxyl-independent mechanisms (Minotti and Aust 1987). In the first mechanism, Fe^{2+} is oxidized in Fe^{3+} by hydrogen peroxide H_2O_2 through the Fenton reaction that also produces hydroxyl radical $OH^{\bullet}$. In cells, Fe^{3+} produced by the Fenton reaction can be reduced back to Fe^{2+} by the oxidation of $O_2^{\bullet-}$ to O_2 originating a catalytic cycle (Fenton, 1894). The formed hydroxyl radical is a highly reactive oxidant (half-life of 10^{-9} s) extracting hydrogen atom from lipid molecules and starting lipid peroxidation as previously mentioned (Yaman and Ayhanci 2021).

In the second mechanism, scientists argue that iron-oxygen complexes, *i.e.,* preferryl and ferryl ions, are strong oxidants that can initiate lipid peroxidation alone (Aruoma *et al,.* 1989). Moreover, during the propagation step of lipid peroxidation, Fe^{2+} can react with LOOH to form alkoxyl radical ($LO^{\bullet}$), which is believed to extract a hydrogen atom from L-H and thus starting another chain of lipid peroxidation (Gardner 1989).

2.2.4 Discovery of ferroptosis and speed of research in this field

The mechanism leading to ferroptosis has evolved from a sequence of atmospheric and ecological events. Since the early days on earth, trace amounts of oxygen was produced from photosynthesis, and then became abundant after the Great Oxygenation Event (Blaustein 2016). O_2 is a strong oxidant that needs to be activated to be reactive. For example, O_2 is a last acceptor of electrons and protons produced by the respiratory chain. The Great Oxygenation Event was the starting point for the formation of free radicals inside eukaryotic cells (Carter 2003). The polyunsaturated fatty acids **(PUFA**) of cell lipid membrane are very susceptible to lipid peroxidation and the abundant iron-dependent cellular mechanisms made this oxidation phenomenon even faster (Fischer, Hemp, and Valentine 2016). Early cell studies suggested the evolution of defense mechanisms to counteract the iron/oxygen-driven lipid peroxidation or to cause cell death (Benzie 2000). Therefore, ferroptosis is an ancestral type of cell death, that was discovered in 2012 by Dixon through pharmacological approaches. Dixon proposed this mechanism as a possible cancer therapy (Dixon *et al*., 2012). Several

complex discoveries have led to the current definition of ferroptosis mechanism. The timeline of these discoveries is presented in **Figure 2.12**. Ferroptosis comes from the Latin word "Ferrum" meaning "iron", and the Greek word "ptosis" that means "to fall" (Sun *et al.,* 2020). It is an emerging form of cell death with 1,285 articles published between 2012 and 2020, where lipid peroxidation catalyzed by iron overload is the main hallmark (Yang and Stockwell 2016). Research concerning targeted cancer therapy *via* ferroptosis is well-advancing. A lot of ferroptosis inducers are spotlighted in recent research for their actions against cancer (Valashedi *et al.,* 2021; Liang *et al.,* 2019). However, the implication and treatment of ferroptosis in several diseases is still an ill-defined subject. According to PubMed statistics, 616 articles concerned with ferroptosis inducers are published, and on the other hand, 279 articles about ferroptosis inhibitors are published in 2021 ("PubMed" n.d.) .

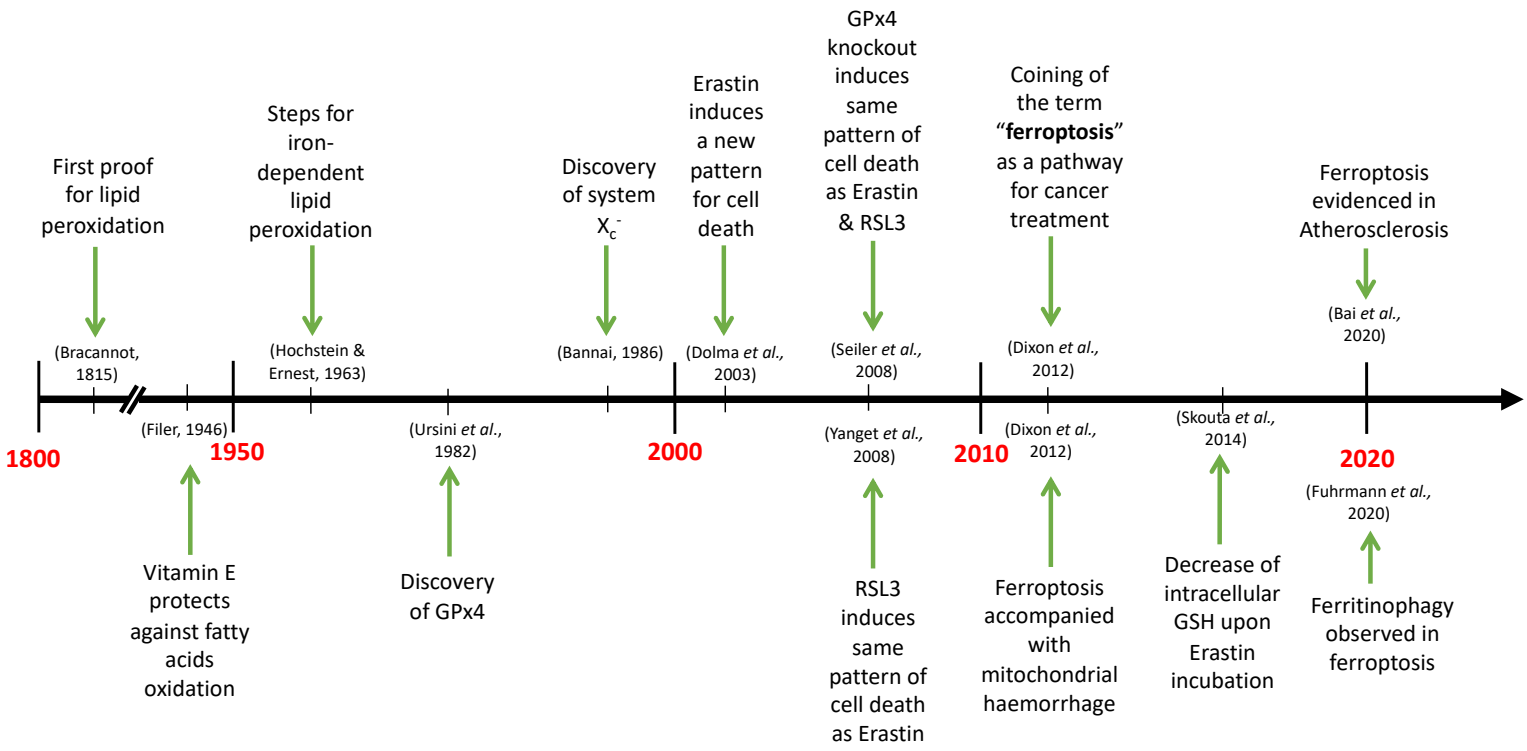

Figure 2.12. Timeline for the major discoveries concerning ferroptosis

2.2.5 Morphological and biochemical features of ferroptosis

Ferroptosis is a regulated form of cell death with distinct morphological and biochemical feature from apoptosis and necrosis (**Table 2.2**). Ferroptosis can propagate to adjacent cells, which are swollen, rounded up and detached from each other *(Riegman et al., 2020; Dixon et al.,* 2012; Yagoda et al. 2007). Nuclear integrity is maintained but chromatin condensation is missing during ferroptosis (Friedmann Angeli *et al.,* 2014). Mitochondrial alterations are the most obvious changes observed during ferroptosis. The mitochondria appears small sized with thick membrane density and reduced crista that will eventually lead to its destruction (Jie Li *et al.,* 2020; Dixon *et al.,* 2012; Dolma *et al.,* 2003). In physiological condition, mitochondrial iron content is regulated by iron exporters and mitochondrial ferritin. However, the mitochondrial iron content is very high in certain ferroptosis-related diseases or in ferroptosis-induced cancer cells (An *et al.,* 2021; Karmi *et al.,* 2021; Alim *et al.,* 2019; Homma, Kobayashi, and Fujii 2020). Iron overload is accompanied with increased mitochondrial ROS production and reduced mitochondrial GSH content (Karmi *et al.,* 2021; Jang *et al.,* 2021; Dixon *et al.,* 2014). Decreased mitochondrial potential and increased mitochondrial permeability are other ferroptosis signs (Chen *et al,*. 2021; Wei *et al.,* 2020). Recently, Jingyi Guo *et al.,* 2021 showed that inhibiting the replication of mitochondrial DNA can induce ferroptosis. Internal lysosomal autophagy of ferritin is also observed in ferroptotic cells. This mechanism is called "ferritinophagy" (Fuhrmann *et al.,* 2020; Wei *et al.,* 2020). Ferroptosis is similar to H_2O_2-induced necrosis by the rupture of plasma membrane but is not accompanied by ATP depletion (Stockwell *et al.,* 2017; Dixon *et al.,* 2012; H. Yang *et al.,* 2010). All in all, ferroptotic cells accumulate iron, lipid peroxides, oxidized NADPH and glutamate. They are depleted in cystine/cysteine and GSH (Mou *et al.,* 2019; J. Li *et al.,* 2020; Shimada *et al.,* 2016a).

Table 2.2. Comparison between apoptosis, necrosis and ferroptosis cell deaths

	Apoptosis	Necrosis	Ferroptosis
Signaling pathway	Physiological caspase-dependent process	Pathological process caused by external toxins	Iron and ROS-dependent process
Biochemical features	Caspase activation DNA fragmentation	Drop in ATP levels	Iron, lipid peroxides and glutamate accumulations GSH and GPx4 downregulations Cysteine/Cystine depletion
Morphology	Cell shrinkage Release of apoptotic bodies	Break down of plasma membrane Inflammation Organelle swelling	Shrunken mitochondria Vanishing of mitochondial crista Ferritinophagy

For properly functioning of cells, biomolecular regulations are fundamental processes that adapt to internal and external environments. Cell oxidation caused by aerobic respiration is a physiologic phenomenon that maintains cell redox homeostasis. Impairments in the homeostatic control between cell oxidation and reduction reactions cause oxidative stress eventually leading to lipid peroxidation and ferroptosis (**Figure 2.13**).

The regulation of intracellular iron content is an important factor for resisting to ferroptosis. Cell iron content is regulated at genes, cytosolic and plasma membrane levels. Indeed, the Iron responsive element protein 2 (**IREBP2**) gene encodes for the iron-responsive element binding protein (**IRE-BP**) that binds to iron-responsive elements (stem loop RNA structures) of many genes such as ferritin heavy chain 1 (**FTH1**) and transferrin receptor (**TFRC**) to control cell iron homeostasis. So, variants in the IREBP2 gene affect the physiological cell iron metabolism and can aid in ferroptosis (Dixon *et al.,* 2012). In the cytosol, ferritinophagy is caused by the upregulation of autophagy-related proteins (**ATG5 and ARC7**), that will release the ferritin-stored iron and thus induce ferroptosis (Hou *et al.,* 2016). Finally, at the plasma membrane, a too high activity of transferrin and transferrin receptor mediates ferroptosis by iron overload inside cells (Gao *et al.,* 2015)

The hallmark of ferroptosis might also be modulated by enzymes implicated in lipid peroxidation processes. Indeed, several cell knockout studies for Acyl-Co1 synthase long-chain family 4 (**ACSL4**) and lysophosphatidyl choline acyl transferase 3 (**LPCAT3**), implicated in the oxidation of membrane constituted of poly-unsaturated fatty acids (Doll *et al.,* 2017; Dixon *et al.,* 2015), revealed resistance for ferroptosis. In addition, lipoxygenase (**LOX**) is a ferroptosis-promoting enzyme that can oxidize phosphatidylethanolamine found in cell membranes (Yang *et al.,* 2016). In a study, Shah *et al.,* (2018) have overexpressed LOX enzyme in kidney human cells by transfection with recombinant DNA resulting in a higher sucepptibility of cells to ferroptosis. Finally, the antioxidant enzyme, glutathione peroxidase 4 (**GPx4**) can reduce peroxidized lipids and thus prevents ferroptosis (*Park et al.,* 2019). Indeed, among the eight human GPxs, GPx4 is the only one that can reduce oxidized phospholipids in membranes, thus its catalytic activity is critically important for cell health and the conditional deficiency of GPx4 in cells causes ferroptosis (*Park et al.,* 2019). GPx4 is a selenoprotein, which requires selenocysteine for its antioxidant activity (Doll and Conrad, 2017). Isopentenyl-PP is an intermediate by-product of the mevalonate pathway that is essential for the synthesis of selenoproteins (Fradejas *et al.,* 2013). The mevalonate pathway produces in addition the coenzyme Q_{10}, which has an antioxidant function at membrane level (Shimada *et al.,* 2016a). Depletion of selenium provokes ferroptosis due to GPx4 misfunctioning (Cardoso *et al.,* 2017). Moreover, the activity of GPx4 strongly relies on the content of GSH inside cells (Ursini and Maiorino, 2020).

The synthesis of intracellular GSH requires cysteine metabolism and/or uptake (Gaucher *et al.,* 2018), which can be either provided *via* the transsulfuration pathway where methionine is converted to *S*-adenosylhomocysteine and cysteine (Mou *et al.,* 2019) or *via* transmembrane proteins responsible for intracellular cysteine transport such as the L-aminoacid transporter (**L-AT**) or the system X_c^-. The system X_c^- is a glutamate/cystine antiporter critical for providing cystine to cells. Cystine is then reduced to cysteine, which is required for GSH synthesis.

In summary, ferroptosis is an intrinsic cellular event that can be modulated by the cell's autonomous properties including iron metabolism and redox reactions. However, the discovery and the understanding of ferroptosis is being initiated in several studies through the action of pharmacological ferroptosis inducers and inhibitors.

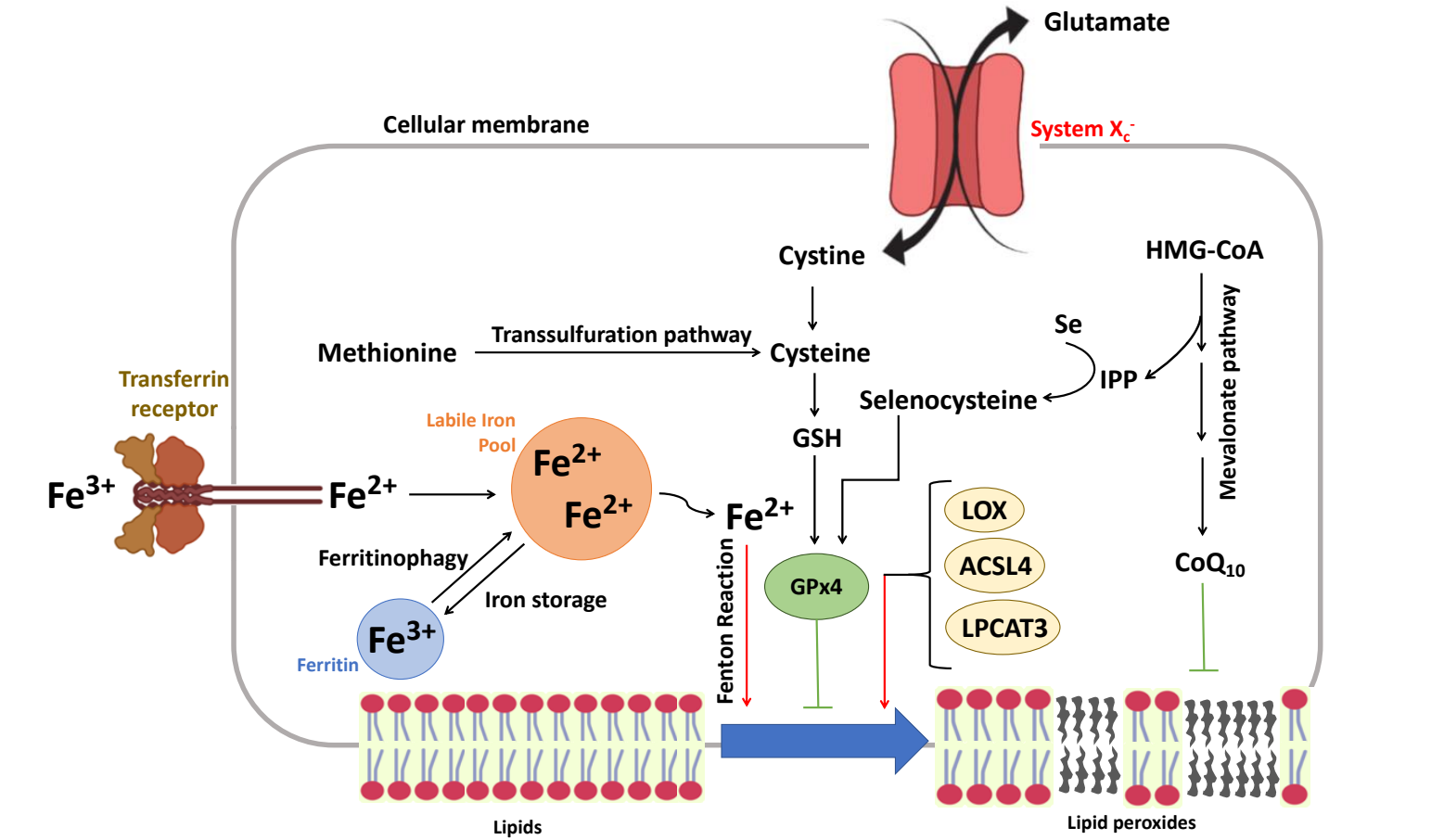

Figure 2.13. Network of ferroptosis signalling pathways

2.2.6 Pharmacological modulation of ferroptosis

2.2.6.1 Ferroptosis inducers

Ferroptosis, as previously clarified, was first discovered as a novel therapeutic approach to kill cancer cells using pharmacological reagents (Dixon *et al.,* 2012). Nowadays, a variety of reagents is used to induce ferroptosis whether to treat cancer or to clarify cell pathways implicated in its development (**Figure 2.14**). Ferroptosis inducers are reviewed in several publications (Hassannia, Vandenabeele, and Berghe, 2019; Stockwell *et al.,* 2017; Cao and Dixon, 2016). The two most popular targets for ferroptosis inducers are, the system X_c^- and the GPx4 (**Figure 2.15**). Inhibitors of the system X_c^- such as erastin, sulfasalazine and sorafenib are class 1 ferroptosis inducing compounds (**FIN I**), whereas inhibitors of GPx4 such as Ras selective lethal 3 (**RSL3**) are class 2 ferroptosis inducing compounds (**FIN II**).

Blocking the system X_c^- is a well-known mechanism to provoke ferroptosis (Dixon *et al.,* 2014). To that purpose, different strategies are at our disposal such as glutamate excess as well as glutaminolysis pathway (Gao *et al.,* 2015), and system X_c^- direct inhibition by erastin. Erastin is a well-known inhibitor of the system X_c^- decreasing the intracellular concentration of GSH (Yang *et al.,* 2014; Skouta *et al.* 2014). It was initially described as a cancer cell killer *via* a pathway different from apoptosis (Dolma *et al.,* 2003), which was lately identified as ferroptosis (Dixon *et al.,* 2012). Erastin-induced ferroptosis can promote endoplasmic reticulum stress (Riegman *et al.,* 2020). Indeed, Erastin has been shown to enhance cell sensitivity to chemotherapy in lung cancer, rhabdomyosarcoma and glioblastoma models (Jipeng Guo *et al.,* 2018; Pennafort *et al.,* 2018; Chen *et al.,* 2015; Yamaguchi *et al.,* 2013) and to alleviate cell resistance to chemotherapeutic drugs in head, neck and ovarian cancer cell (Sato *et al.,* 2018; Roh *et al.,* 2016). Erastin is also a radiosensitizer in radiotherapy (Pan *et al.,* 2019; Shibata *et al.,* 2019; Cobler *et al.,* 2018). However, erastin is rarely tested *in vivo* because of its poor water solubility. Piperazine-erastin (**PE**) and imidazole ketone Erastin **(IKE**) are water soluble erastin-based compounds. PE was shown to decrease tumor cell growth in mice, and IKE induced ferroptosis in B cell lymphoma model (Zhang *et al.,* 2019; Yang *et al.* 2014). Sulfasalazine and sorafenib are also pharmacological reagents that induces ferroptosis in several cancer types by inactivating the system X_c^- (Takayama *et al.,* 2016; Ma *et al.* 2015; Dixon *et al.,* 2014; Lachaier *et al.,* 2014; Louandre *et al.,* 2013; Guo *et al.,* 2011; Gout *et al.,* 2001). However, erastin has a higher inhibitory effect on system X_c^- than the two other

molecules (Dixon *et al.,* 2014). Other pathways have been explored that have similar result to blocking the system X_c^- . Cramer *et al.,* (2017) treated lymphatic leukaemia by engineering "cyst(e)inase", which degrades cellular cystine required for GSH production. Also, GSH synthesis can be inhibited by buthionine sulfoximine through inactivating γ-glutamylcysteine synthase.

The second target to induce ferroptosis is the GPx4. RSL3, a FIN II, reduces the catalytic activity of GPx4 enzyme and thus drives cells to ferroptosis (Shin *et al.,* 2018) in order to treat colorectal cancer for example (Sui *et al.,* 2018). On the contrary, overexpressing GPx4 can inhibit RSL3-driven ferroptosis (Yang *et al.,* 2014). Withaferin A and Altretamine belong as well to FINs II and induce ferroptosis in neuroblastoma as well as ovarian cells, respectively (Hassannia *et al.,* 2018 ; Woo *et al.,* 2015). Other compounds such as ML-210 (DPI10) and ML-162 (DPI7) are also classified as FINs II (Eaton *et al.,* 2018). FIN56 is a ferroptosis inducer classified in the class 3 ferroptosis inducers although it promotes the degradation of GPx4 through a not fully described mechanism (Sun *et al.,* 2021). It can be potentiated by statins (Shimada *et al.,* 2016b). It also binds and activates squalene synthase leading to the depletion of the lipophilic antioxidant, coenzyme Q10. Also, there is $FINO_2$ that indirectly inactivates GPx4 through an unknown pathway. This molecule is an endoperoxide-containing 1,2-dioxolane and can react with Fe^{2+} to produce radicals and aids in lipid peroxidation (Gaschler *et al.,* 2018). Ferroptosis can as well be initiated by increasing the labile iron pool (LIP) through excessive expression of transferrin, limit expression of ferritin or activation of heme-oxygenase (Chang *et al.,* 2018; Hassannia *et al.,* 2018; S. Ma *et al.,* 2016).

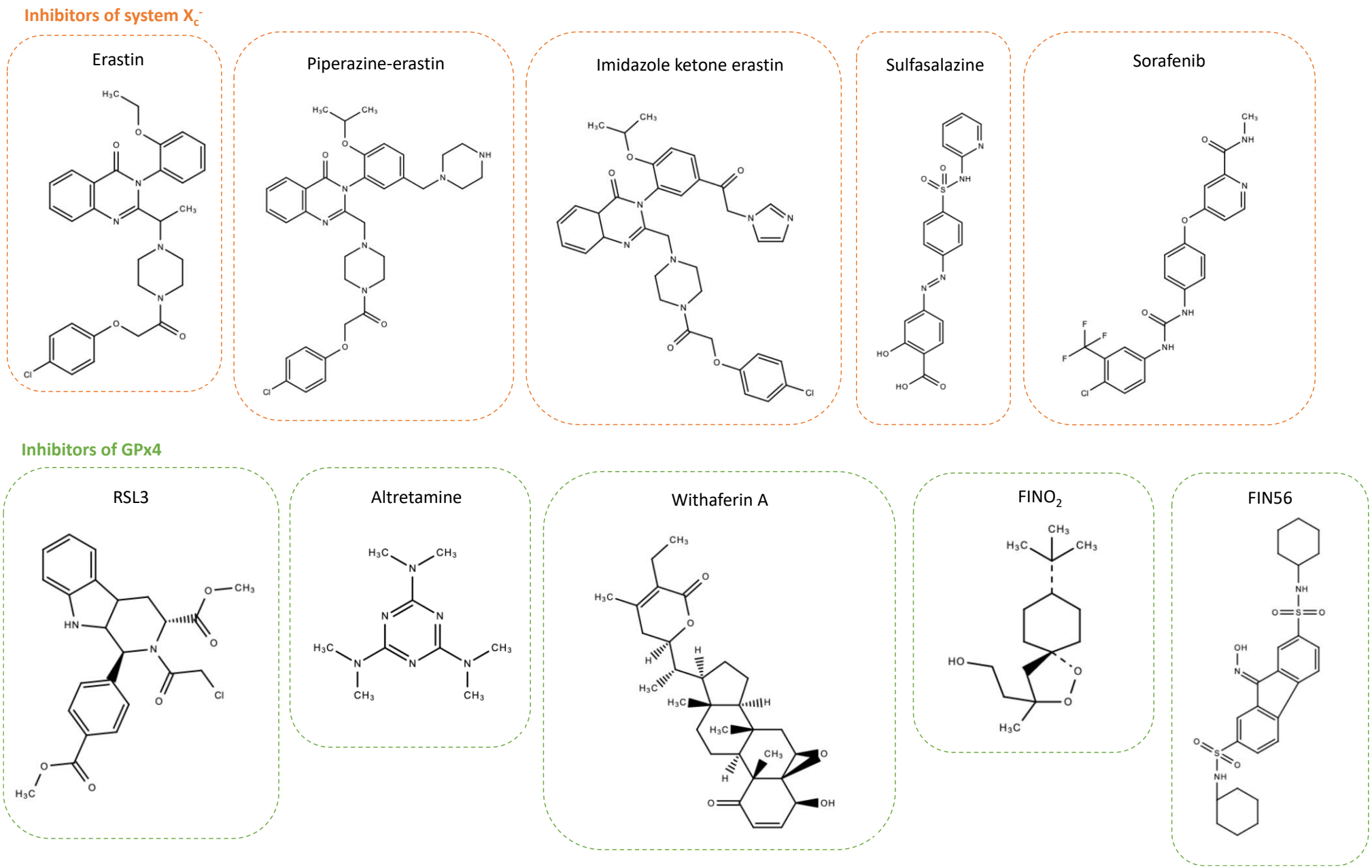

Figure 2.14. Chemical structures for ferroptosis inducers

2.2.6.2 Ferroptosis inhibitors

Following the research around ferroptosis mechanisms, specific ferroptosis inhibitors such as metal-chelators like deferoxamine **(DFO)** and Deferiprone **(DFr),** and lipophilic antioxidants like ferrostatin-1 **(Fer-1),** liproxstatin-1 **(Lip-1),** and vitamin E (α-tocopherol) have been discovered (**Figure 2.15)**.

Deferoxamine (**Figure 2.16, A**) is a metal-chelating agent for trivalent cations such as ferric and aluminium ions. The affinity constants of complex formation are very high, 10^{31} M^{-1} and 10^{25} M^{-1}, respectively, and is carried out on a 1:1 molar basis. DFO is able to bind free iron in plasma or cells to form the ferrioxamine complex. It can also chelate iron bound to ferritin but cannot chelate iron in haemoglobin. As a result, DFO promotes the excretion of iron and aluminium in urine and faeces, thereby reducing their pathological effects in organs. Interestingly, iron and aluminium overload can be screened by the DFO test. This test is based on the fact that DFO does not increase the excretion of iron and aluminium above a certain threshold in healthy subjects. DFO is prescribed for patients suffering from primary hemochromatosis (extra iron builds up in the body to harmful levels caused by gene disorders), which is not curable by phlebotomy, secondary hemochromatosis (extra iron builds up in the body to harmful levels caused by another disease), and renal aluminium poisoning. It can be administered either subcutaneously, intravenously by infusion, intramuscularly, or intraperitoneally. DFO have shown interesting results in ferroptosis-based studies. DFO inhibits ferroptosis in lung cancer cells by decreasing free iron concentration (Cheng *et al.,* 2021), in ovarian cancer cells where the expression of GPx4 is reduced (Li, Zhang, and Chao 2021) and in liver cancer cells (Liu *et al.,* 2021). Spinal cord injury in mice was treated by DFO that decreased iron concentration and promoted the expression of GPx4, system X_c^- and GSH (Yao *et al.,* 2019). DFO is also reported to preserve neurons in the early stages of Parkinson disease (Do Van *et al.,* 2016) and to reduce ROS formation in breast cancer cells and corneal epithelial cells driven to ferroptosis (Otsu *et al.,* 2021; Chen *et al.,* 2017).

Deferiprone (**Figure 2.16, B**) is a bidentate ligand, which binds to iron in a molar ratio of 3:1. Unlike DFO, DFr is a membrane-permeant molecule. DFr promotes iron excretion in transfusion-dependent β-thalassemia. This drug is administered orally and prescribed either as a monotherapy to treat iron-overload when current chelation therapy is unsuitable, or in combination with another chelating drug (mainly DFO) when the monotherapy is not effective

or in case of life-threatening iron overload. To date, DFr has never been tested on a ferroptosis model although it presents similar properties as DFO. For example, it was shown to reduce intracellular iron levels and inhibit lipid peroxidation in hepatocytes (Barnabé *et al.,* 2002). DFr was able also to chelate iron deposits in red blood cells of patients with thalassemia and alleviate plasma membrane dysfunction (Shalev *et al.,* 1995).

Ferrostatin-1 (**Figure 2.16, C**) is a ferroptosis inhibitor that prevents lipid peroxidation by scavenging lipid alkoxyl radicals (Miotto *et al.,* 2020). Dixon *et al.,* (2012), were the first to identify its rescuing effect on glutamate-induced ferroptosis in rat brain. This molecule was also able to restore mitochondrial function in ferroptosis-based neuronal cells model and prevent their death. Furthermore, Fer-1 showed antioxidant effects in cell models of Huntington disease, kidney dysfunction, atherosclerosis, and lung cancer by reducing oxidation of lipids and ROS production, and it had an indirect effect on promoting the expression of GPx4 (Li *et al.,* 2021, Bai *et al.,* 2020; Skouta *et al.,* 2014). These later findings suggest that ferroptosis is a key event in the progression of these diseases.

The other lipophilic antioxidants that showed anti-ferroptosis effects are Lip-1 and vitamin E. The mode of action of Lip-1 is not well explained in literature but it is believed to have a scavenging activity just like Fer-1 due to the presence of 2 amine groups in its structure (**Figure 2.16, D**) (Hinman *et al.,* 2018). This molecule was able to inhibit ferroptosis in mice fibroblasts where GPx4 was knocked-out (Friedmann Angeli *et al.,* 2014). Vitamin E - the lipid soluble form of α-tocopherol that blocks oxidation-chain reaction in the membrane - is less efficient than Fer-1 and Lip-1 (Sun *et al.,* 2020; Princen *et al.,* 1995). Vitamin E suppressed FIN56-induced ferroptosis in fibrosarcoma cells, and prevented lipid peroxidation-induced cell death in acute liver failure (Yamada *et al.,* 2020; Shimada *et al.,* 2016b).

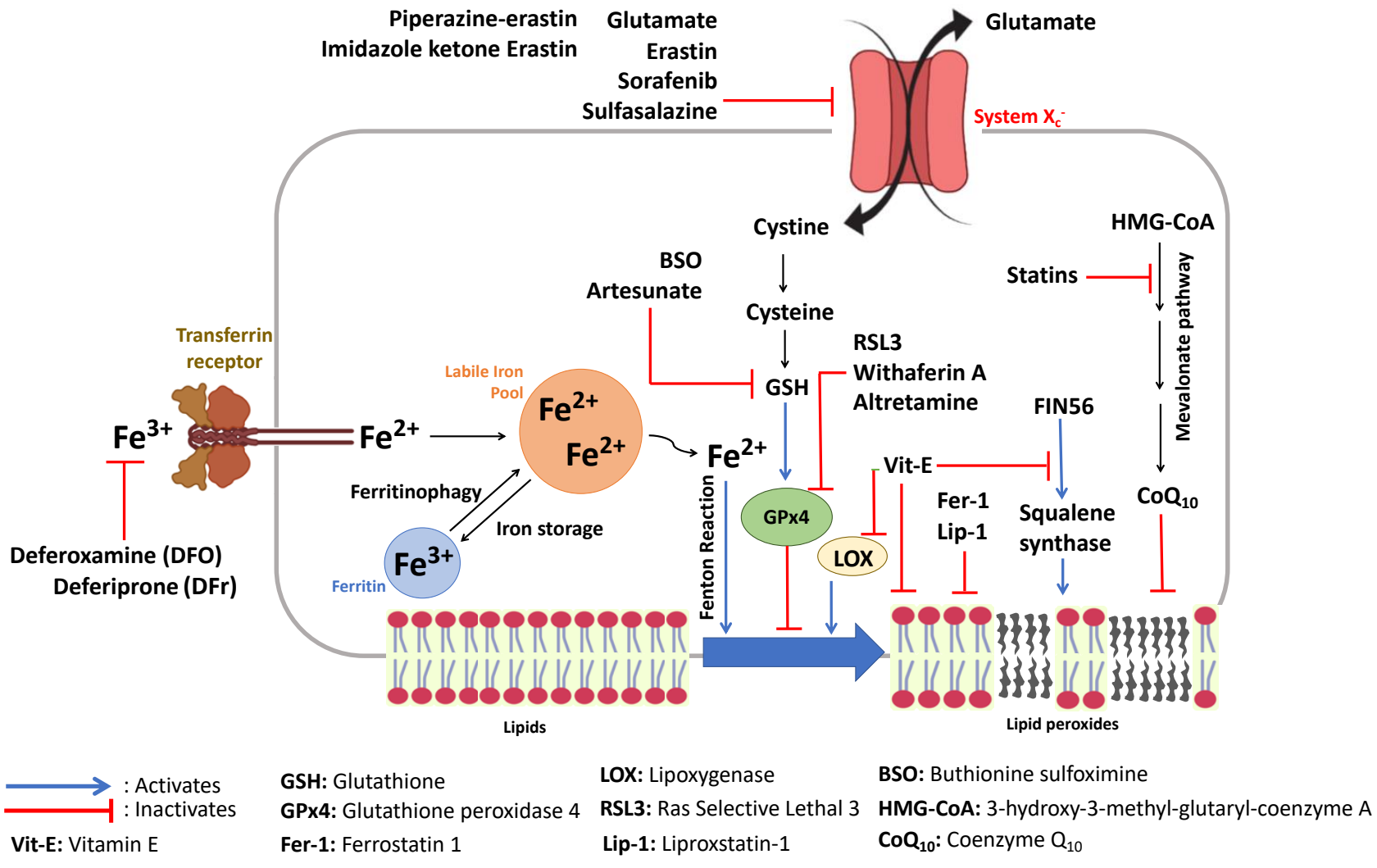

Figure 2.15. Network of ferroptosis inducers and inhibitors

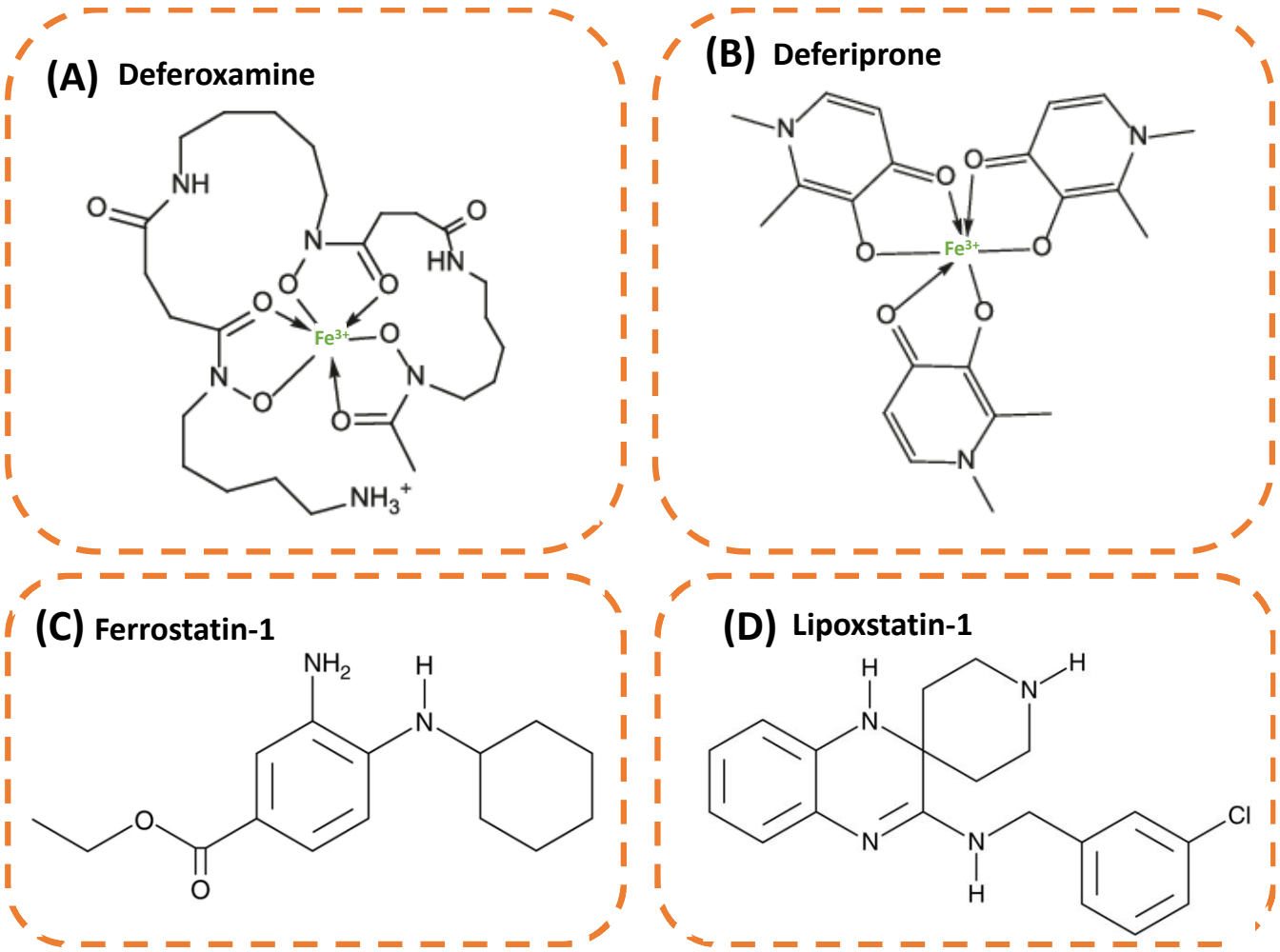

Figure 2.16. Chemical structures of iron chelators: (A) Deferoxamine chelating iron and (B) 3 deferiprones chelating iron, and lipophilic antioxidants: (C) Ferrostatin-1 and (D) Lipoxstatin-1

2.2.7 Ferroptosis and human diseases

2.2.7.1 Bad omen in cardiovascular and neurodegenerative diseases

Atheresclorosis (**AS**) is a cardiovascular disease characterized by the formation of plaques at arteries wall, narrowing the blood flow passage. In a context of inflammation and oxidative stress, AS starts with an endothelial dysfunction associated with LDL entry and oxidation in the sub-endothelium. Macrophages at that site phagocyte oxidized LDL and become foam cells appearing as fatty streaks (Miotto *et al.,* 2020). Although the mechanism leading to AS *via* ferroptosis has not been yet clarified, several studies have provided a reliable correlation between ferroptosis

marker and AS (**Figure 2.17**). Oxidized phospholipids and iron overload are master players in ferroptosis (Li *et al.,* 2018) and they are well-known for their role in the context of oxidative stress leading to AS (Hörkkö *et al.,* 1999; Marques *et al.,* 2019; Wu *et al.,* 2018). Moreover, ferroptosis inhibitors such as Fer-1 and DFO, GPx4, and vitamin E can prevent AS (Wang and Tang 2019; Liu, Xu, and Huang 2017; Veiner *et al.,* 2015). Indeed, Bai *et al.,* (2020) showed that Fer-1 inhibits lipid peroxidation and iron accumulation, and induces GPx4 overexpression as well as GSH production in an AS mice model. Moreover, foam cells of atherosclerotic plaques are found to be overloaded in transferrin-receptor proteins, one of the endogenous ferroptosis inducers (Wei Li *et al.,* 2008). In the same context, LOX overexpression - a cell ferroptosis inducer - also leads to AS (Li et al., 2018). In a recent study, Sampilvanjil *et al.,* (2020) induced ferroptosis in vascular smooth muscle cells with tobacco smoking, which is known since 1998 as a key cause for the development of AS (Howard *et al.,* 1998). Other cardiovascular diseases such as cardiomyopathy and cardiac dysfunction are also induced by iron overload (Gujja *et al.,* 2010; Ravingerová *et al.,* 2020). Indeed, cardiomyopathy appears in cancer patients treated with doxorubicin, due to its ability to accumulate iron and thus to induce ferroptosis (Koleini *et al.,* 2019). According to some studies, ferroptosis is a leading cause for myocardial Ischemia/Reperfusion (**I/R**) injury (tissue damage caused by the return of blood supply after a period of oxygen lack), whose damages can be decreased by Fer-1 and DFO (Li *et al.,* 2019; Fang *et al.,* 2019; Gao *et al.,* 2015).

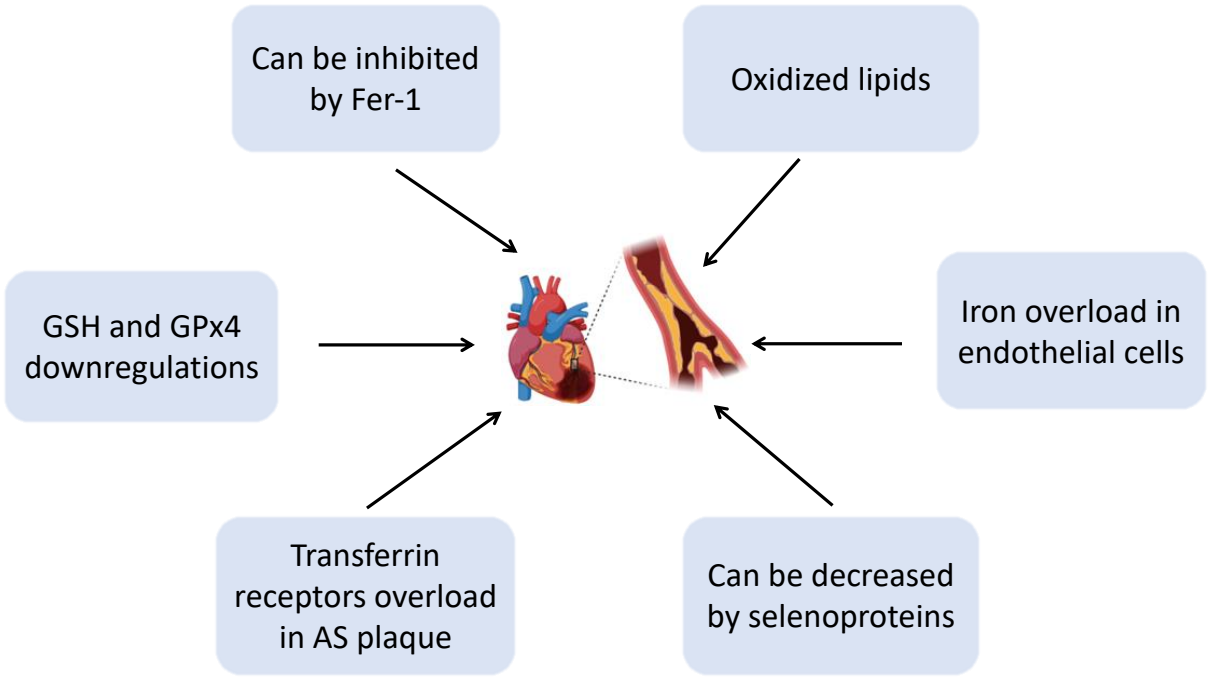

Figure 2.17. Ferroptosis evidence in Atherosclerosis

Several scientific data support the relation between ferroptosis and other chronic disease such as the Huntington disease, a genetic neurodegenerative disease. Biomarkers of this disease are also markers of ferroptosis such as, excessive iron metabolism, glutamate toxicity, dysregulation in GSH-mediated redox potential and lipid peroxidation (Johnson, Wilson-Delfosse, and Mieyal, 2012; Ross and Tabrizi, 2011; Sadagurski *et al.,* 2011). DFO and Fer-1 protected the death of neurons in Huntington models (Skouta *et al.,* 2014; Chen *et al.,* 2013). Alzheimer and Parkinson's diseases are also common neurodegenerative diseases associated with loss of memory and automaticity, respectively. Oxidative destruction of neurons of the hippocampus and substantia nigra are driven by iron accumulation in Alzheimer disease and Parkinson's disease, respectively (Devos *et al.,* 2020; Lane, Ayton, and Bush, 2018; Raven *et al.,* 2013). Neuronal loss in Parkinson disease was prevented by DFO and Fer-1 (Do Van *et al.,* 2016). Traumatic brain injury is as well characterized by ferroptosis features such as elevated iron content, reduced GPx4 activity and ROS accumulation (Xie *et al.,* 2019).

Ferroptosis has contribution in acute and chronic liver disease as well. Indeed, Zhou *et al.,* (2019) and, Afonso Castro and Rodrigues (2019) observed the accumulation of iron and lipid peroxidation in hepatocytes of alcoholic and non-alcoholic liver diseases. In the immune system, GPx4-deficient T-Cells are accompanied with membrane lipid peroxidation (Matsushita *et al.,* 2015). In acute kidney injury model, cell death was prevented by Fer-1 (Skouta *et al.,* 2014) and in a mice model where GPx4 was absent, Lip-1 slowed down renal failure *(Friedmann Angeli et al.,* 2014).

2.2.7.2 A novel landscape in cancer therapy

Ferroptosis was first discovered as a pathway to kill cancer cells. Now, it represents a promising therapy for several types of cancers. Scientists discovered that many drugs such as, the antidiabetic drug, Metformin, the anaesthetic drug, Lidocaine, the anti-malaria drug, Dihydroartemisinin, and the chemotherapeutic drug, Paclitaxel, induce ferroptosis mechanism in cancer cells. Metformin and Lidocaine can lead to ferroptosis in breast and ovarian cancers by destabilizing the system X_c^- (Yang *et al.,* 2021; Sun, Li, and Zhang 2021). Dihydroartemisinin and Paclitaxel revealed their activity to downregulate the expression of system X_c^- and to enhance ferritinophagy in lung and colorectal cancers (Chen *et al.,* 2020; Wei Li *et al.,* 2008; C. Lv *et al.,* 2017; Giannakakou *et al.,* 2001). Ferroptosis inducers, Erastin, Sorafenib and Sulfasalazine promoted ferroptosis in gastric cancer, hepatocellular carcinoma, pancreatic cancer and lung cancer cell lines (Li *et al.,* 2020; Y. Yamaguchi, Kasukabe, and Kumakura 2018; Hao *et al.,* 2017; Louandre *et al.,* 2015). The inactivation of system X_c^- is very efficient in diffuse large B cell lymphoma, that already have a weak transsulfuration pathway making its survival dependent on the extracellular uptake of cystine/ cysteine (Gout *et al.,* 2001). Erastin can attenuate the resistance of leukemic cells to doxorubicin (Yu *et al.,* 2015). Artesunate can provoke ferroptotic cell death by accumulating ROS in adenocarcinoma cell lines (Eling *et al.,* 2015). Ding *et al.,* (2021) provoked ferroptosis in triple negative breast cancer cells by ubiquitinating GPx4 through binding of a small molecule called “DMOCPTL” to GPx4. In fact, the downregulation of GPx4 activity is considered as a biomarker for the efficiency of chemotherapy against breast cancer (Sha *et al.,* 2021).

2.2.8 Conclusion

In summary, the discovery of ferroptosis was a huge scientific progress in the biological domain. The great value of identifying ferroptosis inducers and inhibitors was translated in diseases-treatment studies. No studies have been yet reported the effect of nutrition on ferroptosis. Proteins and peptides provided from natural resources and having metal-chelation activity are interesting bioactive molecules to be studied on ferroptosis models in order to prevent/delay this cellar death pathway.

2.2.9 References

Abbaspour, Hurrell, and Kelishadi. 2014. "Review on Iron and Its Importance for Human Health." *Journal of Research in Medical Sciences : The Official Journal of Isfahan University of Medical Sciences* 19 (2): 164–74.

Afonso, Castro, and Cecília Rodrigues. 2019. "Processes Exacerbating Apoptosis in Non-Alcoholic Steatohepatitis." *Clinical Science (London, England: 1979)* 133 (22): 2245–64. https://doi.org/10.1042/CS20190068.

Alim, Caulfield, Chen, Swarup, Geschwind, Ivanova, Seravalli, et al. 2019. "Selenium Drives a Transcriptional Adaptive Program to Block Ferroptosis and Treat Stroke." *Cell* 177 (5): 1262-1279.e25. https://doi.org/10.1016/j.cell.2019.03.032.

An, Su, Sun, Wang, Fan, Jiang, Yang, and Shi. 2021. "Liraglutide Alleviates Cognitive Deficit in Db/Db Mice: Involvement in Oxidative Stress, Iron Overload, and Ferroptosis." *Neurochemical Research*, September. https://doi.org/10.1007/s11064-021-03442-7.

Andrews, and Schmidt. 2007. "Iron Homeostasis." *Annual Review of Physiology* 69 (1): 69–85. https://doi.org/10.1146/annurev.physiol.69.031905.164337.

Aruoma, Halliwell, Laughton, Quinlan, and Gutteridge. 1989. "The Mechanism of Initiation of Lipid Peroxidation. Evidence against a Requirement for an Iron(II)-Iron(III) Complex." *Biochemical Journal* 258 (2): 617–20.

Ayala, Muñoz, and Argüelles. 2014. "Lipid Peroxidation: Production, Metabolism, and Signaling Mechanisms of Malondialdehyde and 4-Hydroxy-2-Nonenal." *Oxidative Medicine and Cellular Longevity* 2014 (May): e360438. https://doi.org/10.1155/2014/360438.

Bai, Li, Liu, Qiao, and Wang. 2020. "Inhibition of Ferroptosis Alleviates Atherosclerosis through Attenuating Lipid Peroxidation and Endothelial Dysfunction in Mouse Aortic Endothelial Cell." *Free Radical Biology and Medicine* 160 (November): 92–102. https://doi.org/10.1016/j.freeradbiomed.2020.07.026.

Barnabé, Zastre, Venkataram, and Hasinoff. 2002. "DFr Protects against Doxorubicin-Induced Myocyte Cytotoxicity." *Free Radical Biology and Medicine* 33 (2): 266–75. https://doi.org/10.1016/S0891-5849(02)00873-0.

Benzie, 1996. "Lipid Peroxidation: A Review of Causes, Consequences, Measurement and Dietary Influences." *International Journal of Food Sciences and Nutrition* 47 (3): 233–61. https://doi.org/10.3109/09637489609012586.

Benzie, 2000. "Evolution of Antioxidant Defence Mechanisms." *European Journal of Nutrition* 39 (2): 53–61. https://doi.org/10.1007/s003940070030.

Blaustein. 2016. "The Great Oxidation Event." *BioScience* 66 (3): 189–95. https://doi.org/10.1093/biosci/biv193.

Cao and Dixon. 2016. "Mechanisms of Ferroptosis." *Cellular and Molecular Life Sciences* 73 (11–12): 2195–2209. https://doi.org/10.1007/s00018-016-2194-1.

Cardoso, Bush, and Roberts. 2017. "Glutathione Peroxidase 4: A New Player in Neurodegeneration?" *Molecular Psychiatry* 22 (3): 328–35. https://doi.org/10.1038/mp.2016.196.

Carter. 2003. "Oxygen: The Molecule That Made the World." *Journal of the Royal Society of Medicine* 96 (1): 46–47.

Chang, Chiang, Chen, Yu, Chou, and Chang. 2018. "Heme Oxygenase-1 Mediates BAY 11-7085 Induced Ferroptosis." *Cancer Letters* 416 (March): 124–37. https://doi.org/10.1016/j.canlet.2017.12.025.

Chen, Benthani, Wu, Liang, Bian, and Jiang. 2020. "Artemisinin Compounds Sensitize Cancer Cells to Ferroptosis by Regulating Iron Homeostasis." *Cell Death & Differentiation* 27 (1): 242–54. https://doi.org/10.1038/s41418-019-0352-3.

Chen, Marks, Lai, Zhang, Duce, Lam, Volitakis, Bush, Hersch, and Fox. 2013. "Iron Accumulates in Huntington's Disease Neurons: Protection by Deferoxamine." *PLOS ONE* 8 (10): e77023. https://doi.org/10.1371/journal.pone.0077023.

Chen, Li, Liu, Yu, Xue, and Liu. 2015. "Erastin Sensitizes Glioblastoma Cells to Temozolomide by Restraining XCT and Cystathionine-γ-Lyase Function." *Oncology Reports* 33 (3): 1465–74. https://doi.org/10.3892/or.2015.3712.

Chen, Wang, Hsu, Yin, Yeh, Lee, and Tseng. 2017. "CHAC1 Degradation of Glutathione Enhances Cystine-Starvation-Induced Necroptosis and Ferroptosis in Human Triple Negative Breast Cancer Cells via the GCN2-EIF2α-ATF4 Pathway." *Oncotarget* 8 (70): 114588–602. https://doi.org/10.18632/oncotarget.23055.

Chen, Kang, Kroemer, and Tang. 2021. "Organelle-Specific Regulation of Ferroptosis." *Cell Death and Differentiation*, August. https://doi.org/10.1038/s41418-021-00859-z.

Cheng, Feng, Li, Gao, Tang, Liu, Wu, Yue, Li, and Luo. 2021. "Iron Deposition-Induced Ferroptosis in Alveolar Type II Cells Promotes the Development of Pulmonary Fibrosis." *Biochimica Et Biophysica Acta. Molecular Basis of Disease* 1867 (12): 166204. https://doi.org/10.1016/j.bbadis.2021.166204.

Cobler, Zhang, Suri, Park, and Timmerman. 2018. "XCT Inhibition Sensitizes Tumors to γ-Radiation via Glutathione Reduction." *Oncotarget* 9 (64): 32280–97. https://doi.org/10.18632/oncotarget.25794.

Cramer, Saha, Liu, Tadi, Tiziani, Yan, Triplett, et al. 2017. "Systemic Depletion of L-Cyst(e)Ine with Cyst(e)Inase Increases Reactive Oxygen Species and Suppresses Tumor Growth." *Nature Medicine* 23 (1): 120–27. https://doi.org/10.1038/nm.4232.

Devos, Cabantchik, Moreau, Danel, Mahoney-Sanchez, Bouchaoui, Gouel, et al. 2020. "Conservative Iron Chelation for Neurodegenerative Diseases Such as Parkinson's Disease and Amyotrophic Lateral Sclerosis." *Journal of Neural Transmission (Vienna, Austria: 1996)* 127 (2): 189–203. https://doi.org/10.1007/s00702-019-02138-1.

Ding, Chen, Liu, Ge, Wang, Hao, Wang, Chen, and Zhang. 2021. "Identification of a Small Molecule as Inducer of Ferroptosis and Apoptosis through Ubiquitination of GPX4 in Triple Negative Breast Cancer Cells." *Journal of Hematology & Oncology* 14 (1): 19. https://doi.org/10.1186/s13045-020-01016-8.

Dixon, Patel, Welsch, Skouta, Lee, Hayano, Thomas, et al. 2014. "Pharmacological Inhibition of Cystine-Glutamate Exchange Induces Endoplasmic Reticulum Stress and Ferroptosis." *ELife* 3 (May): e02523. https://doi.org/10.7554/eLife.02523.

Dixon, Winter, Musavi, Lee, Snijder, Rebsamen, Superti-Furga, and Stockwell. 2015. "Human Haploid Cell Genetics Reveals Roles for Lipid Metabolism Genes in Nonapoptotic Cell Death." *ACS Chemical Biology* 10 (7): 1604–9. https://doi.org/10.1021/acschembio.5b00245.

Dixon, Lemberg, Lamprecht, Skouta, Zaitsev, Gleason, Patel, et al. 2012. "Ferroptosis: An Iron-Dependent Form of Nonapoptotic Cell Death." *Cell* 149 (5): 1060–72. https://doi.org/10.1016/j.cell.2012.03.042.

Do Van, Gouel, Jonneaux, Timmerman, Gelé, Pétrault, Bastide, et al. 2016. "Ferroptosis, a Newly Characterized Form of Cell Death in Parkinson's Disease That Is Regulated by PKC." *Neurobiology of Disease* 94 (October): 169–78. https://doi.org/10.1016/j.nbd.2016.05.011.

Doll, and Conrad. 2017. "Iron and Ferroptosis: A Still Ill-defined Liaison." *IUBMB Life* 69 (6): 423–34. https://doi.org/10.1002/iub.1616.

Doll, Proneth, Tyurina, Panzilius, Kobayashi, Ingold, Irmler, et al. 2017. "Acsl4 Dictates Ferroptosis Sensitivity by Shaping Cellular Lipid Composition." *Nature Chemical Biology* 13 (1): 91–98. https://doi.org/10.1038/nchembio.2239.

Dolma, Lessnick, Hahn, and Stockwell. 2003. "Identification of Genotype-Selective Antitumor Agents Using Synthetic Lethal Chemical Screening in Engineered Human Tumor Cells." *Cancer Cell* 3 (3): 285–96. https://doi.org/10.1016/s1535-6108(03)00050-3.

Eaton, Furst, Ruberto, Moosmayer, Hillig, Hilpmann, Zimmermann, et al. 2018. "Targeting a Therapy-Resistant Cancer Cell State Using Masked Electrophiles as GPX4 Inhibitors." https://doi.org/10.1101/376764.

Eling, Reuter, Hazin, Hamacher-Brady, and Brady. 2015. "Identification of Artesunate as a Specific Activator of Ferroptosis in Pancreatic Cancer Cells." *Oncoscience* 2 (5): 517–32.

Ems, Lucia, and Huecker. 2021. "Biochemistry, Iron Absorption." In *StatPearls*. Treasure Island (FL): StatPearls Publishing. http://www.ncbi.nlm.nih.gov/books/NBK448204/.

Fang, Wang, Han, Xie, Yang, Wei, Gu, et al. 2019. "Ferroptosis as a Target for Protection against Cardiomyopathy." *Proceedings of the National Academy of Sciences* 116 (7): 2672–80. https://doi.org/10.1073/pnas.1821022116.

Fenton. 1894. "LXXIII.—Oxidation of Tartaric Acid in Presence of Iron." *Journal of the Chemical Society, Transactions* 65 (0): 899–910. https://doi.org/10.1039/CT8946500899.

Fischer, Hemp, and Valentine. 2016. "How Did Life Survive Earth's Great Oxygenation?" *Current Opinion in Chemical Biology* 31 (April): 166–78. https://doi.org/10.1016/j.cbpa.2016.03.013.

Fradejas, Carlson, Rijntjes, Becker, Tobe, and Schweizer. 2013. "Mammalian Trit1 Is a TRNA([Ser]Sec)-Isopentenyl Transferase Required for Full Selenoprotein Expression." *The Biochemical Journal* 450 (2): 427–32. https://doi.org/10.1042/BJ20121713.

Friedmann, Pedro, Schneider, Proneth, Tyurina, Tyurin, Hammond, Herbach, et al. 2014. "Inactivation of the Ferroptosis Regulator Gpx4 Triggers Acute Renal Failure in Mice." *Nature Cell Biology* 16 (12): 1180–91. https://doi.org/10.1038/ncb3064.

Fuhrmann, Mondorf, Beifuß, Jung, and Brüne. 2020. "Hypoxia Inhibits Ferritinophagy, Increases Mitochondrial Ferritin, and Protects from Ferroptosis." *Redox Biology* 36 (September): 101670. https://doi.org/10.1016/j.redox.2020.101670.

Gao, Monian, Quadri, Ramasamy, and Jiang. 2015. "Glutaminolysis and Transferrin Regulate Ferroptosis." *Molecular Cell* 59 (2): 298–308. https://doi.org/10.1016/j.molcel.2015.06.011.

Gardner. 1989. "Oxygen Radical Chemistry of Polyunsaturated Fatty Acids." *Free Radical Biology and Medicine* 7 (1): 65–86. https://doi.org/10.1016/0891-5849(89)90102-0.

Gaschler, Andia, Liu, Csuka, Hurlocker, Vaiana, Heindel, et al. 2018. "FINO2 Initiates Ferroptosis through GPX4 Inactivation and Iron Oxidation." *Nature Chemical Biology* 14 (5): 507–15. https://doi.org/10.1038/s41589-018-0031-6.

Gaucher, Boudier, Bonetti, Clarot, Leroy, and Parent. 2018. "Glutathione: Antioxidant Properties Dedicated to Nanotechnologies." *Antioxidants* 7 (5). https://doi.org/10.3390/antiox7050062.

Giannakakou, Robey, Fojo, and Blagosklonny. 2001. "Low Concentrations of Paclitaxel Induce Cell Type-Dependent P53, P21 and G1/G2 Arrest Instead of Mitotic Arrest: Molecular Determinants of Paclitaxel-Induced Cytotoxicity." *Oncogene* 20 (29): 3806–13. https://doi.org/10.1038/sj.onc.1204487.

Gout, Buckley, Simms, and Bruchovsky. 2001. "Sulfasalazine, a Potent Suppressor of Lymphoma Growth by Inhibition of the x(c)- Cystine Transporter: A New Action for an Old Drug." *Leukemia* 15 (10): 1633–40. https://doi.org/10.1038/sj.leu.2402238.

Guéraud, Atalay, Bresgen, Cipak, Eckl, Huc, Jouanin, Siems, and Uchida. 2010. "Chemistry and Biochemistry of Lipid Peroxidation Products." *Free Radical Research* 44 (10): 1098–1124. https://doi.org/10.3109/10715762.2010.498477.

Gujja, Rosing, Tripodi, and Shizukuda. 2010. "Iron Overload Cardiomyopathy." *Journal of the American College of Cardiology* 56 (13): 1001–12. https://doi.org/10.1016/j.jacc.2010.03.083.

Guo, Duan, He, Li, Wu, Xiang, Bao, et al. 2021. "A Combined Model of Human IPSC-Derived Liver Organoids and Hepatocytes Reveals Ferroptosis in DGUOK Mutant MtDNA Depletion Syndrome." *Advanced Science* 8 (10): 2004680. https://doi.org/10.1002/advs.202004680.

Guo, Xu, Han, Zhou, Xia, Gong, Dai, Li, and Wu. 2018. "Ferroptosis: A Novel Anti-Tumor Action for Cisplatin." *Cancer Research and Treatment : Official Journal of Korean Cancer Association* 50 (2): 445–60. https://doi.org/10.4143/crt.2016.572.

Guo, LHarnedy, O'Keeffe, Zhang, Li, Hou, and FitzGerald. 2015. "Fractionation and Identification of Alaska Pollock Skin Collagen-Derived Mineral Chelating Peptides." *Food Chemistry* 173 (April): 536–42. https://doi.org/10.1016/j.foodchem.2014.10.055.

Guo, Zhao, Zhang, Tan, Zhao, Ge, Liang, et al. 2011. "Disruption of XCT Inhibits Cell Growth via the ROS/Autophagy Pathway in Hepatocellular Carcinoma." *Cancer Letters* 312 (1): 55–61. https://doi.org/10.1016/j.canlet.2011.07.024.

Hao, Yu, He, Huang, Zhao, Liang, Zhang, et al. 2017. "Cysteine Dioxygenase 1 Mediates Erastin-Induced Ferroptosis in Human Gastric Cancer Cells." *Neoplasia* 19 (12): 1022–32. https://doi.org/10.1016/j.neo.2017.10.005.

Hassannia, Vandenabeele, and Berghe. 2019. "Targeting Ferroptosis to Iron Out Cancer." *Cancer Cell* 35 (6): 830–49. https://doi.org/10.1016/j.ccell.2019.04.002.

Hassannia, Wiernicki, Ingold, Qu, Herck, Tyurina, Bayır, et al. 2018. "Nano-Targeted Induction of Dual Ferroptotic Mechanisms Eradicates High-Risk Neuroblastoma." *The Journal of Clinical Investigation* 128 (8): 3341–55. https://doi.org/10.1172/JCI99032.

Hinman, Holst, Latham, Bruegger, Ulas, McCusker, Amagata, et al. 2018. "Vitamin E Hydroquinone Is an Endogenous Regulator of Ferroptosis via Redox Control of 15-Lipoxygenase." *PLOS ONE* 13 (8): e0201369. https://doi.org/10.1371/journal.pone.0201369.

Homma, Kobayashi, and Fujii. 2020. "Cysteine Preservation Confers Resistance to Glutathione-Depleted Cells against Ferroptosis via CDGSH Iron Sulphur Domain-Containing Proteins (CISDs)." *Free Radical Research* 54 (6): 397–407. https://doi.org/10.1080/10715762.2020.1780229.

Hörkkö, Bird, Miller, Itabe, Leitinger, Subbanagounder, Berliner, et al. 1999. "Monoclonal Autoantibodies Specific for Oxidized Phospholipids or Oxidized Phospholipid–Protein Adducts Inhibit Macrophage Uptake of Oxidized Low-Density Lipoproteins." *Journal of Clinical Investigation* 103 (1): 117–28.

Hou, Xie, Song, Sun, Lotze, Herbert J. Zeh, Rui Kang, and Daolin Tang. 2016. "Autophagy Promotes Ferroptosis by Degradation of Ferritin." *Autophagy* 12 (8): 1425–28. https://doi.org/10.1080/15548627.2016.1187366.

Howard, Wagenknecht, Burke, Diez-Roux, Evans, McGovern, Nieto, and Tell. 1998. "Cigarette Smoking and Progression of Atherosclerosis: The Atherosclerosis Risk in Communities (ARIC) Study." *JAMA* 279 (2): 119–24. https://doi.org/10.1001/jama.279.2.119.

Jang, Chapa-Dubocq, Tyurina, St Croix, Kapralov, Tyurin, Bayır, Kagan, and Javadov. 2021. "Elucidating the Contribution of Mitochondrial Glutathione to Ferroptosis in Cardiomyocytes." *Redox Biology* 45 (September): 102021. https://doi.org/10.1016/j.redox.2021.102021.

Johnson, Wilson-Delfosse, and Mieyal. 2012. "Dysregulation of Glutathione Homeostasis in Neurodegenerative Diseases." *Nutrients* 4 (10): 1399–1440. https://doi.org/10.3390/nu4101399.

Karmi, Sohn, Zandalinas, Rowland, King, Nechushtai, and Mittler. 2021. "Disrupting CISD2 Function in Cancer Cells Primarily Impacts Mitochondrial Labile Iron Levels and Triggers TXNIP Expression." *Free Radical Biology & Medicine*, September, S0891-5849(21)00725-5. https://doi.org/10.1016/j.freeradbiomed.2021.09.013.

Knutson. 2017. “Iron Transport Proteins: Gateways of Cellular and Systemic Iron Homeostasis.” *Journal of Biological Chemistry* 292 (31): 12735–43. https://doi.org/10.1074/jbc.R117.786632.

Koleini, Nickel, Edel, Fandrich, Ravandi, and Kardami. 2019. “Oxidized Phospholipids in Doxorubicin-Induced Cardiotoxicity.” *Chemico-Biological Interactions* 303 (April): 35–39. https://doi.org/10.1016/j.cbi.2019.01.032.

Lachaier, Louandre, Godin, Saidak, Baert, Diouf, Chauffert, and Galmiche. 2014. “Sorafenib Induces Ferroptosis in Human Cancer Cell Lines Originating from Different Solid Tumors.” *ANTICANCER RESEARCH*, 6.

Lane, Ayton, and Bush. 2018. “Iron and Alzheimer’s Disease: An Update on Emerging Mechanisms.” *Journal of Alzheimer’s Disease* 64 (s1): S379–95. https://doi.org/10.3233/JAD-179944.

Li, Chen, Liu, Shen, Ding, Gu, Liu, et al. 2018. “CTRP5 Promotes Transcytosis and Oxidative Modification of Low-Density Lipoprotein and the Development of Atherosclerosis.” *Atherosclerosis* 278 (November): 197–209. https://doi.org/10.1016/j.atherosclerosis.2018.09.037.

Li, Zhang, and Chao. 2021. “Significance of Glutathione Peroxidase 4 and Intracellular Iron Level in Ovarian Cancer Cells-"utilization" of Ferroptosis Mechanism.” *Inflammation Research: Official Journal of the European Histamine Research Society ... [et Al.]*, September. https://doi.org/10.1007/s00011-021-01495-6.

Li, Cao, Yin, Huang, Lin, Mao, Sun, and Wang. 2020. “Ferroptosis: Past, Present and Future.” *Cell Death & Disease* 11 (2): 88. https://doi.org/10.1038/s41419-020-2298-2.

Li, Xu, Forssell, Sullivan, and Yuan. 2008. “Overexpression of Transferrin Receptor and Ferritin Related to Clinical Symptoms and Destabilization of Human Carotid Plaques.” *Experimental Biology and Medicine (Maywood, N.J.)* 233 (7): 818–26. https://doi.org/10.3181/0711-RM-320.

Li, Feng, Gauthier, Lokshina, Higashikubo, Evans, Liu, et al. 2019. “Ferroptotic Cell Death and TLR4/Trif Signaling Initiate Neutrophil Recruitment after Heart Transplantation.” *The Journal of Clinical Investigation* 129 (6): 2293–2304. https://doi.org/10.1172/JCI126428.

Li, Chen, Chen, Zhou, Hu, Yang, Chen, et al. 2020. “Targeting Ferroptosis in Breast Cancer.” *Biomarker Research* 8 (1): 58. https://doi.org/10.1186/s40364-020-00230-3.

Liang, Zhang, Yang, and Dong. 2019. “Recent Progress in Ferroptosis Inducers for Cancer Therapy.” *Advanced Materials (Deerfield Beach, Fla.)* 31 (51): e1904197. https://doi.org/10.1002/adma.201904197.

Liu, Xu, and Huang. 2017. “Selenium in the Prevention of Atherosclerosis and Its Underlying Mechanisms.” *Metallomics: Integrated Biometal Science* 9 (1): 21–37. https://doi.org/10.1039/c6mt00195e.

Liu, Tong, Luo, and Gao. 2021. “[Cryptotanshinone May Induce Ferroptosis of Human Liver Cancer HepG2 Cells].” *Zhongguo Yi Xue Ke Xue Yuan Xue Bao. Acta Academiae Medicinae Sinicae* 43 (3): 366–70. https://doi.org/10.3881/j.issn.1000-503X.13115.

Louandre, Ezzoukhry, Godin, Barbare, Mazière, Chauffert, and Galmiche. 2013. “Iron-Dependent Cell Death of Hepatocellular Carcinoma Cells Exposed to Sorafenib.” *International Journal of Cancer* 133 (7): 1732–42. https://doi.org/10.1002/ijc.28159.

Louandre, Marcq, Bouhlal, Lachaier, Godin, Saidak, François, et al. 2015. "The Retinoblastoma (Rb) Protein Regulates Ferroptosis Induced by Sorafenib in Human Hepatocellular Carcinoma Cells." *Cancer Letters* 356 (2, Part B): 971–77. https://doi.org/10.1016/j.canlet.2014.11.014.

Lv, Qu, Zhu, Xu, Xu, Jia, Qing, Li, Wei, and Zhao. 2017. "Low-Dose Paclitaxel Inhibits Tumor Cell Growth by Regulating Glutaminolysis in Colorectal Carcinoma Cells." *Frontiers in Pharmacology* 8: 244. https://doi.org/10.3389/fphar.2017.00244.

Ma, Chen, Wang, Lu, Zhu, Song, Yang, et al. 2015. "Xc- Inhibitor Sulfasalazine Sensitizes Colorectal Cancer to Cisplatin by a GSH-Dependent Mechanism." *Cancer Letters* 368 (1): 88–96. https://doi.org/10.1016/j.canlet.2015.07.031.

Ma, Henson, Chen, and Gibson. 2016. "Ferroptosis Is Induced Following Siramesine and Lapatinib Treatment of Breast Cancer Cells." *Cell Death & Disease* 7 (July): e2307. https://doi.org/10.1038/cddis.2016.208.

Marques, Bermond, Soares Leal, Mageski, Fidelis, Nogueira, Vasquez, Meyrelles, Simões, and Dos Santos. 2019. "Chronic Iron Overload Intensifies Atherosclerosis in Apolipoprotein E Deficient Mice: Role of Oxidative Stress and Endothelial Dysfunction." *Life Sciences* 233 (September): 116702. https://doi.org/10.1016/j.lfs.2019.116702.

Matsushita, Freigang, Schneider, Conrad, Bornkamm, and Kopf. 2015. "T Cell Lipid Peroxidation Induces Ferroptosis and Prevents Immunity to Infection." *The Journal of Experimental Medicine* 212 (4): 555–68. https://doi.org/10.1084/jem.20140857.

Minotti, and Aust. 1987. "The Role of Iron in the Initiation of Lipid Peroxidation." *Chemistry and Physics of Lipids* 44 (2): 191–208. https://doi.org/10.1016/0009-3084(87)90050-8.

Miotto, Rossetto, Di Paolo, Orian, Venerando, Roveri, Vučković, et al. 2020. "Insight into the Mechanism of Ferroptosis Inhibition by Ferrostatin-1." *Redox Biology* 28 (January): 101328. https://doi.org/10.1016/j.redox.2019.101328.

Mou, Wang, Wu, He, Zhang, Duan, and Li. 2019. "Ferroptosis, a New Form of Cell Death: Opportunities and Challenges in Cancer." *Journal of Hematology & Oncology* 12 (1): 1–16. https://doi.org/10.1186/s13045-019-0720-y.

Natto, Kawamura, and Yamamoto. 1993. "Lipid Peroxides as the Initiating Factor of Atherosclerosis." *Annals of the New York Academy of Sciences* 676 (1): 27–45. https://doi.org/10.1111/j.1749-6632.1993.tb38723.x.

Negre-Salvayre, Auge, Ayala, Basaga, Boada, Brenke, Chapple, et al. 2010. "Pathological Aspects of Lipid Peroxidation." *Free Radical Research* 44 (10): 1125–71. https://doi.org/10.3109/10715762.2010.498478.

Nilsson, Regnström, Frostegård, and Stiko. 1992. "Lipid Oxidation and Atherosclerosis." *Herz* 17 (5): 263–69.

Otsu, Ishida, Chinen, Nakamura, Shimazawa, Tsusaki, and Hara. 2021. "Cigarette Smoke Extract and Heated Tobacco Products Promote Ferritin Cleavage and Iron Accumulation in Human Corneal Epithelial Cells." *Scientific Reports* 11 (1): 18555. https://doi.org/10.1038/s41598-021-97956-3.

Pan, Lin, Jiang, Yu, Yang, Zhou, Zhan, et al. 2019. "Erastin Decreases Radioresistance of NSCLC Cells Partially by Inducing GPX4-mediated Ferroptosis." *Oncology Letters* 17 (3): 3001–8. https://doi.org/10.3892/ol.2019.9888.

Park, Park, Lee, Lee, Shin, Kim, Kim, et al. 2019. "Quantitative Proteomic Analyses Reveal That GPX4 Downregulation during Myocardial Infarction Contributes to Ferroptosis in Cardiomyocytes." *Cell Death & Disease* 10 (11): 835. https://doi.org/10.1038/s41419-019-2061-8.

Pennafort, Queiroz, Gomes, and Rocha. 2018. "Instructional Therapeutic Toy in the Culture Care of the Child with Diabetes Type 1." *Revista Brasileira De Enfermagem* 71 (suppl 3): 1334–42. https://doi.org/10.1590/0034-7167-2017-0260.

Princen, van Duyvenvoorde, Buytenhek, van der Laarse, van Poppel, Leuven, and van Hinsbergh. 1995. "Supplementation With Low Doses of Vitamin E Protects LDL From Lipid Peroxidation in Men and Women." *Arteriosclerosis, Thrombosis, and Vascular Biology* 15 (3): 325–33. https://doi.org/10.1161/01.ATV.15.3.325.

"PubMed." n.d. PubMed. Accessed September 20, 2021. https://pubmed.ncbi.nlm.nih.gov/.

Raven, Lu, Tishler, Heydari, and Bartzokis. 2013. "Increased Iron Levels and Decreased Tissue Integrity in Hippocampus of Alzheimer's Disease Detected in Vivo with Magnetic Resonance Imaging." *Journal of Alzheimer's Disease* 37 (1): 127–36. https://doi.org/10.3233/JAD-130209.

Ravingerová, Kindernay, Barteková, Ferko, Adameová, Zohdi, Bernátová, Ferenczyová, and Lazou. 2020. "The Molecular Mechanisms of Iron Metabolism and Its Role in Cardiac Dysfunction and Cardioprotection." *International Journal of Molecular Sciences* 21 (21): 7889. https://doi.org/10.3390/ijms21217889.

Riegman, Sagie, Galed, Levin, Steinberg, Dixon, Wiesner, et al. 2020. "Ferroptosis Occurs through an Osmotic Mechanism and Propagates Independently of Cell Rupture." *Nature Cell Biology* 22 (9): 1042–48. https://doi.org/10.1038/s41556-020-0565-1.

Roh, Kim, Jang, Park, and Shin. 2016. "Induction of Ferroptotic Cell Death for Overcoming Cisplatin Resistance of Head and Neck Cancer." *Cancer Letters* 381 (1): 96–103. https://doi.org/10.1016/j.canlet.2016.07.035.

Ross, and Tabrizi. 2011. "Huntington's Disease: From Molecular Pathogenesis to Clinical Treatment." *The Lancet Neurology* 10 (1): 83–98. https://doi.org/10.1016/S1474-4422(10)70245-3.

Michel, Lewis, Shimada, Yang, MacPherson, Dandapani, et al. 2012. "Development of Small-Molecule Probes That Selectively Kill Cells Induced to Express Mutant RAS." *Bioorganic & Medicinal Chemistry Letters* 22 (4): 1822–26. https://doi.org/10.1016/j.bmcl.2011.09.047.

Sadagurski, Cheng, Rozzo, Palazzolo, Kelley, Dong, Krainc, and White. 2011. "IRS2 Increases Mitochondrial Dysfunction and Oxidative Stress in a Mouse Model of Huntington Disease." *The Journal of Clinical Investigation* 121 (10): 4070–81. https://doi.org/10.1172/JCI46305.

Sampilvanjil, Karasawa, Yamada, Komada, Higashi, Baatarjav, Watanabe, Kamata, Ohno, and Takahashi. 2020. "Cigarette Smoke Extract Induces Ferroptosis in Vascular Smooth Muscle Cells." *American Journal of Physiology. Heart and Circulatory Physiology* 318 (3): H508–18. https://doi.org/10.1152/ajpheart.00559.2019.

Sato, Kusumi, Hamashima, Kobayashi, Sasaki, Komiyama, Izumikawa, Conrad, Bannai, and Sato. 2018. "The Ferroptosis Inducer Erastin Irreversibly Inhibits System x c − and Synergizes with Cisplatin to Increase Cisplatin's Cytotoxicity in Cancer Cells." *Scientific Reports* 8 (1): 968. https://doi.org/10.1038/s41598-018-19213-4.

Sha, Xu, Yuan, Sheng, Wu, Peng, Wang, et al. 2021. "Predictive and Prognostic Impact of Ferroptosis-Related Genes ACSL4 and GPX4 on Breast Cancer Treated with Neoadjuvant Chemotherapy." *EBioMedicine* 71 (September): 103560. https://doi.org/10.1016/j.ebiom.2021.103560.

Shah, Shchepinov, and Pratt. 2018. "Resolving the Role of Lipoxygenases in the Initiation and Execution of Ferroptosis." *ACS Central Science* 4 (3): 387–96. https://doi.org/10.1021/acscentsci.7b00589.

Shalev, Repka, Goldfarb, Grinberg, Abrahamov, and Rachmilewitz. n.d. "DFr (L l) Chelates Pathologic Iron Deposits From Membranes of Intact Thalassemic and Sickle Red Blood Cells Both In Vitro and In Vivo," 6.

Shibata, Yasui, Higashikawa, Miyamoto, and Kuge. 2019. "Erastin, a Ferroptosis-Inducing Agent, Sensitized Cancer Cells to X-Ray Irradiation via Glutathione Starvation in Vitro and in Vivo." *PLoS ONE* 14 (12): e0225931. https://doi.org/10.1371/journal.pone.0225931.

Shimada, Skouta, Kaplan, Yang, Hayano, Dixon, Brown, Valenzuela, Wolpaw, and Stockwell. 2016a. "Global Survey of Cell Death Mechanisms Reveals Metabolic Regulation of Ferroptosis." *Nature Chemical Biology* 12 (7): 497–503. https://doi.org/10.1038/nchembio.2079.

"Global Survey of Cell Death Mechanisms Reveals Metabolic Regulation of Ferroptosis." *Nature Chemical Biology* 12 (7): 497–503. https://doi.org/10.1038/nchembio.2079.

Shin, Kim, Lee, and Roh. 2018. "Nrf2 Inhibition Reverses Resistance to GPX4 Inhibitor-Induced Ferroptosis in Head and Neck Cancer." *Free Radical Biology & Medicine* 129 (December): 454–62. https://doi.org/10.1016/j.freeradbiomed.2018.10.426.

Skouta, Dixon, Wang, Dunn, Orman, Shimada, Rosenberg, et al. 2014. "Ferrostatins Inhibit Oxidative Lipid Damage and Cell Death in Diverse Disease Models." *Journal of the American Chemical Society* 136 (12): 4551–56. https://doi.org/10.1021/ja411006a.

Stockwell, Angeli, Bayir, Bush, Conrad, Dixon, Fulda, et al. 2017. "Ferroptosis: A Regulated Cell Death Nexus Linking Metabolism, Redox Biology, and Disease." *Cell* 171 (2): 273–85. https://doi.org/10.1016/j.cell.2017.09.021.

Sui, Zhang, Liu, Duan, Zhai, Zhang, Han, et al. 2018. "RSL3 Drives Ferroptosis Through GPX4 Inactivation and ROS Production in Colorectal Cancer." *Frontiers in Pharmacology* 9: 1371. https://doi.org/10.3389/fphar.2018.01371.

Sun, Li, and Zhang. 2021. "Lidocaine Promoted Ferroptosis by Targeting MiR-382-5p /SLC7A11 Axis in Ovarian and Breast Cancer." *Frontiers in Pharmacology* 12: 681223. https://doi.org/10.3389/fphar.2021.681223.

Sun, Berleth, Wu, Schlütermann, Deitersen, Stuhldreier, Berning, et al. 2021. "Fin56-Induced Ferroptosis Is Supported by Autophagy-Mediated GPX4 Degradation and Functions Synergistically with MTOR Inhibition to Kill Bladder Cancer Cells." *Cell Death & Disease* 12 (11): 1–14. https://doi.org/10.1038/s41419-021-04306-2.

Sun, Chen, Zhai, Zhang, Xiang, Fang, Xu, et al. 2020. "The Emerging Role of Ferroptosis in Inflammation." *Biomedicine & Pharmacotherapy* 127 (July): 110108. https://doi.org/10.1016/j.biopha.2020.110108.

Takayama, Kubo, Morikawa, Morita, Nagano, and Saya. 2016. "Potential of Sulfasalazine as a Therapeutic Sensitizer for CD44 Splice Variant 9-Positive Urogenital Cancer." *Medical Oncology (Northwood, London, England)* 33 (5): 45. https://doi.org/10.1007/s12032-016-0760-x.

Ursini, and Maiorino. 2020. "Lipid Peroxidation and Ferroptosis: The Role of GSH and GPx4." *Free Radical Biology & Medicine* 152 (May): 175–85. https://doi.org/10.1016/j.freeradbiomed.2020.02.027.

Vaca, Wilhelm, and Harms-Ringdahl. 1988. "Interaction of Lipid Peroxidation Products with DNA. A Review." *Mutation Research/Reviews in Genetic Toxicology* 195 (2): 137–49. https://doi.org/10.1016/0165-1110(88)90022-X.

Valashedi, Najafi-Ghalehlou, Nikoo, Bamshad, Tomita, Kuwahara, Sato, Roushandeh, and Roudkenar. 2021. "Cashing in on Ferroptosis against Tumor Cells: Usher in the next Chapter." *Life Sciences*, September, 119958. https://doi.org/10.1016/j.lfs.2021.119958.

Veiner, Gorbatov, Vardi, Doros, Miller-Lotan, Zohar, Sabo, et al. 2015. "Pharmacogenomic Interaction between the Haptoglobin Genotype and Vitamin E on Atherosclerotic Plaque Progression and Stability." *Atherosclerosis* 239 (1): 232–39. https://doi.org/10.1016/j.atherosclerosis.2015.01.008.

Wang, and Tang. 2019. "PM2.5 Induces Ferroptosis in Human Endothelial Cells through Iron Overload and Redox Imbalance." *Environmental Pollution (Barking, Essex: 1987)* 254 (Pt A): 112937. https://doi.org/10.1016/j.envpol.2019.07.105.

Wei, Qiu, Yao, Wang, Jiang, Jia, Tao, et al. 2020. "Arsenic Induces Pancreatic Dysfunction and Ferroptosis via Mitochondrial ROS-Autophagy-Lysosomal Pathway." *Journal of Hazardous Materials* 384 (February): 121390. https://doi.org/10.1016/j.jhazmat.2019.121390.

Wu, Zhao, Yu, Li, Lin, and Chen. 2018. "Induction of Ferroptosis and Mitochondrial Dysfunction by Oxidative Stress in PC12 Cells." *Scientific Reports* 8 (1): 574. https://doi.org/10.1038/s41598-017-18935-1.

Xie, Wang, Lin, Mao, Feng, Gao, and Jiang. 2019. "Inhibition of Ferroptosis Attenuates Tissue Damage and Improves Long-Term Outcomes after Traumatic Brain Injury in Mice." *CNS Neuroscience & Therapeutics* 25 (4): 465–75. https://doi.org/10.1111/cns.13069.

Yagoda, Rechenberg, Zaganjor, Bauer, Yang, Fridman, Wolpaw, et al. 2007. "RAS–RAF–MEK-Dependent Oxidative Cell Death Involving Voltage-Dependent Anion Channels." *Nature* 447 (7146): 865–69. https://doi.org/10.1038/nature05859.

Yamada, Karasawa, Kimura, Watanabe, Komada, Kamata, Sampilvanjil, et al. 2020. "Ferroptosis Driven by Radical Oxidation of N-6 Polyunsaturated Fatty Acids Mediates Acetaminophen-Induced Acute Liver Failure." *Cell Death & Disease* 11 (2): 144. https://doi.org/10.1038/s41419-020-2334-2.

Yamaguchi, Hsu, Chen, Wang, Hsu, Chang, Du, Ko, Herbst, and Hung. 2013. "Caspase-Independent Cell Death Is Involved in the Negative Effect of EGFR Inhibitors on Cisplatin in Non-Small Cell Lung Cancer Cells." *Clinical Cancer Research : An Official Journal of the American Association for Cancer Research* 19 (4): 845–54. https://doi.org/10.1158/1078-0432.CCR-12-2621.

Yamaguchi, Kasukabe, and Kumakura. 2018. "Piperlongumine Rapidly Induces the Death of Human Pancreatic Cancer Cells Mainly through the Induction of Ferroptosis." *International Journal of Oncology* 52 (3): 1011–22. https://doi.org/10.3892/ijo.2018.4259.

Yaman, and Ayhanci. 2021. *Lipid Peroxidation*. IntechOpen. https://doi.org/10.5772/intechopen.95802.

Yang, Rivera, Jube, Nasu, Bertino, Goparaju, Franzoso, et al. 2010. "Programmed Necrosis Induced by Asbestos in Human Mesothelial Cells Causes High-Mobility Group Box 1 Protein Release and Resultant Inflammation." *Proceedings of the National Academy of Sciences of the United States of America* 107 (28): 12611–16. https://doi.org/10.1073/pnas.1006542107.

Yang, Zhou, Xie, Wang, Li, Chen, Mao, et al. 2021. "Metformin Induces Ferroptosis by Inhibiting UFMylation of SLC7A11 in Breast Cancer." *Journal of Experimental & Clinical Cancer Research: CR* 40 (1): 206. https://doi.org/10.1186/s13046-021-02012-7.

Yang, Kim, Gaschler, Patel, Shchepinov, and Stockwell. 2016. "Peroxidation of Polyunsaturated Fatty Acids by Lipoxygenases Drives Ferroptosis." *Proceedings of the National Academy of Sciences of the United States of America* 113 (34): E4966–75. https://doi.org/10.1073/pnas.1603244113.

Yang, SriRamaratnam, Welsch, Shimada, Skouta, Viswanathan, Cheah, et al. 2014. "Regulation of Ferroptotic Cancer Cell Death by GPX4." *Cell* 156 (1–2): 317–31. https://doi.org/10.1016/j.cell.2013.12.010.

Yang, and Stockwell. 2016. "Ferroptosis: Death by Lipid Peroxidation." *Trends in Cell Biology* 26 (3): 165–76. https://doi.org/10.1016/j.tcb.2015.10.014.

Yao, Zhang, Hao, Duan, Zhao, Sun, Li, et al. 2019. "Deferoxamine Promotes Recovery of Traumatic Spinal Cord Injury by Inhibiting Ferroptosis." *Neural Regeneration Research* 14 (3): 532–41. https://doi.org/10.4103/1673-5374.245480.

Yiannikourides, and Latunde-Dada. 2019. "A Short Review of Iron Metabolism and Pathophysiology of Iron Disorders." *Medicines* 6 (3): 85. https://doi.org/10.3390/medicines6030085.

Yin, Xu, and Porter. 2011. "Free Radical Lipid Peroxidation: Mechanisms and Analysis." *Chemical Reviews* 111 (10): 5944–72. https://doi.org/10.1021/cr200084z.

Yu, Xie, Cao, Yang, Yang, Lotze, Zeh, Kang, and Tang. 2015. "The Ferroptosis Inducer Erastin Enhances Sensitivity of Acute Myeloid Leukemia Cells to Chemotherapeutic Agents." *Molecular & Cellular Oncology* 2 (4): e1054549. https://doi.org/10.1080/23723556.2015.1054549.

Zhang, Tan, Daniels, Zandkarimi, Liu, Brown, Uchida, O'Connor, and Stockwell. 2019. "Imidazole Ketone Erastin Induces Ferroptosis and Slows Tumor Growth in a Mouse Lymphoma Model." *Cell Chemical Biology* 26 (5): 623-633.e9. https://doi.org/10.1016/j.chembiol.2019.01.008.

Zhou, Jie Ye, Bonavita, Daniels, Kainrad, Jogasuria, and You. 2019. "Adipose-Specific Lipin-1 Overexpression Renders Hepatic Ferroptosis and Exacerbates Alcoholic Steatohepatitis in Mice." *Hepatology Communications* 3 (5): 656–69. https://doi.org/10.1002/hep4.1333.

Chapter 3 Electrically switchable nanolever technology for the screening of metal-chelating peptides in hydrolysates

Metal-chelating peptides (MCPs) are considered as indirect antioxidants due to their capacity to inhibit radical chain reaction and oxidation. Here, we propose a new proof-of-concept for the screening of MCPs present in protein hydrolysates for valorizing their antioxidant properties by using emerging time-resolved molecular dynamics technology, switchSENSE®. This method unveils possible interactions between MCPs and immobilized nickel ions using fluorescence and electro-switchable DNA chip. The switchSENSE® method was first set up on synthetic peptides known for their metal-chelating properties. Then, it was applied to soy and tilapia viscera protein hydrolysates **(Figure 3.1)**. Their Cu^{2+}-chelation capacity was, in addition, determined by UV-visible spectrophotometry as a reference method. The switchSENSE® method has displayed a high sensitivity to evidence the presence of MCPs in both hydrolysates. Hence, we demonstrate for the first time that this newly introduced technology is a convenient methodology to screen protein hydrolysates in order to determine the presence of MCPs before launching time-consuming separations.

This chapter has already been published in Journal of Agriculture and Food Chemistry as : El Hajj, S., Sepúlveda Rincón, C.T., Girardet, J.M., Cakir-Kiefer, C., Stefan, S., Zapata Montoya, J.E., Boschi-Muller, S., Gaucher, C., & Canabady-Rochelle, L. Electrically switchable nanolever technology for the screening of metal-chelating peptides in hydrolysates (2021). *J. Agric. Food Chem.* 69 (31) 8819-8827. https://doi.org/10.1021/acs.jafc.1c02199

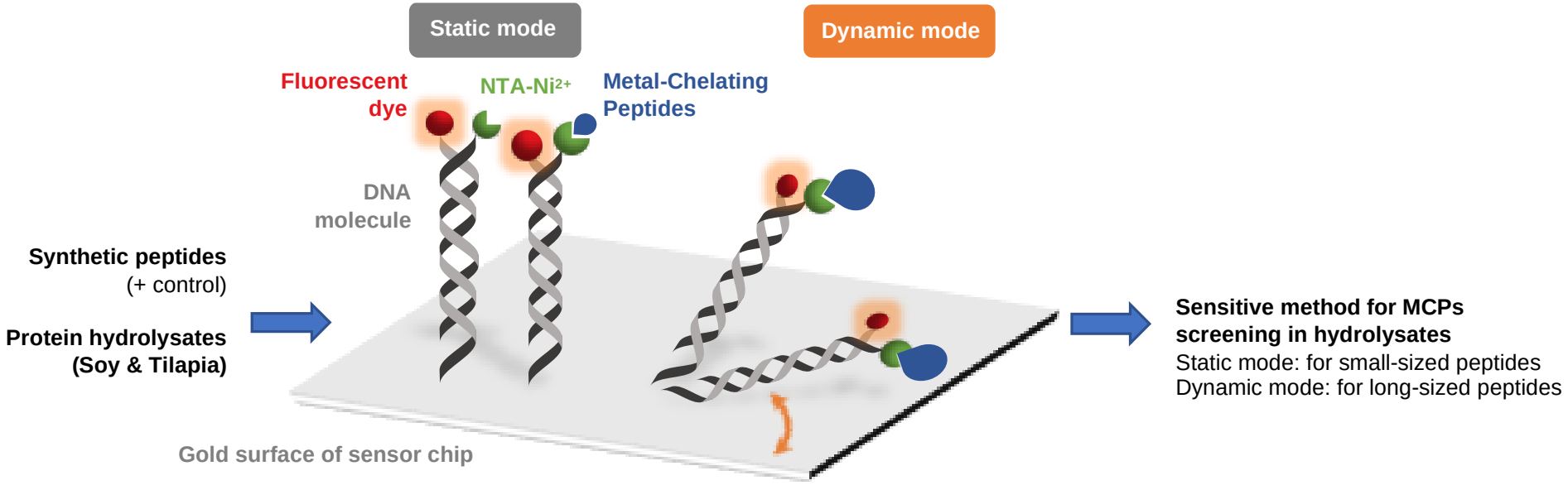

Figure 3.1. The switchSENSE® method was first set up on synthetic peptides known for their metal-chelating properties and on soy and tilapia viscera protein hydrolysates

3.1 Introduction

Nowadays, biomolecules are gaining attention as alternatives to chemicals in various industrial applications such as nutrition, cosmetics, and pharmaceutics. Bioactive peptides with biological activities (*e.g.,* antioxidant, antihypertensive, anticancer activity) (El Hajj *et al.,* 2021) based on their amino acid composition and their primary structures, have been produced by enzymatic hydrolysis (Megías *et al.,* 2007). Metal ion chelation is a functional property commonly investigated in literature (Canabady-Rochelle *et al.,* 2015; Yousef *et al.,* 2019). Indeed, metals ions such as iron, zinc, calcium and copper are essential for several biological functions such as enzyme catalysis, oxygen transport, and neurotransmitter release (Guo *et al.,* 2014). However, their bioavailability is poor due to their low solubility in human fluids (Ma *et al.,* 2019). MCPs contribute to minerals absorption and bioavailability (Ma *et al.,* 2019), thus regulating ion concentrations through selective bindings (Yousef *et al.,* 2019). Finally, iron and copper-chelating peptides - while complexing these transient metal ions - can act as indirect antioxidants by inhibiting *in vivo* the Fenton and Haber-Weiss reactions responsible for the formation of reactive oxygen species (including the hydroxyl radical) and subsequent radical chain reactions.

Protein hydrolysates constitute interesting sources of metal-chelating peptides to explore. Among natural resources, hydrolysates produced from soy proteins (Chen *et al.,* 1998), barley hordein (Bamdad and Chen 2013), and milk whey (Peng *et al.,* 2010), were reported to contain MCPs. In the present study, two sources of potential MCPs were investigated: a tilapia by-product and soy protein isolate. Tilapia is one of the species with the highest aquaculture production in the world, and represents 10% of all finfish species (FAO 2018). Yet, by-products generated by its aquaculture production are about 60% of the animal total weight (Robert *et al.,* 2015). Enzymatic hydrolysis of tilapia by-products is a convenient method to generate protein hydrolysates with high content of bioactive peptides (Gómez *et al.,* 2020; Sierra *et al.,* 2021; S. B. Zhang, Wang, and Xu 2007). In the case of soy protein isolates, enzyme technology is often developed to unveil protein-encrypted bioactive sequences with potential health benefits (*e.g.*, antioxidant activities), and to improve the techno-functional properties for instance (Ashaolu 2020).

To date, the selective separation of bioactive peptides from a hydrolysate is still studied empirically: peptides are separated into various fractions, each one being evaluated for its

bioactivity up to isolate the target peptide and to identify its sequence by tandem mass spectrometry. For MCPs separation, immobilized metal ion affinity chromatography (IMAC) is a technique that takes advantage of the interaction between an immobilized metal ion and a protein or a peptide present in complex biological samples. IMAC can separate peptides or proteins efficiently (Alhazmi *et al.,* 2015) and has been investigated for several years (Helfferich 1961). Nevertheless, the IMAC phase has a moderate sensitivity (Alhazmi *et al.,* 2015), limited performance and flexibility, in addition to the waste of molecules of interest upon the washing up of the non-specific binding molecules (Weinberger, Morris, and Pawlak 2000), which constitute main disadvantages of IMAC.

Hence, MCP screening in hydrolysates is a priority before launching time-consuming separation. Among various screening approaches, the differential analysis of mass spectra of hydrolysates was carried out in the presence and in the absence of metal ion using liquid chromatography coupled to high resolution mass spectrometry in order to detect iron(II)-chelating peptide in protein hydrolysates (Paris *et al.,* 2021). In addition, Surface Plasmon Resonance (SPR) was reported to compare the affinity constant of different tagged proteins bound to metal ions (Bernaudat and Bülow 2005; Kurzątkowska *et al.,* 2014; Nieba *et al.,* 1997) or to study the affinity of His-tag peptides to Ni^{2+} ions (Knecht *et al.,* 2009). Recently, our team developed a strategy to screen MCPs using affinity constants determined in SPR (Canabady-Rochelle *et al.,* 2018) and to simulate their IMAC separation (Muhr *et al.,* 2020). Like SPR, the newly introduced switchSENSE® technology allows to analyse biomolecular interactions in real time. The originality of this latter technology is based on the use of electro-switchable fluorescent DNA nanolevers in which one DNA strand bears a fluorophore while its complementary strand is functionalized by a capture molecule (*i.e.* complexing agent), itself coupled to a ligand (*e.g.,* metal ion) (Langer *et al.,* 2013). Once the target MCP interacts with the metal ion immobilized on the complexing agent, the fluorescence is quenched and the alternating mobility of the DNA nanolevers is altered. These changes allow to determine kinetics and affinity constants in addition to other information related to the analyte (MCPs herein) such as structural and conformational characteristics. As immobilized metals, nickel ions are widely used for protein purification due to their affinity with the exposed side chains of histidine and cysteine in proteins (Hainfeld *et al.,* 1999). With six

coordination sites, Ni^{2+} can strongly bind to a complexing agent such as the tetradentate nitrilotriacetic acid (NTA), while some sites still remain available to interact with the target peptide (Hainfeld *et al.,* 1999).

The aim of this study is to make a proof-of-concept for the screening of metal-chelation activity of peptides present in protein hydrolysates. To that purpose, the switchSENSE® methodology was first set up under static and dynamic modes with small synthetic MCPs, and then with protein hydrolysates, *i.e*. soy protein hydrolysate (SPH) and Tilapia protein hydrolysate (TPH). Prior to that, the global capacity of protein hydrolysates to chelate nickel was checked by standard spectrometry methods.

3.2 Material and Methods

3.2.1 Production of protein hydrolysates

Soy protein hydrolysate. Soy protein isolate (kindly provided by SAS improve, Dury, France) was composed of 87% (w/w) pure proteins. The soy protein isolate powder was dissolved in 50 mM ammonium bicarbonate (2% w/v) and pre-heated at 90 °C for 5 min. Indeed, this ammonium bicarbonate solution has a good buffering capacity in order to regulate well the pH of the medium according to the optimum activity of the enzymes. Besides, this solution does not contain ionic element that might interfere in metal-chelation.

Alcalase® (≥ 2.4 U/g), Protamex® (≥ 1.5 U/g), or Flavourzyme® (≥ 500 U/g), purchased from Sigma-Aldrich (St. Louis, MO, USA) were the proteolytic enzymes used. Hydrolysis was performed with Enzyme/ Substrate ratio equal to 1% (w/w) for 1 h or 3 h, in a beaker equipped with a thermostatic water jacket at the enzymes' optimal working temperature (55 °C) at pH 8.0 (with Alcalase®) and pH 7.0 (with Protamex®, or Flavourzyme®). As described in **Figure 3.2**, enzymes were then inactivated at 100 °C for 15 min by incubating in boiling water. Then, soy protein hydrolysates (SPHs) were cooled at room temperature, centrifuged (10,000 *g,* 15 min), freeze-dried by lyophilization for 48 hours and stored at -20°C until used.

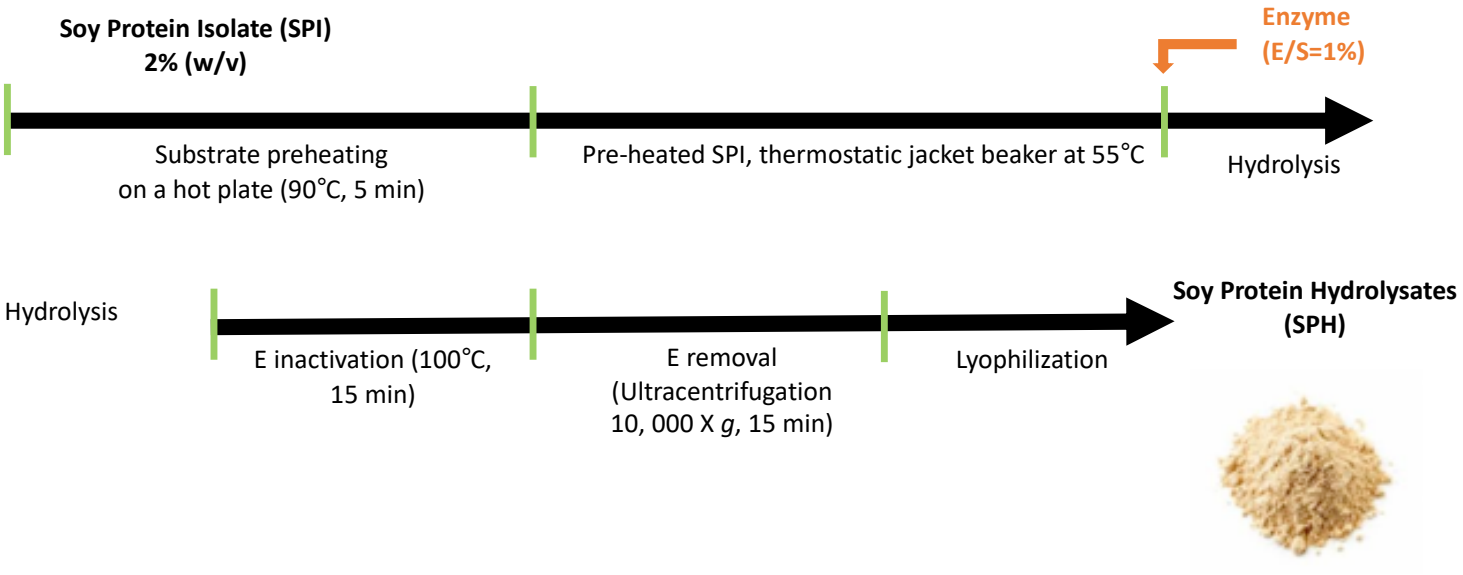

Figure 3.2. Production of the soy protein hydrolysate

Tilapia viscera protein hydrolysate. Fresh red tilapia viscera (*Oreochromis* spp.; kindly provided by Piscícola El Gaitero Antioquia, Colombia) were minced immediately upon arrival using a blender (Black & Decker, Hampstead, MD, USA). Hydrolysate preparation is schematized on **Figure 3.3**. Tilapia viscera were heated at 90 °C for 20 min to inactivate endogenous enzymes. Upon heating, the fat melted and separated from other components of the viscera. Then, sample was frozen at -20 °C for 24 h to easily remove the solidified fat by phase separation. Viscera were then packed in PVC bags and stored at -20 °C until further use. Enzymatic hydrolysis of tilapia viscera was carried out in a batch reactor Bioflo 310 (New Brunswick Scientific Co., Enfield, CT, USA) with pH and temperature maintained at 10 and 59 ºC, respectively, through the automatic control of the Bioflo reactor 310® (New Brunswick Scientific Co., Inc. USA). The reaction was started by the addition of Alcalase® 2.4 L (Novozymes, Copenhagen, Denmark) at enzyme/substrate mass ratio of 1:10. The hydrolysis was monitored by pH-stat method for 3 h. Once produced, the tilapia protein hydrolysate (TPH) was freeze-dried and stored at -20 °C until use. Then, a purification step was carried out on Sep-Pak C18 cartridges (Waters Associates, Milford, MA, USA) to remove salts and other impurities. The cartridges were equilibrated with an aqueous eluent containing 1% (v/v) acetonitrile and 0.01% (v/v) trifluoroacetic acid. The TPH hydrolysate was solubilized at 10 mg/mL in the same equilibration eluent and loaded (1 mL) onto the cartridge. After loading, the cartridge

was washed with the same eluent (3 mL), and TPH was then eluted with a mixture of 30% acetonitrile and 0.01% trifluoroacetic acid in water. The eluted desalted hydrolysate was then freeze-dried and stored at -20 °C until further analyses (Sepúlveda and Zapata 2020).

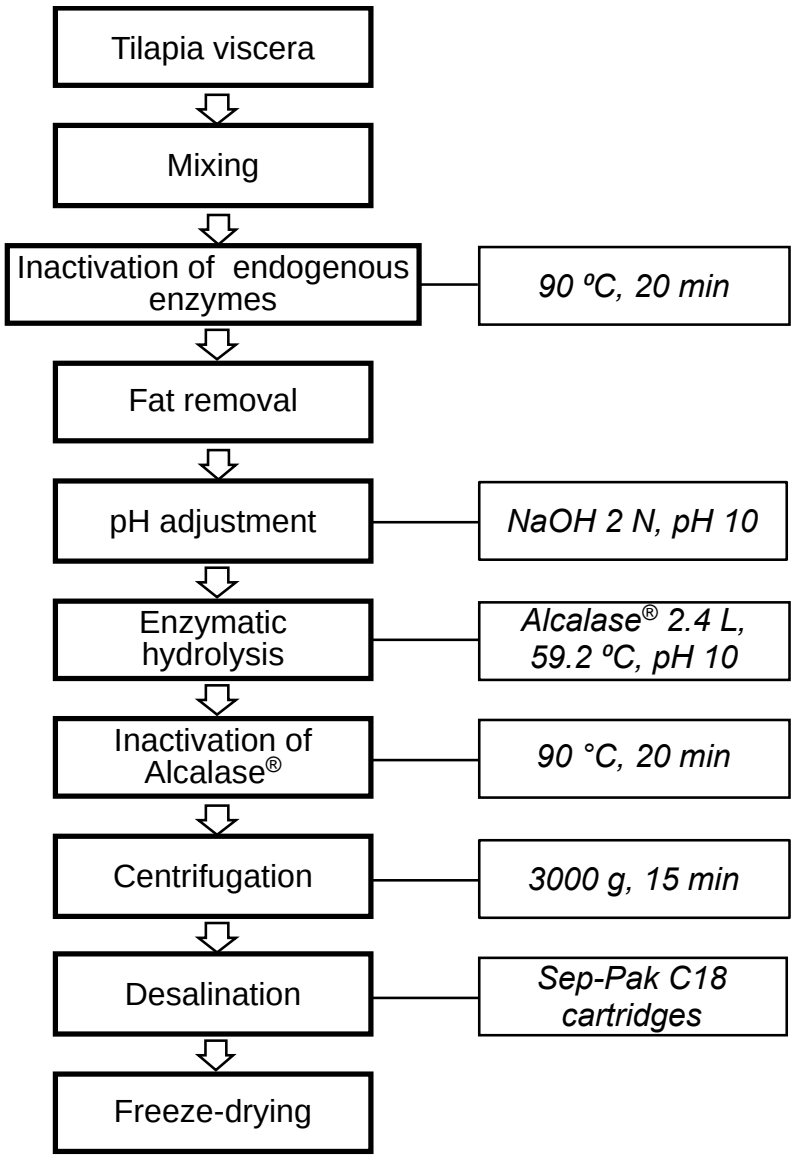

Figure 3.3. Production of the Tilapia protein hydrolysate

3.2.2 Peptide characterization

Peptide concentration in hydrolysates (*i.e.*, TPH and SPHs) was quantified using ortho-phthaldialdehyde-based assay (OPA; ThermoFisher Scientific, Loughborough, UK) in the presence of *N*,*N*-dimethyl-2-mercaptoethyl-ammonium (ThermoFisher) (Canabady-Rochelle et al. 2018; Frister, Meisel, and Schlimme 1988). The results were expressed as mM equivalent (eq.) NH_2 using a calibration curve performed with glycine **(Table 3.1).**

Table 3.1. Peptide concentrations in tilapia protein hydrolysate (TPH) and soy protein hydrolysate (SPH) determined by OPA quantification

Hydrolysates (1g/L)	Peptide concentration (mM eq. NH_2)
SPH (Alcalase® 1 h)	1.39
SPH (Alcalase® 3 h)	1.55
SPH (Protamex® 1 h)	1.19
SPH (Protamex® 3 h)	1.42
SPH (Flavourzyme® 1 h)	0.83
SPH (Flavourzyme® 3 h)	1.19
TPH (Alcalase® 3 h)	0.94

SPHs fractions were analyzed for size distribution by sodium dodecyl sulfate polyacrylamide gel electrophoresis (SDS-PAGE) 15% (v/v) by comparison with molecular weight marker (Bio-Rad, Marnes La Coquette, France) according to the Laemmli method (Laemmli and Favre 1973).

The molecular weight distribution of tilapia hydrolysate was determined by size-exclusion chromatography in a previous study that showed the presence of peptides below 6511 Da, with a striking amount around 336 Da (Sepúlveda *et al.,* 2020).

3.2.3 Real-time switchSENSE® analysis

Synthetic peptides (*i.e.* HHHHHH, HHH, HGH, HW, and β-AH also called carnosine; Sigma-Aldrich), able to bind nickel ions (see peptide chemical structures on **Figure 3.4**), TPH, and SPH were prepared in 10 mM Tris-HCl buffer, pH 7.4, containing 40 mM NaCl, and 0.05% (v/v) Tween 20 (buffer T40). The switchSENSE® experiments were carried out with a biosensor analyzer DRX (SwitchSENSE® Dynamic Biosensors GmbH, Planegg, Germany). An electro-switchable DNA chip MPC-48-2-R1-S containing tris-nitrilotriacetic acid and the fluorescent probe Cy5, was used according to the instructions supplied with the Tris-NTA kit of Dynamic Biosensors. The chip is composed by 6 electrodes connected to 2 spots used as references and 4 sample spots carrying the Ni^{2+} functionalized acid (NTA_3)-tagged DNA nanolevers. The principle of the switchSENSE® technology (**Figure 3.5, panels A and B**) is explained in details by Langer *et al.* Fluorescence static measurements (at 25 °C) were performed on one spot out of the 4 sample spots. Several concentrations of synthetic peptides (0.5, 1 and 10 µM), TPH (5 and 10 µM eq. NH_2), and SPH (10, 100, and 1000 µM eq. NH_2) were injected in the microfluidic device at a flow rate of 10 $\mu L.min^{-1}$ for 10 min (association phase). Then, buffer was injected at 30 $\mu L.min^{-1}$ for 120 min to release the analytes (dissociation phase). All over the kinetic experiments (static measurements), a blank control was performed with peptide-free buffer and subtracted to normalize the signal.

Between the former association and dissociation phases, the flow was stopped, and dynamic measurements were performed with all samples in order to determine the specificity of the interaction. The dynamic response (DR) was deduced from fluorescence relaxation measurements of the switching nanolevers present on all the 6 spots of the chip (reference and sample spots). The difference in motion rates between peptide-free DNA nanolevers and MCP-carrying nanolevers was expressed as relative **Δ**DR (in %). All curves were analysed by nonlinear fitting of single-exponential functions with the switchANALYSIS® software from Dynamic Biosensors. The error presented with the results corresponds to the global fit error of all measurements.

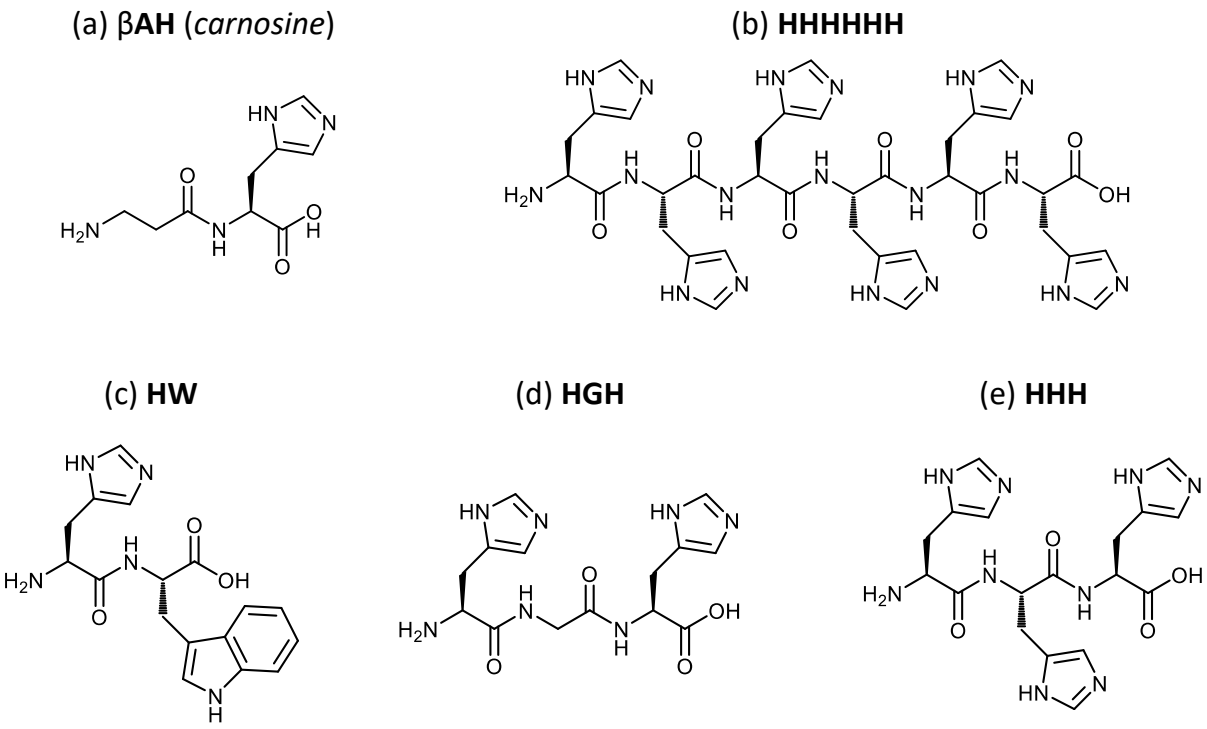

Figure 3.4. Chemical structures of the investigated peptides

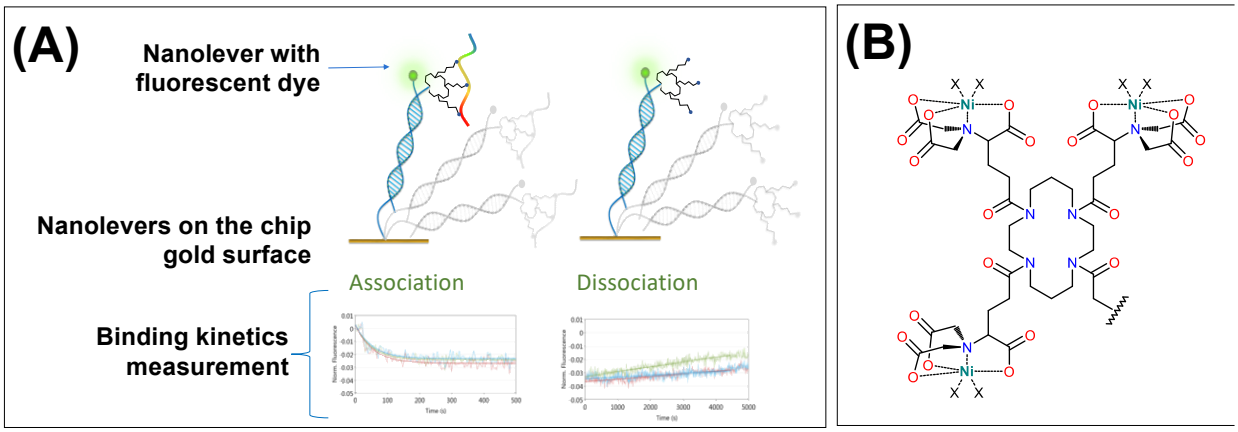

Figure 3.5. (A) Schematic principles of switchSENSE® and **(B)** Structures of the NTA-Ni2+ chelate bound at the extremity of the DNA nanolever and on the surface of the biosensor chip

3.2.4 Metal-chelation test

The global chelation capacity of hydrolysates was determined upon Cu^{2+} chelation by spectrophotometry using murexide as colour indicator. This test was carried out as described in several studies (Canabady-Rochelle et al. 2018; Wong, Leong, and Williamkoh 2006; Wu et al. 2003). Hydrolysates were prepared at different concentrations varying between 2 and 40 $g \cdot L^{-1}$ also expressed in mM eq. NH_2. EDTA and carnosine were both used as positive controls for metal chelation and prepared in a range of 0.4 - 40mM. EDTA, carnosine and hydrolysate solutions were directly diluted in a microplate with hexamine buffer for a total volume of 143 µL. Then, 143 µL of a 3 mM $CuSO_4$ in hexamine buffer and 14 µL of 1 mM murexide solution were added in each well (total volume: 300 µL). The 96-well plate was incubated for 3 min at room temperature and the absorbance was read at two wavelengths, *i.e.* 485 nm and 520 nm, for the copper-murexide complex and the murexide alone, respectively. The A_{485}/A_{520} ratio was considered as proportional to the free copper ion (Cu^{2+}) concentration.

$$Cu^{2+} \text{ complexation } (\%) = \frac{[(A_{485}/A_{520})_0 - (A_{485}/A_{520})_s]}{(A_{485}/A_{520})_0} \times 100 \qquad [1]$$

With $(A_{485}/A_{520})_0$ = ratio of absorbances measured in the absence of sample, and $(A_{485}/A_{520})_s$ = ratio of absorbances measured in the presence of sample (EDTA, carnosine or hydrolysate).

3.3 Results and Discussion

3.3.1 SwitchSENSE® measurements with model peptides

As a starting point, static and dynamic measurements of switchSENSE® were performed with synthetic peptides having 2–6 residues in order to test if this new emerging biosensing technology was sensitive enough to detect the binding of small-sized MCPs. Carnosine, HHHHHH, HHH, HW and HGH are known to chelate transition metals due to the presence of histidine residues (Willett et al. 1995).

Static measurement for fluorescence proximity sensing is a real-time measurement of kinetics responding to changes to the molecular environment upon analyte binding. The fluorescence is partly quenched when the analyte binds to nickel ions (association), which is close to the fluorescent probe while it increases if the analyte is released (dissociation). The real-time

molecular interaction kinetics are shown in **Figure 3.6**. As observed for all the samples, the measured fluorescence signal has always decreased (fluorescence quenching), highlighting an association of the peptides on the immobilized nickel ions. However, the dissociation phase was not observed for the investigated synthetic peptides. This can be explained by their high affinity for nickel ions (three nickel ions are immobilized per DNA nanolever) leading to a very slow dissociation that cannot be observed within the two hours of the dissociation phase measurement.

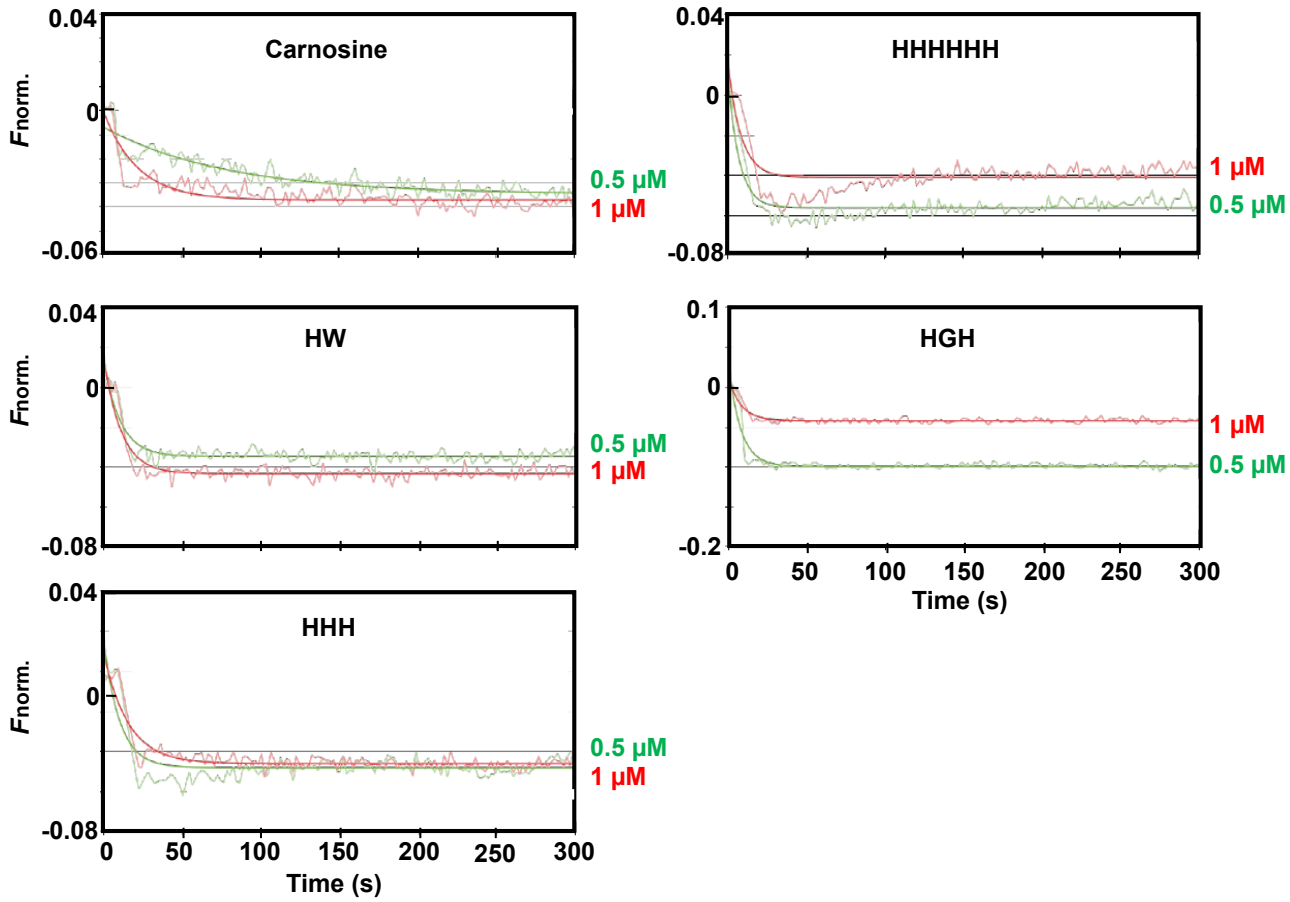

Figure 3.6. Association kinetics analysis of synthetic peptides onto immobilized nickel ions by using the switchSENSE® technology. Raw data are superimposed by global exponential fits for various concentrations of each peptide. A blank control performed with T40 buffer instead of analyte was subtracted to normalize the signal. The k_{obs} were determined for each kinetics measurement. F_{norm}, normalized fluorescence.

The observed rate constant (k_{obs}) determined for carnosine, HHHHHH, HW, HGH and HHH according to the data depicted in **Figure 3.6** are summarized in **Table 3.2**. The results showed no significant variation in the k_{obs} values as a function of peptide concentrations, suggesting that saturation has been reached with the peptide concentrations (K_D < 0.5 µM) used. Due to the low signal intensity, it is not possible to use lower concentrations of peptides. Therefore, the values of the equilibrium constants of association and dissociation (K_A and K_D) cannot be determined. In addition, comparison of the association k_{obs} values at a defined peptide concentration could give information on the relative association rate. Consequently, and according to **Table 3.2**, the fastest observed association rate is obtained with HHHHHH, then with the di- and tri-peptides and finally with carnosine.

Table 3.2. Observed rate constants (kobs) of synthetic peptides, SPHs and TPH association to immobilized nickel ions determined with the switchSENSE® method. Results are presented as mean ± standard deviation.

Sample	k_{obs} **(s^{-1})**[a]	k_{obs} **(s^{-1})**[b]
Carnosine (βAH)	0.013 ± 0.001	0.046 ± 0.003
HHHHHH	0.140 ± 0.015	0.07 ± 0.02
HW	0.095 ± 0.008	0.067 ± 0.007
HGH	0.130 ± 0.006	0.085 ± 0.010
HHH	0.10 ± 0.02	0.064 ± 0.004
SPH (Alcalase® 1 h)	0.09 ± 0.01	0.08 ± 0.01
SPH (Protamex® 1 h)	(1.1 ± 0.9) x10^{-3}	(1.0 ± 0.2) x10^{-3}
SPH (Flavourzyme® 1 h)	not observed	not observed
TPH (Alcalase® 3 h)	(1.9 ± 0.2) x10^{-3}	(29.5 ± 5.4) x10^{-3}

[a] k_{obs} determined at 0.5 µM for synthetic peptides, 5 µM and 0.1 mM eq. NH_2 for TPH and SPHs, respectively

[b] k_{obs} determined at 1 µM for synthetic peptides, 10 µM and 1 mM eq. NH_2 for TPH and SPHs, respectively

In order to find a more sensitive approach, the effect of bounded peptides on molecular motion of the nanolevers was studied by carrying out experiments in dynamic mode. To that purpose, the up-to-down motion of the nanolevers was tracked in real time through fluorescence measurement. Upon binding of an analyte (MCP herein), the hydrodynamic friction and the subsequent motion of the nanolevers are in theory both affected. The dynamic response (**DR**) decreases when an analyte (peptide herein) binds to the immobilized ligand (nickel ions in the present study). The strategy used is explained on **Figure 3.7**. First, T40 buffer (see Materials and Methods) was injected through the microfluidic of the biochip and the DR of the reference electrodes E1 and E2 (in the absence of Ni^{2+} immobilized) and of the sample electrodes E3 to E6 (in the presence of Ni^{2+} immobilized) were determined. Secondly, peptide samples were loaded and the DR was determined.

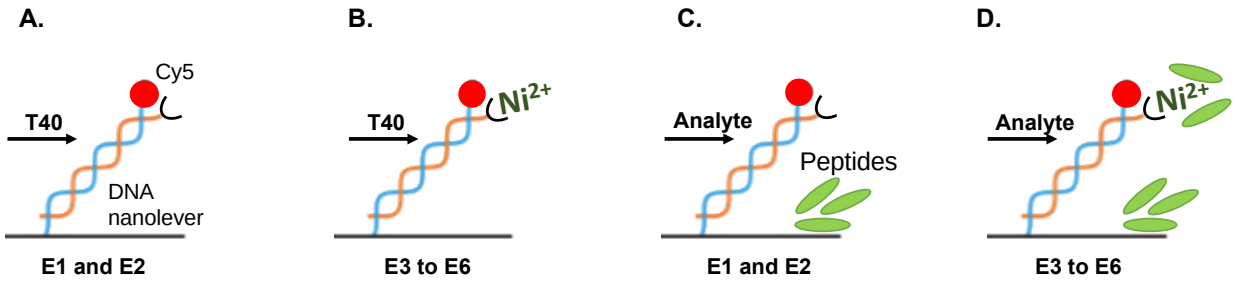

Figure 3.7. Real-time switchSENSE® analysis of molecular interaction between the investigated analyte (synthetic peptides or hydrolysates (TPH, SPHs)) and nickel ions immobilized on DNA nanolevers attached to the gold surface of the chip. The chip is composed of six switchable electrodes, all in contact with the running buffer or analytes loaded into the microfluidic. In molecular dynamics mode, nanolevers are deliberately moved by way of alternating the voltage across the surface. The motion of the levers is tracked in real time. Upon analyte binding, the hydrodynamic friction of the nanolevers and their movement are affected. **(A)** Reference electrodes E1 and E2 in the presence of T40 buffer, **(B)** Sample electrodes E3 to E6 in the presence of T40 buffer, **(C)** Reference electrodes in the presence of analyte (i.e. synthetic peptides or hydrolysates), **(D)** Sample electrodes in the presence of analyte.

Thus, the five synthetic peptides (10 µM in T40 buffer) were investigated by the molecular dynamic mode. The differences of dynamic response between control (*i.e.* peptide-free buffer) and investigated synthetic peptides, defined as **Δ**DR, are depicted in **Figure 3.8**. The conformational study displays poor sensitivity for low-molecular weight and small-sized peptides (2 or 3 amino-acid residues) probably because the molecular friction was not sufficiently slowed down by the binding of such small-sized materials onto the nanolevers. However, it was possible to unveil weak response for HHH, which marked the sensitivity limit of the dynamic mode, while the hexapeptide HHHHHH led to a strong dynamic response.

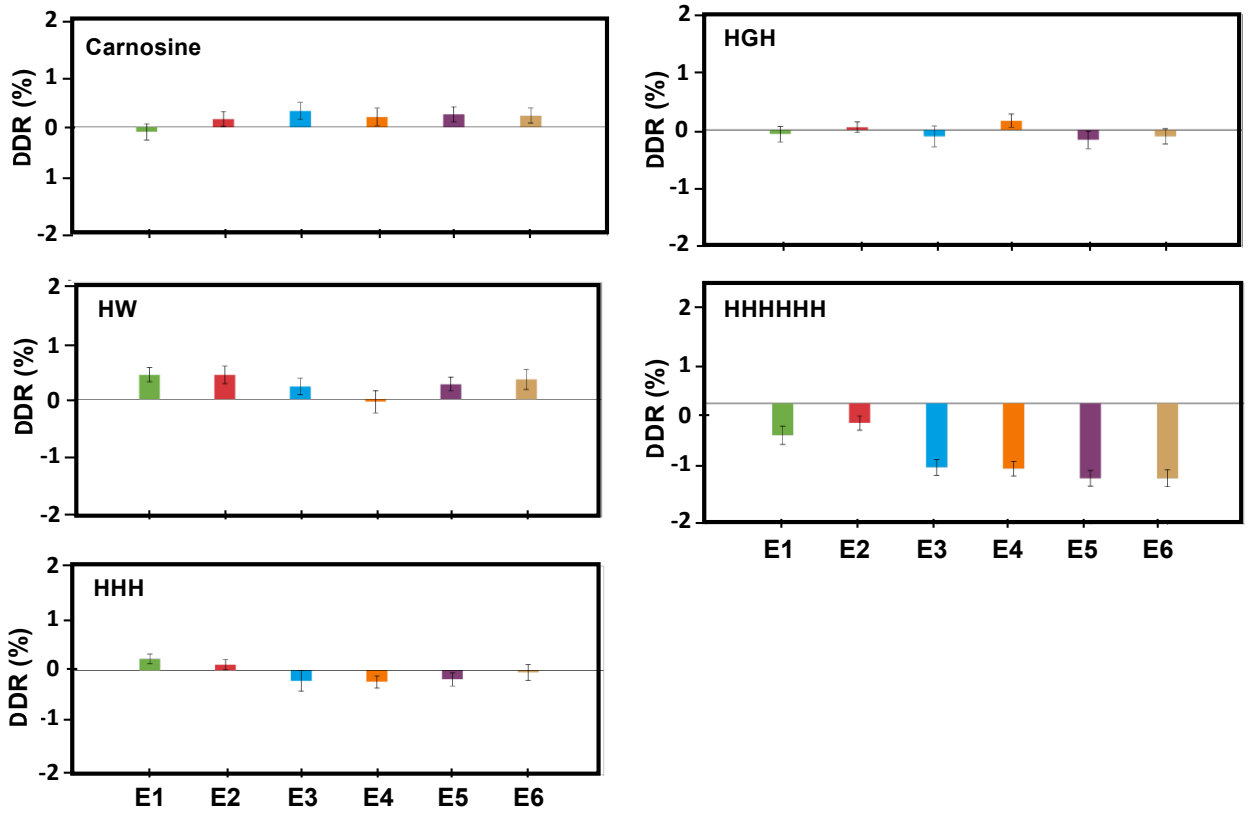

Figure 3.8. Molecular dynamics experiments performed by switchSENSE® technology with synthetic peptides. Experiments were performed in T40 buffer, then in the presence of sample (at 10 µM). Nanolevers' motions were expressed as dynamic response (DR). The relative difference **Δ**DR (in %) was calculated from the various motions determined in the presence and in the absence of sample. Unspecific binding onto the DNA double strands was determined from the **Δ**DR of the reference electrodes E1 and E2 free of nickel, whereas specific interaction with nickel was determined from the **Δ**DR of the sample electrodes E3 to E6

Therefore, these results show that switchSENSE® technology is applicable on small synthetic MCPs and that the two modes can give different information, as the static mode is size-independent but not very sensitive for high affinity MCP-Ni^{2+} association, whereas the dynamic mode seems to have restrictions for very low molecular weight peptides but is much sensitive with peptides able to alter the motion of the nanolevers.

3.3.2 Metal-chelation capacity of Tilapia viscera and soy proteins hydrolysates

Based on their protein composition, and in particular in histidyl residues usually involved in metal ions chelation, soy and Tilapia viscera protein hydrolysates were selected for this study. Indeed, in the soy protein isolate, β-conglycinin 7S (30 His; UniProtKB accession numbers P11827 and P25974) and glycinin G5 (5 His; P04347) represent 80% of the total protein (Adachi *et al.,* 2003; Nishinari *et al.,* 2014). In TPH, histidine was found at a concentration of 12 mg/g of protein (Sepúlveda *et al.,* 2020). Besides, the chelating activity may also be influenced by the presence of negatively charged amino acids, present in 63 mg/g of protein in TPH (Sepúlveda *et al.,* 2020; Zhang, Duan, and Zhuang 2012).

Many studies have extracted and screened metal-chelating peptides after similar enzymatic hydrolysis for soy and tilapia proteins (Charoenphun *et al.,* 2013; Q. Zhang *et al.,* 2018). Alcalase®, Protamex® and Flavourzyme® enzymes are widely listed in literature for producing antioxidant hydrolysates with their hydrolysing optimum conditions (Korhonen and Pihlanto 2006).

Prior to launching switchSENSE® measurements, the ability of TPH and SPH to bind copper ion was investigated by UV-visible spectrophotometry. It is noteworthy to mention that despite the difference in metal ion used, Ni^{2+} in switchSENSE® or Cu^{2+} in spectrophotometry, these two metal ions have similar metal chelation properties in regards to the HSAB theory. Indeed, both belong to the intermediate acids according to the HSAB theory and are able to deprotonate the peptide's amide functions, and induce metal coordination (Sóvágó and Ősz 2006). **Figure 3.9, Panel A,** presents the Cu^{2+} chelation capacity as a function of molar ratio (mM eq. NH_2 of hydrolysate /mM $CuSO_4$). Saturation was observed for all hydrolysates, showing the presence of peptides with affinity for copper. Moreover, a quantitative method previously developed in our group was

applied in order to compare M^{2+} chelation capacities between hydrolysates (Canabady-Rochelle *et al.,* 2018). Two indices, EDTA Equivalent Chelating Capacity (EECC) and Carnosine Equivalent Chelating Capacity (CECC) were calculated from the slopes of the linear parts of the Cu^{2+} chelation graphs of SPH, EDTA and carnosine **(Figure 3.9, Panels A & B)**, where:

$$EECC = (slope)_H / (slope)_{EDTA} \quad [2]$$

$$CECC = (slope)_H / (slope)_{carnosine} \quad [3]$$

The EECC and CECC values were calculated for all hydrolysates (H is either TPH or SPH) and presented in **Table 3.3**. From this latter, TPH is clearly the best preparation in terms of copper chelation activity. Concerning SPHs, a limited hydrolysis time (1 h) is sufficient to reveal metal chelation activity. Besides, the SPH obtained with Flavourzyme® is largely better in terms of chelation capacity than the two other SPHs although hydrolysis by Flavourzyme® is not completed. Note that the hydrolysis with Alcalase® and Protamex® were more extensive as shown by SDS-PAGE analysis (**Figure 3.10**). Therefore, the metal-chelation test validates the presence of MCPs in all investigated hydrolysates.

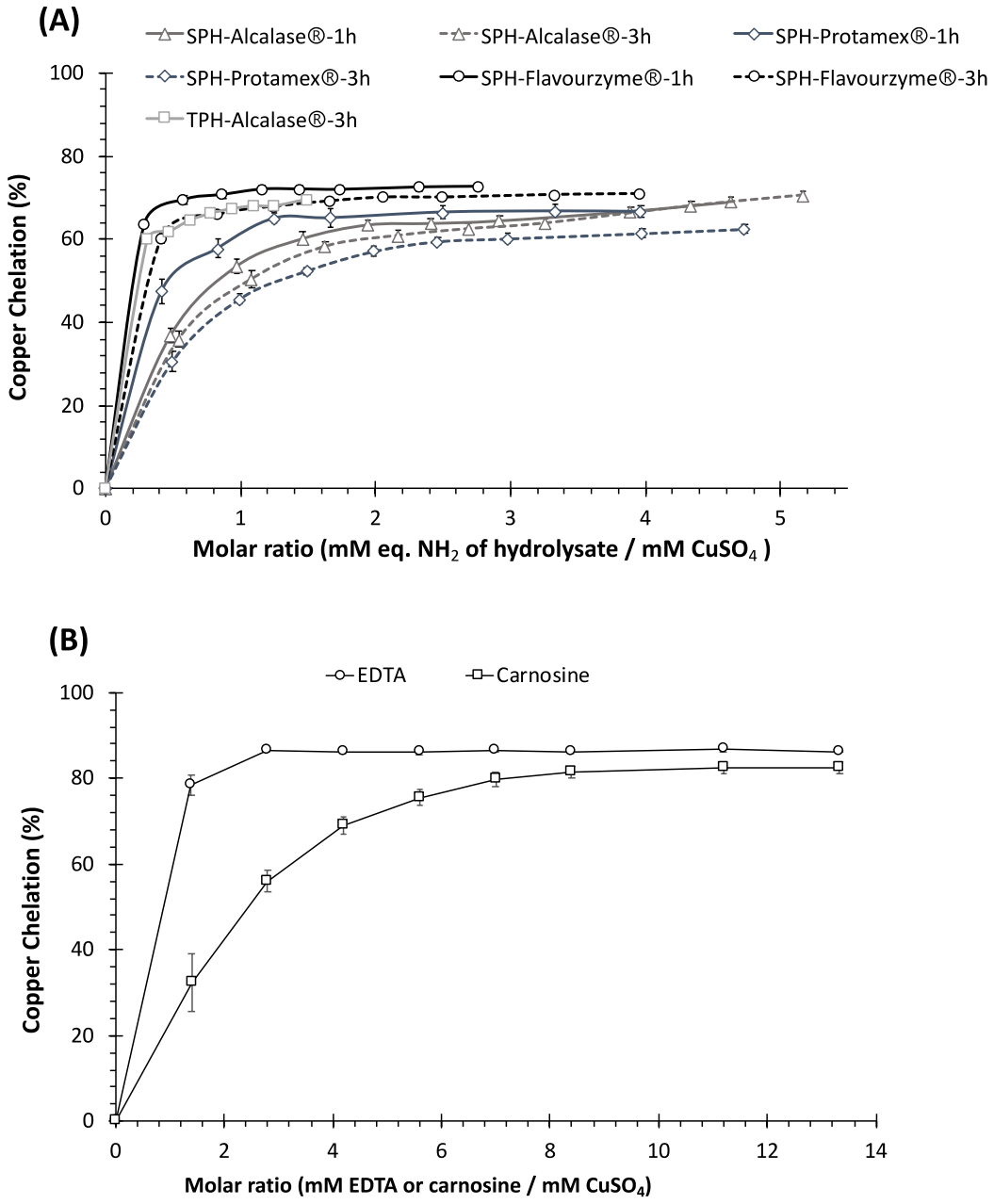

Figure 3.9. Copper chelation capacity (%) of the different hydrolysates **(A),** EDTA and carnosine **(B)** as a function of molar ratio (mM eq NH_2 of hydrolysate or mM EDTA, carnosine/ mM $CuSO_4$). SPHs were prepared by Alcalase®, Protamex®, or Flavourzyme® one- or three-hour treatment. The TPH was prepared by Alcalase® three-hours treatment

Table 3.3. EECC and CECC values determined for TPH and SPHs

	EECC[a]	**CECC**[b]
EDTA	1	-
Carnosine	-	1
SPH (Alcalase® 1 h)	2.53	3.60
SPH (Alcalase® 3 h)	2.85	4.06
SPH (Protamex® 1 h)	4.51	6.41
SPH (Protamex® 3 h)	3.37	4.79
SPH[c] **(Flavourzyme® 1 h)**	11.23	15.96
SPH (Flavourzyme® 3 h)	5.38	7.65
TPH (Alcalase® 3 h)	13.84	19.67

[a]EECC (EDTA Equivalent Chelating Capacity)

[b]CECC (Carnosine Equivalent Chelating Capacity)

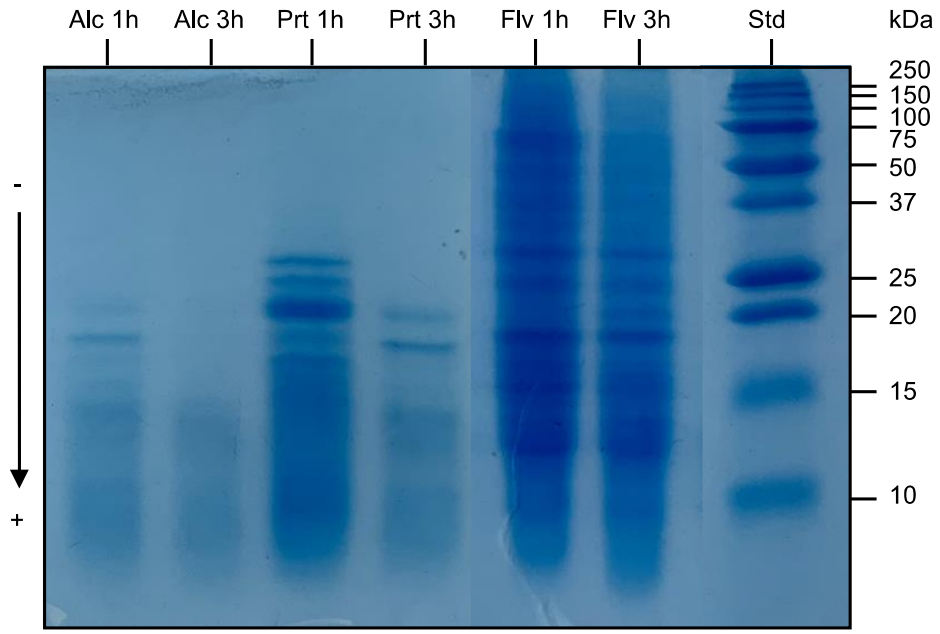

Figure 3.10. SDS-PAGE analysis of the soy protein hydrolysates generated after 1 or 3 h treatment by Alcalase® (Alc), Protamex® (Prt) and Flavourzyme® (Flv). Std, molecular mass standards

3.3.3 SwitchSENSE® measurements for screening MCPs in hydrolysates

To check if the switchSENSE® technology is sensitive enough to detect MCPs present in a complex mixture of peptides, the static and the dynamic fluorescent measurements were applied to SPHs (1 h hydrolysis) and TPH.

The static measurements carried out on all the hydrolysates showed that they display a specific interaction with nickel ions, except the SPH obtained by Flavourzyme® treatment, even at its highest concentration of 1 mM eq. NH_2 (**Figure 3.11 A**). This result suggests that MCP concentration in this latter hydrolysate is lower than in the two other SPHs, as shown by the low yield of hydrolysis of this sample (**Figure 3.10**). In addition, the observed rate constants (k_{obs}) determined for the two other SPHs (obtained by Alcalase® and Protamex®) were largely slower than k_{obs} determined for TPH (**Table 3.2**). Indeed, a minimal concentration of 100 µM eq. NH_2 of each kind of SPH was required to allow the determination of a k_{obs} value with accuracy whereas 5 µM is sufficient for TPH (**Table 3.2**). These results evidence the presence of MCPs able to bind nickel ions specifically, at least in 3 of 4 investigated hydrolysates.

When the dynamic mode was applied for the 4 hydrolysates, no or almost no peptides were stuck onto the DNA nanolevers, showing that there is no unspecific binding also with complex mixtures (reference electrodes E1 and E2) (**Figure 3.11 B**). However, it was difficult to determine any change in the motion of the DNA nanolevers with TPH. Based on the size distribution chromatographic analysis carried out on TPH (Sepúlveda *et al.,* 2020), this can be due to the presence of a majority of small size peptides (di- and tri-peptides). On the other hand, a great change of the molecular friction of the DNA nanolevers was observed for all SPHs. Especially, the hydrolysate produced with Flavourzyme® displayed the most important decrease in motion, probably due to the presence of longer-sized peptides.

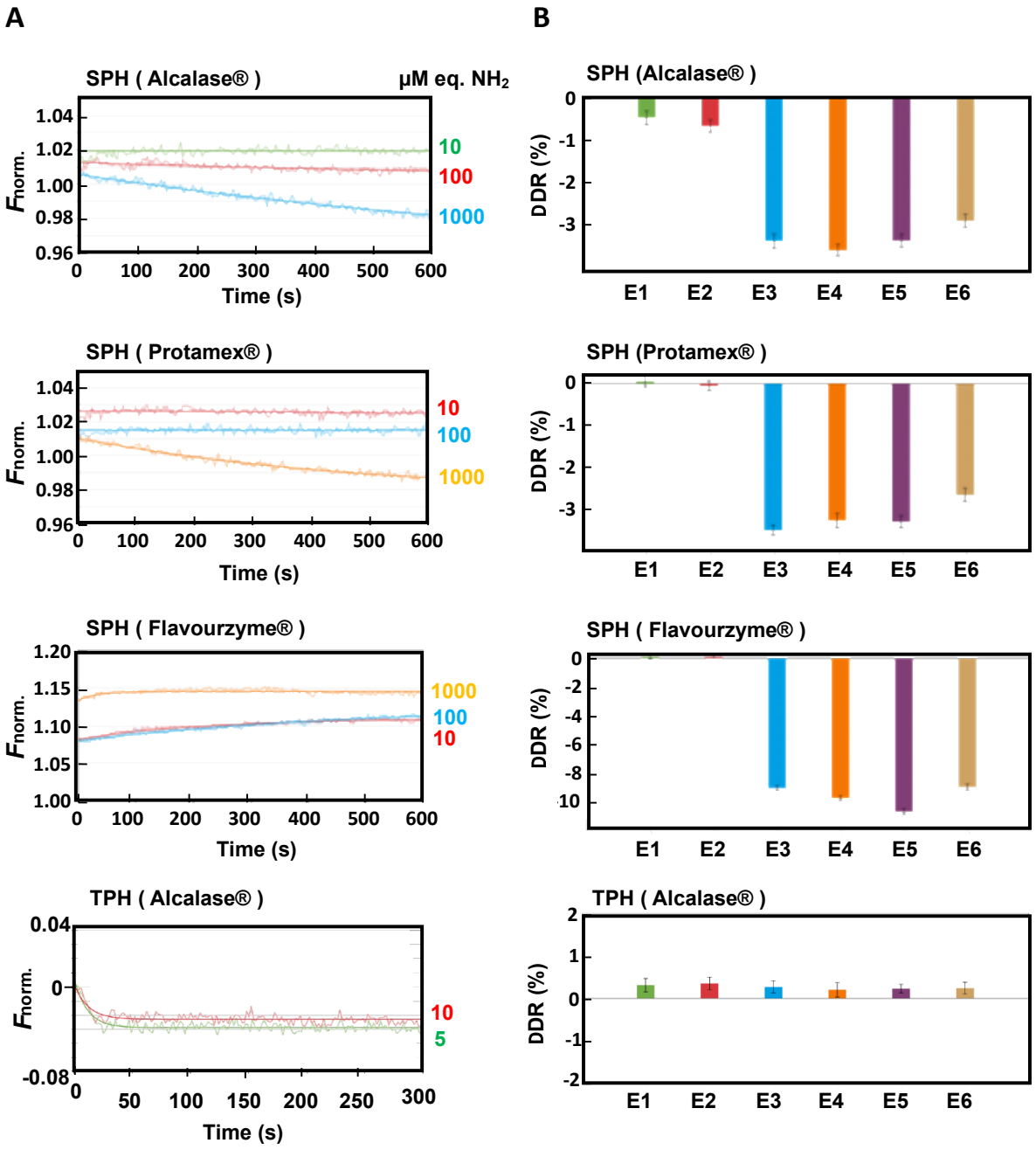

Figure 3.11. Association kinetics analysis (**A**) and Molecular dynamics experiments (**B**) of SPHs and TPH onto immobilized nickel ions by using the switchSENSE® technology. The SPHs were prepared by Alcalase®, Protamex®, or Flavourzyme® one-hour treatment. The TPH was prepared by Alcalase® three-hours treatment. The kinetics raw data are superimposed by global exponential fits for various concentrations of each analyte. The k_{obs} were determined for each kinetics measurement. F_{norm}, normalized fluorescence. For the motion determination, experiments were performed in T40 buffer, then in the presence of sample (SPH at 1000 µM eq. NH_2 & TPH at 100 µM eq. NH_2) and the nanolevers' motions were expressed as dynamic response (DR). The relative difference **Δ**DR (in %) was calculated from the various motions determined in the presence and in the absence of sample. Unspecific binding onto the DNA double strands was determined from the **Δ**DR of the reference electrodes E1 and E2 free of nickel, whereas specific interaction with nickel was determined from the **Δ**DR of the sample electrodes E3 to E6.

Altogether, it is interesting to note that the presence of small MCPs in TPH is only detectable with the static mode, whereas long MCPs present in SPH produced with Flavourzyme® are only revealed with the dynamic mode. Thus, switchSENSE® technology is relevant to screen MCPs in complex mixtures of peptides such as hydrolysates. As already observed for the synthetic peptides, the static and dynamic modes give different but complementary pieces of information. Static mode is relevant for high concentration and small peptides, whereas dynamic mode is more sensitive for longer peptides. Tilapia viscera as well as soy isolates were good sources of MCPs and therefore, their by-products might be studied for their putative biological properties, related especially to their antioxidant properties. For the future, IMAC coupled to mass spectrometry experiments will be performed on-line in order to isolate and to identify some MCPs present in these hydrolysates and that possess potential interesting antioxidant properties.

3.4 References

Adachi, Kanamori, Masuda, Yagasaki, Kitamura, Mikami, and Utsumi. 2003. "Crystal Structure of Soybean 11S Globulin: Glycinin A3B4 Homohexamer." *Proceedings of the National Academy of Sciences* 100 (12): 7395–7400. https://doi.org/10.1073/pnas.0832158100.

Alhazmi, Nachbar, Albishri, Abd El-Hady, Redweik, El Deeb, and Wätzig. 2015. "A Comprehensive Platform to Investigate Protein–Metal Ion Interactions by Affinity Capillary Electrophoresis." *Journal of Pharmaceutical and Biomedical Analysis* 107 (March): 311–17. https://doi.org/10.1016/j.jpba.2015.01.017.

Ashaolu. 2020. "Applications of Soy Protein Hydrolysates in the Emerging Functional Foods: A Review." *International Journal of Food Science & Technology* 55 (2): 421–28. https://doi.org/10.1111/ijfs.14380.

Bamdad, and Chen. 2013. "Antioxidant Capacities of Fractionated Barley Hordein Hydrolysates in Relation to Peptide Structures." *Molecular Nutrition & Food Research* 57 (3): 493–503. https://doi.org/10.1002/mnfr.201200252.

Bernaudat, and Bülow. 2005. "Rapid Evaluation of Nickel Binding Properties of His-Tagged Lactate Dehydrogenases Using Surface Plasmon Resonance." *Journal of Chromatography A* 1066 (1): 219–24. https://doi.org/10.1016/j.chroma.2005.01.079.

Canabady-Rochelle, Harscoat-Schiavo, Kessler, Aymes, Fournier, and Girardet. 2015. "Determination of Reducing Power and Metal Chelating Ability of Antioxidant Peptides: Revisited Methods." *Food Chemistry* 183 (September): 129–35. https://doi.org/10.1016/j.foodchem.2015.02.147.

Canabady-Rochelle, Selmeczi, Collin, Pasc, Muhr, and Boschi-Muller. 2018. "SPR Screening of Metal Chelating Peptides in a Hydrolysate for Their Antioxidant Properties." *Food Chemistry* 239 (January): 478–85. https://doi.org/10.1016/j.foodchem.2017.06.116.

Charoenphun, Cheirsilp, Sirinupong, and Youravong. 2013. "Calcium-Binding Peptides Derived from Tilapia (Oreochromis Niloticus) Protein Hydrolysate." *European Food Research and Technology* 236 (1): 57–63. https://doi.org/10.1007/s00217-012-1860-2.

Chen, Muramoto, Yamauchi, Fujimoto, and Nokihara. 1998. "Antioxidative Properties of Histidine-Containing Peptides Designed from Peptide Fragments Found in the Digests of a Soybean Protein." *Journal of Agricultural and Food Chemistry* 46 (1): 49–53. https://doi.org/10.1021/jf970649w.

El Hajj, Sepulveda-Rincon, Paris, Giraud, Csire, Stefan, Selmeczi, et al. 2021. "Chapter 19 - Application in Nutrition: Mineral Binding." In *Biologically Active Peptides*, edited by Fidel Toldrá and Jianping Wu, 455–94. Academic Press. https://doi.org/10.1016/B978-0-12-821389-6.00016-9.

FAO. 2018. *The State of World Fisheries and Aquaculture 2018: Meeting the Sustainable Development Goals*. The State of World Fisheries and Aquaculture (SOFIA) 2018. Rome, Italy: FAO. https://www.fao.org/documents/card/en/c/I9540EN/.

Frister, Meisel, and Schlimme. 1988. "OPA Method Modified by Use of N,N-Dimethyl-2-Mercaptoethylammonium Chloride as Thiol Component." *Fresenius' Zeitschrift F*[illegible]*r Analytische Chemie* 330 (7): 631–33. https://doi.org/10.1007/BF00473782.

Gómez, Gómez, Zapata, López-García, Cilla, and Alegría. 2020. "Optimization of the Red Tilapia (Oreochromis Spp.) Viscera Hydrolysis for Obtaining Iron-Binding Peptides and Evaluation of In Vitro Iron Bioavailability." *Foods* 9 (7): 883. https://doi.org/10.3390/foods9070883.

Guo, Harnedy, Li, Hou, Zhang, Zhao, and FitzGerald. 2014. "Food Protein-Derived Chelating Peptides: Biofunctional Ingredients for Dietary Mineral Bioavailability Enhancement." *Trends in Food Science & Technology* 37 (2): 92–105. https://doi.org/10.1016/j.tifs.2014.02.007.

Hainfeld, Liu, Halsey, Freimuth, and Powell. 1999. "Ni–NTA–Gold Clusters Target His-Tagged Proteins." *Journal of Structural Biology* 127 (2): 185–98. https://doi.org/10.1006/jsbi.1999.4149.

Helfferich. 1961. "'Ligand Exchange' : A Novel Separation Technique." *Nature* 189 (4769): 1001–2. https://doi.org/10.1038/1891001a0.

Knecht, Ricklin, Eberle, and Ernst. 2009. "Oligohis-Tags: Mechanisms of Binding to Ni2+-NTA Surfaces." *Journal of Molecular Recognition* 22 (4): 270–79. https://doi.org/10.1002/jmr.941.

Korhonen, and Pihlanto. 2006. "Bioactive Peptides: Production and Functionality." *International Dairy Journal*, 4th NIZO Dairy Conference - Prospects for Health, Well-being and Safety, 16 (9): 945–60. https://doi.org/10.1016/j.idairyj.2005.10.012.

Kurzątkowska, Mielecki, Grzelak, Verwilst, Dehaen, Radecki, and Radecka. 2014. "Immobilization of His-Tagged Kinase JAK2 onto the Surface of a Plasmon Resonance Gold Disc Modified with Different Copper (II) Complexes." *Talanta* 130 (December): 336–41. https://doi.org/10.1016/j.talanta.2014.07.013.

Laemmli, and Favre. 1973. "Maturation of the Head of Bacteriophage T4: I. DNA Packaging Events." *Journal of Molecular Biology* 80 (4): 575–99. https://doi.org/10.1016/0022-2836(73)90198-8.

Langer, Hampel, Kaiser, Knezevic, Welte, Villa, Maruyama, et al. 2013. "Protein Analysis by Time-Resolved Measurements with an Electro-Switchable DNA Chip." *Nature Communications* 4 (1): 1–8. https://doi.org/10.1038/ncomms3099.

Ma, Liu, Song, Che, Wang, Feng, Li, and Dai. 2019. "Evaluating the Efficacy of a Ferrous-Ion-Chelating Peptide from Alaska Pollock Frame for the Improvement of Iron Nutritional Status in Rats." *Food & Function* 10 (8): 4888–96. https://doi.org/10.1039/C9FO00310J.

Megías, Pedroche, Yust, Girón-Calle, Alaiz, Millán, and Vioque. 2007. "Affinity Purification of Copper-Chelating Peptides from Sunflower Protein Hydrolysates." *Journal of Agricultural and Food Chemistry* 55 (16): 6509–14. https://doi.org/10.1021/jf0712705.

Muhr, Pontvianne, Selmeczi, Paris, Boschi-Muller, and Canabady-Rochelle. 2020. "Chromatographic Separation Simulation of Metal-chelating Peptides from Surface Plasmon Resonance Binding Parameters." *Journal of Separation Science* 43 (11): 2031–41. https://doi.org/10.1002/jssc.201900882.

Nieba, Nieba-Axmann, Persson, Hämäläinen, Edebratt, Hansson, Lidholm, Magnusson, Karlsson, and Plückthun. 1997. "BIACORE Analysis of Histidine-Tagged Proteins Using a Chelating NTA Sensor Chip." *Analytical Biochemistry* 252 (2): 217–28. https://doi.org/10.1006/abio.1997.2326.

Nishinari, Fang, Guo, and Phillips. 2014. "Soy Proteins: A Review on Composition, Aggregation and Emulsification." *Food Hydrocolloids* 39 (August): 301–18. https://doi.org/10.1016/j.foodhyd.2014.01.013.

Paris, Selmeczi, Ebel, Stefan, Csire, Cakir-Kiefer, Desobry, Canabady-Rochelle, and Chaimbault. 2021. "Metabolomics Approach Based on LC-HRMS for the Fast Screening of Iron(II)-Chelating Peptides in Protein Hydrolysates." *Analytical and Bioanalytical Chemistry* 413 (2): 315–29. https://doi.org/10.1007/s00216-020-03037-1.

Peng, Kong, Xia, and Liu. 2010. "Reducing and Radical-Scavenging Activities of Whey Protein Hydrolysates Prepared with Alcalase." *International Dairy Journal* 20 (5): 360–65. https://doi.org/10.1016/j.idairyj.2009.11.019.

Robert, Zatylny-Gaudin, Fournier, Corre, Le Corguillé, Bernay, and Henry. 2015. "Molecular Characterization of Peptide Fractions of a Tilapia (Oreochromis Niloticus) by-Product Hydrolysate and in Vitro Evaluation of Antibacterial Activity." *Process Biochemistry* 50 (3): 487–92. https://doi.org/10.1016/j.procbio.2014.12.022.

Sepúlveda, and Zapata. 2020. "Effects of Enzymatic Hydrolysis Conditions on the Antioxidant Activity of Red Tilapia (*Oreochromis Spp*.) Viscera Hydrolysates." *Current Pharmaceutical Biotechnology* 21 (12): 1249–58. https://doi.org/10.2174/1389201021666200506072526.

Sepúlveda, Zapata, Martínez-Álvarez, Alemán, Montero, and Gómez-Guillén. 2020. "The Preferential Use of a Soy-Rapeseed Lecithin Blend for the Liposomal Encapsulation of a Tilapia Viscera Hydrolysate." *LWT*, November, 110530. https://doi.org/10.1016/j.lwt.2020.110530.

Sierra, Fan, Zapata, and Wu. 2021. "Antioxidant Peptides Derived from Hydrolysates of Red Tilapia (Oreochromis Sp.) Scale." *LWT* 146 (July): 111631. https://doi.org/10.1016/j.lwt.2021.111631.

Sóvágó, and Ősz. 2006. "Metal Ion Selectivity of Oligopeptides." *Dalton Transactions*, no. 32 (August): 3841–54. https://doi.org/10.1039/B607515K.

Weinberger, Morris, and Pawlak. 2000. "Recent Trends in Protein Biochip Technology." *Pharmacogenomics* 1 (4): 395–416. https://doi.org/10.1517/14622416.1.4.395.

Willett, Gillmor, Perona, Fletterick, and Craik. 1995. "Engineered Metal Regulation of Trypsin Specificity." *Biochemistry* 34 (7): 2172–80. https://doi.org/10.1021/bi00007a010.

Wong, Leong, and Williamkoh. 2006. "Antioxidant Activities of Aqueous Extracts of Selected Plants." *Food Chemistry* 99 (4): 775–83. https://doi.org/10.1016/j.foodchem.2005.07.058.

Wu, Shiau, Chen, and Chiou. 2003. "Antioxidant Activities of Carnosine, Anserine, Some Free Amino Acids and Their Combination." *Journal of Food and Drug Analysis* 11 (2): 6.

Yousef, Sesham, McCabe, Vangala, and Angel. 2019. "Ion Mobility-Mass Spectrometry Techniques for Determining the Structure and Mechanisms of Metal Ion Recognition and Redox Activity of Metal Binding Oligopeptides." *JoVE (Journal of Visualized Experiments)*, no. 151 (September): e60102. https://doi.org/10.3791/60102.

Zhang, Tong, Qi, Wang, Li, Sui, and Jiang. 2018. "Changes in Antioxidant Activity of Alcalase-Hydrolyzed Soybean Hydrolysate under Simulated Gastrointestinal Digestion and Transepithelial Transport." *Journal of Functional Foods* 42 (March): 298–305. https://doi.org/10.1016/j.jff.2018.01.017.

Zhang, Wang, and Ying Xu. 2007. "Optimization of the Aqueous Enzymatic Extraction of Rapeseed Oil and Protein Hydrolysates." *Journal of the American Oil Chemists' Society* 84 (1): 97–105. https://doi.org/10.1007/s11746-006-1004-6.

Zhang, Duan, and Zhuang. 2012. "Purification and Characterization of Novel Antioxidant Peptides from Enzymatic Hydrolysates of Tilapia (Oreochromis Niloticus) Skin Gelatin." *Peptides* 38 (1): 13–21. https://doi.org/10.1016/j.peptides.2012.08.014.

Chapter 4 Metal-chelating activity of soy and pea protein hydrolysates obtained after different enzymatic treatments

In this chapter we talk about how we took advantage of another novel biotechnological tool in order to screen the best hydrolysis condition to produce MCPs in the lab. This technique, called surface plasmon resonance (SPR) has been previously developed to screen MCPs in commercial hydrolysates.

Soy and pea proteins are two rich sources of essential amino acids. The hydrolysis of these proteins reveals functional and bioactive properties of the produced small peptide mixtures. In our study, we employed the hydrolysis of soy protein isolates with the endopeptidases Alcalase® and Protamex®, alone or followed by the exopeptidase Flavourzyme®. The sequential enzyme treatments were the most efficient regarding the degree of hydrolysis. Then, soy and pea protein hydrolysates (SPHs and PPHs, respectively) were ultrafiltrated in order to select peptides of molecular weight ≤ 1kDa. Whatever the protein source or the hydrolysis treatment, the hydrolysates showed similar molecular weight distributions and amino acid compositions. In addition, all the ultrafiltrated hydrolysates possess metal-chelating activities, as determined by UV-spectrophotometry and Surface Plasmon Resonance (SPR). However, the SPR data revealed better chelating affinities in sequentially produced SPHs and PPHs.

This chapter has been recently submitted to Food Chemistry Journal: El Hajj, S., Irankunda, R., Camaño Echavarría, J.A., Arnouc, P., Cédric, P., Stefan, S., Gaucher, C., Boschi-Muller, S., & Canabady-Rochelle, L. Metal-chelating activity of soy and pea protein hydrolysates obtained after different enzymatic treatment

4.1 Introduction

Transition metals, such as iron II (Fe^{2+}) and copper II (Cu^{2+}) ions, are powerful promoters for the production of ROSs since they are able to donate and accept electrons *via* intracellular reactions, such as the Haber-Weiss and Fenton reactions, and thus induce the production of free radicals (Hancock 1992). Brought by nutrition, the exogenous metal-chelators help to reduce oxidative stress resulting from environmental toxins and modern life related factors such as environmental pollution, smoking, UV exposition *etc.* The antioxidant metal-chelating properties of peptides are related to their characteristic amino acid composition and their proper positioning within the peptide sequence. Indeed, certain amino acids can form coordination compounds with metals through their α-amino group, carboxyl group, and R side chain of amino acids. The carboxylate group (COO^-) and the nitrogen atom (N) attach to metals to establish metal carboxylate salt, amine complex, and 5 or 6 membered chelating rings (El Hajj *et al.,* 2021a).

Over the past few decades, protein hydrolysates have been widely engaged in human nutrition applications. Upon proteolysis, the obtained small-sized peptides containing characteristic amino acids are considered as highly advantageous for targeting specific physiological or nutritional requirements (Clemente, 2000). The importance of hydrolysis relies behind the functional changes of proteins. Indeed, with the loss of their native structures, the produced low-molecular-weight peptides enhance their interactions with the environment. Food-derived proteins have popularly undergone proteolysis to obtain a broad range of bioactive and functional peptides, notably MCPs. For instance, the MCPs produced from the proteolysis of milk proteins, especially casein and whey proteins, have been widely reported in the literature. Calcium, iron and zinc binding motifs were discovered in these proteins after submitting them to enzymatic hydrolysis (Vegarud, Langsrud, and Svenning 2000). Calcium-binding peptides were derived from the hydrolysis of tilapia proteins and shrimp processing by-products as well (Chen *et al.,* 2014; Charoenphun *et al.,* 2013; Cheung *et al.,* 2012). Other protein hydrolysates produced for instance from chickpea, rapeseed, sunflower, and bean protein contain also bioactive MCPs *(Xie et al., 2015; Carrasco-Castilla et al.,* 2012; Torres-Fuentes *et al.,* 2011; Megías *et al.,* 2007) . As for the choice of digestive enzymes, many various proteinases and their combinations – including pure (*e.g.*, trypsin, pepsin, thermolysin) and crude (Alcalase®, Protamex®, Flavourzyme®, *etc*.) enzymes – were

listed in literature with their hydrolysing optimum conditions (Korhonen and Pihlanto 2006). Different hydrolysis conditions can lead to the production of hydrolysates with variations among their physio-chemical characteristics and bioactivities, such as the metal-chelating activity.

Soy and peas are the two most produced legumins in France (Simmen and Lacampagne 2020). Soy proteins, generally cheaper than other proteins, are the only vegetable protein sources that contain all the essential amino acids, and are considered as relevant substitutes of animal proteins, especially for vegetarians and vegans. They are linked to multiple health benefits for pregnancy, cardiovascular and gastrointestinal systems, cancer prevention, and lactose intolerance condition (Barrett 2006; Montgomery 2003). Similarly, pea proteins are also a low-cost source of proteins and can be used as substitute for animal proteins, mainly in smoothies and shakes to increase protein content. As main advantage, pea proteins do not cause allergic reactions, aids in kidneys and heart health, weight loss, and muscle growth and repair (Strauch and Lila 2021; Babault *et al.,* 2015; Tömösközi *et al.,* 2001). Certain studies have identified MCPs with antioxidant activities in soy and pea protein hydrolysates produced by different enzymatic treatments. For example, Lv *et al.,* (2009) used IMAC to identify iron-chelating peptides from soy proteins hydrolysates produced by protease M. Also, Bao *et al.,* (2008) used FTIR to study complexes formed between peptides of soy hydrolysates produced after pepsin, flavourzyme® and protease M treatments. Iron-chelating activity was determined as well using UV-spectrophotometry in pea protein hydrolysates produced by thermolysin (Pownall, Udenigwe, and Aluko 2010).

The aim of this research is to compare the effect of different enzymatic hydrolysis conditions and of two types of interesting protein sources (soy and pea) on the production of metal-chelating peptides.

4.2 Material and Methods

4.2.1 Production of protein hydrolysates

The raw materials, soy protein isolates (**SPI**) and pea protein isolates (**PPI**), were kindly provided from SAS IMPROVE (Dury, France). The two protein isolates (2%, w/v) were dispersed in 50 mM ammonium bicarbonate buffer and preheated at 90°C for 5 minutes. Their enzymatic hydrolysis was performed in thermostatically controlled reaction vessels at 55°C with various proteases. The enzymes Alcalase® (Protease from Bacillus licheniformis, ≥ 2.4 U/g, Sigma-Aldrich; **Alc**) and Protamex® (Protease from Bacillus sp., ≥ 1.5 U/g, Sigma-Aldrich; **Prt**) were added individually to the SPI solution for a complete 1-hour and 3-hours hydrolysis, carried out at pH = 8 for the Alcalase® treatment or pH = 7 for the Protamex® treatment. Two sequential hydrolysis were also performed on SPI and PPI solutions using an additional enzymatic treatment with Flavourzyme® (Protease from Aspergillus oryzae, ≥ 500 U/g, Sigma-Aldrich; **Flv**). For these sequential treatments, Alcalase® was applied for 1 hour (pH = 8) followed by Flavourzyme® treatment for 2 hours (pH = 7; **Alc+Flv**). Similarly, Protamex® was applied for 1 hour followed by Flavourzyme® treatment for 2 hours, both at pH = 7 (**Prt+Flv**). The enzyme to substrate ratio (E/S) was always set at 1% (v/v). Whatever the enzymatic treatment, the mixture was stirred while monitoring and maintaining the temperature and pH. The first enzyme was always inactivated at 95°C for 15 min before adding the second enzyme. Following the hydrolysis by the second enzyme, this latter was also inactivated at 95°C for 15 min and the samples were centrifuged (10 000 *g*; 15min) in order to precipitate and remove both large unhydrolyzed proteins and both enzymes. Finally, the six SPHs and the two PPHs prepared were lyophilized to obtain a powder, subsequently stored at -20°C until further analysis. The hydrolysates were named by their respective protein source (**SPH** or **PPH**) followed by their enzymatic treatment (**Alc, Prt, Alc+Flv, Prt+ Flv**) and the time defined for their hydrolysis.

4.2.2 Ultrafiltration

Parts of the hydrolysates were dispersed in MilliQ water (18 mΩ·cm^{-1}) and fractionated under stirring, using consecutively 10 kDa and 1 kDa Ultracel® ultrafiltration membranes (Millipore, Jaffry, USA) in 100 mL ultrafiltration cell (Millipore, Jaffery, USA). Ultrafiltration through 10 kDa membrane was first required in order to facilitate then the ultrafiltration of the

hydrolysates through the 1 kDa membrane. The retentates were frozen at -20°C and denoted as > 10 kDa fraction, while the permeates were passed through the 1 kDa membrane, thus forming two fractions for each hydrolysate: a first fraction comprised within 1-10 kDa (frozen at -20°C) and a second one less or equal to 1 kDa (lyophilized for further assays).

4.2.3 Efficiency of the different hydrolysis protocols

4.2.3.1 OPA quantification

The molar concentration of each hydrolysate defined as the primary amino groups revealed by hydrolysis was determined by the OPA (for *o*-phthaldialdehyde) quantification. This method was adapted from Canabady-Rochelle *et al.,* (2018). The OPA solution was prepared by dissolving 40 mg of OPA (ThermoFisher Scientific, Loughborough, UK) in 1 mL of pure methanol and 100 mg of *N,N*-dimethyl-2-mercaptoethyl ammonium (ThermoFisher Scientific) in a few milliliters of Borax buffer (sodium tetraborate 100 mM, 1% w/v sodium dodecyl sulfate, pH 9.3, Sigma-Aldrich). These two former solutions were mixed in a volumetric flask, qsf 50 mL Borax buffer. Each solution of peptide hydrolysate (20 µL, 1 $mg.mL^{-1}$) prepared in Borax buffer was mixed with the OPA solution (200 µL) directly in a 96-well plate (Nunclon™ Delta Surface, ThermoFicher Scientific). The absorbance was read at 340 nm (Multiskan Go spectrophotometer, ThermoFicher Scientific) after 3 min of incubation under stirring at room temperature. The molar concentration of each peptide hydrolysate was calculated in mM eq. glycine with the help of a Glycine calibration curve (1-5 mM).

4.2.3.2 Determination of the degree of hydrolysis

The degree of hydrolysis (**DH**) defined as the proportion of cleaved peptide bonds in a protein hydrolysate was evaluated by the OPA quantification of the primary amino groups liberated during hydrolysis. The value of DH (%) was calculated according to the following formula conducted from Romero-Garay *et al.,* (2020).

$$\mathrm{DH}(\%) = \frac{(\mathrm{NH_{2(t)}} - \mathrm{NH_{2(0)}})}{(\mathrm{NH_{2(max)}} - \mathrm{NH_{2(0)}})} \times 100 \qquad [1]$$

Where $NH_{2(t)}$ = concentration of amino groups in 1g/L hydrolysates at the end of hydrolysis, $NH_{2(0)}$ = concentration of amino groups of SPI (without hydrolysis), and $NH_{2(max)}$ = concentration of amino groups after a complete chemical hydrolysis of SPI, performed with 6N HCl at 130°C for 24 h (Romero-Garay *et al.,* 2020).

Note that the DH was only determined for whole soy protein hydrolysates, not those submitted to an ultrafiltration step. Indeed, upon ultrafiltration, some peptides are lost, which do affect the DH determination.

4.2.4 Physico-chemical characterization of the produced hydrolysates

4.2.4.1 Size exclusion chromatography (SEC)

The molecular weight distribution of the 1 kDa-ultrafiltrated SPHs and PPHs was determined by GFC (for gel filtration chromatography) using a Waters 515 HPLC pump, a degazer and a RID 10-A Shimadzu detector. The mobile phase was composed of a water containing sodium nitrate at 0.1 M and sodium azide at 0.2% (w/v). The stationary phase was composed of a Phenomenex PolySep-GFC-P 2000 (7.8 x 35 mm) guard column to help remove contaminants and free amino acids, followed by a same phase column (7.8 x 300 mm) that have a separation range comprised between 0.1 and 10 kDa. Each sample (200 µL) was injected at 5 mg/mL and separated at room temperature with a flow rate of 0.7 mL/min. PolyEthylenGlycol (**PEG**: 200, 600, 1000, 3000 and 8000 Da, Sigma Aldrich, USA) were used as standards for GFC calibration. Data were collected and analysed with the software ASTRA (Wyatt Technology).

4.2.4.2 Identification of amino acid composition

Quantitative analysis of amino acids was realized on a UHPLC system (Thermo Fisher Scientific) in-line with an Orbitrap ID-X Tribrid mass spectrometer (Thermo Fisher Scientific) equipped with an atmospheric pressure ionization interface.

Five microliters of samples (SPI, PPI, and 4 hydrolysates: 1kDa-Ultrafiltrated SPH and PPH, either prepared by Alcalase® followed by Flavourzyme® or by Protamex® followed by Flavourzyme®) were separated on C18 Alltima reverse phase column (150 x 2.1mm, 5µm – Grace/Alltech, Darmstadt, Germany) equipped with a C18 Alltima pre-column (7.5 x2.1mm, 5µm) at 10°C. The flow rate was set at 0.2 $mL.min^{-1}$ and the mobile phases consisted in water supplemented with nonafluoropentanoic acid (20 mM) as ion-pairing reagent for A and pure acetonitrile for B. Amino acids were eluted using a linear gradient from 5 % to 25 % of B for 12 min, and then an isocratic step at 25 % of B for 18 min. Mass analysis was carried out in heated electrospray positive ion mode ($H\text{-}ESI^{+}$) and mass spectrometry conditions were as follows: spray voltage was set at 4.0 kV; source gases were set (in arbitrary units/min) for

sheath gas, auxiliary gas and sweep gas at 30, 5, and 5, respectively; vaporizer temperature and ion transfer tube temperature were both set at 300°C. MS scans were performed from 70 to 210 m/z at 60 K resolution (full width of the peak at its half maximum, fwphm, at 200 m/z) with MS parameters as follows: RF-lens, 35%; maximum injection time, 50 ms; data type, profile; AGC target: custom; normalized AGC target: 25 %. The mass spectrometer calibration was performed using the Pierce FlexMix calibration solution (Thermo Scientific). MS data acquisition was carried out utilizing the Xcalibur v. 4.3 software (Thermo Scientific).

4.2.5 Determination of the metal-chelation properties

4.2.5.1 UV-spectrophotometry

The Cu^{2+} chelation properties of the 1 kDa-ultrafiltrated SPHs and PPHs were determined as an indirect antioxidant capacity and measured by spectrophotometry using murexide as colour indicator, similarly as in Canabady-Rochelle *et al.,* 2018. Hydrolysates were prepared in hexamine buffer between 0.42 and 40 g/L, and then, their concentration was expressed in mM eq. NH_2. As good complexing agents, EDTA and carnosine were both considered as positive controls and prepared in a range of 0.42–40 mM. EDTA, carnosine and the 1 kDa-ultrafiltrated hydrolysate solutions were directly diluted in a microplate with hexamine buffer for a total volume of 143 µL. Then, 143 µL of a 3 mM $CuSO_4$ solution in hexamine buffer and 14 µL of a 1 mM murexide solution were added in each well (total volume: 300 µL). The 96-well plate was incubated for 3 min at room temperature and the absorbance was measured at two wavelengths*, i.e.,* 485 nm and 520 nm, for the copper-murexide complex and the murexide alone, respectively. The ratio of absorbance (A_{485}/A_{520}) was considered proportional to the free copper ion (Cu^{2+}) concentration.

$$Cu^{2+}\ \text{complexation}\ (\%) = \frac{[(A_{485}/A_{520})_0 - (A_{485}/A_{520})_s]}{(A_{485}/A_{520})_0} \times 100 \qquad [2]$$

With $(A_{485}/A_{520})_0$ = ratio of absorbances measured in the absence of sample, and $(A_{485}/A_{520})_s$ = ratio of absorbances measured in the presence of sample (EDTA, carnosine or hydrolysate).

4.2.5.2 Surface Plasmon Resonance

SPR experiments were carried out similarly to Canabady-Rochelle *et al.,* (2018). The binding affinity of protein hydrolysates for Ni^{2+} was analysed by SPR at 25°C using a Biacore X100

instrument (GE Healthcare, Uppsala, Sweden) equipped with Ni^{2+}-NTA sensor chips. All binding experiments were performed at a flow rate of 20 µL.min^{-1}.

First, Ni^{2+} was injected for 1 min onto the NTA chip using a $NiCl_2$ solution (500 mM, Biacore kit) and followed by a 1-min stabilization. The NTA flow channel uncharged in Ni^{2+} was used as a reference channel in order to determine the importance of aspecific interactions. Then, each peptide sample was injected on both channels for 270 s followed by 270 s undisturbed dissociation time. The chip was regenerated between each studied concentration with a two steps protocol involving successively imidazole (500 mM) at a flow rate of 20 µL.min^{-1} for 1 min and SDS (0.5 % v/v) at a flow rate of 40 µL.min^{-1} for 1 min.

The sensorgrams obtained from the SPR experiments were processed with BIAevaluate software. The isotherms obtained were expressed in Resonance Unit (**RU**, corrected by the offset value) as a function of the concentration of protein hydrolysate (expression in mM equivalent glycine according to the OPA quantification). The dissociation constants (K_D, mM equivalent glycine) were determined at equilibrium by fitting the experimental data with the 1:1 binding model. The affinity constant (K_A, mM^{-1} equivalent glycine) was calculated as the inverse of the dissociation constant.

4.3 Results and Discussion

4.3.1 Efficiency of the different hydrolysis protocols

Alcalase® and Protamex® are two serine endopeptidases obtained from *Bacillus.* Both comprise the so-called "Subtilisin" enzyme, which has a broad hydrolysing specificity. Yet, according to the literature, these two different commercialized crude enzymes led to different but efficient DH when incubated with soy isolates (Zhang, Huang, and Jiang, 2014; Seo, Lee, and Baek 2008; Penta-Ramos and Xiong, 2002). The degree of hydrolysis (**DH**) of SPI hydrolysates varies from 13 % (Protamex® 1h) to 32 % (Alcalase® 1h + Flavourzyme® 2h) **(Figure 4.1)** depending on the enzyme used, the hydrolysis time, and individual or sequential enzymatic hydrolysis. After 1 hour of hydrolysis, Alcalase® shows a higher DH than Protamex® (19.3 % and 13.2 %, respectively). Raising up the time of hydrolysis by Alcalase® to 3 hours does not significantly improve the DH. However, 3 hours of Protamex® treatment increases

the DH to 19.7 %. So Alcalase® is more efficient than Protamex®, resulting in a greater number of peptides after 1 h of hydrolysis, but not after 3 hours.

Being an exopeptidase, Flavourzyme® is widely used as a second protease in sequential hydrolysis studies with an endopeptidase being the first hydrolysing enzyme**.** After a sequential enzymatic treatment, using either Alcalase® followed by Flavourzyme® or Protamex® followed by Flavourzyme®, the DH increased to 31.8 % and 29 % respectively. So, a sequential enzymatic treatment gives a clear advantage in terms of quantities of generated peptides. Hence, our results are in agreement with the literature, which reports that the primary use of an endopeptidase facilitates the reaction of the exopeptidase in order to reach a better hydrolysis (Vioque *et al.,* 1999; Ugolini *et al.,* 2015).

In our work, we demonstrated similar DH than certain other studies. For example, Zhang *et al., (2018*) had a DH value of 20% after a 3-hour Alcalase® treatment of soy protein isolates (24% in our study). After a 10-hours Protamex® treatment of soy protein isolate, Xie *et al.,* (2012) obtained a DH of 16.6 % (19% after 3 hours in our study). Concerning sequential hydrolysis with Alcalase® followed by Flavourzyme®, we have obtained a larger DH (31.8%) than Ma *et al.,* (2013) (24%).

According to the literature, the increased DH value could be correlated to an increased antioxidant activity of hydrolysates, including metal-chelating property (Zhang, Huang, and Jiang, 2014; Theodore, Raghavan, and Kristinsson 2008; Raghavan and Kristinsson, 2008). Moreover, the hydrolysate fraction collected after ultrafiltration – thus, constituted of low molecular weight peptides – could have better antioxidant activities than the one containing high molecular weight peptides (He *et al.,* 2013; Ranamukhaarachchi, Meissner, and Moresoli, 2013; Tsou *et al.,* 2010; Ren *et al.,* 2010). Thus, we focus our attention on examining the 1kDa-ultrafiltrated samples in this study.

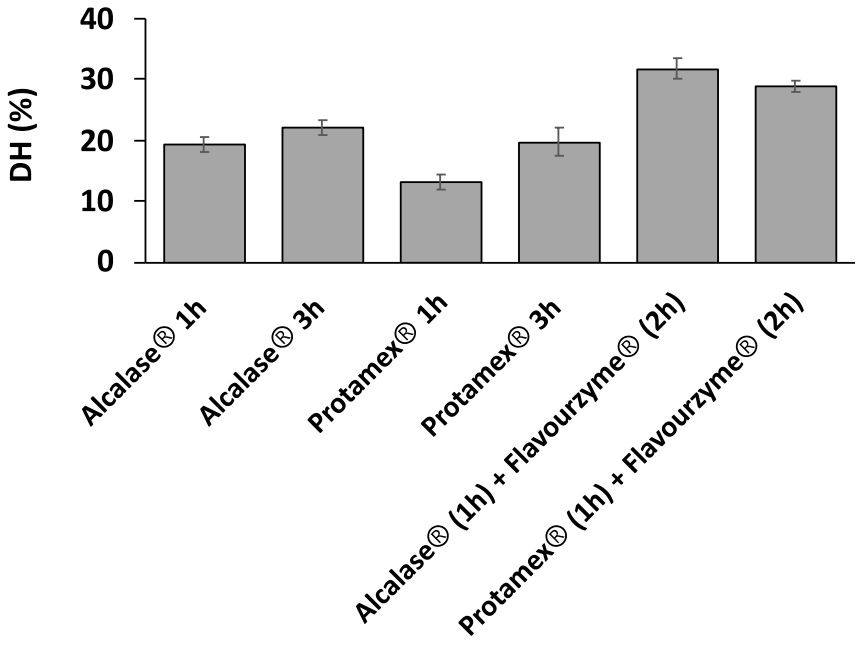

Figure 4.1. Degree of hydrolysis (DH%) of soy protein isolates treated with different enzymes for different durations. Non-filtrated soy hydrolysates are analysed for DH. Results are presented as mean ± standard deviation from 5 replicates

4.3.2 Characterization of the produced hydrolysates

The molecular weight distribution (%) of the 1 kDa-ultrafiltrated SPHs and PPHs was evaluated according to the linear regression of Log (MW) and elution chromatograms obtained by SEC (**Figure 4.2**). The results indicate that the molecular masses of the SPHs (except SPH by Protamex® 1h) and PPHs are mostly distributed among 400-200 Da. The highest percentages of peptides in this former range are collected for the SPH by Alcalase® 1h followed by Flavourzyme® 2h (57%) and for SPH treated by Protamex 3h (65%).

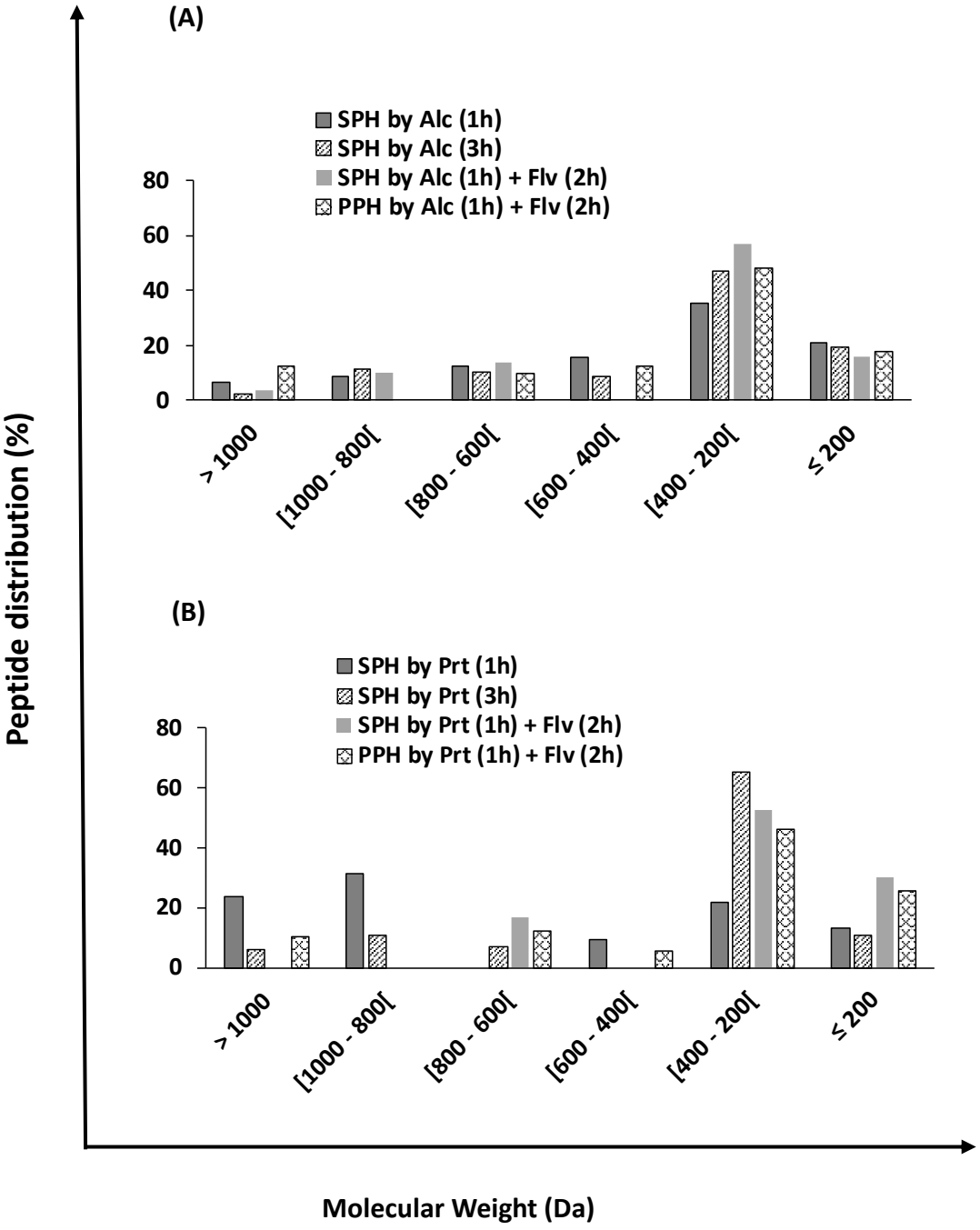

Figure 4.2. Molecular weight distribution of the 1kDa-ultrafiltrated SPHs and PPHs after (A) Alcalase® treatment for 1 h or 3 h or 1 h followed by 2 h of Flavourzyme® treatment, and (B) Protamex® treatment for 1 h or 3 h or 1 h followed by 2 h of Flavourzyme® treatment. PPHs were produced only by Alcalase® 1 h (or Protamex® 1 h) followed by 2 h of Flavourzyme®. SPH: Soy Protein Hydrolysate. PPH: Pea Protein Hydrolysate. Alc (1h): Alcalase® treatment for 1 h; Alc (3h): Alcalase® treatment for 3 h; Prt (1h): Protamex® treatment for 1 h; Prt (3h): Protamex® treatment for 3 h; Alc (1h) + Flv (2h): Alcalase® treatment for 1 h followed by Flavourzyme® treatment for 2 h; Prt (1h) + Flv (2h): Protamex® treatment for 1 h followed by Flavourzyme® treatment for 2 h

The amino acid composition of four hydrolysates is shown in **figure 4.3**. These compositions are globally similar regardless of the protein source and the hydrolysis process, with some differences. Indeed, regarding acidic amino acids (Asp and Glu), well known for their ability to chelate metal ions through their carboxylic groups (Lv *et al.,* 2013), the highest percentages are observed in PPH by Alcalase® (1h) followed by Flavourzyme® (2h) with 20% and 12.9%, respectively. Both sequential SPHs show high percentages of aspartic acid as well (14.8 % and 7.9 %, respectively). Besides, the SPH generated by Protamex® (1h) followed by Flavourzyme® (2h) contains 11.8% of histidine, which is a well-known metal-chelating amino acid (Chen, Shen, and Xia, 2020; Zhang *et al.,* 2018; Sun *et al.,* 2017; Torres-Fuentes, Alaiz, and Vioque, 2011). Finally, proline, arginine and lysine, which are present at similar percentages in SPHs and PPHs, were previously found in Ca^{2+}-chelating peptides (Bredderman and Wasserman, 2002). Therefore, those results suggest that the metal-chelating activity observed for the different hydrolysates could reflect the presence of a great variety of MCPs.

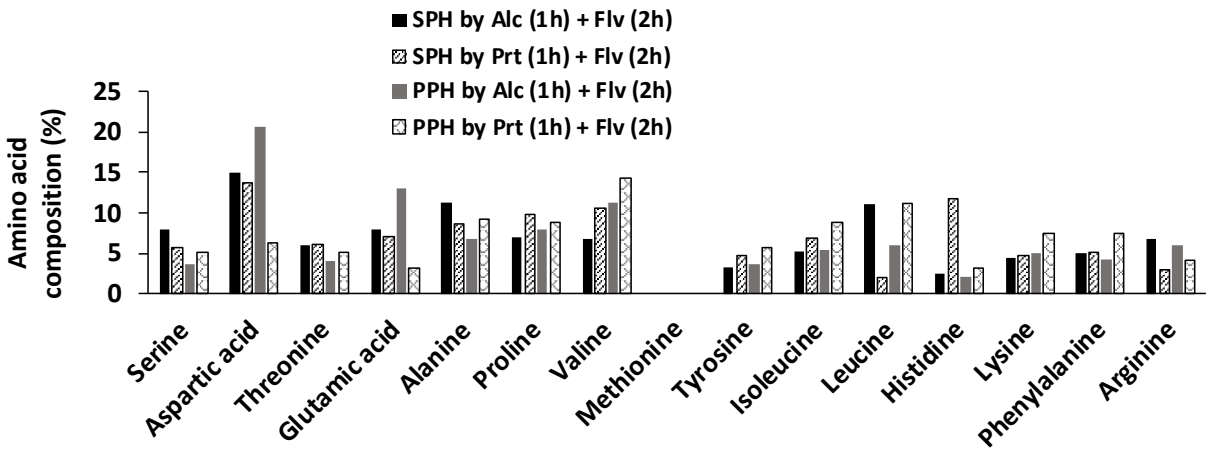

Figure 4.3. Amino acid composition of 1kDa-ultrafiltrated SPH and PPH produced by sequential hydrolysis treatment, i.e., Alcalase® or Protamex® followed by Flavourzyme®. SPH: Soy Protein Hydrolysate. PPH: Pea Protein Hydrolysate. Alc (1h): Alcalase® treatment for 1 h; Alc (3h): Alcalase® treatment for 3 h; Prt (1h): Protamex® treatment for 1 h; Prt (3h): Protamex® treatment for 3 h; Alc (1h) + Flv (2h): Alcalase® treatment for 1 h followed by Flavourzyme® treatment for 2 h; Prt (1h) + Flv (2h): Protamex® treatment for 1 h followed by Flavourzyme® treatment for 2 h

4.3.3 Determination of the metal-chelation properties

4.3.3.1 By UV-spectrophotometry

The copper-chelation capacities of the 1kDa-ultrafiltrated SPHs and PPHs were evaluated by spectrophotometry and expressed as a function of the molar ratio (mM equiv Glycine for hydrolysate / mM $CuSO_4$) (**Figure 4.4**). Whatever the hydrolysate treatment, we observed a Langmuir-shaped graphs and a saturation plateau, indicating the presence of peptides able to bind copper ions in all the 1kDa-ultrafiltrated hydrolysates, with similar capacities. From these presented graphs, we determined various indices similarly as in Canabady-Rochelle *et al.,* 2015 and 2018. **Table 4.1** shows the EDTA and carnosine equivalent chelating capacities (**EECC** and **CECC**, no unit) calculated for all the samples. The EECC and CECC values ranged between [1.54 – 2.52] and [2.19 – 3.58] respectively, without significant differences between each hydrolysate. This implies that the ultrafiltrated soy and pea hydrolysates contain copper-chelating peptides, but the spectrophotometry method has a low sensitivity in differentiating between the chelation power of the different hydrolysates. In fact, screening of bioactive peptides by UV-spectrophotometry often depends on their concentration in the hydrolysates.

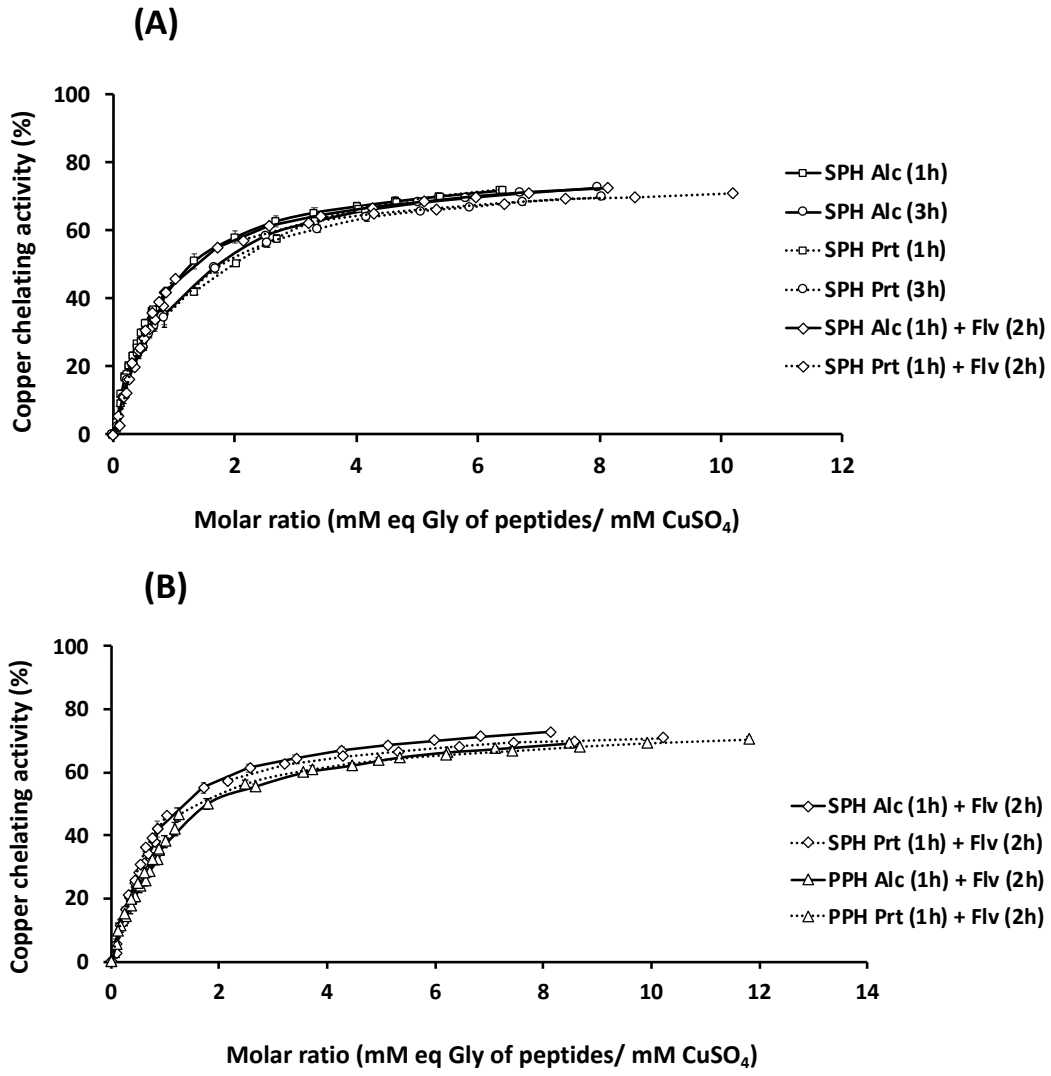

Figure 4.4. Copper chelating activity (%) of the different 1-kDa ultrafiltrated (A) SPHs and (B) PPHs as a function of molar ratio (mM eq Glycine of hydrolysate / mM $CuSO_4$). SPH: Soy Protein Hydrolysate. PPH: Pea Protein Hydrolysate. Alc (1h): Alcalase® treatment for 1 h; Alc (3h): Alcalase® treatment for 3 h; Prt (1h): Protamex® treatment for 1 h; Prt (3h): Protamex® treatment for 3 h; Alc (1h) + Flv (2h): Alcalase® treatment for 1 h followed by Flavourzyme® treatment for 2 h; Prt (1h) + Flv (2h): Protamex® treatment for 1 h followed by Flavourzyme® treatment for 2 h

Table 4.1. EDTA equivalent chelating capacity (EECC) and carnosine equivalent chelating capacity (CECC) values determined for 1kDa-ultrafiltrated SPHs and PPHs. Results are presented as mean ± standard deviation from 5 replicates

	EECC	± SEM	CECC	± SEM
SPH Alc (1h)	2.52	0.06	3.58	0.08
SPH Alc (3h)	1.94	0.02	2.76	0.03
SPH Alc (1h) + Flv (2h)	2.10	0.01	2.98	0.02
SPH Prt (1h)	2.33	0.05	3.31	0.07
SPH Prt (3h)	1.95	0.04	2.77	0.06
SPH Prt (1h) + Flv (2h)	2.08	0.01	2.96	0.02
PPH Alc (1h) + Flv (2h)	1.81	0.15	2.57	0.21
PPH Prt (1h) + Flv (2h)	1.54	0.02	2.19	0.03

SPH: Soy Protein Hydrolysate

PPH: Pea Protein Hydrolysate

Alc 1h: Alcalase® treatment for 1 h

Alc 3h: Alcalase® treatment for 3 h

Prt 1h: Protamex® treatment for 1 h

Prt 3h: Protamex® treatment for 3 h

Alc (1h) + Flv (2h): Alcalase® treatment for 1 h followed by Flavourzyme® treatment for 2 h

Prt (1h) + Flv (2h): Protamex® treatment for 1 h followed by Flavourzyme® treatment for 2 h

4.3.3.2 By Surface Plasmon Resonance

SPR is a sensitive and selective method for MCPs screening (Canabady-Rochelle *et al.,* 2018; Maalouli *et al.,* 2011; Knecht *et al.,* 2009). The SPR signal is detected when the peptide is interacting and surrounding the metal-ion in its favourable geometry, producing accurate and comparable information about the hydrolysates. The immobilized Ni^{2+} was used due to its similarities with Cu^{2+} in regards to its coordination properties with amino acids according to the HSAB theory (Sóvágó and Ősz, 2006).

The SPR response (RU) is plotted as a function of the hydrolysate concentrations (mM equiv. Glycine) **(Figure 4.5).** These so-called sorption isotherms indicate the binding response of investigated hydrolysates on the immobilized Ni^{2+} at equilibrium. They are presented either

as a function of the enzymatic treatment applied to soy protein (panel A) or as a function of the source of protein used for proteolysis (soy or pea), using the same enzymatic treatment (panel B). Whatever the enzymatic treatment or protein source used, the isotherms show hyperbolic profiles with saturation or a tendency for saturation. The differences are more visible in the saturation plateau of the metal-binding response, unlike UV-spectrophotometry data. Different parameters are obtained from the fitting of these binding isotherms and reported in **Table 4.2**.

For single protease hydrolysis of SPI, and considering the K_A values, apparent affinity of peptides for Ni^{2+} ion varied from 0.12 to 0.38 mM^{-1} equiv Gly. Hydrolysates produced by Alcalase® treatment present better apparent affinity compared to those produced by Protamex® treatment, and the best apparent affinity is observed for only 1 hour of Alcalase® treatment. This shows that there is no direct correlation between DH and apparent affinity for Ni^{2+}. Moreover, addition of exopeptidase (Flv treatment for 2 h) in the hydrolysis procedure give rise to an increase of the apparent affinity (from 0.38 to 0.42 and 0.12 to 0.23 mM^{-1} equiv Gly, for Alc 1h and Prt 1h, repectively). Finally, the results are independent from the protein source, since similar affinities are observed for PPH after sequential hydrolysis with Flv (0.45 and 0.27 mM^{-1} equiv Gly for Alc 1h and Prt 1h, respectively). This could be probably due to the fact that both soy and pea are legumins. All in all, sequential hydrolysis processes are better compared to a one step process in terms of metal-chelating properties of the obtained hydrolysates, *i.e.* these hydrolysates globally contain peptides with better affinity for Ni^{2+}.

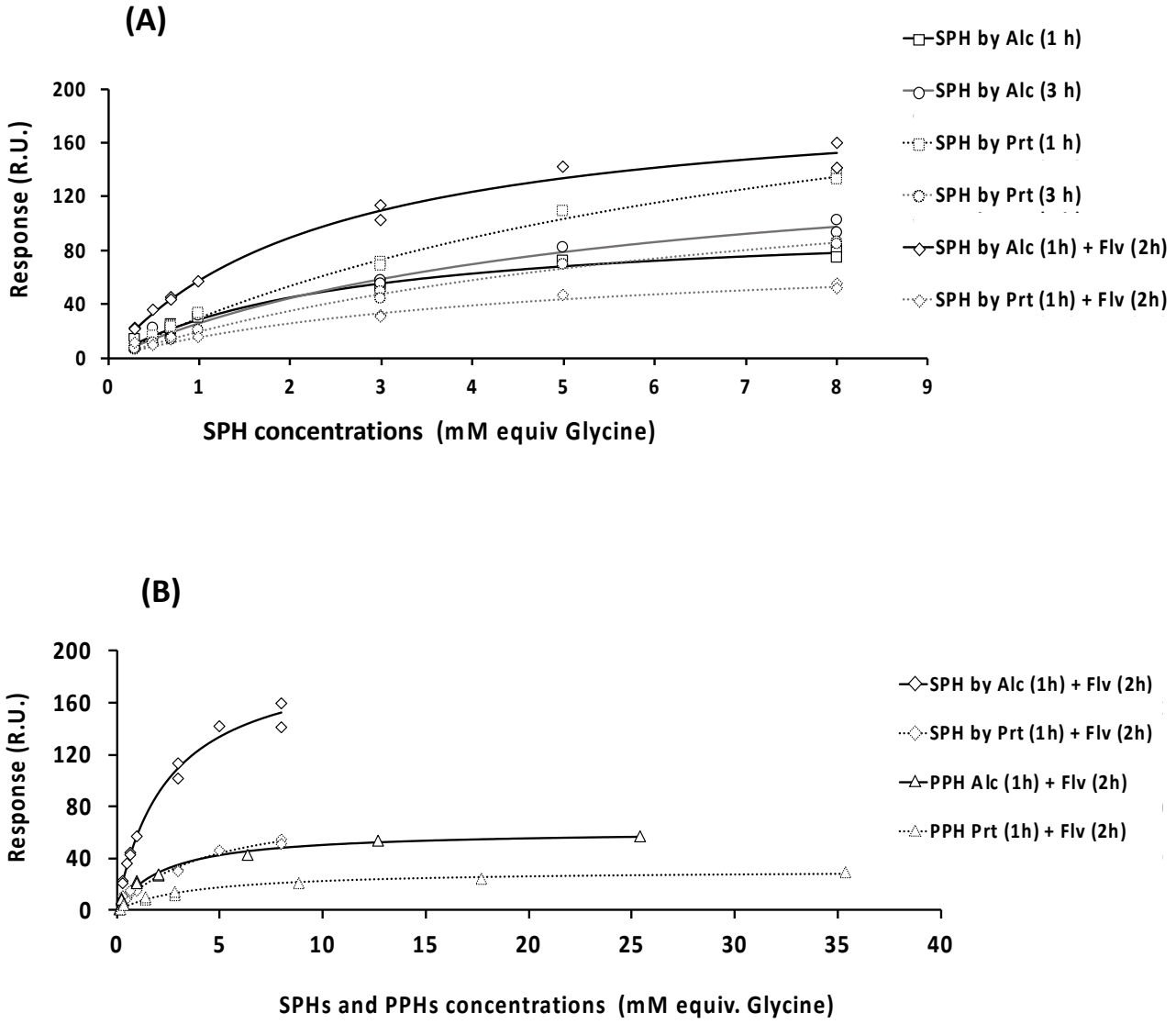

Figure 4.5. SPR response signal (R.U.) of the different 1-kDa ultrafiltrated (A) SPHs and (B) PPHs as a function of different molar concentrations (mM eq Glycine of hydrolysate). SPH: Soy Protein Hydrolysate. PPH: Pea Protein Hydrolysate. Alc (1h): Alcalase® treatment for 1 h; Alc (3h): Alcalase® treatment for 3 h; Prt (1h): Protamex® treatment for 1 h; Prt (3h): Protamex® treatment for 3 h; Alc (1h) + Flv (2h): Alcalase® treatment for 1 h followed by Flavourzyme® treatment for 2 h; Prt (1h) + Flv (2h): Protamex® treatment for 1 h followed by Flavourzyme® treatment for 2 h

Table 4.2. Peptide concentration (mM equivalent glycine) determined by OPA dosage, Dissociation (KD, mM), Affinity constants (KA, mM-1), and Rmax (R.U) determined by SPR ± standard deviation for the 1kDa-ultrafiltrated SPHs and PPHs

Sample	Peptide concentration (mM equiv Gly for 1g/L SPH)	K_D (mM equiv Gly)	STD (K_D)	K_A (mM^{-1} equiv Gly)	R*max* (RU)	STD (R_{max})
SPH by Alc (1h)	1.91	2.59	0.59	0.38	109.32	4.9
SPH by Alc (3h)	2.39	5.35	1.80	0.19	157.01	21
SPH by Prt (1h)	1.92	8.18	1.50	0.12	270.34	24
SPH by Prt (3h)	2.41	7.43	1.00	0.13	166.49	11
SPH by Alc (1h) + Flv (2h)	1.29	2.43	0.64	0.42	192.24	10
SPH by Prt (1h) + Flv (2h)	3.06	4.44	2.60	0.23	84.43	16
PPH by Alc (1h) + Flv (2h)	2.54	2.23	0.44	0.45	67.84	3
PPH by Prt (1h) + Flv (2h)	3.54	3.76	0.96	0.27	27.56	2

SPH: Soy Protein Hydrolysate

PPH: Pea Protein Hydrolysate

Alc 1h: Alcalase® treatment for 1 h

Alc 3h: Alcalase® treatment for 3 h

Prt 1h: Protamex® treatment for 1 h

Prt 3h: Protamex® treatment for 3 h

Alc (1h) + Flv (2h): Alcalase® treatment for 1 h followed by Flavourzyme® treatment for 2 h

Prt (1h) + Flv (2h): Protamex® treatment for 1 h followed by Flavourzyme® treatment for 2 h

4.4 Conclusion

In conclusion, soy and peas, which are the two most produced legumins in France, constitute rich sources of metal-chelating peptides. The fact that both soy and pea are from the legume family and that both proteins are complete might reflect the global similarities observed in the molecular weight distributions and amino acid compositions regardless of the hydrolysis condition employed. The hydrolysis treatments had an effect on the metal-chelating activity of the ultrafiltrated produced hydrolysates. A sequential treatment with an endopeptidase (Alcalase® or Protamex®) followed by an exopeptidase (Flavourzyme®) is more efficient than individual hydrolysis by an endopeptidase and the small-sized peptides (≤ 1kDa) produced have better metal-chelating affinity. This difference could only be detected by a sensitive screening method like SPR.

As perspective of this work, the MCPs present in hydrolysates could be identified by MS experiments (Paris *et al.,* 2021). In addition, IMAC coupled to mass spectrometry experiments is currently under development in order to isolate and determine some MCPs present in these hydrolysates. Then, these MCPs will be purified in order to increase their concentration for further applications related to human oral ingestion.

4.5 References

Babault, Païzis, Deley, Guérin-Deremaux, Saniez, Lefranc-Millot, & A. Allaert. (2015). Pea Proteins Oral Supplementation Promotes Muscle Thickness Gains during Resistance Training: A Double-Blind, Randomized, Placebo-Controlled Clinical Trial vs. Whey Protein. *Journal of the International Society of Sports Nutrition* 12 (1): 3. https://doi.org/10.1186/s12970-014-0064-5.

Bao, Lv, Yang, Ren, & Guo. (2008). A Study of the Soluble Complexes Formed during Calcium Binding by Soybean Protein Hydrolysates. *Journal of Food Science* 73 (3): C117–121. https://doi.org/10.1111/j.1750-3841.2008.00673.x.

Barrett. (2006). The Science of Soy: What Do We Really Know? *Environmental Health Perspectives* 114 (6): A352–358. https://doi.org/10.1289/ehp.114-a352.

Bredderman, & Wasserman. (1974). Chemical Composition, Affinity for Calcium, and Related Properties of the Vitamin D Dependent Calcium-Binding Protein. *ACS Publications* 13(8): 1687-1694. https://doi.org/10.1021/bi00705a021.

Canabady-Rochelle, Selmeczi, Collin, Pasc, Muhr, & Boschi-Muller. (2018). SPR Screening of Metal Chelating Peptides in a Hydrolysate for Their Antioxidant Properties. *Food Chemistry* 239: 478–485. https://doi.org/10.1016/j.foodchem.2017.06.116.

Carrasco-Castilla, Hernández-Álvarez, Jiménez-Martínez, Jacinto-Hernández, Alaiz, Girón-Calle, Vioque, & Dávila-Ortiz. (2012). Antioxidant and Metal Chelating Activities of Peptide Fractions from Phaseolin and Bean Protein Hydrolysates. *Food Chemistry* 135 (3): 1789–1795. https://doi.org/10.1016/j.foodchem.2012.06.016.

Charoenphun, Cheirsilp, Sirinupong, & Youravong. (2013). Calcium-Binding Peptides Derived from Tilapia (Oreochromis Niloticus) Protein Hydrolysate. *European Food Research and Technology* 236 (1): 57–63. https://doi.org/10.1007/s00217-012-1860-2.

Chen, Mu, Huang, Nie, Liu, & Zeng. (2014). Isolation of a Calcium-Binding Peptide from Tilapia Scale Protein Hydrolysate and Its Calcium Bioavailability in Rats. *Journal of Functional Foods* 6: 575–584. https://doi.org/10.1016/j.jff.2013.12.001.

Chen, Shen, & Xia. (2020). Effect of Molecular Weight of Tilapia (Oreochromis Niloticus) Skin Collagen Peptide Fractions on Zinc-Chelating Capacity and Bioaccessibility of the Zinc-Peptide Fractions Complexes in Vitro Digestion. *Applied Sciences* 10 (6): 2041. https://doi.org/10.3390/app10062041.

Cheung, Cheung, Tan, & Li-Chan.(2012). The Role of Molecular Size in Antioxidant Activity of Peptide Fractions from Pacific Hake (Merluccius Productus) Hydrolysates. *Food Chemistry* 134 (3): 1297–1306. https://doi.org/10.1016/j.foodchem.2012.02.215.

Clemente. (2000). Enzymatic Protein Hydrolysates in Human Nutrition. *Trends in Food Science & Technology* 11 (7): 254–262. https://doi.org/10.1016/S0924-2244(01)00007-3.

Coscueta, Amorim, Voss, Nerli, Picó, & Pintado. (2016). Bioactive Properties of Peptides Obtained from Argentinian Defatted Soy Flour Protein by Corolase PP Hydrolysis. *Food Chemistry*, Total Food 2014: Exploitation of agri-food chain wastes and co-products, 198: 36–44. https://doi.org/10.1016/j.foodchem.2015.11.068.

El Hajj, Sepulveda-Rincon, Paris, Giraud, Csire, Stefan, Selmeczi, Girardet, Desobry, Muhr, Gaucher, & Canabady-Rochelle. (2021a). Application in Nutrition: Mineral Binding." In Fidel Toldrá and

Jianping Wu, (Eds), *Biologically Active Peptides* (pp. 455–494). https://doi.org/10.1016/B978-0-12-821389-6.00016-9.

He, Girgih, Malomo, Ju, & Aluko. (2013). Antioxidant Activities of Enzymatic Rapeseed Protein Hydrolysates and the Membrane Ultrafiltration Fractions. *Journal of Functional Foods* 5 (1): 219–227. https://doi.org/10.1016/j.jff.2012.10.008.

Knecht, Ricklin, Eberle, & Ernst. (2009). Oligohis-Tags: Mechanisms of Binding to Ni^{2+}-NTA Surfaces. *Journal of Molecular Recognition* 22 (4): 270–279. https://doi.org/10.1002/jmr.941.

Korhonen, & Pihlanto. (2006). Bioactive Peptides: Production and Functionality. *International Dairy Journal*, 4th NIZO Dairy Conference - Prospects for Health, Well-being and Safety, 16 (9): 945–960. https://doi.org/10.1016/j.idairyj.2005.10.012.

Lv, Bao, Liu, Ren, & Guo. (2013). Purification and Characterization of Caclium-Binding Soybean Protein Hydrolysates by Ca2+/Fe3+ Immobilized Metal Affinity Chromatography (IMAC). *Food Chemistry* 141 (3): 1645–1650. https://doi.org/10.1016/j.foodchem.2013.04.113.

Lv, Liu, Bao, Tang, Yang, & Guo. (2009). Identification and Characteristics of Iron-Chelating Peptides from Soybean Protein Hydrolysates Using IMAC-Fe^{3+}. *Journal of Agricultural and Food Chemistry* 57 (11): 4593–4597. https://doi.org/10.1021/jf9000204.

Ma, Wang, Sun, Ma, Zhang, Gao, & Liu. (2013). Study on Hydrolysis Conditions of Flavourzyme in Soybean Polypeptide Alcalase Hydrolysate. *Advanced Materials Research* 652–654: 435–38. https://doi.org/10.4028/www.scientific.net/AMR.652-654.435.

Maalouli, Gouget-Laemmel, Pinchemel, Bouazaoui, Chazalviel, Ozanam, Yang, Burkhard, Boukherroub, & Szunerits. (2011). Development of a Metal-Chelated Plasmonic Interface for the Linking of His-Peptides with a Droplet-Based Surface Plasmon Resonance Read-Off Scheme. *Langmuir* 27 (9): 5498–5505. https://doi.org/10.1021/la2005437.

Megías, Pedroche, Yust, Girón-Calle, Alaiz, Millán, & Vioque. (2007). Affinity Purification of Copper-Chelating Peptides from Sunflower Protein Hydrolysates. *Journal of Agricultural and Food Chemistry* 55 (16): 6509–6514. https://doi.org/10.1021/jf0712705.

Montgomery. (2003). Soy Protein. *The Journal of Perinatal Education* 12 (3): 42–45. https://doi.org/10.1624/105812403X106946.

Paris, Selmeczi, Ebel, Stefan, Csire, Cakir-Kiefer, Desobry, Canabady-Rochelle, & Patrick Chaimbault. (2021). Metabolomics Approach Based on LC-HRMS for the Fast Screening of Iron(II)-Chelating Peptides in Protein Hydrolysates. *Analytical and Bioanalytical Chemistry* 413 (2): 315–329. https://doi.org/10.1007/s00216-020-03037-1.

Penta-Ramos, & Xiong. (2002). Antioxidant Activity of Soy Protein Hydrolysates in a Liposomal System. *Journal of Food Science* 67 (8): 2952–2956. https://doi.org/10.1111/j.1365-2621.2002.tb08844.x.

Pownall, Udenigwe, & Aluko. (2010). Amino Acid Composition and Antioxidant Properties of Pea Seed (Pisum Sativum L.) Enzymatic Protein Hydrolysate Fractions. *Journal of Agricultural and Food Chemistry* 58 (8): 4712–4718. https://doi.org/10.1021/jf904456r.

Raghavan, & Kristinsson. (2008). Antioxidative Efficacy of Alkali-Treated Tilapia Protein Hydrolysates: A Comparative Study of Five Enzymes. *Journal of Agricultural and Food Chemistry* 56 (4): 1434–1441. https://doi.org/10.1021/jf0733160.

Ranamukhaarachchi, Meissner, & Moresoli. (2013). Production of Antioxidant Soy Protein Hydrolysates by Sequential Ultrafiltration and Nanofiltration. *Journal of Membrane Science* 429: 81–87. https://doi.org/10.1016/j.memsci.2012.10.040.

Ren, Zheng, Liu, & Liu. (2010). Purification and Characterization of Antioxidant Peptide from Sunflower Protein Hydrolysate. *Food Technology and Biotechnology* 48 (4): 519-523. ISSN 1330-962

Romero-Garay, Martínez-Montaño, Hernández-Mendoza, Vallejo-Cordoba, González-Córdova Montalvo-González, & García-Magaña. (2020). Bromelia Karatas and Bromelia Pinguin: Sources of Plant Proteases Used for Obtaining Antioxidant Hydrolysates from Chicken and Fish by-Products. *Applied Biological Chemistry* 63 (1): 41. https://doi.org/10.1186/s13765-020-00525-x.

Seo, Lee, & Baek. (2008). Evaluation of Bitterness in Enzymatic Hydrolysates of Soy Protein Isolate by Taste Dilution Analysis. *Journal of Food Science* 73 (1): S41–46. https://doi.org/10.1111/j.1750-3841.2007.00610.x.

Simmen, & Lacampagne. (2020). The Market of Legumes in France, 51.

Sóvágó, & Ősz. (2006). Metal Ion Selectivity of Oligopeptides. *Dalton Transactions*, no. 32 (August): 3841–3854. https://doi.org/10.1039/B607515K.

Strauch, & Lila. (2021). Pea Protein Isolate Characteristics Modulate Functional Properties of Pea Protein–Cranberry Polyphenol Particles. *Food Science & Nutrition* 9 (7): 3740–3751. https://doi.org/10.1002/fsn3.2335.

Sun, Cui, Jin, Wu, Wang, & Lin. (2017). Contributions of Molecular Size, Charge Distribution, and Specific Amino Acids to the Iron-Binding Capacity of Sea Cucumber (Stichopus Japonicus) Ovum Hydrolysates. *Food Chemistry* 230 (September): 627–636. https://doi.org/10.1016/j.foodchem.2017.03.077.

Theodore, Raghavan, & Kristinsson. (2008). Antioxidative Activity of Protein Hydrolysates Prepared from Alkaline-Aided Channel Catfish Protein Isolates. *Journal of Agricultural and Food Chemistry* 56 (16): 7459–7466. https://doi.org/10.1021/jf800185f.

Tömösközi, Lásztity, Haraszi, & Baticz. (2001). Isolation and Study of the Functional Properties of Pea Proteins. *Die Nahrung* 45 (6): 399–401. https://doi.org/10.1002/1521-3803(20011001)45:6<399::AID-FOOD399>3.0.CO;2-0.

Torres-Fuentes, Alaiz, & Vioque. (2011). Affinity Purification and Characterisation of Chelating Peptides from Chickpea Protein Hydrolysates. *Food Chemistry* 129 (2): 485–490. https://doi.org/10.1016/j.foodchem.2011.04.103.

Tsou, Kao, Tseng, & Chiang. (2010). Enhancing the Anti-Adipogenic Activity of Soy Protein by Limited Hydrolysis with Flavourzyme and Ultrafiltration. *Food Chemistry* 122 (1): 243–248. https://doi.org/10.1016/j.foodchem.2010.02.070.

Ugolini, Cinti, Righetti, Stefan, Matteo, D'Avino, & Lazzeri. (2015). Production of an Enzymatic Protein Hydrolyzate from Defatted Sunflower Seed Meal for Potential Application as a Plant Biostimulant. *Industrial Crops and Products* 75 (November): 15–23. https://doi.org/10.1016/j.indcrop.2014.11.026.

Vegarud, Langsrud, & Svenning. (2000). Mineral-Binding Milk Proteins and Peptides; Occurrence, Biochemical and Technological Characteristics. *British Journal of Nutrition* 84 (S1): 91–98. https://doi.org/10.1017/S0007114500002300.

Vioque, Sánchez-Vioque, Clemente, Pedroche, Bautista, & Millan. (1999). Production and Characterization of an Extensive Rapeseed Protein Hydrolysate. *Journal of the American Oil Chemists' Society* 76 (7): 819–823. https://doi.org/10.1007/s11746-999-0071-x.

Xie, Huang, Li, Cheng, Wang, Yin, & Yan. (2015). Affinity Purification and Characterisation of Zinc Chelating Peptides from Rapeseed Protein Hydrolysates: Possible Contribution of Characteristic Amino Acid Residues. *Food Chemistry* 173: 210–217. https://doi.org/10.1016/j.foodchem.2014.10.030.

Xie, Liang, Wei, Zhao, He, Lu, Huo, and Ma. (2012). Optimization of Glutamine Peptide Production from Soybean Meal and Analysis of Molecular Weight Distribution of Hydrolysates. *International Journal of Molecular Sciences* 13 (6): 7483–7495. https://doi.org/10.3390/ijms13067483.

Zhang, Huang, & Jia-Xin Jiang. (2014). Iron Binding Capacity of Dephytinised Soy Protein Isolate Hydrolysate as Influenced by the Degree of Hydrolysis and Enzyme Type. *Journal of Food Science and Technology* 51 (5): 994–999. https://doi.org/10.1007/s13197-011-0586-7.

Zhang, Tong, Qi, Wang, Li, Sui, & Jiang. (2018). Changes in Antioxidant Activity of Alcalase-Hydrolyzed Soybean Hydrolysate under Simulated Gastrointestinal Digestion and Transepithelial Transport. *Journal of Functional Foods* 42: 298–305. https://doi.org/10.1016/j.jff.2018.01.017.

Zhang, Zhou, Liu, & Zhao. (2018). Particulate Nanocomposite from Oyster (Crassostrea Rivularis) Hydrolysates via Zinc Chelation Improves Zinc Solubility and Peptide Activity. *Food Chemistry* 258: 269–277. https://doi.org/10.1016/j.foodchem.2018.03.030.

Chapter 5 Development of a ferroptosis model on Aortic smooth muscle cells

The biological interest in exploring metal-chelating activity in hydrolysates, with tools mentioned in chapters 3 and 4, is to eventually evaluate their antioxidant power *in cellulo*. These peptides could be promising for ferroptosis inhibition by chelating excess iron ions and thus contribute to the prevention of cell death in several diseases including Atherosclerosis **(AS)**. In this chapter, we described how we aimed to develop a ferroptosis model (induction and rescuing) on human aortic smooth muscle cells to mimic ferroptosis happening during AS development.

5.1 Introduction

Toxic iron ions catalyze the formation of hydroxyl radicals *via* the Haber-Weiss reaction (Haber and Weiss 1934), or can be a direct reactant for their production such as Fe(II) in Fenton reaction (Fenton 1894). Normally, adult males absorb only 1.5 mg of iron per day but adult females require additional 1.5-2 mg per day in order to compensate the losses during menstrual bleeding. Maintaining iron homeostasis is critically essential for human health to prevent diseases such as iron deficiency anemia and hemochromatosis caused by iron overload. Concentration of intracellular iron ions is regulated at several cellular levels that comprise: iron (Fe^{3+}) uptake *via* transferrin receptors (TFR1 and TFR2), iron (Fe^{3+}) storage in ferritin, and iron (Fe^{2+}) export *via* ferroportin. Dysregulation of iron homeostasis causes iron-mediated cell death, recently described as ferroptosis, which is genetically, biochemically and morphologically different from apoptosis and necrosis (Mou *et al*. 2019; Tang *et al*. 2019). **(See Figure 2.13, page 95)**

Ferroptosis has been reported in several diseases such as hepatic cancer, renal and cardiovascular diseases (heart failure, atherosclerosis). The hallmark feature of ferroptosis is the iron-dependent accumulation of oxidized phospholipids (*i.e.*, lipid peroxides). Ferroptosis

can be induced by the inactivation of system X_c^- (glutamate/cystine antiporter) using either erastin, sorafenib, sulfasalazine, or excess glutamate but also, by the inhibition of the glutathione peroxidase 4 **(GPx4)** using Ras Selective Lethal 3 **(RSL3)** (Kobayashi *et al.,* 2018) **(See Figure 2.15, page 101)**. Indeed, the inhibition of the system X_c^- induces the depletion of intracellular cysteine pool, the limiting amino acid required for glutathione **(GSH)** synthesis. Yet, the decrease of intracellular GSH concentration causes an imbalance in cell redox homeostasis and antioxidant capacity. Indeed, it inhibits the glutathione-dependent enzymes, such as the **GPx4** that catalyzes the reduction of lipid peroxides while oxidizing GSH and protects cells from oxidative stress-induced plasma membrane injury (Martin and Teismann 2009).

Ferroptosis can be prevented by natural and/or chemical compounds. Vitamin E is a natural exogeneous lipophilic antioxidant that can inhibit ferroptosis by reducing lipid peroxides, so does the synthetic ones such as ferrostatins and Trolox (a hydrophilic analog of vitamin E). Metal-chelating agents such as deferoxamine **(DFO)** and deferiprone **(DFr)** can chelate iron ions ($Fe^{2+/3+}$) in excess and thus inhibits their catalytic effect known to induce ferroptosis (Cao and Dixon 2016). Although ferroptosis has been identified as a cell death pathway occurring in cardiovascular diseases such as atherosclerosis, very few studies in the literature report treatments inhibiting ferroptosis. Moreover, to the author's knowledge, there is no model of ferroptosis based on cardiovascular cells in order to test molecules able to inhibit ferroptosis with potential application in cardiovascular diseases treatment.

Hence, the objective of this study is to develop a cell-based ferroptosis model upon the inhibition of the system Xc^- antiporter and triggering lipid peroxidation with Fe(III) overload. This model will be used to investigate potential Fe(III) chelators using DFO and Dfr as positive controls.

5.2 Material and Methods

5.2.1 Reagents

Erastin (E7781, Sigma-Aldrich) was prepared at an initial concentration of 10 mM in 100% Dimethyl sulfoxide **DMSO** (FLUKA), aliquoted and stored at -80°C. Ferric citrate (F3388-Sigma-Aldrich) was prepared at an initial concentration of 25 mM in warm PBS (37°C) and stored at

4°C. Deferoxamine (D0160000, European Pharmacopia) was prepared at an initial concentration of 30 mM in PBS, aliquoted, and stored at -80°C. Deferiprone (Y0001976, European Pharmacopia) was prepared at an initial concentration of 134 mM in warm ultra-pure water, aliquoted and stored at -80°C.

5.2.2 Cell culture

Smooth muscle cells derived from human aorta, AoSMC (CC-2571, LONZA, France) were grown (37°C, 10% CO_2) in smooth muscle complete cell growth medium (CC-3182, LONZA, France) containing SmBM™ Basal Medium and SmGM™ 2 SingleQuots supplements. Supplements comprise 5% (v/v) of fetal bovine serum (FBS), 0.1% (v/v) insulin, 0.2% (v/v) of human basic fibroblast growth factor (hFGF-B), 0.1% (v/v) of gentamicin, 0.1% (v/v) of amphotericin-B, and 0.1% (v/v) of human epidermal growth factor (hEGF).

5.2.3 Cytocompatibility test

The cytocompatibility of Erastin at a concentration range comprised between 0.01 and 10 µM was evaluated by the MTT test. The AoSMC were seeded at a density of 60.10^3 cells/mL of complete growth medium in 96-well plate. After 24 h, cells were incubated with the different concentration of Erastin for another 24 h at 37°C. Then, 50 µL of 3-(4,5-dimethylthiazol-2-yl)-2,5-diphenyltetrazolium bromide (MTT) solution (5 mg/mL) were added to each well for 3 h at 37°C. In viable cells, cellular oxidoreductase can reduce MTT to its insoluble form, called formazan that have a purple color. The formazan crystals were dissolved with 50 µL of 100% DMSO in each well, and the absorbance was read at 570 nm.

5.2.4 Induction of ferroptosis

AoSMCs were seeded at a density of 60.10^3 cells/mL of complete growth medium in 6-well microplate for further GSH, MDA and protein quantifications. Prior to incubations, DMSO (100%), erastin, ferric citrate, deferoxamine, and deferiprone were diluted in warm (37°C) incubation medium (complete cell growth medium either undiluted or diluted 2 times with PBS) in order to obtain final concentrations of 1 %, 100 µM, 500 µM, 500 µM, and 1500 µM, respectively. Finally, the molecules were further diluted 10 times for 16 hours of incubation (37°C, 10% CO_2) with AoSMC. Final volume in each well was 1 mL.

5.2.5 Quantification of intracellular glutathione concentration

After incubation, the cells were lysed with 250 µL of 3.3% (v/v) cold perchloric acid (Sigma-Aldrich) and centrifuged at 10,000 *g* during 15 min at 4°C. 200 µL of the supernatant was neutralized by 11.5 µL NaOH-40%, whereas the pellet was collected and resuspended in 200 µL of lysis buffer (0.5 M Tris-HCl 1.5 M NaCl, 10% SDS, and pure Triton) and frozen at -80°C for further protein dosage assay **(see section 5.2.7)**. The neutralized supernatant was diluted (4 times for control condition, 2 times for erastin condition, and 1.3 times for erastin + ferric citrate condition and for Erastin + ferric citrate + deferoxamine or deferiprone condition) in a solution containing HCl (0.1 M; Sigma Aldrich) and EDTA (2 mM; Titriplex). Then, 60 µL of each previously diluted supernatant were deposited in triplicates in 96-well black microplate (ThermoFischer Scientific). 120 µL of borate buffer (0.4 M; pH 9.2; Merk) and 20 µL of 2,3-naphthalene dicarboxaldehyde (NDA, 5.4 mM; Fluka) were then added to each well. The plate was incubated for 25 minutes at 4°C. The fluorescence intensity was measured at λ_{exc}= 485 nm and λ_{em}= 538 nm using the microplate reader *Synergy2 – Bioteck* and the *Gen5 – 1.08* software. The GSH concentration in each sample was determined from a calibration curve presenting fluorescence intensity as a function of GSH concentration ranging from 0.325 µM to 3.25 µM.

5.2.6 Quantification of peroxidized lipids

Malondialdehyde (MDA) was quantified as a final product of lipid peroxidation using the TBARS method (Janero, 1990). After incubation, cells were lysed in 200 µL of 10 % (v/v) perchloric acid to collect MDA and centrifuged at 10,000 *g* for 15 min at 4°C for further protein collection. The supernatant was then separated from the pellet. The pellet was resuspended in 200 µL of lysis buffer (0.5 M Tris-HCl, 1.5 M NaCl, 10 % (v/v) SDS, and 10 % (v/v) pure Triton) and frozen at -80°C for further protein dosage **(see section 5.2.7)**. 200 µL of TBA solution (15 g of trichloroacetic acid (Sigma-Aldrich) and 0.38 g of thiobarbatic acid (Sigma-Aldrich) dissolved in 100 mL of 0.25 M HCl) and 2 µL of butylated hydroxytoluene (Fluka) 2% (w/v in absolute ethanol (Sigma-Aldrich)) were added to each supernatant. Samples were incubated at 95°C for 1 h, then placed in ice for 3 minutes. The MDA-TBA adduct was then extracted with 400 µL of butanol-1 (Sigma-Aldrich) and centrifuged at 15,000 *g* for 5 min at 4°C. 120 µL of each supernatant were deposited in triplicates in 96-well black microplate (ThermoFischer Scientific). The fluorescence intensity was measured at λ_{exc}= 485 nm and λ_{em}= 538 nm using

the microplate reader *Jasco* and the *Spectra Manager – 2.10.01* software. The concentration of MDA in each sample was determined from the plotted calibration curve representing the fluorescence intensity as a function of MDA concentration ranging from approximately 0.0625 µM to 2.5 µM. Note that the initial concentration of MDA was validated using UV spectrophotometry and by Beer Lambert equation at each experiment.

5.2.7 Quantification of intracellular proteins

The intracellular protein concentration was quantified to evaluate the number of cells remaining after the incubations. The intracellular protein concentration was determined using the bicinchoninic acid (BCA) assay kit (ThermoFisher Scientific) including a calibration curve of bovine serum albumin (BSA) ranging from 25 µg/mL to 1000 µg/mL. 25 µL of each resuspended pellet were deposited in triplicates in 96-well microplate and added with 200 µL working buffer (50 volumes of reagent A: sodium carbonate, sodium bicarbonate, BCA and sodium tartrate in 0.1 M NaOH; 1 volume of reagent B: 4% (w/v) of copper sulfate). The absorbance was read at 570 nm after 30 min incubation at 37°C using the spectrophotometer equipped with a microplate reader *BioTeck 800TS, J80.13*.

5.2.8 Statistical analysis

Results are shown as mean ± standard error of the mean (SEM), based on 3 independent experiments. The statistical analysis was performed using GraphPad Prism 9 software with a t-test or one-way ANOVA test followed by a Tukey's post-test. Differences were considered significant when $p < 0.05$.

5.3 Results and Discussion

The development of the ferroptosis model on AoSMCs was done by first testing the cytocompatibility of Erastin, and then by following the two biomarkers: intracellular concentration of GSH and lipid peroxidation, normalized in reference of the protein content.

5.3.1 Cytocompatibility of Erastin

A range of erastin concentrations (0.01 µM - 10 µM) was tested for evaluating their cytocompatibility on AoSMCs as a first required step in order to set the maximum concentration of erastin to be used in developing the ferroptosis model without killing the cells. **Figure 5.1** shows approximately 80% ± 20% of cell viability for all tested concentrations

of erastin. Thus, AoSMCs have maintained their functional properties and growing abilities after 24 hours of treatment with erastin, whatever the investigated concentration. According to some studies, 10 µM of erastin is the commonly used concentration to induce ferroptosis (Zhang et al., 2020; Sato et al., 2018; Dixon et al., 2014). Therefore, 10 µM of erastin is the first chosen concentration for the development of the ferroptosis model on AoSMC in our experiments.

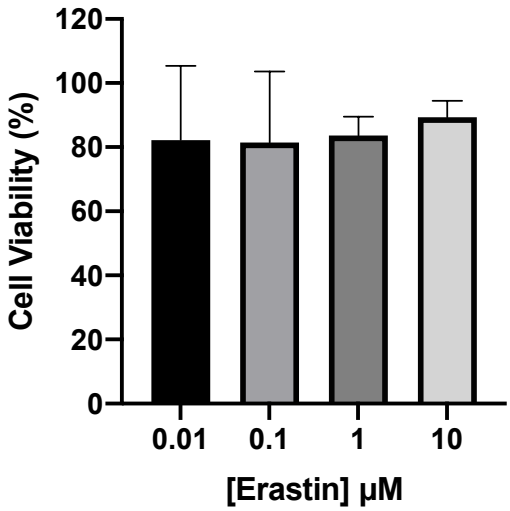

Figure 5.1. AoSMC cell viability after 24 h incubation of different erastin concentration. Results are presented as mean ± sem of n=3 and compared using one-way ANOVA. Results are calculated in respect to 100% viability, which is for [Erastin]=0 µM.

5.3.2 Ferroptosis evaluation upon Erastin incubation in different media by GSH quantification

Erastin was incubated in complete culture medium, this latter being either non-diluted, diluted 2 times, or 10 times. Indeed, cystine and glutamate present in culture medium can have inhibitory effect on erastin activity itself when present at high concentrations. Yet, the concentration of these 2 amino acids could not be communicated by LONZA - the culture medium supplier - due to confidentiality.

Figure 5.2 shows the intracellular concentration of GSH and proteins before and after incubation of AoSMC with erastin in different incubation media (diluted or not). In complete medium (non-diluted) and in the absence of erastin, the physiological concentration of GSH is stated at 10 µM ± 1.4 µM **(Figure 5.2, A)** and the protein concentration at 520 ± 80 µg/mL **(Figure 5.2, B)**. Following erastin overnight incubation in complete culture medium, the

intracellular GSH concentration **(Figure 5.2, A)** decreased by 9 times compared to the control condition. The intracellular protein concentration was determined to evaluate the number of cells remaining after the incubation. No significant change was observed in protein concentration between the control condition (520 ± 80 µg/mL) and the erastin condition (390 ± 20 µg/mL) **(Figure 5.2, B)**. In complete medium diluted 2 times, the intracellular GSH concentration decreased by 5 times after overnight incubation with 10 µM erastin in comparison to the control **(Figure 5.2, C),** and the protein concentration remained constant 450 ± 20 µg/mL for both conditions **(Figure 5.2, D)**. Finally, in complete medium diluted 10 times the concentration of intracellular GSH decreased by 2 times following erastin overnight incubation **(Figure 5.2, E)**, and protein concentrations observed were similar for both control and erastin conditions **(Figure 5.2, F)**. GSH and protein concentrations of AoSMC in complete medium diluted 10 times are respectively, 3 µM ± 0.5 µM and 63 µg/mL ± 22 µg/mL (for the control) and, 1.5 µM ± 0.2 µM and 70 µg/mL ± 20 µg/mL (in the erastin condition). These former values are much lower than those observed in non-diluted complete medium and complete medium diluted 2 times. So, although erastin can significantly decrease intracellular GSH in complete medium diluted 10 times, cells in this latter medium are suffering after an overnight incubation, even in the absence of erastin. Therefore, only the non-diluted and the 2 times-diluted mediums are not deleterious for AoSMC viability after overnight incubation and for these 2 media, erastin did inhibit the system X_c^- and deprived cells from cystine/cysteine necessary for GSH synthesis.

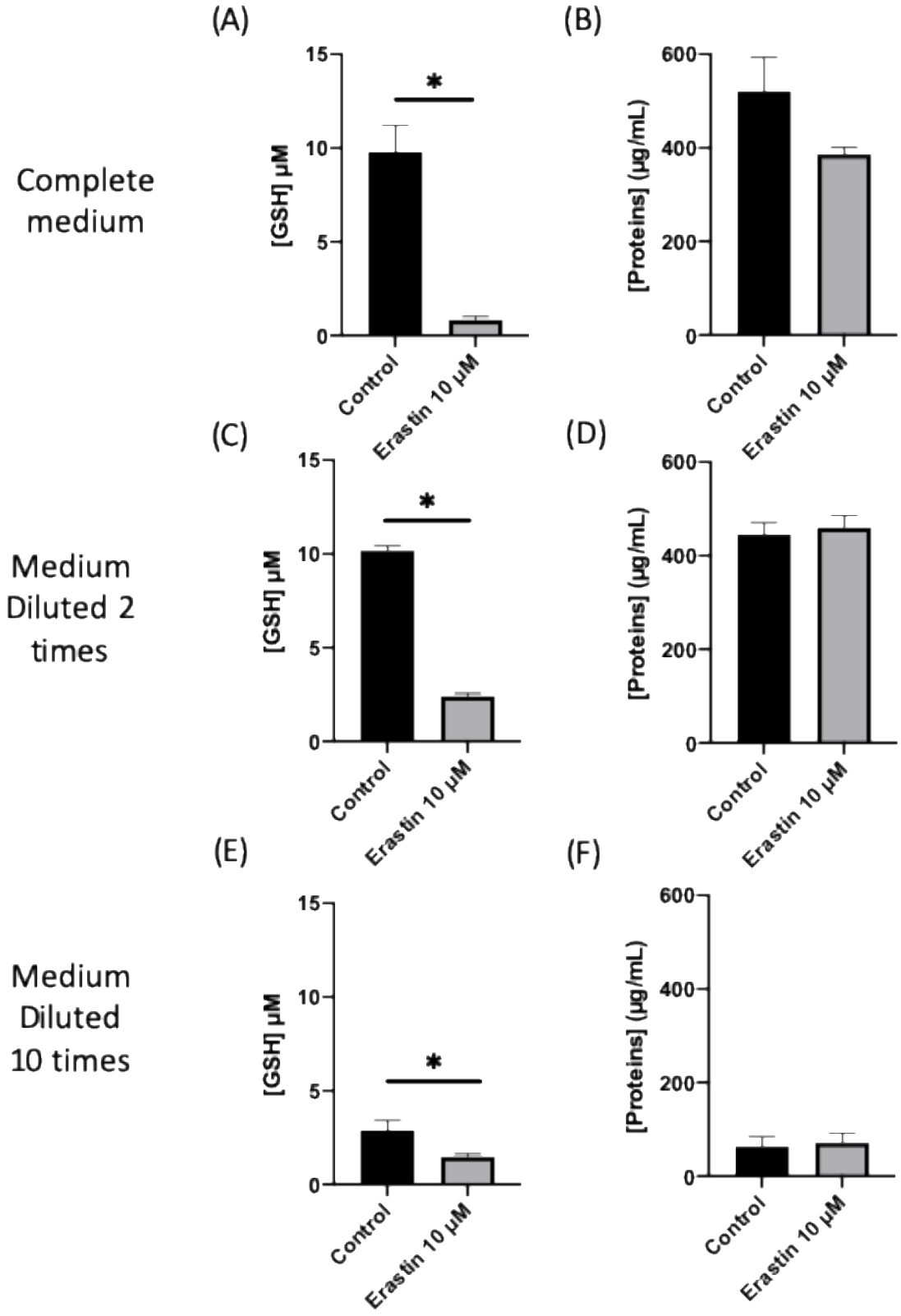

Figure 5.2. GSH and proteins concentrations in AoSMCs after an overnight incubation with and without erastin in non-diluted complete medium (A & B), complete medium diluted 2 times (C & D) and complete medium diluted 10 times (E & F). Results are presented as mean ± sem of n=3 and compared using one sample t test; *p < 0.05.

5.3.3 Ferroptosis evaluation upon erastin incubation in different media by MDA quantification

MDA was quantified to evaluate lipid peroxidation – the second ferroptosis biomarker - state of cells after overnight incubation with 10 µM Erastin in non-diluted and in 2 times diluted complete media. In non-diluted complete medium, MDA concentration **(Figure 5.3, A)** and protein concentration **(Figure 5.3, B)** were determined at 0.1 ± 0.02 µM and 470 ± 50 µg/mL, respectively, and remained constant whatever the investigated conditions (control or in the presence of erastin). In 2 times-diluted medium, MDA concentration fluctuated between 0.08 ± 0.05 µM in control condition and 0.016 ± 0.05 µM in erastin condition, without significant difference between both conditions **(Figure 5.3, C)**. Protein concentration in both media (complete or 2 times-diluted) was approximately 400 ± 80 µg/mL **(Figure 5.3, D)**. So, blocking the system X_c^- with erastin does not provoke lipid peroxidation in AoSMCs in both media after an overnight incubation. This result was expected as lipid peroxidation is induced by hydroxyl radicals, produced upon the Haber-Weiss reaction resulting from iron ions oxidation. Therefore, in order to induce lipid peroxidation, we decided to introduce 50 µM of ferric citrate (FC) during erastin incubation, as a provider for Fe^{3+} ions.

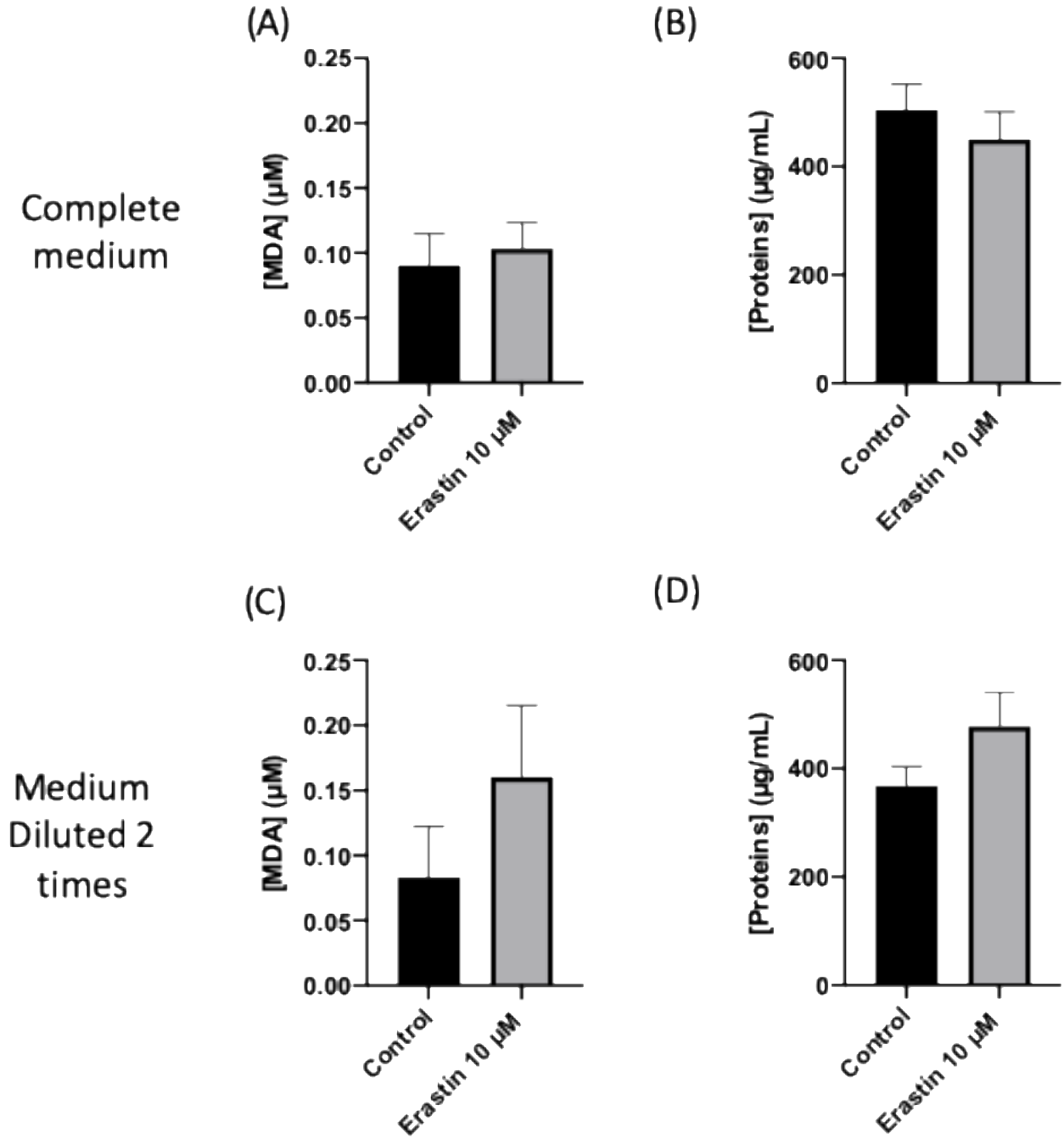

Figure 5.3. MDA quantification and protein dosage of AoSMC after an overnight incubation with and without erastin in non-diluted complete medium (A & B) and, complete medium diluted 2 times (C & D). Results are presented as mean ± sem of n=3 and compared using one sample t test; *p < 0.05.

5.3.4 Ferroptosis evaluation upon iron introduction in different media by MDA quantification

MDA concentration in non-diluted complete medium after overnight incubation of AoSMCs with 10 µM Erastin + 50 µM FC did not significantly change compared both to the control and to the 10 µM Erastin conditions **(Figure 5.4, A)**. However, the protein concentration decreased by 3 times in the 10 µM Erastin + 50 µM FC compared to the control and the 10 µM Erastin conditions **(Figure 5.4, B)**. This means that, in complete medium, the introduction of 50 µM FC is deleterious to cells. Note that the initial concentration of iron ions in the complete medium could not be communicated by the medium supplier. In complete medium diluted 2 times, the 10 µM Erastin + 50 µM FC condition and the 10 µM Erastin condition have increased MDA concentration by 3.75 and 2 times compared to the control, respectively **(Figure 5.4, C).** In the meantime, the protein concentration remained constant at approximately 420 ± 70 µg/mL in those 3 conditions **(Figure 5.4, D).** This implies that, in complete medium diluted 2 times, 10 µM Erastin + 50 µM FC promote lipid peroxidation without leading to cell death.

Therefore, inducing ferroptosis was validated by GSH and MDA quantification upon overnight incubation with 10 µM Erastin (to act on GSH synthesis) + 50 µM FC (to induce lipid peroxidation) in complete medium diluted 2 times.

To be able to use this ferroptosis model based on AoSMC as a positive control on which testing antioxidant molecules such as metal-chelating peptides, a rescue ferroptosis model should be developed as well, using reagents well known for their metal-chelating properties such as Deferoxamine (DFO) and Deferiprone (DFr).

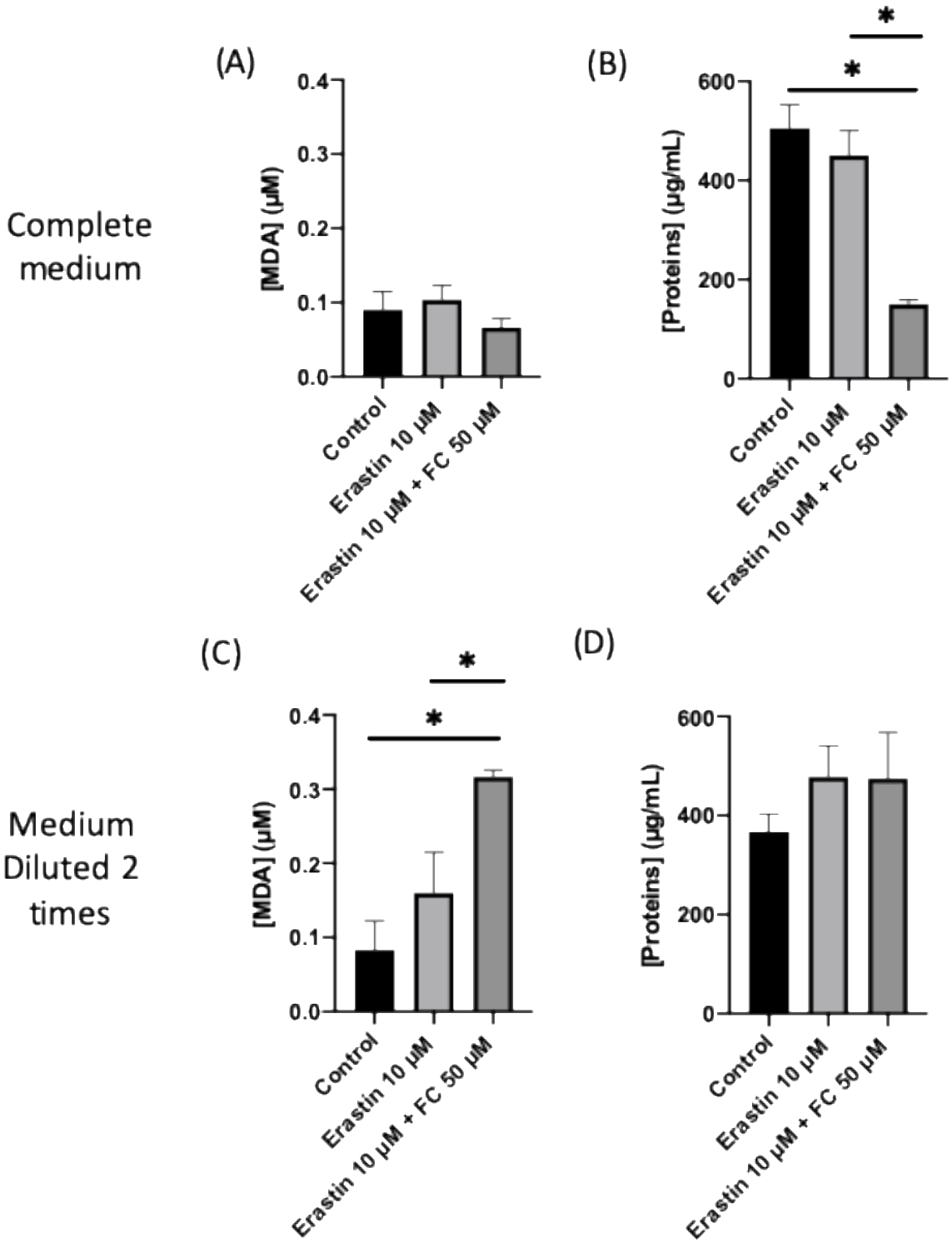

Figure 5.4. MDA quantification and protein dosage of AoSMC after an overnight incubation with and without erastin ± 50 µM ferric citrate (FC) in non-diluted complete medium (A & B) and in complete medium diluted 2 times (C & D). Results are presented as mean ± sem of n=3 and compared using one way ANOVA; *$p < 0.05$ (Tukey's multiple comparisons test).

5.3.5 Ferroptosis rescue model evaluation by GSH and MDA quantifications

Intracellular GSH concentration was evaluated by plotting the ratio of GSH quantity (nmol) over protein mass (mg). The **Figure 5.5, A** show that this ratio is non-significantly increased by 50 µM DFO in comparison to the incubation with 10 µM erastin + 50 µM FC and is equivalent to GSH ratio in 10 µM erastin condition. However, 150 µM DFr is able to restore GSH ratio compared to the 10 µM Erastin + 50 µM FC condition, but not significantly compared to the control condition (ratio = 30 nmol/mg ± 1 nmol/mg).

Similarly, MDA concentration was evaluated by plotting also MDA quantity (nmol) over protein mass (mg). MDA concentration is non-significantly decreased after incubation with 50 µM DFO but significantly decreased by 4 times after incubation with 150 µM DFr in comparison to the incubation with 10 µM erastin + 50 µM FC. So, by chelating Fe^{3+} in 1:1 ratio (Velasquez and Wray 2021), DFO tends to inhibit ferroptosis caused by 10 µM erastin + 50 µM FC condition but might requires an adaptation of incubation conditions, such as the time of incubation or DFO concentration in order to render its effect significant. However, DFr in those conditions of time (16 h) and concentration (150 µM) stop lipid peroxidation induced by combatant use of erastin and FC. Dfr binds Fe^{3+} in 3:1 molar ratio and its small structure allows it to be a cell permeant metal-chelator, unlike DFO (Galanello, 2007). Therefore, 150 µM Dfr rescues our ferroptosis model based on AoSMCs.

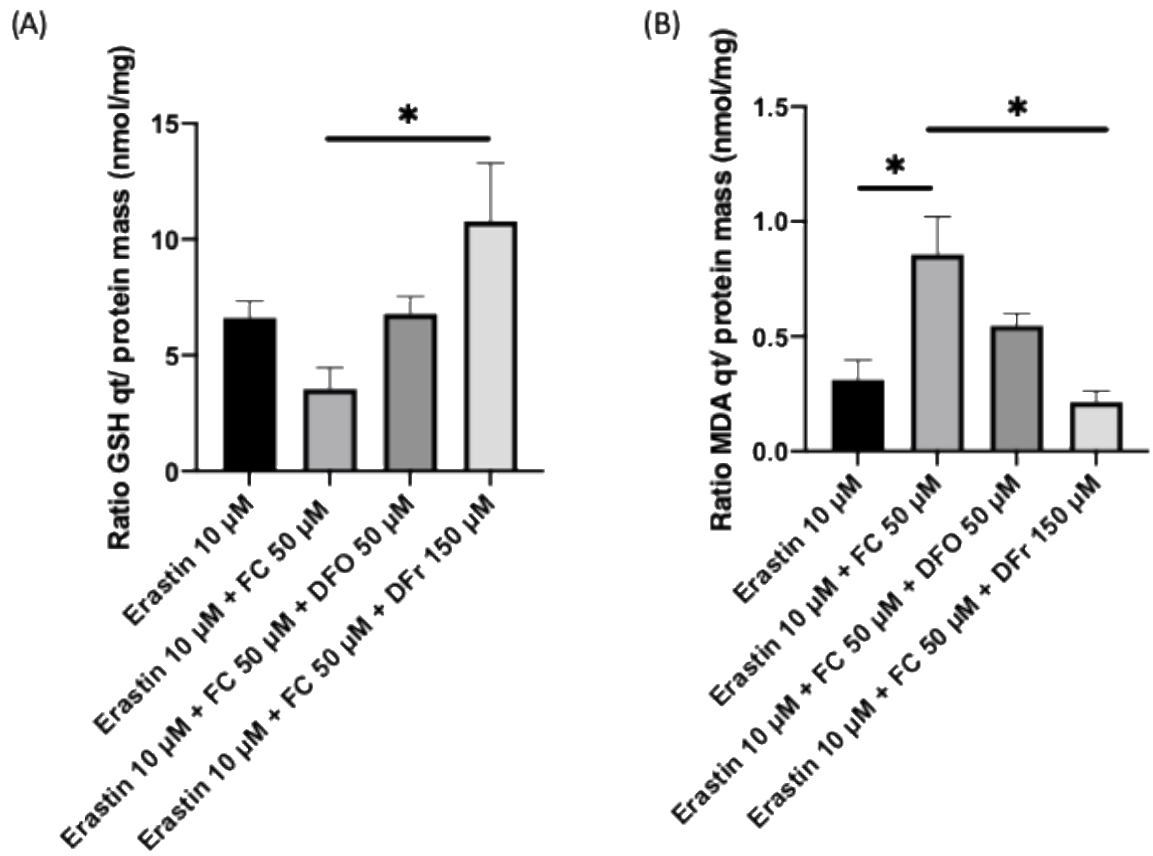

Figure 5.5. Ratio of GSH quantity over protein mass (A) and the ratio of MDA quantity over protein mass (B) Smooth muscle cells were incubated in complete medium diluted 2 times for 1 night with and without erastin ± 50 µM ferric citrate ± 50 µM deferoxamine (or 150 µM deferiprone). Results are presented as mean ± sem of n=3 and compared using one-way ANOVA; *p < 0.05 (Tukey's multiple comparisons test).

5.4 Conclusion and Perspectives

In conclusion, the ferroptosis model is validated using GSH and MDA as biomarkers upon the overnight incubation of AoSMCs with Erastin 10µM and FC 50 µM. Erastin induced GSH depletion while ferric citrate - containing ferric ions (Fe^{3+}) - induced lipid peroxidation. DFO (50 µM) was not effective on AoSMCs for rescuing ferroptosis, unlike DFr (150 µM).

In perspectives, our ferroptosis model adapted to AoSMC investigation should be reinforced by following a third ferroptosis biomarker, which is the ROS production. In addition to inhibiting lipid peroxidation, inhibiting ROS production can also be a biomarker for measuring metal chelation efficiency since iron ions, notably Fe^{2+} are well-known to catalyze ROS via the Fenton reaction. It would be interesting to study the effect of synthetic metal-chelating peptides such as HHH, HHHHHH, HGH and carnosine in inhibiting ferroptosis since it could be

the start for a protein-based therapy (or prevention) for iron-overload diseases and then to investigate the effect of metal-chelating peptides discovered from protein hydrolysates.

5.5 References

Cao, and Dixon. 2016. "Mechanisms of Ferroptosis." *Cellular and Molecular Life Sciences* 73 (11–12): 2195–2209. https://doi.org/10.1007/s00018-016-2194-1.

Dixon, Patel, Welsch, Skouta, Lee, Hayano, Thomas, et al. 2014. "Pharmacological Inhibition of Cystine–Glutamate Exchange Induces Endoplasmic Reticulum Stress and Ferroptosis." *ELife* 3 (May): e02523. https://doi.org/10.7554/eLife.02523.

Fenton, 1894. "LXXIII.—Oxidation of Tartaric Acid in Presence of Iron." *Journal of the Chemical Society, Transactions* 65 (0): 899–910. https://doi.org/10.1039/CT8946500899.

Galanello. 2007. "Deferiprone in the Treatment of Transfusion-Dependent Thalassemia: A Review and Perspective." *Therapeutics and Clinical Risk Management* 3 (5): 795–805.

Haber, and Weiss. 1934. "The Catalytic Decomposition of Hydrogen Peroxide by Iron Salts." *Proceedings of the Royal Society of London. Series A - Mathematical and Physical Sciences* 147 (861): 332–51. https://doi.org/10.1098/rspa.1934.0221.

Janero. 1990. "Malondialdehyde and Thiobarbituric Acid-Reactivity as Diagnostic Indices of Lipid Peroxidation and Peroxidative Tissue Injury." *Free Radical Biology and Medicine* 9 (6): 515–40. https://doi.org/10.1016/0891-5849(90)90131-2.

Kobayashi, Suhara, Baba, Kawasaki, Higa, and Matsui. 2018. "Pathological Roles of Iron in Cardiovascular Disease." *Current Drug Targets* 19 (9): 1068–76. https://doi.org/10.2174/1389450119666180605112235.

Martin, and Teismann. 2009. "Glutathione—a Review on Its Role and Significance in Parkinson's Disease." *The FASEB Journal* 23 (10): 3263–72. https://doi.org/10.1096/fj.08-125443.

Mou, He, Zhang, Duan, and Li. 2019. "Ferroptosis, a New Form of Cell Death: Opportunities and Challenges in Cancer." *Journal of Hematology & Oncology* 12 (1): 1–16. https://doi.org/10.1186/s13045-019-0720-y.

Sato, Kusumi, Hamashima, Kobayashi, Sasaki, Komiyama, Izumikawa, Conrad, Bannai, and Sato. 2018. "The Ferroptosis Inducer Erastin Irreversibly Inhibits System x c − and Synergizes with Cisplatin to Increase Cisplatin's Cytotoxicity in Cancer Cells." *Scientific Reports* 8 (1): 968. https://doi.org/10.1038/s41598-018-19213-4.

Tang, Kang, Berghe, Vandenabeele, and Kroemer. 2019. "The Molecular Machinery of Regulated Cell Death." *Cell Research* 29 (5): 347–64. https://doi.org/10.1038/s41422-019-0164-5.

Velasquez, and Wray. 2021. "Deferoxamine." *StatPearls*, May. https://www.statpearls.com/ArticleLibrary/viewarticle/20309.

Zhang, Fan, Pang, Shen, Wang, Zhao, Li, et al. 2020. "Neuroprotective Effect of Deferoxamine on Erastin-Induced Ferroptosis in Primary Cortical Neurons." *Neural Regeneration Research* 15 (8): 1539–45. https://doi.org/10.4103/1673-5374.274344.

Chapter 6 General Conclusion and Perspectives

Living organisms constantly produce ROS, which are highly reactive and toxic substances for cells. Cells are normally able to fight against these ROS using intrinsic enzymes or antioxidant molecules. However, an imbalance between ROS and antioxidant defenses leads to oxidative stress, a condition that is the starting point of many diseases such as atherosclerosis. Free metal ions, particularly iron ions, are often responsible for oxidative stress. Cell death caused by iron overload has been defined as “ferroptosis” and to date there is no cell-based ferroptosis model that mimic the cell signaling pathway in AS disease. Humans are recommended to take exogenous antioxidants in order to counteract the excess ROS production caused by the toxic environmental surroundings. Since the consumption of certain synthetic antioxidants have been linked to adverse effects, researchers are now turning to natural molecules, including bioactive peptides derived from various natural proteins. Currently, the purification of new bioactive peptides from protein hydrolysates is performed empirically *via* fastidious and high cost separation and identification techniques. The goal of this PhD was to evaluate modern biotechnological techniques to screen MCPs is hydrolysates and to apply them on cardiovascular cell-based ferroptosis model to assess their chelation capacity in a biological environment.

This last chapter summarizes the contributions made to achieve the aforementioned goal and it stresses out work that still need to be done **(Figure 6.1)**.

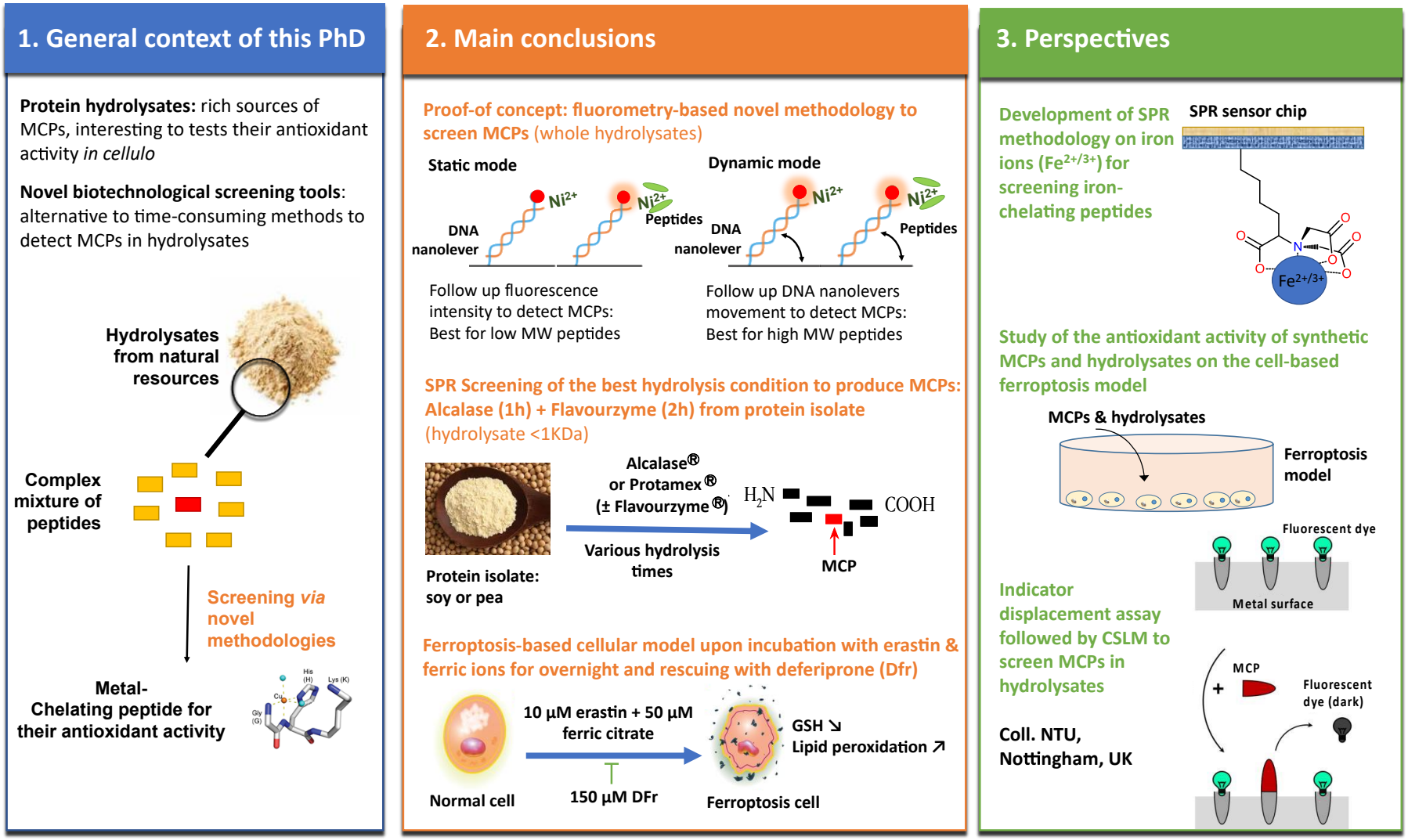

Figure 6.1. Schematic representation for this PhD's goal, achievements and proposed future work.

6.1 Conclusion

Meantime, the development of innovative biosensors relies on studying real-time biological interactions involving small molecules, peptides, membrane proteins, biologics and other molecules even in crude reaction mixtures. SwitchSENSE® is a recent methodology, which is based on short DNA nanolevers that can switch on gold surface spots on a microfluidic chip. For the author's knowledge, this methodology has never been adapted to the screening of metal-chelating peptides in hydrolysates. For this purpose, switchSENSE® technology was adjusted by immobilizing NTA-Ni^{2+} to the surface of its sensor chip. First, the methodology was validated with pure synthetic peptides well-known for their nickel-chelating properties and then applied to enzymatic hydrolysates used in food industry. This methodology was able to categorize the metal-chelating activities of the studied hydrolysates according to the enzymatic treatment or the protein source: Tilapia viscera or soy isolates.

Enzymatic hydrolysis is nowadays the most promising method to produce bioactive peptides, especially from natural resources. The bioactivity of produced hydrolysates relies on several factors implicated in the hydrolysis procedure such as protein source, type of proteases used, enzyme-to-substrate ratio, time of incubation… etc. Bioactive peptides are normally of 10 amino acids long. So, ultrafiltration is often performed after hydrolysis to obtain these specific fractions of peptides in hydrolysates. In this thesis, we took in advantage a previously developed MCPs-screening modern methodology to identify the best hydrolysis conditions to produce MCPs. This methodology, called Surface Plasmon Resonance (SPR) is based on real-time interaction of MCPs with immobilized Ni^{2+}. After the hydrolysis of soy and pea isolate by Alcalase® and Protamex® enzymes, either individually for 1 and 3 hours or sequentially with Alcalase® or Protamex® for 1 hour followed by Flavourzyme® enzyme for 2 hours, hydrolysates were then ultrafiltrated and characterized according to their molecular weight distribution and amino acid content. Finally, their affinity bindings towards Ni^{2+} were determined by SPR. The sequential hydrolysis of soy protein isolate by Alcalase® followed by Flavourzyme® was the best treatment to produce MCPs.

The biological interest in exploring metal-chelating activity in these hydrolysates is to evaluate their antioxidant power *in cellulo*. These target peptides could be promising for ferroptosis inhibition by chelating iron ion in excess and thus contribute to the prevention of cell death in several diseases including atherosclerosis (AS). However, in literature, ferroptosis induction in

cells is only well described to kill cancer cells but not as a model of diseased cells. For this purpose, we aimed to develop a ferroptosis model (induction and rescuing) on human aortic smooth muscle cells to mimic ferroptosis happening during AS development. The ferroptosis model was developed in three steps taking into consideration three essential parameters such as the concentration of ferroptosis inducers (erastin and ferric ions), the time and the medium of incubation. At each step, 2 biomarkers, *i.e.,* intracellular concentration of GSH and lipid peroxidation, were followed by NDA and TBARS methods, respectively. Finally, the ferroptosis model was validated upon 10 µM Erastin and 50 µM ferric ions incubation during 16 hours in a complete medium diluted 2 times. Erastin succeeded in blocking the system X_c^- leading to the depletion of intracellular cysteine necessary for GSH synthesis. Adding ferric ions have accelerated oxidative reactions, notably the Fenton reaction, producing reactive species that have attacked lipid membranes in cells and caused lipid peroxidation. The rescue of the ferroptosis model was validated using metal chelators such as DFO and DFr, which are also control molecule regarding MCP activity. Only 150 µM of DFr was able to inhibit lipid peroxidation caused by erastin and ferric ion.

The outcomes of this interdisciplinary PhD project at the professional and personal level are summarized hereafter **(Figure 6.2)**. In terms of publications, we have published a book chapter about applications of mineral-binding peptides, and an original article concerning the fluorometry-based MCP screening (Chapter 3 in this thesis; El Hajj *et al.,* 2021). We have recently submitted the manuscript for the screening of MCPs in soy and pea protein hydrolysates after different enzymatic hydrolysis treatments (Chapter 4 in this thesis; El Hajj, *et al.,* in submission). We also aim to valorize the ferroptosis work with a review on ferroptosis (Chapter 2, section 2.2) and a publication concerning the ferroptosis model development adapted to human aortic smooth muscle cells (Chapter 5 of this thesis). Our results have been presented and discussed at several national and international conferences. Also, collaborations with laboratories from/or outside Université de Lorraine have allowed us to make connections between the different disciplines implicated in this PhD and to produce those scientific outcomes. Finally, this PhD have provided beneficial trainings (professional and inter-personal), and scientific mediation opportunities.

Publications

El Hajj et al., Electrically switchable nanolever technology for the screening of metal-chelating peptides in hydrolysate. *Journal of Agricultural and Food Chemistry* (IF: 4.192), **2021,** 69 (31): 8819–27.
El Hajj et al., Metal-chelating activity of soy and pea protein hydrolysates obtained after different enzymatic treatments. Submitted at *Food Chemistry*.
El Hajj et al., "Chapter 19 - Application in Nutrition: Mineral Binding." In *Biologically Active Peptides*, Elsevier book edited by Fidel Toldrá and Jianping Wu, **2021,** 455–94.

Conferences

El Hajj et al., Investigating the antioxidant activity of metal-chelating peptides in soy hydrolysates on a cell-based ferroptosis model. 29th international conference for Functional Food Center (FFC). Dallas, TX, United-States, **29th – 30th April 2021**. Oral communication
El Hajj et al., Metal-chelating peptides in hydrolysates: biocatalysis production, characterization and screening. Seminar of IMPACT BIOMOLECULE. Palma de Mallorca, Spain, **3th – 25th October 2019.** Poster and Flash presentation.
El Hajj et al., SPR screening of metal-chelating peptides for their antioxidant properties in laboratory-produced hydrolysates: effect of proteolysis conditions. 17ème édition du congrés de la SFGP. Nantes, France, **15th – 17th October, 2019.** Oral communication.

Scientific Collaborations

Laboratories of Université de Lorraine (UR AFPA, L2CM, LCPM, LIBIO, IMoPA) and **3 platforms** (PASM, ASIA, B2S).
Internship at Institute of Chemistry, Université de Strasbourg (1 week): Spectrophotometric screening of metal-chelating peptides using ascorbate oxidation monitoring in the presence of NTA-Fe^{3+}.
International mobility at School of Science & Technology, Nottingham Trent University, United Kingdom (2 months): Development of a screening method for metal-chelating peptides in protein hydrolysates by confocal laser scanning microscopy (CLSM).
International grant obtained for supporting this mobility (DrEAM 5 project).

Trainings

Followed courses: Chromatography, electrochemical methods, calorimetry and thermo-gravimetric analysis, molecular synthesis and their characterization (RMN, FT-IR, DRX, UV-visible and fluorescence spectroscopies), drug and nanoparticle development.
Management trainings: Culture of scientific integrity, R&D professions, MOOC Doctorate and Career Development.
Mentoring: Participation in the supervision / scientific training of students (Bibliography, experiments).

Scientific mediation

Participation at the science festival in October 2018. « How to make a battery from a lemon? ».
Interview at the ''Factuel, l'info de l'Université de Lorraine'' Portrait of a researcher, international human rights day woman on March 8, 2020.
Application to L'oreal-UNESCO program for women in Science in April 2021.

Figure 6.2. The outcomes of this PhD

6.2 Perspectives

This present interdisciplinary project aimed at discovering and testing new MCPs produced from proteolysis and evidenced by setting up new original screening methodologies. SPR and switchSENSE® are techniques developed on Ni^{2+}. Although Ni^{2+} physico-chemical properties are similar to Cu^{2+}, its biological relevance in terms of oxidative stress reactions is poor. So, the development of those two methodologies based on iron ions (Fe^{2+} or Fe^{3+}) is mandatory. However, applying these 2 ions on biosensor is challenging. Indeed, Fe^{3+} rapidly precipitates in non-acidic pH such as at physiological pH (pH 7.4) and Fe^{2+} rapidly oxidizes into Fe^{3+} in the presence of oxygen. To rise these blocks, we can propose to prepare Fe^{3+} in acidic solution and gradually increase the pH until reaching the physiological value. For Fe^{2+}, we could consider working in an anaerobic glovebox.

The next step is to identify iron-chelating peptides in hydrolysates using an original methodology based on IMAC coupled to MS. This methodology has already been developed in the frame of another PhD thesis (PhD student: Cédric Paris; Director: Stéphane Désobry Co-Directress: Laetitia Canabady-Rochelle; PhD defended in April 2021). IMAC directly coupled on line with MS (IMAC-MS) is also a novel approach for a direct, sensitive and untargeted screening of iron(II)-chelating peptides in complex mixtures. After identification of the best MCPs using IMAC-MS, their production and modification into pseudopeptides by chemical synthesis will allow to obtain sufficient amount of pure bioactive peptides and will be advantageous for *in vivo* applications since pseudopeptides are known to be preserved from degradation by digestive enzymes and their bioavailability will be increased.

Testing hydrolysates containing MCPs and/or pure MCPs on a cell model of oxidative stress is necessary to guarantee their bioactivity. The interest in this PhD was to test the inhibitory action of MCPs on the developed ferroptosis model. The ferroptosis model based on human aortic smooth muscle cells still requires some validation as for example, by following a 3rd biomarker such as the ROS production. After validating the ferroptosis rescue model, MCPs and hydrolysates will be tested on the ferroptosis model and their inhibitory effect can be compared to that of DFO and DFr. Hydrolysates and pure MCPs could require different incubation conditions to observe their inhibitory effect. So, setting up their concentrations and incubation time can be also challenging and time-consuming. After validation of their

effect on the ferroptosis model, the samples will require to be tested for their bioavailability through the intestinal barrier in order to move to their evaluation in *in vivo* models.

Finally, in the frame of a collaboration between our team and the Biomolecular and Materials Interface Research Group (Nottingham Trent University, England), an application for a DrEAM grant (offered by LUE for researchers) have been accepted and a 2 months internship at the the Biomolecular and Materials Interface Research Group is ongoing meanwhile. The goal of this research visit is to discover new technique related to MCPs screening. The technique is based on indicator displacement assays and followed up by Confocal Scanning Laser Microscopy (CSLM). Using a metal oxide surface (notably nickel oxide surface) and a fluorophore, the indicator displacement assay can provide measurements of interactions based on the direct observation of competitive binding between the fluorophore and the metal-chelating peptide of interest.